Theory of dynamical solvent and guest-host correlated quantum dynamics

Henning Gustav Alois Kirchberg

UNIVERSITÄT HAMBURG

1·9·1·9

Hamburg

2020

Theory of dynamical solvent and guest-host correlated quantum dynamics

Dissertation
zur Erlangung des Doktorgrades
an der Fakultät für Mathematik, Informatik, Naturwissenschaften
Fachbereich Physik
der Universität Hamburg

vorgelegt von
Henning Gustav Alois Kirchberg
aus Braunschweig

Hamburg
2020

Gutachter der Dissertation: Prof. Dr. Michael Thorwart
Prof. Dr. Abraham Nitzan

Zusammensetzung der Prüfungskommission: Prof. Dr. Michael Thorwart
Prof. Dr. Abraham Nitzan
Prof. Dr. Christian Bressler
Prof. Dr. Daniela Pfannkuche
Prof. Dr. Michael Potthoff

Datum der Disputation: 12.05.2020

Vorsitzender Fach-Promotionsausschuss PHYSIK: Prof. Dr. Günter Hans Walter Sigl

Leiter des Fachbereichs PHYSIK: Prof. Dr. Wolfgang Hansen

Dekan an der Fukultät MIN: Prof. Dr. Heinrich Graener

Contents

For you will see many particles there stirred by unseen blows change their course and turn back, driven backwards on their path, now this way, now that, in every direction everywhere. [...] And so the movement passes upwards from the first-beginnings, and little by little comes forth to our senses, so that those bodies move too, which we can descry in the sun's light [...]

Lucretius, *De rerum natura (On the nature of things)*, book II, ll. 116-149, translated by C. Bailey (Oxford University Press, London, 1910)

Abstract

This thesis is devoted to quantum dynamical processes in dissolved atoms and molecules when non-stationary time-dependent changes within the solvent-solute configuration occur. The strong spatial and temporal changes of the solvent produce statistical configurations far away from thermal equilibrium and strongly modify the properties of the solute such as time-dependent modifications of optical absorption or of charge transfer.

In the first part of the thesis, I investigate optical absorption of an atom in a non-equilibrated solvent as signature of energy absorption. To this end, I consider the dynamics of a generic molecular dipole which is embedded in an Onsager sphere with specific time-dependent geometric configurations. We solve a non-stationary Langevin equation for the molecular dipole moment of the solute and use the reduced description of the solvent based on the Onsager continuum model of solvation. Central macroscopic properties such as the molecular polarization, the dielectric constants and the relaxation time of the solvent, which are all experimentally measurable, enter in that model. First, I generically study the relaxation and absorption properties of a central molecular dipole moment embedded in the center of a shrinking and a breathing Onsager cavity. The relaxation rate of the dipole moment inside the shrinking sphere is enhanced in comparison to the static sphere while the relaxation within the breathing cavity is reduced. The calculated linear absorption spectrum for the breathing sphere additionally shows a dramatic reduction of the broadening of the linewidth. Second, the model of a shrinking Onsager sphere is connected to a bimodal time-dependent Stokes shift and provides an extension to the Bagchi-Oxtoby-Fleming theory. Thus, the Stokes shift can be decomposed into the bulk water relaxation and the self-motion or extensional changes of the solute. Afterward, the Onsager solvation model is extended to describe a dynamical formation of the hydration shell. For a growing hydrophobic hydration shell around a neutralized iodine, the calculated absorption spectrum shows a noticeable time-dependent blue shift. Experimental data from X-ray absorption spectroscopy confirm this shift which thus provides a clear signature of hydrophobic solvation.

In the second part of the thesis, I investigate charge transfer through solvated molecular junctions mediated by a nonadiabatic solvent. Under equilibrium condition, the celebrated Marcus theory explains the charge transfer by successive hopping where the charge configuration on the conducting molecule leads to a readjustment of the surrounding solvent molecules. A central assumption in equilibrium Marcus theory is the complete relaxation of the solvent according to the charge configuration before each new hopping while thermal solvent fluctuations around the equilibrium account for the charge transfer. In this thesis, I go beyond equilibrium Marcus theory and study charge transfer under the action of nonequilibrium fluctuations. For this, I consider a finite relaxation time, during which the solvent molecules adjust in between the successive charge-transfer processes. In general, they do not entirely thermalize between two sequential hops. To this end, a diffusion equation (Smoluchowski equation) is formulated for an effective solvent coordinate representing its configuration. I determine its solution for a low and overdamped solvent relaxation. By employing a Monte Carlo simulation for the successive single-electron transfer, a characteristic Kramers-like turnover in the current-damping behavior of the molecular junction is found. For a well chosen applied bias voltage and solvent reorganization energy, the characteristic turnover can be inverted. The calculated current autocorrelation function grows for an enhanced damping which shows a strong influence of the solvent relaxation on the current. Finally, I propose a way to tune the solvent-induced damping using geometrical control of the solvent dielectric response in nanostructured solvent channels.

Zusammenfassung

In der vorliegenden Dissertation werden dynamische quantenmechanische Prozesse in solvatisierten Atomen und Molekülen unteruscht, wenn nicht stationäre zeitliche Änderungen in der Konfiguration von Solvens und gelöstem Stoff sich vollziehen. Die starken örtlichen und zeitlichen Lösungsmitteländerungen induzieren statistische Konfigurationen fern vom thermischen Gleichgewicht und beeinflussen mittelbar die Eigenschaften des solvatisierten Moleküls, wie zeitabhängige Modifikationen der optischen Absorption oder des Ladungstransfers.

Im ersten Teil der Dissertation untersuche ich die optische Absorption eines Atoms in einem Nichtgleichgewichtssolvens als Merkmal der Energieabsorption. Zu diesem Zweck betrachte ich die Dynamik eines generischen molekularen Dipols, welcher im Zentrum einer Onsagersphäre mit spezifischen geometrischen Konfigurationen situiert ist. Wir lösen dann die nicht stationäre Langevin Gleichung für das molekulare Dipolmoment eines solvatisierten Stoffes und nutzen die reduzierte Beschreibung des Solvens mit dem Onsager Model, einem Kontinuumsmodel. Zentrale makroskopische Größen, die auch experimentell zugänglich sind, wie die molekulare Polarisation, die dielektrischen Konstanten und die Relaxation des Solvens, fließen in dieses Model ein. Zunächst studiere ich generisch das Relaxations- und Absorptionsvehaltens eines zentralen molekularen Dipolmoments in einer schrumpfenden und einer atmenden Onsagerkavität. Die Relaxationsrate des Dipolmoments in der schrumpfenden Kavität wird im Vergleich zum statischen Fall erhöht, während die Relaxtion für die atmende Kavität reduziert wird. Das berechnete lineare Absorptionsspektrum zeigt hier zusätzlich eine drastische Reduktion der Linienbreite für die atmende Kavität. Sodann wird das Model der schrumpfenden Onsagerkugel mit einem biomodalen Verhalten im zeitabhängigen Stokes-Shift verknüpft und liefert so eine Erweiterung der Bagchi-Oxtoby-Fleming Theorie. Der Stokes-Shift kann somit in die kollektive Solvensrelaxation und in die mögliche Eigenbewegungen oder Größenänderungen des zentralen Moleküls zerlegt werden. Anschließend erweitere ich das

Onsagermodell für die dynamische Bildung einer Solvationshülle. Für eine hydrophobe Hydrathüllenausbildung um ein neutralisiertes Iodmolekül zeigt das berechnete Absorptionsspektrum eine deutliche zeitliche Blauverschiebung. Experimentelle Daten aus der Röntgenabsorptionsspektroskopie bestätigen die Verschiebung und geben einen klaren Hinweis auf hydrophobe Solvatation.

Im zweiten Teil der Dissertation untersuche ich den nicht-adiabatischen solvensbedingten Landungstransfer durch einen solvatisierten molekularen Leiter. Unter Gleichgewichtsbedingungen beschreibt die berühmte Marcus-Theorie den Ladungstransfer mittels sukzessiver Hüpfprozesse, wobei jede Ladungsänderung des zentralen leitenden Moleküls eine Neuausrichtung der umgebenden Solvensmoleküle bedingt. Eine zentrale Annahme der Marcustheorie ist hierbei die vollständige Relaxation des Solvens gemäßdes Ladungszusatandes des Molekls vor jedem Hüpfprozess, wobei die thermischen Fluktuationen des Solvens um das Gleichgewicht den Landungstransfer bedingen. In der Dissertation untersuche ich den Ladungstransfer unter der Wirkung von Nichtgleichgewichtsfluktuationen jenseits der Marcus-Theorie. Daher betrachte ich eine endliche Relaxationszeit, während welcher sich die Solvensmoleküle neu ausrichten. Im Allgemeinen thermalisieren diese nicht vollständig zwischen den sequenziellen Hüpfvorgängen. Zu diesem Zweck wird eine Diffussionsgleichung (Smoluchowski-Gleichung) für eine effektive Koordinate formuliert, welche die zeitabhängige Solvenskonfiguration darstellt. Ich bestimme sodann die Lösungen für die Grenzfälle einer stark und schwach gedämpften Solvensrelaxation. Eine anschließende Monte-Carlo Simulation für den Ein-Elektronen-Transfer zeigt ein charakteristisches Kramers Umkehrverhalten in der Strom-Dämpfungs-Abhängigkeit. Für eine geschickte Wahl der angelegten Spannung und der Solvensreoganisationsenergie kann das Verhalten umgekehrt werden. Die berechnete Stromautokorrelationsfunktion wächst bei einer erhöhten Dämpfung, was einen starken Einfluss des Solvensrelaxationsverhaltens auf den Strom zeigt. In einem letzten Schritt zeige ich eine geschickte Methode das Dämpfungsverhalten des Solvens zu steuern, indem ich die veränderte dielektrische Antwort des Solvens aufgrund geometrischer Einschnürungen im Bereich weniger Nanometer nutze.

Chapter 1

Introduction

Since the early days in physics one is interested in dynamics of objects ranging from the macroscopic world to the smallest particles known today. While in the macroscopic world Hamilton's equations, or simply Newton's equation, adequately describe their time evolution, one exploits the Schrödinger equation for the dynamics of quantum objects. During time evolution they will interact with other particles of 'the rest of the world' and may exchange energy, charge or spin. These interactions significantly affect the dynamics of the particle of interest and result in *dissipation* [1, 2, 3, 4, 5, 6], and *decoherence* [7]. The latter, being an inherent quantum effect, disturbs the quantum phase relation, such that relevant information of the *system* is lost in the *environment* or *bath*.

A historic example of observing and quantifying trajectories of classical particles is the jittery motion of pollen grains suspended in water studied by the Botanist Robert Brown in 1827 [8]. Albert Einstein in 1905 [9], Marian Smoluchowski in 1906 [10] and later Paul Langevin in 1908 [11] formulated phenomenological equations of motion for such a particle trajectory leading to a diffusion constant, which depends on the temperature of the solution and the mobility of the observed particle related to its mean free path.

1.1 Brownian motion and open quantum systems

To retrace equations of motion from the microscopic perspective, the idea of small coupled quantum objects forming a many-body system arises which can eventually be reduced to the dynamics of few significant degrees of freedom. Therefore, John von Neumann introduced in 1927 a formalism of density matrices where he effectively describes the time evolution of a quantum (sub-)system of particular interest interacting with a bath of which the detailed dynamics is insignificant [12]. The global Hamiltonian $H = H_S + H_B + H_I$ is split into a relevant system Hamiltonian H_S, a bath Hamiltonian H_B and a system-bath interaction H_I. The time-dependent expectation value of a system observable $\mathbf{A}$ can be obtained by $\langle \mathbf{A}(t) \rangle = \mathrm{tr}_S\{\boldsymbol{\rho}_S(t)\mathbf{A}\}$, where the density operator of the system $\boldsymbol{\rho}_S(t) = \mathrm{tr}_B\{\boldsymbol{\rho}(t)\}$ results from a partial trace over the bath states for the overall density matrix $\boldsymbol{\rho}(t)$ which describes the system, the bath and their interaction [12] [1]. In performing the trace over the many bath degrees of freedom, one considers the bath composed of a great number of identical constituents obeying the laws of statistical mechanics. Particularly, if the bath is large in comparison to the small subsystem of interest, the bath is thought to be in thermal equilibrium. With the reduced description for the bath at hand one can formulate equations of motion for the system which may now depend on a few macroscopic variables. The Fokker-Planck equation for a Brownian motion [15], the Bloch equations for magnetic relaxation [14] or the master equation for an atom interacting with the radiation field [16] are just few examples which follow this spirit [17]. While the isolated system obeys reversible dynamics determined by the Hamiltonian H_S and the initial probability density $\boldsymbol{\rho}_S(t_0)$, its interaction with the bath leads to *irreversible* time evolution. In this case, the equation of motion for $\boldsymbol{\rho}_S(t)$ comprises a reversible part entering via the Poisson bracket (classically) or the commutator (quantum mechanically) [18] and an irreversible part related to correlation functions of the system variable coupling to the bath characterized by *Green-Kubo*-type formulae in linear order of perturbation theory [19, 20]. The quantum statistical environment acts via *fluctuating* forces like the solution particles exerts them on the pollen grain in the Brownian experiment. The fluctuating forces cause decoherence and damping of the quantum system where measurements of relevant dynamical system observables are related to entities of the macroscopic world. The fundamental principle of the *fluctuation-dissipation theorem* relates dissipation of energy and fluctuations of a noise force where the notion of a local equilibrium exists [20]. Multiple ansatzes are available to solve the equation of motion of $\boldsymbol{\rho}_S(t)$ ranging from simple master equations [21, 22], when the interactions between the system and the environment is weak and the equations can be solved in a pertubative manner, to exact numerical methods [23, 24, 6]. The latter are needed for strong system-bath interaction in the non-Markovian regime when memory effects of previous system states due to bath interaction strongly influence the momentary time-evolution of the system.

---

[1] The formalism of density matrices or density operators is independently introduced by John von Neumann [12] in 1927, Lev Landau in 1927 [13] and Felix Bloch in 1946 [14].

1.2 Experimental approach to dynamical solvents

In experimental setups, one probes dynamical processes of quantum systems by applying an external force which drives the system (and bath) slightly or far away from equilibrium. The time-dependent response to this force enlightens different dynamical system behavior determined by the interaction with the bath. Standard experimental methods are quasi-elastic and inelastic scattering of light [25], electrons or neutrons off a sample under investigation. The line shapes of the associated spectra reveal the underlying system's dynamics influenced by the bath relaxation [26]. More advanced nonlinear spectroscopy techniques exploit three or multiple light pulses interacting successively with the probe and, thus, provide more detailed information on the system's time evolution and its correlation dynamics which is not resolved in linear spectroscopy. 2D spectra may offer for example information about prominent vibrational mode couplings and, hence, directly enlightens the energy transfer dynamics in molecules up to femtosecond time resolution [27]. In all such experiments, the system's response to an external force yields information about the dynamical properties of fluctuations and the ensuing dissipation of energy into the bath.

A prominent example to study dynamical properties of a central system within a huge bath is the chemical process of photodissociation and possible recombination of iodine $I_2 \rightarrow I + I$ in solution which totally dissociates in the gas phase [28, 29]. The potential energy surfaces of dissolved iodine depend on the distance of the center of mass of the two I atoms and describe bound and repulsive states of I_2. Upon photoexcitation from a stable ground state, iodine may reach a dissociative energy level which leads to a separation of the I atoms due to the repulsive Coulomb potential. The separating atoms encounter solvent molecules, exchange energy with them and, thus, can be forced to recombine or may completely dissociate. The molecular absorption spectrum at a wavelength of 500 nm is first bleached out, but recovers after 30-50 ps, signaling the recombination of I_2 in CCl_4 [30]. At 350 nm, the transient states can be probed, and their life time varies from 60 ps in alkane solvents to 2.7 ns in CCl_4 [28, 31]. Since the life time depends on the solvent, multiple theoretical ansatzes have been used to explain its influence. A simplest model stems from Smoluchoswki [32] who has considered diffusion-controlled reactions where the rate for interstate transition, $k_D = 4\pi D\sigma$, depends only on the solvent diffusion constant D and the length of the relative free reactive path σ between the reactants [2]. This model has further developed, such that, e.g., the 'cage effect' in liquids, where radicals are screened by the solvent disabling the separation, is taken into account [33]. Further developments include

---

[2] Smoluchowski has considered ideal spherical reactants [32].

non-spherical solvent geometry [34] or spin statistical factors [35] which clearly hint to consider the molecular aspect of the solvent. Then, vibration-vibration transfer pathways between solute and solvent eventually become important [29]. A molecular dynamics (MD) simulation for the solvent molecules in the vicinity of the reactants may provide numerical solutions for such a *many-body* problem [36].

1.3 Discrete and continuum models of solvation

Albeit MD simulations recover with high accuracy dynamical processes such as reaction rates of dissolved reactants, the simulation effort increases with the number of solvent molecules taken into account. The main ingredients here are the forces modifying the positions of the individual solvent molecules. In most cases, one uses simple force-field representations of molecular features, such as harmonic spring forces for bond lengths and angles or the Coulomb law for van der Waals or electrostatic interactions. Once the effective forces acting on the individual atom are obtained, mostly, classical Newton's equation is applied to calculate accelerations and velocities to iteratively update the atom positions. The integration of movements is done numerically where the individual time steps normally rank between 1 and 3 fs for MD simulations. Biological or chemical processes up to microseconds require iteration over 10^9 calculation cycles [37]. Yet, MD simulations remain essentially a description on the classical level.

One effective way to incorporate quantum mechanical effects are *continuum solvation models*. In an enormously complex network of interactions that characterizes the liquid, one may obtain dynamical information of a subsystem by simply focusing on the component of interest, the *solute*, while treating the rest as responsive continuum medium, the *solvent*. In 1936, Lars Onsager was the first who has effectively described the polarization of the solvent as back action on the solute dipole moment by means of a fluctuating force field, the *reaction field* [38]. His concept of molecular dipole moments acting on the continuum dipolar solvent with a resulting back action opened up the way to describe the solute dynamics quantum mechanically, e.g., as a two level system with distinct dipole moments for the ground and excited states [39, 40]. As a result, the vacuum Hamiltonian of the isolated molecular system becomes an effective Hamiltonian, where the solute-solvent interaction and the solvent Hamiltonian are taken into account according to the approach in terms of a system-bath model. Since the polarization of the solvent is induced by the solute while the solute is subsequently polarized by the solvent, an iterative self-consistent field approach represents the solution of such a problem which is an often used quantum mechanical method [40]. This implicit sampling of the solvent relies on macroscopic properties, such as the dielectric permittivity and the refractive index of the solvent, which furthermore take into account long-range electrostatic interactions and polarization effects. These are often neglected in discrete MD approaches [40].

1.4 Nonequilibrium quantum solvation and irreversible time-dependent phenomena

The main focus of this thesis is to study *nonequilibrium quantum solvation and irreversible as well as non-stationary time-dependent phenomena*. The relevant time dependence in continuum models is contained in the frequency dependent dielectric function $\epsilon(\omega)$ of the solvent where information on the precise functional form is known experimentally or from effective models such as the Debye [41] or the Drude [42] model. With $\epsilon(\omega)$ and a suitable Fourier transform, one obtains a time-dependent polarization by exploiting the theory of linear response [20]. Within the framework of a continuum model, a separation of the solvent response into a fast, mostly associated with electronic motion, and a slow contribution, due to nuclear and molecular motion, is commonly performed. The slow delays of solvent polarization upon fast changes in the structure or in the electronic charge distribution are then used to simulate the solvation dynamics. These nonequilibrium effects are used to describe chemical reaction dynamics in a condensed environment, electron-transfer processes [43, 44] or (non-linear) vibrational spectroscopies [45, 46]. In all these models, the relaxation process of the solvent polarization is not completely coupled to the source of relaxation, i.e., the charge transfer or energy absorption, but, instead, is activated by such a source [40] and thus is based on linear response theory. The solvent then freely relaxes according to the functional form of $\epsilon(\omega)$ and its corresponding time-dependent characteristics follow in linear response theory a time translation symmetry reflecting stationarity. A model extension away from solvent equilibrium requires that the relaxation of the system (the source of nonequilibrium) and the solvent are coupled from the initial moment to the final re-equilibration such that non-stationary effects in time are encountered [40].

1.5 Aim of the thesis

Modern picosecond and femtosecond resolved X-ray spectroscopy provides an experimental tool to reveal solute-induced changes of water structure such as the hydrogen-bond strength, the tetrahedral order, or the presence of dangling (non-hydrogen-bonded) OH groups in the hydration shell of the solute [47, 48, 49]. In this case, the continuum model alone is limited and has to be adapted to recover possible time-dependent anisotropies in solute-solvent interactions. Hence, the configuration departs from thermal equilibrium and the solvent becomes a true nonequilibrium entity. Here, chemical intuition or preliminary MD simulations may help to follow the real-time geometrical structure changes of the solvent around the solute. From largely adiabatic simulations, one may extract some representative configurations within the first layer of the hydration shell(s) and exploit them to quantum mechanically model the molecule combined with a continuum description of the solvent that takes into account bulk and longer-range effects [47]. Phenomenological continuum models using molecular cavities like the Onsager model [38] can then be adjusted to describe evolving non-stationary polarization effects in given spatial regions of the solvent. This concept is followed within the first part the thesis. We shall use a continuum model of a polar solvent hosting a solute described by an Onsager-type geometric cavity. Structural changes in the solvent are included in time-dependent changes of geometrical properties of the solute cavity, e.g., its radius, its solvation shell layer. An externally provided time protocol will be used to mimic a dynamic environment. Then, the time-dependent relaxation and absorption properties in this nonequilibrium solvent will be determined, leading to clear signatures of the dynamic solvent which become measurable via physical observables associated to the solute. This realizes a time-dependent observation of dynamical solvent properties by considering dynamical information of the solute alone. This is newly established and will be studied in detail in the *first part* of this thesis.

Chemical reaction in an equilibrium solution is well studied and the first theoretical treatment of the dynamic influence of the solvent on an activated reaction stems from Kramers in 1940 [50]. He found that the solvent dynamics may lead to a breakdown of the reaction rate of reactants in chemical equilibrium covered by the conventional transition state theory in two distinct ways [51]. First, solvent collisions with the reactants may lead to a recrossing of the reaction barrier and may, in the extreme case, turn into a diffusive passage over the barrier. By exploiting the model of a Brownian motion (Langevin and Fokker-Planck equations) for the solvent, Kramers has introduced a damping force experienced by the reacting particles which interact with the solvent. For large damping the reaction rate is strongly reduced. The damping is often associated with the viscosity of the solvent by exploiting a hydrodynamic argument of Stokes' law[52]. In a second way, for sufficiently low friction and mostly at low pressure, a system-solvent energy transfer is required for reactive activation, and, thus, the reaction rate grows with friction. The regime of low friction is observed in isomerization reactions or unimolecular processes, whereas the high-friction limit is valid for most processes where atoms are transferred between reactant and product states [28]. This theory can be extended to metal-molecule-metal junctions in solution, such that solvent features can be read of from the charge current and its fluctuations through the molecular bridge. In the simplest model, when the molecule supports only one electronic site, this site may be successively occupied and de-occupied as an electron hops between the metal and the molecule. Every hopping is accompanied by solvent relaxation due to a change of the charging state of the molecule and, thus, due to a change of the polarization state of the solvent. In the most prominent Marcus electron transfer theory [43, 44] the solvent fully relaxes before a new event occurs. In this case, only equilibrium fluctuations of the solvent polarization affect the charge on the molecule. When solvent relaxation happens on a finite time scale, successive electron hopping events are highly correlated in time and the Marcus theory has to be extended to the realm of nonequilibrium fluctuations. Such a generalization of the Marcus theory to nonequilibrium is the main focus of the *second part* of this thesis.

1.6 Structure of this thesis

This implies the following structure of the thesis: In Chapter 2, I establish the basic and the conceptual ideas of open quantum systems to study the energy absorption and charge transfer in molecules in a highly fluctuating solvent. Therefore, I investigate the time evolution of relevant system degrees of freedom such as the molecular dipole moment. I start with the derivation of the quantum Langevin equation from a microscopic model in Sec. 2.1 to obtain an equation of motion for the relevant system variable. To further specify the environmental solvent, I continue in Sec. 2.2 with a description of continuum solvation models and exploit dielectric properties such as the dielectric constants and relaxation properties related to the underlying molecular characteristics of the solvent. I briefly recapitulate a molecular system coupled to the electromagnetic field in Sec. 2.3 to link important relaxation and absorption properties of the molecule determined in linear spectroscopy, e.g. the absorption coefficient, to the solvent characteristics. In Sec. 2.4, I review the spin-boson model to describe the electron transfer in polar solution. In the nonadiabatic regime, important dielectric properties are related to a characteristic spectral density of the bath to describe the solvent mediated electron transfer.

In Chapter 3, I formulate a novel nonequilibrium theory for time-irreversible changes of the geometrical structure of the solute or solvent. I extend the cavity model of Onsager in Sec. 3.1 to describe a molecule in solution. In Sec. 3.2, a theory of nonequilibrium quantum solvation based on the Onsager model is formulated in which geometric parameters of the solvent are explicitly depending on time. The relaxation and absorption properties of a test molecular point dipole in a dielectric solvent is used to reveal the solvent dynamics for two cases: a shrinking Onsager sphere, and a breathing Onsager sphere. The idea of the shrinking sphere is used in Sec. 3.3 to develop a model for a bimodal behavior in the time-dependent fluorescence Stokes shift. In Sec. 3.4, I address the dynamic build-up of the hydration shell around a hydrophobic solute on the basis of this time-dependent dielectric continuum model. Interestingly, it turns out that the build-up of the hydration shell can be revealed by a time-dependent Stokes' shift of the solute's absorption spectrum.

In Chapter 4, I consider the effect of a finite solvent-induced relaxation on the 'hopping' conduction in molecular junctions, which goes beyond the standard treatments of transport in solvated molecular junctions that rely on equilibrium Marcus theory. I develop a generalization of Marcus theory to nonequilibrium.

Furthermore, I predict an effective way to suitably tune the solvent relaxation and, hence, the current as well as its correlation, by changing the dielectric properties of the solvent in strong geometrical confinements on the nanoscale. Strong surface effects of nanostructured solvent channels strongly modify the relaxation properties of a bulk solvent, opening the way to control relaxation and dephasing rates by geometric means.

Chapter 5 concludes the thesis and provides an outlook. Three Appendices A, B and C are included.

Chapter 2

Theory of nonequilibrium quantum dynamics in a continuous solvent

Energy absorption and charge transfer in a molecule dissolved in a dynamical solvent with many degrees of freedom portray prominent quantum dynamical processes. Externally imposed photons or electrons, e.g. by a light source or by a bias voltage, drive the molecule-solvent system out of its initial thermally equilibrated state which, on the one hand, lead to charge and energy redistribution of the molecule itself, but, on the other hand, also induce a solvent reorganization. The latter has to adapt to the varying energy or charge state of the molecule, and consequently, strongly acts back on the molecule and alters its energy and charge states. Thus, the solvent dynamics influences energy relaxation properties of the dissolved molecule and changes its charge transfer abilities.

To study energy absorption and charge transfer in such enormous *open quantum systems*, one utilizes the framework of quantum statistical mechanics for many-body systems to understand the origin of macroscopic irreversible behavior, such as energy dissipation, resulting from the underlying microscopic process of many individual interacting particles [17]. It arises the idea to reduce the many-body system into a (sub-)system of interest, the molecule or *solute*, which interacts with an environment, the *solvent* [12]. This concept may be translated into a simple formal expression where the whole system is partitioned into three parts: the system or *solute*, the *environment* or *solvent* and their *interaction.* Thus, the Hamiltonian reads on the lines of the system-bath formalism

$$H(\mathbf{q},\mathbf{r}) = H_S(\mathbf{q}) + H_B(\mathbf{r}) + H_I(\mathbf{q},\mathbf{r}), \tag{2.1}$$

where $\mathbf{q}$ and $\mathbf{r}$ describe the degrees of freedom of the solute and the individual solvent molecules, respectively, e.g. their position or angle of distortion. Having such a model at hand, one wants now to understand the microscopic origin of relaxation dynamics of a specific system observable, e.g. the molecular dipole moment to study molecular energy absorption. These system-plus-bath models allow a full quantum mechanical treatment as, despite its complexity in detail, the total given Hamiltonian H of Eq. (2.1) determines the dynamical process. In general, the time evolution of closed systems with finite degrees of freedom, such as usually described by H_S, can be solved by unitary operations acting on the the system. For open systems with 'infinite' many degrees of freedom, the dynamics of the system cannot by accurately described using unitary operators alone due to the interactions between the system and its environment [26]. Refs. [21, 22, 23], as some examples of many for energy absorption and electron transfer dynamics of the system, introduce quantum master equations for distinct observables, while, e.g. Refs. [24, 6] exploit exact numerical techniques to include memory effects of the solvent related to strong molecule-solvent correlations for system-plus-bath models.

In this context, the general concept of *continuum solvation models* to determine the time evolution of the system is to preserve the accurate description of the central solute, or at least parts of it, e.g. a distinct electronic transition, and to reduce the degrees of freedom of the large solvent molecular assembly by means of a continuous dielectric description. There is a large variety of many-body systems for which such a reduction may be profitably used. The single solute molecule in a dilute solvent is just one example of many ones, which may be also a defect inside a crystal, an active part of an enzyme or a a single molecule in a pure gas [53]. The reduction procedures exploit, for example, projection operator techniques to relevant observables and thermal averaging of the remaining solvent degrees of freedom [17]. The resulting continuous polar solvent imposes a fluctuating environment and responds electrodynamically to the charging or energy state of the central solute. Thus, the dynamics of the system observable of interest can be determined in terms of a generalized (quantum) Langevin equation for the motion [17, 26]. The damped (quantum) mechanical harmonic oscillator is the simplest model of a dissipative quantum system [54, 4, 26]. A central harmonic oscillator is coupled linearly via its displacement q to the fluctuating coordinates of a dynamical bath of harmonic oscillators. After formulating the equation of motion for the displacement q, or for another relevant system observable in the quantum case, one can study its relaxation dynamics which is fully described by the *spectral density* $J(\omega)$. The spectral function covers the coupling to each individual bath mode and bears all collective influence of the harmonic bath on the system, such as energy relaxation or dephasing of initially fixed system's quantum phase relations. To obtain the spectral density for continuum solvation models, one may consider a generic molecular two-level system interacting electrodynamically with a huge collection of solvent modes which are eventually related to a continuous solvent. Thereafter, dielectric properties and solvent relaxation times enter in the spectral description for the bath (see Sec. 2.4). The resulting theoretical framework is based on the *spin-boson model* which has become one of the central models of theoretical physics with applications in chemistry and biology [31]. Caldeira and Leggett were among the first who applied this model to study quantum mechanical tunneling in macroscopic systems [4, 55].

The aim of the present chapter is to establish the important theoretical framework for solute dynamics embedded in a continuous and mostly stationary solvent by exploiting the continuum model of solvation which is later utilized and extended towards non-stationary changes of solute/solvent configurations for energy absorption in Chapter 3 and for charge transfer in Chapter 4. In Section 2.1, the system-bath model is revisited to derive the generalized quantum Langevin equation for observables whose dynamics can be used for energy absorption and charge transfer processes. Section 2.2 revisits the electrostatic description of the continuum model of the solvent to connect macroscopic dielectric properties to its molecular origins of solvent fluctuations. Section 2.3 focuses on linear absorption spectroscopy of light by using the Hamiltonian of minimal coupling Hamiltonian of the molecular system to the radiation field. In Section 2.4, the spin-boson model is reviewed to describe charge transfer processes in solution. Finally, I show how a spectral density relies on dielectric properties.

2.1 System-bath model

The aim of the system-bath model is to achieve a generalized equation of motion for a system observable of particular interest.

In this model, the quantum system is realized by a particle of mass M moving in a potential $V(\mathbf{q})$ with the position operator $\mathbf{q}$ as the relevant degree of freedom [1]. The system Hamiltonian reads,

$$H_S = \frac{\mathbf{p}^2}{2M} + V(\mathbf{q}), \tag{2.2}$$

---

[1] The presentation essentially follows Refs. [26, 31].

where $\mathbf{p}$ is the momentum operator. The huge environment is represented by a bath of N independent harmonic oscillators of mass m_α with displacement operators $\mathbf{x}_\alpha$ and momentum operators $\mathbf{p}_\alpha$. The bath and system-bath interaction Hamiltonian reads

$$H_B + H_I = \sum_{\alpha}^{N} \left(\frac{\mathbf{p}_\alpha^2}{2m_\alpha} + \frac{1}{2} m_\alpha \omega_\alpha^2 (\mathbf{x}_\alpha - \frac{c_\alpha}{m_\alpha \omega_\alpha^2} \mathbf{q})^2 \right), \tag{2.3}$$

where the interaction appears via a bi-linear coupling term $\mathbf{q} \sum_\alpha c_\alpha \mathbf{x}_\alpha$ with the coupling constants c_α to the individual oscillators. This coupling represents the first term in the expansion of a general interaction $V_I(\mathbf{q}, \mathbf{x}_1, ..., \mathbf{x}_N) = V_I(\mathbf{q}_0) + V_I(\mathbf{x}_0^N) + \frac{1}{2} \sum_\alpha k_\alpha (\mathbf{q} - \mathbf{q}_0)(\mathbf{x}_\alpha - \mathbf{x}_{\alpha,0})$ between the system and the bath displacements, where the notation $\mathbf{x}^N = (\mathbf{x}_1, ..., \mathbf{x}_N)$ is used and where the coupling constant is $k_\alpha = (\partial^2 V / \partial \mathbf{q} \partial \mathbf{x}_\alpha)|_{\mathbf{q}_0, \mathbf{x}_{\alpha,0}} = 2c_\alpha$. One sets $\mathbf{q}_0 = \mathbf{x}_0^N = 0$ and $V_I(\mathbf{q}_0) = V_I(\mathbf{x}_0^N) = 0$ in the following discussion. The counter term $\sum_\alpha \frac{c_\alpha^2 \mathbf{q}^2}{2 m_\alpha \omega_\alpha^2}$ in the Hamiltonian of Eq. (2.3) has the effect that the minimum of the total potential experienced by the particle at any displacement $\mathbf{q}$ in $\mathbf{q}$-direction remains at the minimum of $V(\mathbf{q})$. The quantum mechanical equations of motion in the Heisenberg picture for the system and bath operators are

$$\ddot{\mathbf{q}} = -\frac{1}{M} \frac{\partial}{\partial \mathbf{q}} V(\mathbf{q}) - \frac{1}{M} \sum_{\alpha}^{N} c_\alpha \left(\frac{c_\alpha}{m_\alpha \omega_\alpha^2} \mathbf{q} - \mathbf{x}_\alpha \right), \tag{2.4}$$

and

$$\ddot{\mathbf{x}}_\alpha = -\omega_\alpha^2 \mathbf{x}_\alpha + \frac{c_\alpha}{m_\alpha} \mathbf{q}. \tag{2.5}$$

The dynamical equation (2.5) for the oscillator displacement operator $\mathbf{x}_\alpha(t)$ is an ordinary second order linear differential equation with inhomogeneity $c_\alpha / m_\alpha \mathbf{q}(t)$. This equation is solved by standard Green function techniques. The solution evolving from the initial values $\mathbf{x}_\alpha^{(0)}$ and $\mathbf{p}_\alpha^{(0)}$ at $t_0 = 0$ reads

$$\mathbf{x}_\alpha(t) = \mathbf{x}_\alpha^{(0)} \cos[\omega_\alpha t] + \frac{\mathbf{p}_\alpha^{(0)}}{m_\alpha \omega_\alpha} \sin[\omega_\alpha t] + \frac{c_\alpha}{m_\alpha \omega_\alpha} \int_0^t dt' \sin[\omega_\alpha (t - t')] \mathbf{q}(t'). \tag{2.6}$$

Integrating the last term by parts, one obtains a functional of the particle's velocity $\dot{\mathbf{q}}(t)$

and position $\mathbf{q}(t)$ in the form

$$\begin{aligned}\mathbf{x}_\alpha(t) =& \mathbf{x}_\alpha^{(0)}\cos[\omega_\alpha t] + \frac{\mathbf{p}_\alpha^{(0)}}{m_\alpha\omega_\alpha}\sin[\omega_\alpha t] \\ &+ \frac{c_\alpha}{m_\alpha\omega_\alpha^2}\Big(\mathbf{q}(t) - \cos[\omega_\alpha t]\mathbf{q}(0) - \int_0^t dt'\cos[\omega_\alpha(t-t')]\dot{\mathbf{q}}(t')\Big).\end{aligned} \tag{2.7}$$

One can now eliminate the bath degrees of freedom by inserting Eq. (2.7) into Eq. (2.4). The equation of motion for $\mathbf{q}(t)$ alone follows as

$$M\ddot{\mathbf{q}}(t) + M\int_0^t dt'\gamma(t-t')\dot{\mathbf{q}}(t') + \frac{\partial}{\partial\mathbf{q}}V(\mathbf{q}) = \boldsymbol{\xi}(t). \tag{2.8}$$

This equation for the dynamics of $\mathbf{q}(t)$ is the generalized quantum *Langevin equation* where the interaction with the environmental bath appears via a memory-friction, second term of Eq. (2.8), and a random external force $\boldsymbol{\xi}(t)$. To this end one introduces the memory-friction kernel

$$\gamma(t) = \Theta(t)\frac{1}{M}\sum_\alpha \frac{c_\alpha^2}{m_\alpha\omega_\alpha^2}\cos[\omega_\alpha t], \tag{2.9}$$

and the external force term

$$\boldsymbol{\xi}(t) = \sum_\alpha c_\alpha\Bigg(\bigg[\mathbf{x}_\alpha^{(0)} - \frac{c_\alpha}{m_\alpha\omega_\alpha^2}\mathbf{q}(0)\bigg]\cos[\omega_\alpha t] + \frac{\mathbf{p}_\alpha^{(0)}}{m_\alpha\omega_\alpha}\sin[\omega_\alpha t]\Bigg). \tag{2.10}$$

The equation of motion (2.8) is an integro-differential equation in which the environment affects the system non-instantaneously by a memory function $\gamma(t-t')$ at time $t-t'$ of the past interaction between them producing in general a *non-Markovian* dynamics. The Markovian limit is obtained when this kernel is instantaneous, i.e., $\gamma(t-t') = 2\gamma\delta(t-t')$. This term induces friction for the position operator $\mathbf{q}$.

The external force represents a stochastic force that acts on $\mathbf{q}$ and conveys energy absorption and emission of single quanta $\hbar\omega_\alpha$ into and from the environment. Coming from the microscopic picture, the stochastic nature roots in the lack of information of initial values of $\bar{\mathbf{x}}_\alpha^{(0)} = \mathbf{x}_\alpha^{(0)} - \frac{c_\alpha}{m_\alpha\omega_\alpha^2}\mathbf{q}(0)$ and $\mathbf{p}_\alpha^{(0)}$. As one assumes the bath in thermal equilibrium at initial time, one samples their momenta and position out of an equilibrium

Boltzmann distribution. Their statistics satisfies [2]

$$\begin{aligned}
&\langle \bar{\mathbf{x}}_\alpha^{(0)} \rangle_{\boldsymbol{\rho}_B^{(0)}} = \langle \mathbf{p}_\alpha^{(0)} \rangle_{\boldsymbol{\rho}_B^{(0)}} = 0; \\
&2m_\alpha\omega_\alpha \langle \bar{\mathbf{x}}_\alpha^{(0)} \bar{\mathbf{x}}_\beta^{(0)} \rangle_{\boldsymbol{\rho}_B^{(0)}} = \frac{2}{m_\alpha\omega_\alpha} \langle \mathbf{p}_\alpha^{(0)} \mathbf{p}_\beta^{(0)} \rangle_{\boldsymbol{\rho}_B^{(0)}} = \hbar[1 + 2n(\omega_\alpha)]\delta_{\alpha\beta},
\end{aligned} \tag{2.11}$$

where $n(\omega_\alpha) = [\exp(\beta\hbar\omega_\alpha) - 1]^{-1}$ is the single-particle Bose distribution.

With this relation at hand, one finds for the mean force $\langle \boldsymbol{\xi}(t) \rangle_{\boldsymbol{\rho}_B^{(0)}} = 0$ and for the force-force or environment auto-correlation function (for $t > s$)

$$\langle \boldsymbol{\xi}(t)\boldsymbol{\xi}(s) \rangle_{\boldsymbol{\rho}_B^{(0)}} = \hbar \sum_\alpha^N \frac{c_\alpha^2}{2m_\alpha\omega_\alpha} \Big[\coth[\beta\hbar\omega_\alpha/2] \cos[\omega_\alpha(t-s)] - i \sin[\omega_\alpha(t-s)] \Big]. \tag{2.12}$$

If the number N of bath oscillators is large, the Poincaré recurrence time exceeds all relevant time scales of the system. Thus, one may replace the sum over the discrete bath modes by a frequency integral by introducing a *spectral density*

$$J(\omega) = \pi \sum_\alpha^N \frac{c_\alpha^2}{2m_\alpha\omega_\alpha} \delta(\omega - \omega_\alpha), \tag{2.13}$$

such that one obtains

$$\langle \boldsymbol{\xi}(t)\boldsymbol{\xi}(s) \rangle_{\boldsymbol{\rho}_B^{(0)}} = \frac{\hbar}{\pi} \int_0^\infty d\omega J(\omega) \Big[\coth[\beta\hbar\omega/2] \cos[\omega(t-s)] - i \sin[\omega(t-s)] \Big] \tag{2.14}$$

and

$$\gamma(t) = \frac{2}{\pi M} \int_0^\infty d\omega \frac{J(\omega)}{\omega} \cos[\omega t]. \tag{2.15}$$

In the classical limit $k_BT \gg \hbar\omega$ the environmental correlation function (Eq. (2.14)) becomes $\langle \boldsymbol{\xi}(t)\boldsymbol{\xi}(s) \rangle_{\boldsymbol{\rho}_B^{(0)}} = Mk_BT\gamma(t-s)$ such that the quantum Langevin equation becomes formally the classical one.

The relaxation induced by the environment is entirely determined by the properties of

---

[2] The canonical distribution of the shifted bath oscillators in equilibrium reads $\boldsymbol{\rho}_B^{(0)} = Z^{-1} \exp\Big(-\beta \sum_\alpha \Big[\frac{\mathbf{p}_\alpha^{(0)2}}{2m_\alpha} + \frac{m_\alpha\omega_\alpha^2}{2} \bar{\mathbf{x}}_\alpha^{(0)2} \Big] \Big)$, where Z is the partition function and $\beta^{-1} = k_BT$.

the spectral density (Eq. (2.13)). An *Ohmic* bath is described by

$$J(\omega) = \eta\omega e^{-\omega/\omega_c}, \tag{2.16}$$

such that Eq. (2.15) becomes

$$\gamma(t) = \frac{2\eta}{\pi M}\frac{1/\omega_c}{(1/\omega_c)^2 + t^2}, \tag{2.17}$$

where ω_c is a cutoff frequency beyond which the density of states in the environment drops rapidly. If ones defines the constant $\eta = \gamma M$ and chooses a short memory time $\tau_{mem} = \pi/(2\omega_c) \to 0$, the memory-friction kernel in Eq. (2.15) becomes Markovian $\gamma(t) = 2\gamma\delta(t)$. Thus, the force-force auto-correlation (Eq. (2.12)) in the classical Markovian regime reads $\langle \boldsymbol{\xi}(t)\boldsymbol{\xi}(s)\rangle_{\boldsymbol{\rho}_B^{(0)}} = 2M\gamma k_B T\delta(t-s)$. Markovianity requires that the bath relaxes fast relative to the system, which is realized when ω_c is chosen larger than all relevant system frequencies or energy spacing.

2.2 Continuum model of the solvent

In the previous section a generalized Langevin equation for the dynamics of a relevant system observable, e.g. $\mathbf{q}(t)$ in Eq. (2.8), is formulated. All relevant impact of the solvent on the system observable enters via the non-Markovian friction term $\int_0^t dt'\gamma(t-t')\dot{\mathbf{q}}(t)$ and the random force $\boldsymbol{\xi}(t)$. In performing the thermal average for the initial positions and momenta in Eq. (2.12) for the bath oscillators, one continues with a coarse-grained description of the bath. In such a continuum approach individual solvent molecules are described by their collective action on the system. It is of great interest in system-solvent models to compare the time scales of the system or solute variable of interest to that one of the solvent. Characteristic timescales in molecular systems with electronic processes are around $10^{-15} - 10^{-16}$s, $10^{-14} - 10^{-15}$s for vibrational motions and $> 10^{-12}$s for rotations, librations and center of mass motion [56, 31]. A typical timescale for solvent relaxation, e.g. for water bulk water at room temperature, is about $\tau = 8.2$ps [39, 57]. Obviously this timescale is longer than characteristic electronic or vibrational motions in the solute and clearly hints a non-Markovian treatment in formulating the relevant Langevin equation since past solvent configurations influences the momentary dynamics of the solute. In the limit where the solvent relaxation is short relative to the characteristic system time, e.g. time scale for rotational motion of the solute or nonadiabatic charge transfer (see

Subsec. 2.4.3), the solvent response is instantaneous and expressed by a constant damping coefficient and by a white-noise character of the random force, a signature of Markovianity.

The idea now arises to formulate an effective Hamiltonian for continuous models of solvation which leads to a generalized Langevin-type equation for the relevant observable for the non-Markovian limit. We introduce an appropriate solvent response function $Q(\mathbf{x}, \mathbf{x}'; t, t')$ in the solute-solvent interaction term to effectively describe the solvent action on the system. $\mathbf{x}$ and $\mathbf{x}'$ represent two individual vectors, pointing in the continuous solvent, which are correlated. Together with t and t', describing the correlation between solvent events at different times, we gain dynamical information of the coarse-grained and continuous solvent. The effective Hamiltonian then reads

$$H_{eff}(\mathbf{q}, \mathbf{x}) = H_S(\mathbf{q}) + H_I(\mathbf{q}, Q(\mathbf{x}, \mathbf{x}'; t, t')). \tag{2.18}$$

Here, we neglect the solvent Hamiltonian H_B of Eq. (2.1) as we are only interested in its action on the system and the system dynamics itself. The introduced response function or *susceptibility* is related to the introduced spectral density of Eq. (2.13) for a stationary process in time via the identity $J(\omega) \propto \mathrm{Im}[Q(\omega)]$ and is independent of the position $\mathbf{x}$ for a homogeneous and isotropic solvent [26] (see further details in the following Subsec. 2.2.1). A spectral density for an continuous solvent will be studied and formulated in greater detail by means of electrostatics in Sec. 2.4.

This section revisits basic electrostatic descriptions of a continuous solvent coming from its 'atomistic' nature. In Subsec. 2.2.1, I derive an appropriate response function for a continuous dielectric medium to an applied external electric field which may be associated to charge distortion described by the solute coordinate $\mathbf{q}$. In Subsec. 2.2.2, the time scales and origins of the nonequilibrium dynamic response of the solvent are reviewed. Finally, a dielectric description for a continuous solvent based on the molecular polarizability is presented in Subsec. 2.2.3.

2.2.1 Electrostatics in continuous dielectric solvents

We determine the response function of a solvent described by an continuous dielectric medium to a test charge [58]. To this end, we consider a solvent in a box whose dimension is such that all effects induced by solvent-wall interaction can be neglected. We place a small test charge (density) in the center of the solvent box at the position $\mathbf{x}$ and and ask for the electric field at this point which is created by all other charges in the material. The total solvent box is assumed charge-neutral neglecting the small test charge. The charge distribution for the m-th solvent molecule reads

$$\rho_m(\mathbf{x}) = -e \sum_{j=1}^{N_{el}^{(m)}} \delta(\mathbf{r}_j^{(m)} - \mathbf{x}) + e \sum_{n=1}^{N_{nuc}^{(m)}} z_n^{(m)} \delta(\mathbf{R}_n^{(m)} - \mathbf{x}), \tag{2.19}$$

where the first term describes the electrons of elementary charge $-e$ and the second term the nucleons of charge e or zero counted by $z_n^{(m)} = 0; 1$. m is the index of the respective molecule. Using stationary Maxwell's equation, one obtains the scalar electrostatic potential from the Poisson equation $\Delta\Phi(\mathbf{x}) = -4\pi\rho(\mathbf{x})$ in the form (we use cgs-units)

$$\Phi(\mathbf{x}) = \int d^3x' \frac{\rho(\mathbf{x}')}{|\mathbf{x} - \mathbf{x}'|}, \tag{2.20}$$

where the electric field $\mathbf{E}(\mathbf{x}) = -\nabla\Phi(\mathbf{x})$ is induced by the complete molecular charge distribution $\rho(\mathbf{x}) = \sum_m \rho_m(\mathbf{x})$ at the point $\mathbf{x}$ of our test charge.

It is often more relevant to determine the macroscopic electric field as average over the individual microscopic molecular contributions. This averaging is equivalent to the elimination of the short range of the electric field expressions from the individual solvent molecules. We further discuss individual molecular contributions to the electric field in the following Subsec. 2.2.3. To this end, one divides the macroscopic solvent volume into smaller volumes $\Delta V(\mathbf{x}_s)$ that still contain a large number of molecules, where the vector $\mathbf{x}_s$ points to the s-th volume element. Since we are only interested in the long-range contributions of the charges located in $\Delta V(\mathbf{x}_s)$ to the potential, we perform a multipole expansion up to the dipole contribution for a vector $\mathbf{x}$ far away $\mathbf{x}_s$. By expanding the term $|\mathbf{x} - \mathbf{x}_s - (\mathbf{x}' - \mathbf{x}_s)|^{-1} \approx |\mathbf{x} - \mathbf{x}_s|^{-1} - (\mathbf{x}' - \mathbf{x}_s)\nabla_{\mathbf{x}}|\mathbf{x} - \mathbf{x}_s|^{-1}$ with respect to $\mathbf{x}' - \mathbf{x}_s$ the potential reads

$$\begin{aligned}\Phi(\mathbf{x}) &= \sum_s \frac{1}{|\mathbf{x} - \mathbf{x}_s|} \int_{\Delta V(\mathbf{x}_s)} d^3\mathbf{x}' \rho(\mathbf{x}') + \int_{\Delta V(\mathbf{x}_s)} d^3\mathbf{x}' (\mathbf{x}' - \mathbf{x}_s)\rho(\mathbf{x}') \frac{\mathbf{x} - \mathbf{x}_s}{|\mathbf{x} - \mathbf{x}_s|^3} \\ &= \sum_s \frac{1}{|\mathbf{x} - \mathbf{x}_s|} \int_{\Delta V(\mathbf{x}_s)} d^3\mathbf{x}' \rho(\mathbf{x}') + \mathbf{d}_s \frac{\mathbf{x} - \mathbf{x}_s}{|\mathbf{x} - \mathbf{x}_s|^3}.\end{aligned} \tag{2.21}$$

The first term is the monopole term, which is assumed to be zero, since the solvent contains no free charges disregarding the small test charge. The second term is the dipole term by introducing the dipole moment $\mathbf{d}_s = \int_{\Delta V(\mathbf{x}_s)} d^3\mathbf{x}'(\mathbf{x}' - \mathbf{x}_s)\rho(\mathbf{x}')$ of the volume element $\Delta V(\mathbf{x}_s)$. Higher-order multipole moments are assumed to be small compared to the dipole term. The dipole moment $\mathbf{d}_s$ of the small volume may be traced back to the individual molecular dipole moments $\mathbf{d}_s = \sum_{m \in \Delta V(\mathbf{x}_s)} \mathbf{d}_m = \sum_m \int d^3\mathbf{x}'\mathbf{x}'\rho_m(\mathbf{x}')$. We note that not all molecules such as H_2 our CCl_4 have a permanent dipole moment. However, once an external electric field is applied, the molecular charge density can be distorted and an dipole moment is induced. Other molecules, e.g. H_2O or NH_3, have permanent dipole moments and form polar dielectrics [58].

Regarding the effective Hamiltonian approach of Eq. (2.18), the aim is to reduce the degrees of the individual solvent molecules (or subunits of collection of them) discretized by the vector $\mathbf{x}_s$ of the volume $\Delta V(\mathbf{x}_s)$ to a continuous description. To this end, we introduce the coarse-grained dipole density or the *polarization* by $\mathbf{P}(\mathbf{x}_s) = \mathbf{d}_s/\Delta V(\mathbf{x}_s)$, such that the sum of the second term of the potential of Eq. (2.21) can be replaced by an integral over the system volume, i.e.,

$$\begin{aligned}\Phi_P(\mathbf{x}) &= \sum_s \mathbf{d}_s \frac{\mathbf{x}-\mathbf{x}_s}{|\mathbf{x}-\mathbf{x}_s|^3} \approx \int d^3\mathbf{x}'\mathbf{P}(\mathbf{x}')\frac{\mathbf{x}-\mathbf{x}'}{|\mathbf{x}-\mathbf{x}'|^3} \\ &= \int d^3\mathbf{x}'\mathbf{P}(\mathbf{x}')\nabla_{\mathbf{x}'}\frac{1}{|\mathbf{x}-\mathbf{x}'|} = -\int d^3\mathbf{x}'\frac{\nabla_{\mathbf{x}'}\mathbf{P}(\mathbf{x}')}{|\mathbf{x}-\mathbf{x}'|}.\end{aligned} \tag{2.22}$$

The resulting electric field in the solvent obeys the relation $\nabla\mathbf{E}(\mathbf{x}) = 4\pi\rho_P(\mathbf{x})$ and is induced by the polarization charge density $\rho_P(\mathbf{x}) = -\nabla\mathbf{P}(\mathbf{x})$ of the solvent.

So far, we have discussed how a given polarization charge density $\rho_P(\mathbf{x})$ within the solvent results in an electric field. We now come back to the initial idea of the effective Hamiltonian of Eq. (2.18) for the solute, where we have reduced the solute-solvent interaction by means of the response function $Q(\mathbf{x},\mathbf{x}';t,t')$ of the solvent to the solute degrees of freedom. To this end, we may ask how an external electric field, e.g., induced by the charge displacement $\mathbf{q}$ of the solute (cf. Chapter 3), leads to a change of the charge distribution in the solvent, characterized in terms of its polarization.

In general, the answer to this question is that the polarization of the solvent is a complicated functional of the acting electric field, $\mathbf{P} = \mathbf{P}[\mathbf{E}]$. For a weak perturbation of the solvent due to the external field, a linear relation between the electric field and the polarization is justified in the form

$$\mathbf{P}(\mathbf{x},t) = \int d\mathbf{x}' \int dt' \boldsymbol{\chi}(\mathbf{x},\mathbf{x}';t,t')\mathbf{E}(\mathbf{x}',t'). \tag{2.23}$$

Here, $\boldsymbol{\chi}$ is the tensor of electric susceptibility, because the direction of $\mathbf{P}$ can differ from that of the electric field $\mathbf{E}$. For an isotropic solvent, $\mathbf{P}$ and $\mathbf{E}$ are parallel and $\boldsymbol{\chi} = \chi\mathbb{I}$ where χ is a scalar and $\mathbb{I}$ is the unit tensor. The dependence of $\boldsymbol{\chi}(\mathbf{x}, \mathbf{x}'; t, t')$ on time and position dependence reflects the fact that an applied field at some position at some time may cause a response at another position at a later time [31]. In a homogeneous and stationary solvent, $\boldsymbol{\chi}(\mathbf{x}, \mathbf{x}'; t, t') = \boldsymbol{\chi}(\mathbf{x} - \mathbf{x}'; t - t')$ and the susceptibility depends only on position and time differences. For a local susceptibility in time and position and an isotropic solvent, we even have that $\chi(\mathbf{x} - \mathbf{x}'; t - t') = \chi\delta(\mathbf{x} - \mathbf{x}')\delta(t - t')$, which implies $\mathbf{P} = \chi\mathbf{E}$. We assume that the electric field in the solvent results from an externally controlled charge density $\rho_{ex}(\mathbf{x})$, e.g. from a solute molecule, an the polarization charge density of the solvent $\rho_P(\mathbf{x})$. Therefore, the relation for the overall electric field in the solvent $\nabla\mathbf{E}(\mathbf{x}) = 4\pi(\rho_{ex}(\mathbf{x}) + \rho_P(\mathbf{x}))$ holds. The dielectric displacement field, which obeys $\nabla\mathbf{D}(\mathbf{x}) = 4\pi\rho_{ex}(\mathbf{x})$ and where $\mathbf{D} = \mathbf{E} + 4\pi\mathbf{P}$, may be interpreted as the external field induced by $\rho_{ex}(\mathbf{x})$. For vacuum and, hence, in absence of the polarizable solvent $\mathbf{D} = \mathbf{E}$.

With the definition of the (local) dielectric constant $\epsilon = 1 + 4\pi\chi$, one can write the relation $\mathbf{D} = \mathbf{E} + 4\pi\mathbf{P}$ as $\mathbf{E} = \epsilon^{-1}\mathbf{D}$. In dielectric media, $\epsilon > 1$ holds such that the electric field $\mathbf{E}$ inside the solvent is smaller than the applied field outside the solvent which we identify the dielectric displacement vector $\mathbf{D}$ [58]. This reduction of the field is a clear signature of the polarization of the solvent. The electric susceptibility χ for molecules is further revisited in Subsec. 2.2.3.

2.2.2 Dynamic response of the polarization

One key feature of interest is to describe nonequilibrium or time-dependent processes, when the dynamics of the solvent, characterized by the stationary response $Q(t-t')$ (see effective Hamiltonian of Eq. (2.18) for a response local in space), occurs on the same timescale as the dynamics of the solute described by its coordinate $\mathbf{q}$ in a non-Markovian way. If the charge distribution of the solute varies appreciably during a time period, the response of the microscopic solvent particles, i.e., molecules, atoms or electrons, will not be sufficiently rapid to build up a new equilibrium polarization, such that the actual polarization $\mathbf{P}$ of the continuous solvent will lag behind the changing charge distribution of the solute [53]. For an isotropic and homogeneous solvent which is local in position, the polarizability α is given according to the applied external field $\mathbf{D} = \epsilon^{-1}\mathbf{D} + 4\pi\mathbf{P}$ outside as

$$\mathbf{P}(t) = \frac{1}{4\pi}\int_{-\infty}^{t} dt'[\delta(t - t') - \epsilon^{-1}(t - t')]\mathbf{D}(t') \equiv \frac{1}{4\pi}\int_{-\infty}^{t} dt'\alpha(t - t')\mathbf{D}(t'). \qquad (2.24)$$

The assumption of locality is valid if the spatial variation of the actual external electric field $\mathbf{D}(t)$ is small on the scale of atomic or molecular extensions inducing the polarization. Causality requires that $\alpha(t) = 0$ for $t < 0$. Carrying out a Fourier transform of Eq. (2.24), we get $\mathbf{P}(\omega) = \alpha(\omega)\mathbf{D}(\omega)$. Using the relation $\mathbf{D}(\omega) = \epsilon(\omega)\mathbf{E}(\omega)$ (see Subsec. 2.2.1) we obtain the polarizability

$$\alpha(\omega) = \frac{1}{4\pi}[1 - \epsilon^{-1}(\omega)]. \tag{2.25}$$

For many realistic physical situations, it is reasonable to split the polarization $\mathbf{P} = \mathbf{P}_{fast} + \mathbf{P}_{slow}$ into a fast and slow part. The fast part of the solvent response is associated with the distortion of the molecular electronic charge distribution by the external field and its typical response time τ_e is of the order 10^{-16}s [53, 31]. This polarization may respond to high-frequency external fields. The slow part is related to the orientational relaxation of nuclei on a time scale $\tau_n \sim 10^{-12}$s [53, 31]. Therefore, this term is more sensitive to electric fields of lower frequencies. The separation of $\mathbf{P}$ into a high- and low-frequency part enters in the *Debye* [41] dielectric relaxation function $2\pi\epsilon(t) = \epsilon_\infty\delta(t) + \tau_D^{-1}(\epsilon_S - \epsilon_\infty)\exp[-t/\tau_D]\Theta(t)$ or in Fourier space [3]

$$\epsilon(\omega) = \left[\epsilon_\infty + \frac{\epsilon_s - \epsilon_\infty}{1 + i\tau_D\omega}\right]. \tag{2.26}$$

In the high-frequency range ($\omega \to \infty$), the dielectric function in Eq. (2.26) approaches the value ϵ_∞, whereas for very low frequencies ($\omega \to 0$) it goes to the static dielectric constant ϵ_s. The intermediate, frequency-dependent range is characterized by the Debye relaxation time τ_D. Inserting an external monochromatic electric field $\mathbf{D}$ with a low frequency $\omega_{ex} \ll \tau_n^{-1}$ in Eq. (2.25), the polarization $\mathbf{P} \approx (4\pi)^{-1}[1 - \epsilon_s^{-1}]\mathbf{D}$ follows. For a high-frequency external $\mathbf{D}$ with $\omega_{ex} \sim \tau_e^{-1}$ one can deduce the fast polarization $\mathbf{P}_{fast} = (4\pi)^{-1}[1 - \epsilon_\infty^{-1}]\mathbf{D}$. Since the resulting $\mathbf{P}$ contains also the fast electronic contribution, the slow orientational polarization alone is $\mathbf{P}_{slow} = \mathbf{P} - \mathbf{P}_{fast} = (4\pi)^{-1}[\epsilon_\infty^{-1} - \epsilon_s^{-1}]\mathbf{D}$. This decomposition of the response function into two terms goes back to Pekar and Marcus, such that the resulting polarizability for the slow orientational solvent relaxation, $c_P = \epsilon_\infty^{-1} - \epsilon_s^{-1}$, is named as *Pekar* factor [43]. For very fast processes, e.g. vertical electronic transitions, only the electronic polarization will be involved, whereas for slower processes, such as, e.g., the time-resolved fluorescence Stokes shift measurements, the com-

---

[3] The Fourier transform is defined by $\mathcal{F}[f(t)] = \int_{-\infty}^{\infty} dt \exp(i\omega t) f(t)$.

plete solvent dynamic response, including induced and orientational polarization, will be faced [59, 31].

2.2.3 Molecular polarizability

In this subsection, we further investigate the relationship between molecular properties of the solvent and the macroscopic susceptibility χ (cf. Eq. (2.23)).

First, one distinguishes between the macroscopic electric field $\mathbf{E}$ and the actual near field $\mathbf{E}_i$ which acts on the individual molecules in the solvent. In dilute solvents the distance between the molecules is large enough that there is no further contribution to the macroscopic electric field coming from the neighboring molecules, whereas in dense solvents an internal field $\mathbf{E}_i$ acts on the individual molecules in addition to the macroscopic field $\mathbf{E}$ in the solvent. To determine the internal field $\mathbf{E}_i$, Lorentz proposed to first remove the nearest neighbor molecules of a chosen central solvent molecule [60]. Afterwards one lays a sphere around the molecule and calculates the electric field $\mathbf{E}_P$ which arises from the polarization of the surrounding medium which is now assumed to be a continuous dielectric solvent [60, 61]. One then determines the electric near field $\mathbf{E}_n$ arising from the nearest neighboring molecules which one has removed. The calculated difference between these two contribution gives rise to the actual internal field $\mathbf{E}_i = \mathbf{E}_n - \mathbf{E}_P$ which acts on the individual molecules. The polarization field is calculated from a volume integral [61] to $\mathbf{E}_P = -4\pi\mathbf{P}/3$, while $\mathbf{P}$ represents the polarization in the sphere. The field arising from the neighboring atoms is found to cancel to zero, $\mathbf{E}_n = 0$, due to symmetry of the molecular cluster of nearest neighbors [60] [4]. The total polarization $\mathbf{P}$ can be expressed by the mean individual molecular dipole moment $\mathbf{d}_m$ of N molecules and reads $\mathbf{P} = N\langle\mathbf{d}_m\rangle$. The induced molecular dipole moment $\langle\mathbf{d}_m\rangle$ is proportional to the total electric field in the solvent and reads $4\pi\langle\mathbf{d}_m\rangle = \alpha_m(\mathbf{E} + \mathbf{E}_i)$, where the molecular polarizability α_m itself is assumed to be independent of the field.

In combining the equations one obtains

$$4\pi\mathbf{P} = N\alpha_m\left(\mathbf{E} + \frac{4\pi}{3}\mathbf{P}\right), \tag{2.27}$$

where we have assumed $\mathbf{E}_n = 0$. Using the relation $\mathbf{P} = \chi\mathbf{E}/4\pi$, the susceptibility of a

---

[4] Lorentz has calculated in [60] for illustration the electric field at the origin of a cube which stems from parallel dipole moments located at the eight vertices. In some amorphous substances one may express the near field contribution $\mathbf{E}_n$ in terms of the polarization $\mathbf{P}$ related via a traceless tensor $s_{\alpha\beta}$.

solvent follows as

$$\chi = \frac{N\alpha_m}{1 - \frac{1}{3}N\alpha_m}. \tag{2.28}$$

This relation relates the susceptibility χ, a macroscopic parameter of the solvent, with the molecular polarizability, a microscopic parameter. The dielectric constant ϵ, which relates the electric field outside the solvent (dielectric displacement) $\mathbf{D}$ to that one inside the solvent $\mathbf{E}$ via $\mathbf{E} = \epsilon^{-1}\mathbf{D}$, is connected to the susceptibility χ via $\epsilon = 1 + \chi$ (by exploiting Eqs. (2.23) and (2.25)) such that one obtains the *Clausius-Mossotti relation*

$$\alpha_m = \frac{3}{N}\frac{\epsilon - 1}{\epsilon + 2}. \tag{2.29}$$

Mossotti (in 1850) and Clausius (in 1879) have independently found that the relation $(\epsilon - 1)/(\epsilon + 2)$ is proportional to the density of the dielectric matter [62, 63]. This relation holds mostly for gases and liquids with small dielectric constants whereas for liquids and solids with large ϵ this relation holds only approximatively.

2.3 Molecular absorption spectroscopy

Laser absorption spectroscopy is a common technique to study the energy absorption of molecular systems by means of its absorption spectrum. In this section, I investigate the coupling of a molecular system to light, or more general, to the radiation field to enlighten linear absorption properties when the system forms a continuous dielectric medium.

The minimal-coupling Hamiltonian of a molecular system with electrons and nuclei interacting with the radiation field reads

$$\mathbf{H} = \sum_u \frac{1}{2m_u}\left[\mathbf{p}_u - \frac{q_u}{c}\mathbf{A}(\mathbf{x}_u, t)\right]^2 + \frac{1}{2}\sum_{u \neq v} \frac{q_u q_v}{|\mathbf{x}_u - \mathbf{x}_v|} + H_R, \tag{2.30}$$

where m_u, q_u, c, $\mathbf{p}_u$ and $\mathbf{x}_u$ are the mass, the charge, the speed of light in vacuum, the momentum and position operator of the nuclei and electrons composing the molecular system.[5] The first term describe their coupling to the external vector field $\mathbf{A}(\mathbf{r}, t)$ and the kinetic energy while the second term of the Hamiltonian in Eq. (2.30) describes the

---

[5] I use cgs-units here.

Coulomb interaction between the molecular constituents. The last term is the Hamiltonian of the external radiation field. One usually neglects the fields induced by the motion of the charges bound in the molecular system. Further, one disregards here molecule-molecule interactions responsible for intermolecular charge and energy transfer.

The Hamiltonian of the external radiation field is given by

$$H_R = \frac{1}{8\pi} \int dr [\mathbf{E}^2(\mathbf{r}) + \mathbf{B}^2(\mathbf{r})], \tag{2.31}$$

where the external electric and magnetic field are defined by the vector potential $\mathbf{A}(\mathbf{r}, t)$ via

$$\mathbf{B}(\mathbf{r}, t) = \nabla \times \mathbf{A}(\mathbf{r}, t) \tag{2.32}$$

$$\mathbf{E}(\mathbf{r}, t) = -\frac{1}{c} \frac{\partial \mathbf{A}(\mathbf{r}, t)}{\partial t}. \tag{2.33}$$

The choice of the Coulomb gauge $\nabla \mathbf{A}(\mathbf{r}, t) = 0$ makes the vector potential a transverse field $\mathbf{A}(\mathbf{r}, t) \equiv \mathbf{A}^{\perp}(\mathbf{r}, t)$ with respect to its propagation. Due to the specific gauge the external electric field $\mathbf{E}(\mathbf{r}, t) \equiv \mathbf{E}^{\perp}(\mathbf{r}, t)$ is transverse. One assumes that there are no free charges which give rise to respective densities or currents, which would contribute to the longitudinal electric field. The contribution of the external electric and magnetic field, H_R, in the Hamiltonian (Eq. (2.30)) is neglected as we are in this section specifically interested in the molecule-field interaction. Another simplification arises by restricting the wavelength of the external fields to exceed the spatial extension of the molecular system. Within this long-wavelength approximation, the vector potential in Eq. (2.30) can be written as $\mathbf{A}(\mathbf{X}_m, t)$, where $\mathbf{X}_m$ represents a single specific point, e.g., the center of mass, of the $m-$th molecule [58].

We next transform the Hamiltonian (Eq. (2.30)) by neglecting H_R with the unitary operator

$$D(t) = \exp\left[-\frac{i}{\hbar c} \sum_u q_u \mathbf{x}_u \mathbf{A}(\mathbf{X}_m, t) \right] = \exp\left[-\frac{i}{\hbar c} \boldsymbol{\mu}_m \mathbf{A}(\mathbf{X}_m, t) \right], \tag{2.34}$$

where $\boldsymbol{\mu}_m = \sum_u q_u \mathbf{x}_u$ is the dipole operator associated to the $m-$th molecule. The transformed Hamiltonian for the electronic and nuclear coupling to the radiation field thus becomes

$$\tilde{H}(t) = D(t)HD^{\dagger}(t) + i\hbar\left(\frac{\partial D(t)}{\partial t}\right)D^{\dagger}(t) = \sum_{u} \frac{1}{2m_u}\mathbf{p}_u{}^2 + \frac{1}{2}\sum_{u\neq v} \frac{q_u q_v}{|\mathbf{x}_u - \mathbf{x}_v|} - \boldsymbol{\mu}_m \mathbf{E}(\mathbf{X}_m, t). \tag{2.35}$$

Here one uses the transformed momentum operator $D(t)\mathbf{p}_u D^{\dagger}(t) = \mathbf{p}_u + \frac{q_u}{c}\mathbf{A}(\mathbf{X}_m, t)$ and $i\hbar\left(\frac{\partial D(t)}{\partial t}\right)D^{\dagger}(t) = \frac{1}{c}\boldsymbol{\mu}_m\frac{\partial \mathbf{A}(\mathbf{r},t)}{\partial t} = -\boldsymbol{\mu}_m\mathbf{E}(\mathbf{X}_m, t)$ together with Eq. (2.33). The resulting Hamiltonian (2.35) reproduces with its two first terms the molecular Hamiltonian, while its last term $\boldsymbol{\mu}_m\mathbf{E}(\mathbf{X}_m, t)$ represents the interaction of the molecular dipole moment $\boldsymbol{\mu}_m$ of molecule m with the electric field at the specifically chosen point $\mathbf{X}_m$. We note that the radiation-matter interaction term in the Hamiltonian of Eq. (2.30) may also contain a higher-order term $\propto \mathbf{A}^2$ which vanishes within the long-wavelength and after applying the unitary transformation.

In order to obtain spectroscopic information of condensed phase situation beyond individual molecules, we make several assumptions according to reference [58]:

(i) One neglects magnetization effects and effects leading to a magnetic field within the medium, especially displacement currents.

(ii) The molecules forming the condensed medium are polarized as dipoles, while one neglects higher order multipoles of the polarization.

(iii) One assumes no free charge and current in the medium.

(iv) One considers spectroscopic setups that probes macroscopic properties, i.e., electromagnetic fields of wavelengths longer than the individual molecular size.

For *macroscopic* spectroscopic information of the molecular assembly, an important assumption is to only look at *far field* contributions of the electromagnetic field coming from the sample. In terms of the experimental setup, the spectrometer is far away from the illuminated sample. The key quantity is the polarization field $\mathbf{P}(\mathbf{x}, t)$ generated by the molecules in response to their interaction with the incoming electric field (see Subsec. 2.2.2). In doing so, we proceed as in Eq. (2.22) and consider a coarse-grained polarization field of a small volume element ΔV, which still contains a sufficiently large number of molecules. The applied field should vary only slightly on the length scale of this volume. Each volume element $\Delta V(\mathbf{x})$ is labeled by the spatial vector $\mathbf{x}$ which is its center of mass. It will become a continuous quantity when sums are considered. The resulting polarization of the medium reads

$$\mathbf{P}(\mathbf{x},t) = \frac{1}{\Delta V(\mathbf{x})} \sum_{m \in \Delta V} \mathbf{d}_m(t), \tag{2.36}$$

where $\mathbf{d}_m(t)$ is the time-dependent expectation value of one individual molecular dipole moment according to $\mathbf{d}_m(t) = \mathrm{tr}\{\boldsymbol{\rho}_{eq} U^\dagger(t,t_0)\boldsymbol{\mu}_m U(t,t_0)\}$ [6].

For the total Hamiltonian $H(t) = H_{mol} + H_{int}(t)$, one uses the light-matter interaction Hamiltonian derived in Eq. (2.35) and sum over individual molecular contributions

$$H_{int}(t) = -\sum_m \mathbf{E}(\mathbf{X}_m, t)\boldsymbol{\mu}_m. \tag{2.37}$$

For an ensemble of identical molecules with $\Delta V(\mathbf{x})$ one may replace the summation over the individual molecular dipole moments in Eq. (2.36) by an effective dipole moment at $\mathbf{x}$ multiplied by the volume density n_{mol} of the molecules in the sample volume [58], i.e.,

$$\mathbf{P}(\mathbf{x},t) = n_{mol}\mathbf{d}(\mathbf{x},t). \tag{2.38}$$

We then consider the light absorption of the collectivity of individual dipoles represented by $\mathbf{P}$.

By using Maxwell's equations for dielectric media, using the relation $\mathbf{D} = \mathbf{E} + 4\pi\mathbf{P}$ and the assumption of vanishing free charges and currents and a nonmagnetic material, one obtains a closed equation for the electric field and the polarization according to

$$\left[\frac{\partial^2}{\partial t^2} - c^2\Delta\right]\mathbf{E} = -4\pi\frac{\partial^2}{\partial t^2}\mathbf{P}[\mathbf{E}]. \tag{2.39}$$

To determine the functional $\mathbf{P}[\mathbf{E}]$, we use the sum over the resulting time-dependent expectation values for the individual molecular dipole moments as given in Eq. (2.36). The speed of light in vacuum is $c = \sqrt{\mu_0^{-1}\epsilon_0^{-1}}$.

If the polarization depends linearly on the external field $\mathbf{P} = \chi\mathbf{E}$ (see Eq. (2.23) in Subsec. 2.2.1), Eq. (2.39) can be solved by a plane wave ansatz. To be specific, we use a dielectric platelet of thickness d in z-direction, while there are no geometric restrictions

---

[6] The initial equilibrium statistical operator in absence of the radiation field is $\boldsymbol{\rho}_{eq} = Z^{-1}\exp[-\beta H_{mol}]$, where Z is the partition function and $\beta^{-1} = k_B T$. $U(t,t_0) = \hat{T}\exp\left[-i/\hbar\int_{t_0}^{t} dt' H(t)\right]$ is the time-evolution operator with the time-ordering operator $\hat{T}$.

in x- and y-direction. The monochromatic light is assumed to propagate along the z-direction. Since one neglects reflecting boundary conditions for a thickness much larger than the wavelength of the light in the platelet, $d \gg \lambda_{med}$, one finds

$$\mathbf{E}(z,t) = \mathbf{n}e^{i\omega t}\Bigg[\Theta(-z)\Bigg[E_0 e^{ik_{vac}z} + E_R e^{-ik_{vac}z}\Bigg] + \Theta(z)E_T e^{ik_{med}z}\Bigg] + c.c., \tag{2.40}$$

where we discriminate between the transmitted part in the medium with amplitude E_T and wave number $k_{med} = \omega\sqrt{\epsilon(\omega)}/c$ and the incoming field with amplitude E_0 and the reflected field E_R in vacuum with wave number $k_{vac} = \omega/c$. $\mathbf{n}$ defines the polarization unit vector and $\epsilon(\omega)$ is the complex frequency dependent dielectric constant (cf. Eq. 2.26 in Subsec. 2.2).

The absorption is defined as the decay of the field intensity inside the medium and, thus, determined by the imaginary part of k_{med}. According to Beer's law $I(z) = I(0)e^{-az}$, where $I(z) = |E(z)|^2$, the absorption coefficient is frequency dependent and reads $a(\omega) = 2\omega\,\mathrm{Im}[\sqrt{\epsilon(\omega)}]/c$. After inserting the electric field of Eq. (2.40) together with relation $\mathbf{P} = \chi\mathbf{E}$ in Eq. (2.39), one finds the relation $\sqrt{\epsilon(\omega)} = \sqrt{1 + 4\pi[\mathrm{Re}[\chi(\omega)] + i\,\mathrm{Im}[\chi(\omega)]]} = n(\omega) + i\kappa(\omega)$. Therefore, $\mathrm{Im}[\sqrt{\epsilon(\omega)}] = \kappa(\omega) = 2\pi\,\mathrm{Im}[\chi(\omega)]/n(\omega)$ where $n(\omega) = \mathrm{Re}[\sqrt{\epsilon(\omega)}]$ is the frequency dependent index of refraction. The absorption coefficient reads

$$a(\omega) = \frac{4\pi\omega}{n(\omega)c}\,\mathrm{Im}[\chi(\omega)], \tag{2.41}$$

which is proportional to the imaginary part of the susceptibility. Moreover, in most cases $n^2 \gg \kappa^2$, such that the index of refraction is $n(\omega) = \sqrt{1 + 4\pi\,\mathrm{Re}[\chi(\omega)]}$.

The actual frequency dependence of the dielectric susceptibility $\chi(\omega)$ is strongly determined by the geometry of the dielectric medium and the molecular system as well as the underlying model under investigation. The absorption may also strongly depend on time according to time-dependent varying molecular assembly inside the medium (cf. Chapter 3).

2.4 Electron transfer processes in solution

Electron transfer (ET) is the basis the most chemical reaction processes. Chemical phenomena ranging from photosynthesis to electrochemistry a governed by oxidation-reduction processes where ET is involved in the essential steps for oxygen production or corrosion. A typical working definition of ET is a spontaneous charge redistribution between an initially prepared state, the *donor* state, and a specific product state, the *acceptor* state [58, 64, 65]. The transferred electron remains in a bound state with respect to the particular molecular system and is not activated above the ionization threshold. During the ET the electronic charge distribution and, hence, the internal electric field of the molecule is changed. This may cause new equilibrium positions of the nuclei, and, in case the ET takes place in a polarizable environment such as a polar solvent, may lead to polarization and a rearrangement of the solvent molecules. This process may be seen as the motion of the electron carrying along a polarization cloud [58, 64, 65]. Typical vacuum molecular ionization potential are of the order of $(100 - 300)k_BT$ at $T = 300\text{K}$. Therefore, the stabilization of the reactants by the solvent is associated with the reason that ET occurs in solution at room temperature [31]. For the adequate description of ET, there exists a similarity between the introduced system-bath model in Sec. 2.1 such that the donor and acceptor state, the system of interest, are coupled to the degrees of freedom of the solvent which change their equilibrium configuration if the electronic charge density on the molecule is modified due to the ET. Conversely, the overall free-energy landscape of the donor and acceptor state strongly depends on the momentary solvent configuration. This dependence is mostly considered for a *reaction coordinate*, a particularly chosen collective coordinate for the solvent degrees of freedom. Generically, one considers a double-well potential where its minima are related to the reactant and product states being in equilibrium with the respective solvent configuration. A tractable approximation for the regime of high enough barriers, separating the states, is to approximate the potential wells by harmonic wells.

In the following, I will apply the system-bath Hamiltonian of Sec. 2.1 to model ET in Subsec. 2.4.1 in solution. Afterwards, in Subsec. 2.4.2, we will interpret the displacement of the bath coordinate as solvent dielectric fluctuations influencing on the ET processes in solution. Then, we evaluate in detail the nonadiabatic ET rates for different temperature regimes in Subsec. 2.4.3. Finally, I will relate, in Subsec. 2.4.4, the spectral density for the ET rates to dielectric properties of the solvent.

2.4.1 The system-bath model of dielectric solvation

We consider a quantum two-state system, representing the donor and acceptor state, which couples linearly to the solvent, modeled as collection of harmonic oscillators (cf. Sec. 2.1),

$$\begin{aligned}H =& \left[E_A + \sum_\alpha g_A^\alpha \mathbf{x}_\alpha\right] |A\rangle\langle A| + \left[E_D + \sum_\alpha g_D^\alpha \mathbf{x}_\alpha\right] |D\rangle\langle D| + V_{DA}|D\rangle\langle A| + V_{AD}|A\rangle\langle D| \\ &+ \sum_\alpha \left[\frac{\mathbf{p}_\alpha^2}{2m_\alpha} + \frac{1}{2}m_\alpha\omega_\alpha^2\mathbf{x}_\alpha^2\right],\end{aligned} \tag{2.42}$$

where $g_N^\alpha = V_N^\alpha\sqrt{2m_\alpha\omega_\alpha/\hbar}$ is the strength of coupling between the donor ($N = D$) and acceptor ($N = A$) and the individual harmonic oscillators of the bath. The coupling is diagonal in the local donor- and acceptor- state, such that the bath induces fluctuations in the local state energies E_A and E_D. $|A\rangle$ and $|D\rangle$ describe the donor and acceptor states respectively. One neglects the off-diagonal bath coupling to the interstate transition from donor to acceptor state and vice versa. $\mathbf{p}_\alpha$, $\mathbf{x}_\alpha$, m_α, ω_α describe the momentum operator, the position operator, the mass and frequency of the harmonic bath mode, respectively. We use the *Condon approximation* that neglects any dependence of V_{DA} or V_{AD} on the momentum or position of the harmonic bath modes because we are interested in the onsite vibrational dynamics. Next, we use the unitary polaron transformation of the Hamiltonian with $\mathbf{U} = \Pi_{N=A,D}\exp\left[i\hbar|N\rangle\langle N|\Omega_N\right]$, where $\Omega_N = \sum_\alpha \Omega_N^\alpha$ and $\Omega_N^\alpha = \frac{g_N^\alpha \mathbf{p}_\alpha}{\hbar m_\alpha \omega_\alpha^2}$. The donor and acceptor states are orthogonal, i.e., $\langle N|N'\rangle = \delta_{N,N'}$. The transformed Hamiltonian $\tilde{H} = \mathbf{U}^\dagger H \mathbf{U}$ reads

$$\begin{aligned}\tilde{H} =& \sum_{N=A,D}\left[E_N - \left[\sum_\alpha \frac{g_N^{\alpha\,2}}{2m_\alpha\omega_\alpha}\right]\right]|N\rangle\langle N| + \sum_{N'\neq N=A,D} V_{NN'}e^{-i(\Omega_N-\Omega'_N)}|N\rangle\langle N'| \\ &+ \sum_\alpha\left[\frac{\mathbf{p}_\alpha^2}{2m_\alpha} + \frac{1}{2}m_\alpha\omega_\alpha^2\mathbf{x}_\alpha^2\right].\end{aligned} \tag{2.43}$$

The first and the last term describe the uncoupled system and bath, while the donor and acceptor state energies are shifted due to the coupling to the bath. This means that for the present case, we do not use a counter term in the model in comparison to the model introduced in Sec. 2.1. The interstate coupling is transformed to $V_{NN'}|N\rangle\langle N'| \rightarrow V_{NN'}e^{-i(\Omega_N-\Omega'_N)}|N\rangle\langle N'|$. To see its significance, one writes the eigenstates of the system and bath as $|N,\mathbf{v}\rangle = |N\rangle\varphi_\mathbf{v}\{\mathbf{x}_\alpha\}$, where the elements v_α of the vector $\mathbf{v}$ denote the state of the different modes α. $\varphi_\mathbf{v}\{\mathbf{x}_\alpha\} = \Pi_\alpha\varphi_{v_\alpha}\{\mathbf{x}_\alpha\}$ are the set of eigenstates of the bath Hamiltonian. The coupling between two vibronic state $|N,\mathbf{v}\rangle$ and $|N',\mathbf{v}'\rangle$ is given by the bare interstate coupling $V_{NN'}$ with am additional renormalization term

$$\begin{aligned}\varphi_{\mathbf{v}}(\{\mathbf{x}_\alpha\})V_{NN'}e^{-i(\Omega_N-\Omega'_N)}\varphi'_{\mathbf{v}}(\{\mathbf{x}_\alpha\}) &= V_{NN'}\Pi_\alpha\varphi_{v_\alpha}\{\mathbf{x}_\alpha\}e^{-\lambda_\alpha^{N,N'}(\partial/\partial\mathbf{x}_\alpha)}\varphi_{v'_\alpha}\{\mathbf{x}_\alpha\} \\ &= V_{NN'}\Pi_\alpha\varphi_{v_\alpha}\{\mathbf{x}_\alpha\}\varphi_{v'_\alpha}\{\mathbf{x}_\alpha-\lambda_\alpha^{N,N'}\},\end{aligned} \tag{2.44}$$

where $\lambda_\alpha^{N,N'} = (g_N^\alpha - g_{N'}^\alpha)/(\hbar m_\alpha \omega_\alpha^2)$. The absolute square of the term in Eq. (2.44) is known as *Franck-Condon factor*. Here, we have introduced the eigenstates of the total Hamiltonian (Eq. (2.42)) by a product of the eigenstates of the system and the bath. This product ansatz may be a good description if one further investigates the system and bath contributions, especially the resulting dynamics of their degrees of freedom. Once noticeably different time scales for the system of interest and of the solvent bath are identified, the eigenfunctions separate.

The most prominent example in this context is the *Born-Oppenheimer approximation*, where one splits a molecular system dynamics in their fast electronic and de facto static nuclear contributions. The main reasoning here is the huge mass difference between electron and nuclei which results in different time scale for the underlying motions. The nuclei are about 2000 times heavier than electrons, which results in a much faster dynamics of the electrons [66]. In Subsec. 2.2.2, we have used the same argument to split the polarization in a fast, electronic, and slow, nuclear part. In the Born-Oppenheimer picture the molecular states have the form $\Phi_n(\mathbf{r},\mathbf{R})\varphi_{n,\mathbf{v}}(\mathbf{R})$ where $\mathbf{r}$ and $\mathbf{R}$ denote the fast electronic and slow nuclear positions, respectively. $\Phi_n(\mathbf{r},\mathbf{R})$ are the eigenfunctions of the electronic states with eigenvalue $E_{el}^{(n)}(\mathbf{R})$ which depend parametrically on the fixed nuclear position $\mathbf{R}$ due to the slow nuclear motion relative to the electronic motion. $\varphi_{n,\mathbf{v}}(\mathbf{R})$ are the nuclear wavefunctions associated with the given n-th electronic state within the calculated static potential surface $E_{el}^{(n)}(\mathbf{R})$, which is formed by electronic eigenenergies. Often, a good approximation is to expand the nuclear potential surfaces $E_{el}^{(n)}(\mathbf{R})$ up to quadratic order in a Taylor expansion about the solvent configuration of the minimal energy $E_{el,eq}^{(n)}$. The nuclear normal mode coordinates $\mathbf{x}^{(n)} \equiv \{x_\alpha^{(n)}\}$ and the corresponding frequencies $\{\omega_\alpha^{(n)}\}$ result from the nuclear eigenvectors and corresponding eigenfunctions of the Hessian matrices of the n-th surface, $H_{\alpha,\alpha'}^{(n)} = (\partial^2 E_{el}^{(n)}(\mathbf{R})/\partial\mathbf{R}_\alpha\partial\mathbf{R}_{\alpha'})_{eq}$ [31]. The resulting potential surfaces in this harmonic approximation are

$$E_{el}^{(n)}(\mathbf{R}) = E_n + \frac{1}{2}\sum_\alpha m_\alpha \omega_\alpha^{(n)2} x_\alpha^{(n)2}, \tag{2.45}$$

where $E_n = E_{el,eq}^{(n)}$. If the vibrational energies are independent of the actual electronic state, we have that $\{\omega_\alpha^{(n)}\} = \{\omega_\alpha\}$ which one also assumes in the Hamiltonian of (2.42). Then, the harmonic potential surfaces of the n-th electronic state are shifted with respect to each other according to Eq. (2.43) and we have

$$E_{el}^{(n)}(\mathbf{R}) = E_n + \frac{1}{2}\sum_\alpha m_\alpha \omega_\alpha^2 (x_\alpha - \lambda_\alpha^{(n)})^2 \tag{2.46}$$

$$= E_n + \sum_\alpha \hbar\omega_\alpha (\bar{x}_\alpha - \bar{\lambda}_\alpha^{(n)})^2, \tag{2.47}$$

where we have used the dimensionless coordinates $\bar{x}_\alpha \equiv x_\alpha\sqrt{m_\alpha\omega_\alpha/2\hbar}$ and shifts $\bar{\lambda}_\alpha^{(n)} \equiv \lambda_\alpha^{(n)}\sqrt{m_\alpha\omega_\alpha/2\hbar}$ in Eq. (2.47). Experimental evidence for identical normal-mode coordinates for different electronic state is given in molecular spectroscopy, especially for low-lying electronic states [31].

We now reconsider the two distinct donor and acceptor electronic states introduced in the Hamiltonian of Eq. (2.43) and identify the nuclear modes of the introduced Born-Oppenheimer picture with the solvent modes. Fig. 2.1 represents a schematic view of the potential surfaces involved for the transition from the donor D to the acceptor A while each state couples to the same harmonic normal modes ω_α of the solvent. The normal mode shift $\bar{\lambda}_\alpha^A \equiv \bar{\lambda}_\alpha$ express the deviation of the equilibrium position of the acceptor state, while one sets $\bar{\lambda}_\alpha^D = 0$ for the donor state. We identify their (shifted) equilibrium energies $E_D \equiv \left[E_D - \left[\sum_\alpha \frac{{g_D^\alpha}^2}{2m_\alpha\omega_\alpha}\right]\right]$ and E_A, respectively. $E_R^\alpha = \hbar\omega_\alpha\bar{\lambda}_\alpha^2$ is the single mode reorganization energy, while $E_R = \sum_\alpha E_R^\alpha$ is the total reorganization energy after a vertical transition from the donor to the energy minimum of the acceptor state has occurred. We will discuss the reorganization energy in Subsec. 2.4.3 in greater detail.

A vertical transition between the two potential surfaces may occur in a photoinduced transition where the needed energy is carried by the absorbed photon. For ET processes in solution at high-temperature when photon is involved, the only available energy is thermal. Marcus [43, 31] observed that in this case, the transition between two electronic states is only possible if these two states are energetically equal and degenerate due to a specific solvent configuration respectively. The solvent coordinates x_α therefore determine the transition state for the ET process, while the dynamics of these coordinates determines the ET rate (see Subsec. 2.4.3 for nonadiabatic ET and Chapter 4 for nonequilibrium solvent dynamics). In the low-temperature limit, nuclear solvent tunneling between the

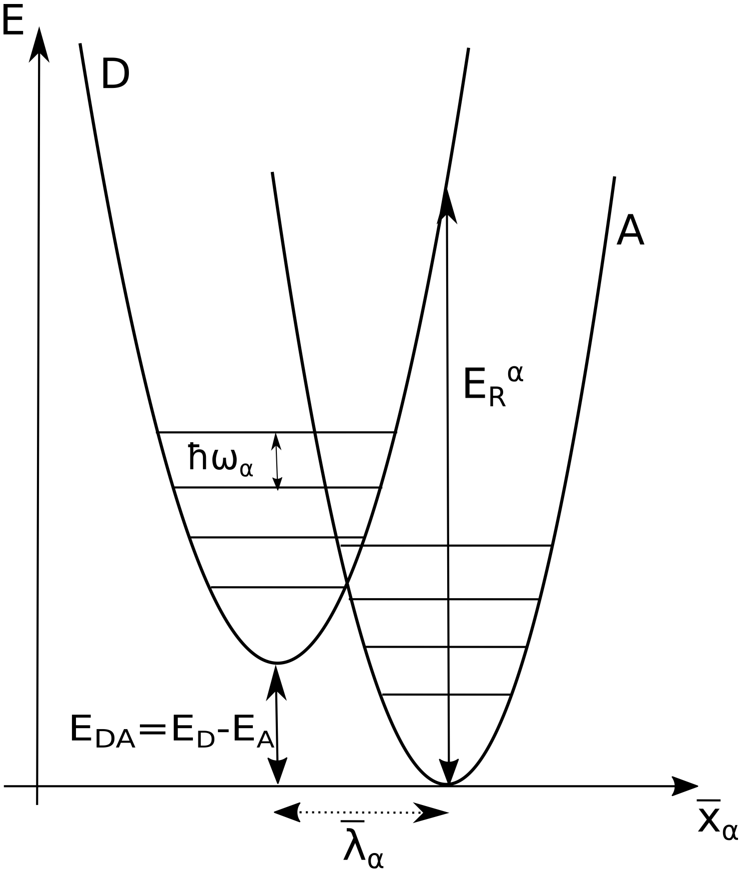

Figure 2.1: Schematic view of the shifted potential surfaces for the donor (D) and acceptor (A) state for a single mode ω_α.

two surfaces is the dominant process that accompanies the ET. Then, the solvent nuclear wavefunctions are localized in wells which are relatively far from each other and, hence, their mutual overlap is small [31].

In the following subsection, we will associate a physical meaning to the solvent coordinates x_α for high-temperature by using the notion of a fluctuating polarization within a continuous dielectric solvent.

2.4.2 Continuum dielectric theory for ET in solution

An ET process is a change of the electronic charge distribution in the molecular system. The polarization of the surrounding solvent molecules due to this charge rearrangement, which implies a change of the electric field, can be described in a continuum approach by the relation $\mathbf{P} = \chi\mathbf{E}$ of Eq. (2.23), where $\chi = (\epsilon - 1)/4\pi$ results from Eq. (2.25) and the displacement field $\mathbf{D} = \epsilon\mathbf{E}$. According to the discussion in Subsec. 2.2.2 the polarization can be split into a fast, electronic, and a slow, nuclear (solvent) part $\mathbf{P} = \mathbf{P}_e + \mathbf{P}_n$. The electronic part may be related to $\mathbf{P}_{el} = (\epsilon_e - 1)\mathbf{E}/4\pi$ and the nuclear part to $\mathbf{P}_n = (\epsilon - \epsilon_e)\mathbf{E}/4\pi$. Following the Marcus theory, the energy of the electronic states immediately before and after the ET are equal, while the solvent molecules can not adjust instantaneously [43, 31]. Thus, an ET occurs if a solvent fluctuation matches a configuration where the donor and acceptor state are energetically equivalent. The fluctuation acts before the ET takes place at a given fix charge distribution.

Based on this picture, we study in the following the changes in the solvent configuration, where we are especially interested in $\mathbf{P}_n$, i.e., the slow fluctuations due to thermal motion of the solvent nuclei. We consider the ET transfer from the donor to the acceptor state where ρ_D and ρ_A are the molecular charge distributions associated with these two states. Starting in the donor state, we first determine the fluctuations in the nuclear solvent polarization $\mathbf{P}_n$ associated to charge configuration ρ_D. A charge fluctuation is generated by a fictitious charge distribution $\rho_\Theta = \rho_D + (\rho_A - \rho_D)\Theta$ where the fluctuation is recorded with $0 \leq \Theta \leq 1$. In turn, ρ_Θ induces a nuclear polarization $\mathbf{P}_{n\Theta}$ in equilibrium with this fictitious charge distribution. Thus, in the donor state, where $\rho = \rho_D$, $\mathbf{P}_{n\Theta}$ defines a fluctuation departing from equilibrium and being characterized by the parameters ρ_A and Θ [31]. For illustration, let us consider an ideal conducting sphere as test molecule with radius a and varying charge $q_D \rightarrow q_\Theta$ embedded in a continuous and homogeneous dielectric solvent [43, 31]. We calculate the free energy difference ΔG, in being the reversible work at constant temperature and pressure, where the charge on the sphere remains q_D but the nuclear polarization of the solvent is $\mathbf{P}_{n\Theta}$. The latter is the same as in the equilibrium state with the charge q_Θ on the sphere. In the first step, we calculate the difference $\Delta G_{\Theta\rightarrow D'}$ in free energy for a charge transfer $q_\Theta \rightarrow q_D$ while the polarization remains at the value for the charge q_Θ. The state D' represents a charge q_D on the sphere with the fixed polarization $\mathbf{P}_{n\Theta}$ of the state and the charge q_Θ. D' is hence a nonequilibrium state in view of the nuclear degrees of freedom. The electrostatic potential on the surface of the sphere can be written as a vacuum term and a term from the solvent polarization in the form

$$\Phi_\Theta = \frac{q_\Theta}{\epsilon a} = \frac{q_\Theta}{a} + \left[\frac{1}{\epsilon} - 1\right]\frac{q_\Theta}{a}. \tag{2.48}$$

Under the condition that the nuclear polarization $\mathbf{P}_{n\Theta}$ remains fixed, the addition of a small amount of charge ξ leads to the modified potential

$$\Phi(\xi) = \frac{q_\Theta}{\epsilon a} + \frac{\xi}{\epsilon_e a}, \tag{2.49}$$

where only the electronic polarization responds quickly. The first term of the potential in Eq. (2.49) stems from the fixed polarization induced by the charge q_Θ while the second term in Eq. (2.49) results from the electronic polarization during the charging. The charging process proceeds until $\xi = q_D - q_\Theta$. The reversible work from this charging process is $\Delta G_{\Theta \to D'} = \int d\xi \Phi(\xi)$ from $\xi = 0$ to $\xi = q_D - q_\Theta$. The free energy with the substitution $q_\Theta = q_D + (q_A - q_D)\Theta$ leads to

$$\Delta G_{\Theta \to D'} = \int_0^{q_D - q_\Theta} d\xi \Phi(\xi) = \frac{q_D(q_D - q_A)}{\epsilon a}\Theta + \frac{(q_A - q_D)^2}{a}\left[\frac{1}{2\epsilon_e} - \frac{1}{\epsilon}\right]\Theta^2. \tag{2.50}$$

Next, we determine the free energy $\Delta G_{\Theta \to D}$ where the nuclear polarization reacts to the given charge of the sphere. The corresponding free energy thus reads with $q_\Theta = \rho_D + (q_A - q_D)\Theta$

$$\Delta G_{\Theta \to D} = \int_{q_\Theta}^{q_D} dq' \Phi(q') = \int_{q_\Theta}^{q_D} dq' \frac{q'}{\epsilon a} = \frac{q_D(q_D - q_A)}{\epsilon a}\Theta - \frac{(q_D - q_A)^2}{2\epsilon a}\Theta^2. \tag{2.51}$$

The potential surface for the fluctuations of the nuclear polarization of the solvent about the equilibrium donor state with the charge q_D on the sphere results out of the difference $\Delta G_{D \to D'} = \Delta G_{\Theta \to D'} - \Delta G_{\Theta \to D}$ as

$$\Delta G_{D \to D'} = \frac{(q_D - q_A)^2}{2a}\left[\frac{1}{\epsilon_e} - \frac{1}{\epsilon}\right]\Theta^2. \tag{2.52}$$

The theory of linear response of the dielectric continuum yields a harmonic potential surface quadratic in the charge fluctuation Θ which may be associated with a solvent reaction coordinate for the ET from the donor to the acceptor. The potential surface in Eq. (2.52) represents the thermal fluctuation of the solvent nuclei inducing a polarization field $\mathbf{P}_{n\Theta}$ while the charge on the molecule remains q_D. The resulting curvature of the harmonic surface may be directly connected to physical parameters: the dielectric constants ϵ_e and ϵ, the initial (q_D) and final (q_A) charge as well as a geometry factor, the radius a of the test sphere. The result of Eq. (2.52) can be directly compared to the potential energy surface given in Eq. (2.47) which originated in a two-state model coupled to a bath of harmonic oscillators. Once we have identified a prominent bath mode to which the donor and acceptor states couple, the introduced frequency ω_α of the harmonic bath modes gets a physical meaning via Eq. (2.52). Moreover, the displacement $\bar{x}_\alpha$ in Eq. (2.47) or Θ in Eq. (2.52) may be then understood as a reaction coordinate which determines the ET rate. The resulting energy surfaces for both processes consequently are

$$E_D(\Theta) = E_D + \frac{(q_D - q_A)^2}{2a}\left[\frac{1}{\epsilon_e} - \frac{1}{\epsilon}\right]\Theta^2, \tag{2.53}$$

$$E_A(\Theta) = E_A + \frac{(q_D - q_A)^2}{2a}\left[\frac{1}{\epsilon_e} - \frac{1}{\epsilon}\right][1-\Theta]^2, \tag{2.54}$$

where E_D and E_A are the energies for the donor and acceptor equilibrium state, respectively, when the nuclear polarization $\mathbf{P}_{n\Theta}$ is in equilibrium with the states $n = D$ or $n = A$.

2.4.3 Rate for the nonadiabatic electron transfer

One of the crucial parameter for ET is the interstate coupling V_{AD} between the donor and acceptor state given in Eq. (2.43). This quantity is directly associated with the time scale $t_{el} = \hbar/|V_{AD}|$ for electronic transition on which the electronic wave function moves from the donor and acceptor site. The donor-acceptor system is coupled to different harmonic modes ω_α of the solvent bath. They can be characterized by a mean frequency ω_{vib} to determine the time scale $t_{vib} = 2\pi/\omega_{vib}$ for the change of configuration of the solvent nuclei if we assume that the motion is not overdamped [58].

For the case $t_{vib} \gg t_{el}$, the electron will move many times between the donor and acceptor before any relevant change in the solvent nuclear configuration occurs. Therefore, the electronic wave function is delocolized over the whole donor-acceptor system and the electron in an *adiabatic* state. This situation may be compared to the introduced (adiabatic) Born-Oppenheimer approximation where one separates the time scales for the nuclear and electronic motion (see Subsec. 2.4.1). This situation is referred to an adiabatic ET.

The opposite situation is encountered for $t_{vib} \ll t_{el}$. Here, the solvent vibrational motion is much faster than the electronic motion on the molecule. This type of operation is called *nonadiabatic* ET. The donor and acceptor states are spatially localized and the reaction coordinate describing the motion within the solvent evolves very rapidly. So, the electronic wave function does not have enough time to move completely from the donor to the acceptor, such that only a small fraction of the electronic probability amplitude reaches the donor site [7]. Since the coupling V_{DA} is small in this case, one can describe the ET by a perturbation expansion with respect to V_{DA}. In the lowest order of perturbation theory one can use *Fermi's golden rule* to describe the ET rate which is valid at any temperature [58]. We focus on the nonadiabatic ET because the bridge-mediated ET over large distances usually proceeds in this limit such as the problem of the nonadiabatic ET through a molecule coupled between a source and a drain electrode in non-equilibrated solution studied in Chapter 4.

To this end, we proceed with the thermally averaged rate for the ET between the donor and acceptor $D \to A$. Since the relaxation in the bath is fast relative on the time scale of the ET, we can assume the bath being in thermal equilibrium state during the whole process. Thus, the overall donor state and the acceptor state can be written as product states in the form $|N, \mathbf{v}\rangle = |N\rangle \Pi_\alpha |v_\alpha\rangle$. The ET rate follows from Fermi's golden rule [58, 31] as

$$k_{DA} = \frac{2\pi}{\hbar} \sum_{\mathbf{v}} P_{\mathbf{v}} \sum_{\mathbf{v}'} |\langle \mathbf{v}|\hat{V}_{DA}|\mathbf{v}'\rangle|^2 \delta(E_D - E_A + E(\mathbf{v}) - E(\mathbf{v}')), \tag{2.55}$$

where $P_{\mathbf{v}} = Z^{-1} \exp[-H_B/k_B T]$ is the statistical operator [8]. The interstate coupling term of Eq. (2.43) reads, after using the product ansatz for the donor and acceptor states, $\hat{V}_{DA} = V_{DA} e^{\sum_\alpha \bar{\lambda}_\alpha^{D,A} (\hat{a}_\alpha^\dagger - \hat{a}_\alpha)}$, where we use the formulation in terms of creation and annihilation operators for $\bar{\mathbf{p}}_\alpha$ and dimensionless coordinates. After using the identity $\delta(x) = (2\pi\hbar)^{-1} \int dt e^{ixt/\hbar}$ and the Bloch theorem, $\langle e^{c(\hat{a}^\dagger + \hat{a})} \rangle_T = e^{\langle [c(\hat{a}^\dagger + \hat{a})]^2 \rangle_T}$ [31], for thermal averaging, Eq. (2.55) reads

$$\begin{aligned} k_{DA} &= \frac{1}{\hbar^2} \int_{-\infty}^{\infty} dt e^{i\omega_{DA} t} \sum_{\mathbf{v}} P_{\mathbf{v}} \langle \mathbf{v}| e^{iH_B t/\hbar} \hat{V}_{DA} e^{-iH_B t/\hbar} \sum_{\mathbf{v}'} |\mathbf{v}'\rangle \langle \mathbf{v}'| \hat{V}_{AD} |\mathbf{v}\rangle \\ &= \frac{|V_{DA}|^2}{\hbar^2} e^{-\sum_\alpha \bar{\lambda}_\alpha^{(D,A)2} [2n(\omega_\alpha)+1]} \int_{-\infty}^{\infty} dt e^{i\omega_{DA} t + \sum_\alpha \bar{\lambda}_\alpha^{(D,A)2} \{n(\omega_\alpha) e^{i\omega_\alpha t} + [n(\omega_\alpha)+1] e^{-i\omega_\alpha t}\}} \\ &= \frac{|V_{DA}|^2}{\hbar^2} e^{-\int_0^\infty d\omega J_{DA}(\omega)[2n(\omega)+1]} \int_{-\infty}^{\infty} dt e^{i\omega_{DA} t + \int_0^\infty d\omega J_{DA}(\omega) \{n(\omega) e^{i\omega t} + [n(\omega)+1] e^{-i\omega t}\}}, \end{aligned} \tag{2.56}$$

---

[7] One uses the term 'electronic probability density' in order to determine the transition quantum mechanically. It is meaningless to follow the velocity of the electron itself within the ET process without any measurement[58].

[8] The state $\mathbf{v}$ are described by $H_B = \sum_\alpha \left[\frac{\mathbf{p}_\alpha^2}{2m_\alpha} + \frac{1}{2} m_\alpha \omega_\alpha^2 \mathbf{x}_\alpha^2 \right]$ and Z is the partition function.

where $\hbar\omega_{DA} = E_{DA} = E_D - E_A$ and $n(\omega) = (e^{\beta\hbar\omega} - 1)^{-1}$ is the thermal boson occupation number. We further exploit the unitary operator relation $\mathbb{I} = \sum_{\mathbf{v}'} |\mathbf{v}'\rangle \langle\mathbf{v}'|$ in Eq. (2.56). In the last equality of Eq. (2.56), we have introduced the spectral density $J_{DA}(\omega) = \sum_\alpha \bar{\lambda}_\alpha^{(D,A)2}\delta(\omega - \omega_\alpha)$, since we assume that the number of the different vibrational solvent modes becomes large.

This form of ET rate reminds one of the fact that the spectral density is interpreted as the density of bath oscillators weighted by its specific coupling constant to the subsystem of interest (cf. Sec. 2.1). We further introduce $G(t) = \int_0^\infty d\omega J_{DA}(\omega)\cos[\omega t][1 + 2n(\omega)] - i\int_0^\infty d\omega J_{DA}(\omega)\sin[\omega t]$ [9] such that the ET rate in Eq. (2.56) reads

$$k_{DA} = \frac{|V_{DA}|^2}{\hbar^2} e^{-G(0)} \int_{-\infty}^{\infty} dt e^{i\omega_{DA}t + G(t)}. \tag{2.57}$$

We next derive the high-temperature limit for the ET rate of Eq. (2.57). To this end, we require that the spectral density goes to zero beyond a certain cutoff frequency ω_c (see Eq. (2.16)). For $\omega_c|t| \ll \pi/2$, $\exp[G(t) - G(0)]$ rapidly approaches zero since the real part of the exponent $\cos[\omega t] - 1$ is negative. For $\omega_c|t| \gg \pi/2$ the different frequency contributions to the time integral may interfere destructively, since the number of the different vibrational solvent modes is large. In the high-temperature limit $k_B T \gg \hbar\omega_c$, we may introduce the approximation $1 + 2n(\omega) \approx 2k_B T/\hbar\omega \gg 1$ for all frequencies less the ω_c. One may approximate then by $G(t) \approx -\int_0^\infty d\omega(\omega t)^2 \frac{k_B T}{\hbar\omega} J_{DA}(\omega) - i\int_0^\infty d\omega(\omega t) J_{DA}(\omega)$ in the exponent by the leading order terms of sine and cosine which is known as the short-time expansion. Hence, the ET rate of Eq. (2.57) in the high-temperature limit follows as

$$k_{DA} = \frac{|V_{DA}|^2}{\hbar^2} \int_{-\infty}^{\infty} dt \exp\left\{ i\frac{(E_{DA} - \hbar\int_0^\infty d\omega J_{DA}(\omega)\omega)t}{\hbar} \right\} \exp\left\{ -\frac{\int_0^\infty d\omega J_{DA}(\omega)\omega k_B T t^2}{\hbar} \right\}. \tag{2.58}$$

Finally, we define the reorganization energy

$$\hbar\int_0^\infty d\omega J_{DA}(\omega)\omega = E_R \tag{2.59}$$

---

[9] The spectral density $J_{DA}(\omega)$ introduced here has a different dimension than $J(\omega)$ introduced in Eq. (2.13). They are related via $J_{DA}(\omega)\omega^2 = J(\omega)$, which follows the different conventions in the different scientific communities.

and perform the Gaussian time integral in Eq. (2.58). The ET rates becomes then

$$k_{DA} = \frac{2\pi}{\hbar}|V_{DA}|^2 \frac{1}{\sqrt{4\pi k_B T E_R}} \exp\left\{-\frac{(E_{DA}-E_R)^2}{4E_R k_B T}\right\}. \tag{2.60}$$

This celebrated expression that follows upon introducing E_R is the Marcus rate of ET, named after R. A. Marcus [43, 58] who received the Nobel prize for this concept in 1992. We may compare the Marcus rate of Eq. (2.60) with the *Arrhenius* type ET rate given by $k_{DA} \propto \exp\{-E_{act}/k_B T\}$ for chemical reactions. By this we may identify the activation energy $E_{act} = (E_{DA}-E_R)^2/(4E_R)$ [67, 68], which is the energy needed to cross the potential energy barrier separating the donor and acceptor state in their equilibrium.

The difference $E_{DA} - E_R$ in the expression for the activation energy may be understood with the following consideration. Initially, the electron is at the donor site and then suddenly reaches the acceptor. This transfer is accompanied by a change in the electronic charge density, where the solvent has to readjust. In order to reorganize the surrounding molecules, the energy E_R has to be removed from the available system energy which is given by the transition energy E_{DA}. Therefore, the energy E_R is called *reorganization energy* or *polarization energy*. It was formally introduced in Eq. (2.47) in Subsec. 2.4.1 for the system coupled to a bath of harmonic oscillators. A major advance of the reorganization energy is that it reduces all solvent degrees of freedom to a single number because it is the integral over all bath modes.

One can further easily derive the rate for the back transfer from the acceptor to the donor k_{AD} in the used model of identical parabolic potentials of the donor and acceptor states (Eq. (2.43)). One only has to change the sign of $E_{DA} \to -E_{DA} \equiv E_{AD}$. One obtains

$$k_{AD} = k_{DA}(-E_{DA}) = e^{-E_{DA}/k_B T} k_{DA}(E_{DA}), \tag{2.61}$$

where the ratio of the forward and backward rate fulfills the detailed balance condition $\exp\{-E_{DA}/k_B T\}$, a clear signature for processes at thermal equilibrium.

2.4.4 Spectral density for the fluctuations in polar solvents

Now, we are ready to derive the spectral density $J(\omega)$ entering in the ET rate of Eq. (2.60) for an ET process in polar solvents by using a macroscopic dielectric description. To this end, we introduce a free energy functional $F_P[\mathbf{P}_{fast}, \mathbf{P}_{slow}, \mathbf{D}]$ which depends on the fast and slow solvent polarization (cf. Subsec. 2.2.2) as well as on the displacement field $\mathbf{D}$

produced by the charge distribution of donor and acceptor state.

Again, we may separate the ET process into different time scales. k_{DA}^{-1} describes the time scale for an ET process between the donor and acceptor, τ_n and τ_e characterize the nuclear and electronic polarization relaxation, respectively. This enables us to introduce a reduced free energy that only depends on the fluctuating properties of the slow orientational nuclear solvent polarization. The fast electronic polarization is described by its equilibrium values due to its quasi-instantaneous adaptation to the actual state. One further assumes that the electron is either at the donor or the acceptor. Any intermediate sates are neglected. Hence, we obtain two diabatic reduced free energy expressions for the donor ($n = D$) and the acceptor ($n = A$) state, respectively, as

$$F_n[\tilde{\mathbf{P}}, \mathbf{D}_n] = E_n - \frac{1}{2c_{el}} \int d^3\mathbf{x}\mathbf{D}_n^2(\mathbf{x}) + \frac{2\pi}{c_p} \int d^3\mathbf{x}\tilde{\mathbf{P}}^2(\mathbf{x}, t) - \int d^3\mathbf{x}\mathbf{D}_n(\mathbf{x})\tilde{\mathbf{P}}(\mathbf{x}, t), \tag{2.62}$$

where $\mathbf{D}_n$ is fixed for the electronic degree of freedom at the donor or acceptor, $\tilde{\mathbf{P}} = \mathbf{P}_{slow}/\epsilon_\infty$, the Pekar factor c_p (cf. Subsec. 2.2.2), and $c_{el} = 4\pi(1 - \epsilon_\infty^{-1})^{-1}$ [10]. The electronic levels E_n get renormalized with the *Born solvation energy*, which is the second term of Eq. (2.62) and which reflects the fact to have the charges at the donor or acceptor in a polar solvent. This gives rise to a displacement field in which the fast dielectric electronic part of solvent enters. The third term is the energy of the freely fluctuating orientational polarization, while the last term is the energy due to the coupling of the solvent polarization and the electric displacement field. The diabatic potential surfaces of the donor-acceptor complex, as introduced in Eq. (2.52) for the system-bath model, can be directly deduced from Eq. (2.62). To this end, we identify $F_n[\tilde{\mathbf{P}}, \mathbf{D}_n]$ with the potential energy surface $U_n[\tilde{\mathbf{P}}]$. This identification is valid since the free energy functional depends on a quasistatic field without any kinetic energy contribution [58]. The equilibrium polarization of $U_n[\tilde{\mathbf{P}}_m^{(eq)}]$ is obtained from the condition $\partial U_m/\partial\tilde{\mathbf{P}} = 0$ and is given by $\tilde{\mathbf{P}}_m^{(eq)} = (4\pi)^{-1}c_p\mathbf{D}_m$.

The total free energy at equilibrium polarization then reads $U_m[\tilde{\mathbf{P}}_m^{(eq)}] = E_m - (8\pi)^{-1}(1 - \epsilon_s^{-1}) \int d^3\mathbf{x}\mathbf{D}_m^2(\mathbf{x})$ which describes the solvent in total equilibrium, including its fast electronic as well as its slow orientational contributions, to the given charge state. We are now able to compute the reorganization energy as energy difference between the product state (electron at the acceptor), but with the equilibrium polarization of the donor state and

---

[10] The derivation of the reduced functional is described in the textbook of May and Kühn [58].

the equilibrium free energy for the acceptor state. The reorganization energy thus reads

$$E_R = U_A[\tilde{\mathbf{P}}_D^{(eq)}] - U_A[\tilde{\mathbf{P}}_A^{(eq)}] = \frac{c_p}{8\pi}\int d\mathbf{x}^3[\mathbf{D}_A(\mathbf{x}) - \mathbf{D}_D(\mathbf{x})]^2. \tag{2.63}$$

We then rewrite the transfer rate of Eq. (2.57) and eventually express it in terms of the dielectric function of the polar solvent. To this end, we retrace the rate equation (2.56) and write it as

$$k_{DA} = \frac{|V_{DA}|^2}{\hbar^2}\int dt e^{i\Delta E t/\hbar}\,\mathrm{tr}\left\{\boldsymbol{\rho}_{eq}^D S_{AD}(t,0)\right\}. \tag{2.64}$$

Here, $\boldsymbol{\rho}_{eq}^D$ is the statistical operator of the solvent in thermal equilibrium with the donor state. Furthermore, the operator $S_{AD}(t,0)$ is specified below. One identifies the difference Hamiltonian $H_A - H_D$ with the difference of the free energy of Eq. (2.62) between the acceptor and donor state such that ΔE in Eq. (2.57) is the operator-free part of $H_A - H_D$. In principle one has to define a proper expression for the kinetic energy of the polarization field to obtain a Hamiltonian. However, the kinetic energy contribution cancels in $H_A - H_D$. Further, one has to quantize the polarization field $\tilde{\mathbf{P}} \to \hat{\mathbf{P}}$. Since $\hat{\mathbf{P}}$ will eventually be used to define a quantum statistical correlation function associated to the dielectric function, we omit further discussion on the details of the quantization [58, 69, 70, 71, 72].

Overall, the difference Hamiltonian thus reads

$$H_A - H_D = -\Delta E - \int d^3\mathbf{x}\Delta\mathbf{D}_{AD}(\mathbf{x})\hat{\mathbf{P}}(\mathbf{x}), \tag{2.65}$$

where $\Delta\mathbf{D}_{AD}(\mathbf{x}) = \mathbf{D}_A - \mathbf{D}_D$ and $\Delta E = E_D - E_A - \frac{1}{2c_{el}}\int d^3\mathbf{x}\big[\mathbf{D}_D^2(\mathbf{x}) - \mathbf{D}_A^2(\mathbf{x})\big]$. This includes the renormalization of the state energies by the Born solvation energy. Furthermore, we have $S_{AD}(t,0) = \hat{T}\exp\Big\{-\frac{i}{\hbar}\int_0^t dt'\Delta H_{AD}^{(D)}(t')\Big\}$, with $\Delta H_{AD}^{(D)}(t) = U_D^\dagger(t)[H_A - H_D + \Delta E]U_D(t) = -\int d\mathbf{x}^3\Delta\mathbf{D}_{AD}(\mathbf{x})\hat{\mathbf{P}}^{(D)}(\mathbf{x},t)$, the time ordering operator $\hat{T}$ and $U_D(t) = \exp\big\{-\frac{i}{\hbar}H_D t\big\}$.

Next, we perform a second-order cumulant approximation of $\mathrm{tr}\left\{\boldsymbol{\rho}_{eq}^D S_{AD}(t,0)\right\} \equiv \langle S_{AD}(t,0)\rangle \approx \exp\{-\Gamma_1(t) - \Gamma_2(t)\}$, where $\Gamma_n(t)$ is of $n-$th order in $\Delta H_{AD}^{(D)}$. For $\Gamma_1(t)$

one obtains

$$\begin{aligned}\Gamma_1(t) &= \frac{i}{\hbar}\int_0^t dt_1 \langle \Delta H_{AD}^{(D)}(t_1)\rangle_D \qquad (2.66)\\ &= -\frac{i}{\hbar}\int_0^t dt_1 \int d^3\mathbf{x}\Delta\mathbf{D}_{AD}(\mathbf{x})\langle\hat{\mathbf{P}}(\mathbf{x},t_1)\rangle_D\\ &= -\frac{i}{\hbar}t\int d^3\mathbf{x}\Delta\mathbf{D}_{AD}(\mathbf{x})\tilde{\mathbf{P}}_D^{(eq)}(\mathbf{x})\\ &= -\frac{i}{\hbar}t\frac{c_p}{4\pi}\int d^3\mathbf{x}\Delta\mathbf{D}_{AD}(\mathbf{x})\mathbf{D}_D(\mathbf{x}),\end{aligned}$$

where the expectation value of the polarization operator can be replaced by the equilibrium polarization $\tilde{\mathbf{P}}_D^{(eq)}$ for the electron at the donor. The quantity $\Gamma_2(t)$ has the form

$$\Gamma_2(t) = \frac{1}{2}\Gamma_1^2(t) + \frac{1}{\hbar^2}\int_0^t dt_1\int_0^{t_1} dt_2 \int d^3\mathbf{x}_1 d^3\mathbf{x}_2 \Delta D_{AD}(\mathbf{x}_1)\langle\hat{\mathbf{P}}(\mathbf{x}_1,t_1)\hat{\mathbf{P}}(\mathbf{x}_2,t_2)\rangle_D\Delta D_{AD}(\mathbf{x}_2) \qquad (2.67)$$

$$\begin{aligned}&= \frac{1}{2}\Gamma_1^2(t) + \frac{1}{\hbar^2}\int_0^t dt_1\int_0^{t_1} dt_2 \int d^3\mathbf{x}_1 d^3\mathbf{x}_2\\ &\times \Delta D_{AD}(\mathbf{x}_1)\langle[\tilde{\mathbf{P}}_D^{(eq)}(\mathbf{x}_1) + \Delta\hat{\mathbf{P}}^{(D)}(\mathbf{x}_1,t_1)][\tilde{\mathbf{P}}_D^{(eq)}(\mathbf{x}_2) + \Delta\hat{\mathbf{P}}^{(D)}(\mathbf{x}_2,t_2)]\rangle_D\Delta D_{AD}(\mathbf{x}_2)\\ &= \frac{1}{\hbar^2}\int_0^t dt_1\int_0^{t_1} dt_2 \int d^3\mathbf{x}_1 d^3\mathbf{x}_2 \Delta D_{AD}(\mathbf{x}_1)\langle\Delta\hat{\mathbf{P}}^{(D)}(\mathbf{x}_1,t_1)\Delta\hat{\mathbf{P}}^{(D)}(\mathbf{x}_2,t_2)\rangle_D\Delta D_{AD}(\mathbf{x}_2).\end{aligned}$$

Here, we have split the polarization operator according to $\hat{\mathbf{P}}(\mathbf{x},t) = \tilde{\mathbf{P}}_D^{(eq)}(\mathbf{x}) + \Delta\hat{\mathbf{P}}(\mathbf{x},t)$ into its equilibrium value plus the deviation from this equilibrium polarization. The deviation $\Delta\hat{\mathbf{P}}(\mathbf{x},t)$ is related to a fluctuation and does not depend on the electronic charge at the donor. Therefore, this quantity can be related to the dielectric function. To this end, we further neglect spatial dispersion and anisotropy in the correlation function of the polarization fluctuations $C_P(\mathbf{x}_1,t_1;\mathbf{x}_2,t_2) = \langle\Delta\hat{\mathbf{P}}^{(D)}(\mathbf{x}_1,t_1)\Delta\hat{\mathbf{P}}^{(D)}(\mathbf{x}_2,t_2)\rangle_D \to \delta(\mathbf{x}_1-\mathbf{x}_2)C_p(t_1-t_2)$ to obtain a scalar, coordinate-independent and stationary correlation function in time, see Eq. (2.69) in Subsec. 2.2.1 for the polarizability tensor. Using the expression for the solvent reorganization energy in Eq. (2.63), one finds

$$\Gamma_2(t) = \frac{8\pi E_R}{\hbar^2 c_p}\int_0^t dt_1\int_0^{t_1} dt_2 C_P(t_1-t_2). \qquad (2.68)$$

The linear polarizability is connected to the polarization via $\alpha(t_1 - t_2) = -\frac{i}{\hbar}\Theta(t_1 -$

$t_2)\Big\langle \big[\Delta\hat{\mathbf{P}}^{(D)}(t_1), \Delta\hat{\mathbf{P}}^{(D)}(t_2)\big] \Big\rangle_D$, where [...] denotes the commutator. Therefore, we introduce the antisymmetrized correlation function $C_P^-(t) = C_p(t) - C_P^*(t)$ [11] to replace the commutator which leads to $\alpha(t_1 - t_2) = -\frac{i}{\hbar}\Theta(t_1 - t_2)C_P^-(t_1 - t_2)$. Performing a Fourier transform of the polarization results in[12]

$$\alpha(\omega) = \int \frac{d\omega'}{2\pi\hbar}\frac{C_P^-(\omega')}{\omega - \omega' + i\nu}, \nu > 0. \tag{2.69}$$

The equation (2.69) relates $\mathrm{Im}[\alpha(\omega)] = -C_P^-(\omega')/2\hbar$, while according to Eq. (2.25) in Subsec. 2.2.2, $\mathrm{Im}[\alpha(\omega)] = -\mathrm{Im}[\epsilon(\omega)^{-1}]/4\pi \equiv \mathrm{Im}[\epsilon(\omega)]/4\pi|\epsilon(\omega)|^2$. One finds [13]

$$C_P(t) = -\frac{\hbar}{4\pi^2}\int_0^\infty d\omega \Big\{ e^{-i\omega t}[1 + n(\omega)] + e^{i\omega t}n(\omega) \Big\} \frac{\mathrm{Im}[\epsilon(\omega)]}{|\epsilon(\omega)|^2}. \tag{2.70}$$

After carrying out the double time integration in Eq. (2.68) and Eq. (2.70) one obtains with the Bose-Einstein distribution $n(\omega)$

$$\Gamma_2(t) = \frac{2E_R}{\pi\hbar c_p}\int_0^\infty \frac{d\omega}{\omega^2}\frac{\mathrm{Im}[\epsilon(\omega)]}{|\epsilon(\omega)|^2}\Big\{ [e^{-i\omega t} - 1][1 + n(\omega)] + [e^{i\omega t} - 1]n(\omega) + i\omega t \Big\}. \tag{2.71}$$

If one compares this result with the function $G(t)$ in Eq. (2.57), we find the expression for the spectral density for the polar solvent

$$J(\omega) = -\frac{2E_R}{\pi\hbar c_p}\frac{1}{\omega^2}\frac{\mathrm{Im}[\epsilon(\omega)]}{|\epsilon(\omega)|^2}. \tag{2.72}$$

With the relation $E_R = \hbar\int_0^\infty d\omega\omega J(\omega)$, we have $\Gamma_2(t) = G(0) - G(t) - iE_R t/\hbar$. The final expression for the ET rate with the free energy difference according to Eq. (2.62) $\Delta F^{(eq)} = F_D^{(eq)}(\mathbf{D}_D) - F_A^{(eq)}(\mathbf{D}_A)$ reads

$$k_{DA} = \frac{1}{\hbar^2}|V_{DA}|^2 \int dt \exp\Big\{ \frac{i}{\hbar}\Delta F^{(eq)}t + G(t) - G(0) \Big\}. \tag{2.73}$$

We observe that the energy difference E_{DA} in the rate in Eq. (2.60) is shifted by the complete equilibrium Born solvation energy which includes fast electronic and slow orien-

---

[11] $C_p^*(t)$ denotes complex conjugate of $C_p(t)$.

[12] The heavy side function can be expressed by the Fourier integral $-\int \frac{d\omega}{2\pi i}\exp(-i\omega t)/(\omega + i\epsilon)$ and $C_P^-(\omega) \equiv \mathrm{Re}[C_p^-(\omega)]$.

[13] One uses the relation between the time-dependent correlation function and its Fourier-transformed antisymmetrized version $C_{uv}(t) = \int_0^\infty \frac{d\omega}{2\pi}[e^{-i\omega t}[1 + n(\omega)]C_{uv}^-(\omega) + e^{i\omega t}n(\omega)C_{vu}^-(\omega)]$ [58].

tational contributions. This reflects the influence of the polarity of the solvent surrounding an electron transfer reaction on the ET rate. The solvent fluctuations enter in $G(t)$ via a frequency dependent spectral density which is proportional to the imaginary part of the dielectric function.

The assumption of an ET rate being much smaller than the rate of the orientational polarization, $k_{DA} \ll \tau_n^{-1}$, enables us to find the free energy expression and a spectral density, $J(\omega) \propto \mathrm{Im}[\epsilon(\omega)]$, for the ET process of Eq. (2.73). Once an electron is transferred, the slowest contribution of the solvent relaxes fast enough, such that solvent vibrational states $|\mathbf{v}\rangle$ are in thermal equilibrium before a new possible ET occurs. To this end, we describe the initial solvent state distribution in Eq. (2.56) by the Bose-Einstein distribution $n(\omega)$. In high temperature limit $k_B T \gg \hbar\omega_c$ [14] the function $G(t)$ stemming from the coupling to the bath goes quickly to zero and a Marcus-type ET rate will be found according to Eq. (2.60).

In the opposite limit of a slow ET, for a rate $k_{DA} > \tau_n^{-1}$ the solvent states do not relax fast enough to their thermal equilibrium and cannot be described by $n(\omega)$ for a stationary density of solvent microstates, especially if a cascade of ET events between the donor and acceptor happens or a successive electron transmission between the molecule-lead interfaces occurs. Moreover, we expect a time-dependent ET rate which depends on the time span elapsed since the previous charge rearrangement due to the previous ET. During this time span, the solvent readjusts to the newly formed charge configuration but does not reach its equilibrium configuration before the new ET process occurs. Thus, the ET is strongly *solvent-controlled* [58]. The impact of the solvent dynamics on the *nonequilibrium* ET rates for chemical reactions was studied in great detail by H. A. Kramers [50]. To this end, he has introduced a solvent-induced friction in the dynamics of a generalized reaction coordinate in terms of a Fokker-Planck equation. This nonequilibrated ET rates will be extended in Chapter 4 to study the successive electron transmission processes through a molecule between two electronic leads embedded in a nonequilibrated solvent.

---

[14] ω_c may be associated with the highest energy of the thermal bath

Chapter 3

Nonequilibrium molecular relaxation dynamics in a dynamic solvent

Electronic spectroscopy of photoexcited molecules dissolved in a polar medium measures the response of molecular electronic states to applied time-dependent electric fields, but also reveals the interplay of the dissolved molecule (the solute) and the solvent as signature of a quantum many-body system (see Sec. 2.1) [53, 58]. Since the early days of spectroscopic measurements, it has been established that the solvent induces pronounced features in the molecular response. Prominent examples are the broadening of spectral lines and the Stokes shift between absorption and emission lines which both reflect the omnipresent influence of the solvent relaxation properties in energy absorption processes [58, 53, 31, 73].

A new type of spectroscopic phenomena arises if changes of the charge configuration of the solute are accompanied by timely irreversibly structural changes of the solute or the solvent. Such a situation, when the solvent/solute changes its configuration as a function of time, clearly goes beyond the time-dependent reorganization of the continuous solvent to the newly formed charge configuration described by the dynamic, but stationary, response of the polarization in Subsec. 2.2.2.

A recent study [74] of a sequence of electronic transitions between a low-spin and a high-spin electronic configuration of aqueous Fe-II complexes has provided possible hints of fast non-stationary dynamical changes in the first hydration shell which accompany the electronic transitions in the central molecule. In the experiment, an increase of the lengths of the bonds between the central Fe-atom and the nearest neighbor atoms in the complex was identified as being induced by the electronic transitions. The experimental data have been interpreted such that the transition from the low-spin to the high-spin configuration due to photoexcitation is accompanied by a structural change of the hydration layer: On average two shell water molecules are expelled from the hydration shell into the bulk solvent. The distribution of the water molecules in the shell is modified during the transition influencing the electronic relaxation. This experiment is consistent with earlier theoretical predictions [75, 76] obtained on the basis of ab initio molecular dynamics simulations. Another example is the structural dynamics of photoexcited of $[\mathrm{Co(terpy)}_2]^{2+}$ in aqueous solution investigated with ultrafast X-ray diffuse scattering [77]. Accompanying density functional theory calculations showed that the photoexcitation leads to elongation of the Co-N bonds.

X-ray absorption spectroscopy (XAS) is even able to probe the transition form hydrophilic to hydrophobic solvation and the dynamic built-up of the hydrophobic solvation shell with atomic scale resolution on a short time scale [49]. The process of the formation of a solvation shell is usually observed if the central molecule abruptly changes its charge configuration, e.g., from its ionic to its neutral, and hence, hydrophobic state. This can be achieved by a strong-field removal of one electron of the solute. The picosecond XAS study reveals the creation of a network of hydrogen bonded water molecules in the first solvation shell within 5ps around a iodine molecule which has been neutralized just before. The experimental data further demonstrate the dynamic expansion of the solvent layer after the transfer $I^- \to I^0$ with an increase of the radius of the hydrated cluster by up to 80% [49, 78]. The experimental data have been corroborated by ab initio molecular dynamics simulations. Further experimental studies have been carried out, see Ref. [79] for an excellent recent account on the present status.

These experimental observations of time-dependent and highly nonequilibrium features, i.e., changes in molecular bond lengths and/or solvent reorganization require theoretical descriptions beyond established models of solvation. The aim of this chapter is to develop and solve a theoretical model describing the response of a dissolved molecule facing time-dependent configurational changes of its structure or of the solvent to an external electric field. To this end, different situations for non-stationary and timely strongly changing configuration of the solute (Sec. 3.2 and 3.3) and solvent, i.e., a timely varying solvation shell (Sec. 3.4), are studied for the absorption spectrum of the central molecule according to the experimental observations described above.

This leads to the following structure of the present chapter. First, I introduce the basic concepts of the Onsager continuum model of solvation in Sec. 3.1. In Sec. 3.2, I then establish a time-dependent Onsager model to determine the optical linear absorption of a molecule with geometric configurations varying explicitly over time. I exploit the derived model to explain the bimodal behavior of the time-dependent fluorescence Stokes shift in Sec. 3.3. In Sec. 3.4, I examine a molecule where a layer of a hydration shell grows around the central Onsager sphere by developing the time-dependent Onsager model. We will see that the predictions of this time-dependent Onsager model are confirmed by measured X-ray absorption spectra.

3.1 Onsager's model of solvation

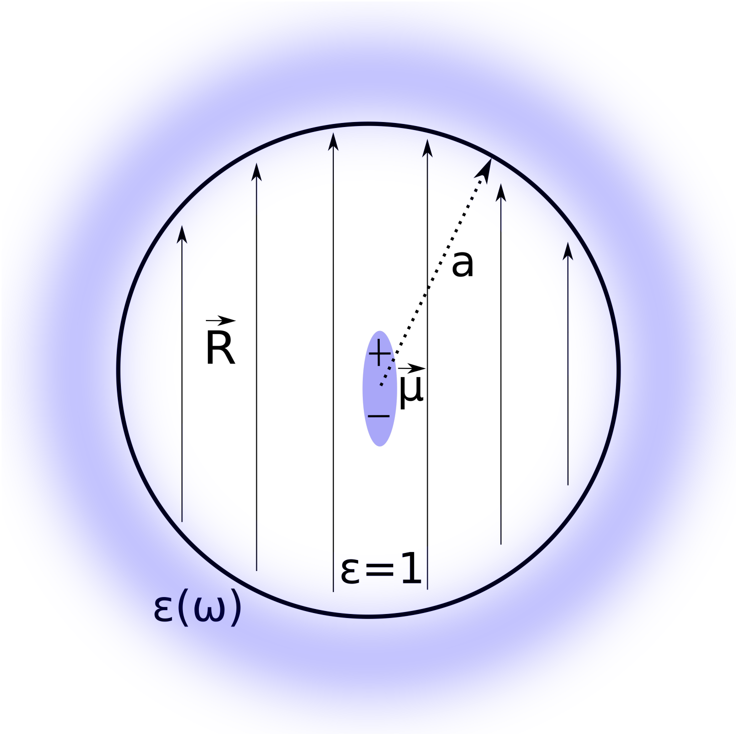

Figure 3.1: Onsager's model of solvation. The molecular dipole moment $\boldsymbol{\mu}$ is embedded inside an empty vacuum cavity ($\epsilon = 1$) of radius a which is surrounded by a polar solvent with dielectric function $\epsilon(\omega)$. The dipole polarizes the solvent which in turn creates an electric reaction field $\mathbf{R}$ acting back on the dipole.

The starting point of Onsager's model of solvation model is captured by the generalized Hamiltonian of Eq. (2.18) in Sec. 2.2 for continuum solvation models based on the system-bath description. The tremendous reduction of solvent (bath) degrees of freedom leads effectively to a solvent response function which indicates the reaction to changes of solute (system) degrees of freedom and which contributes to the system dynamics as main result in system-bath approaches (cf. Sec. 2.1).

The earliest polarizable and simplest continuum model of solvent was developed by Born in 1920 [80] who assumed a solute with a spherical charge distribution in the center of an effective molecular cavity with an unknown time-independent radius. This molecular cage itself is placed in a classical dielectric continuum. Inside the molecular cavity, vacuum is assumed. The solute-solvent interaction is determined by the net electric charge q of the solute. In view of the later developments, the total charge of the sphere can be viewed as the first term of a multipole expansion of the charge distribution of the sphere. The interaction $V_I = q\Phi$ results, where Φ is the electrostatic potential stemming from the back-action of the solvent polarization to the net molecular charge q.

Later, Kirkwood [81] and Onsager [38] have extended this model to include the second and higher-order multipole terms of the electrostatic potential generated by the solute. The latter is described as a point dipole located at the center of a spherical (Kirkwood) or an ellipsoidal (Onsager) molecular cavity which, again, is static and whose unknown parameters are empirical and used as fit parameters. The model gives then rise to a dipole-dipole interaction between the central molecule and the solvent. The interaction has the form $V_I = -\boldsymbol{\mu} \cdot \mathbf{R}$ (cf. minimal coupling Hamiltonian of Eq. (2.35) for a molecule coupling to an applied electric field in Sec. 2.3) where $\boldsymbol{\mu}$ is the dipole moment of the solute and $\mathbf{R}$ the electric *reaction field* at the location of the dipole moment as result of its solvent polarization (see Fig. 3.1). The reaction field can be obtained from linear response theory yielding

$$\mathbf{R}(t) = \int_{-\infty}^{t} dt' X(t-t')\boldsymbol{\mu}(t'), \tag{3.1}$$

where $X(t-t')$ is the susceptibility function (in general a tensor). One assumes an isotropic, homogeneous and local-in-space response function such that X is a scalar function which we have discussed for the electric susceptibility in Eq. (2.23) in Subsec. 2.2.1 in greater detail. The formulation of Eq. (3.1) reflects the fact that the dipole moments of solvent molecules do not adjust instantaneously to the central dipole moment, but rather lag behind the changing dipole in time. Causality requires that $X(t) = 0$ for $t < 0$. The Fourier transform of Eq. (3.1) using the convolution theorem reads $\mathbf{R}(\omega) = X(\omega)\boldsymbol{\mu}(\omega)$ [1].

---

[1] The Fourier transform is defined by $\mathcal{F}[f(t)] = \int_{-\infty}^{\infty} dt \exp(i\omega t) f(t)$.

To obtain a appropriate equation for $X(\omega)$ which is the response of the idealized homogeneous dipolar solvent to the molecular dipole moment, one has to solve the time-dependent electrostatic problem. The dielectric displacement $\mathbf{D}_i$ in any phase i, i.e. $i = I$, inside, $i = A$, outside the Onsager sphere, is related to the electric field $\mathbf{E}_i$ and polarization $\mathbf{P}_i$ by $\mathbf{D}_i(\mathbf{x}, t) = \mathbf{E}_i(\mathbf{x}, t) + 4\pi\mathbf{P}_i(\mathbf{x}, t)$, see Subsec. 2.2.1. In linear response, the polarization is related to the electric field via $\mathbf{P}_i(\mathbf{x}, \omega) = \alpha_i(\omega)\mathbf{D}_i(\mathbf{x}, \omega)$ (cf. Eq. (2.24)) and $\mathbf{D}_i(\mathbf{x}, \omega) = \epsilon_i(\omega)\mathbf{E}_i(\mathbf{x}, \omega)$ with $\epsilon_i(\omega) = (1 + 4\pi\alpha_i(\omega))^{-1}$. Here, $\alpha_i(\omega)$ is the respective polarizability (see Eq. (2.25) of Subsec. 2.2.2) of the medium inside and outside the sphere. To obtain the response function X and the corresponding reaction field $\mathbf{R}$ one has to know the electrostatic potential in the cavity in the presence of the dipole and due to its interaction with the solvent. Taking the center of the dipole as the origin of a coordinate system and choosing the dipole vector in alignment with the $z-$ axis, $\boldsymbol{\mu} = \mu\hat{\mathbf{e}}_z$, we are able to solve the Laplace equation $\Delta\Phi = 0$ for the potential as the net charge is zero. The resulting solution exploits the spherical symmetry and is $\Phi_i = \sum_{n=0}^{\infty} \big(A_n^{(i)} r^n + \frac{B_n^{(i)}}{r^{n+1}}\big) P_n[\cos\Theta]$, where P_n are the Legendre polynomials and Θ is the angle with respect to the $z-$axis [73]. We set the potential $(\Phi_A)_{r\to\infty} = 0$ far outside. Furthermore, we require the continuity of the potential yielding the condition $(\Phi_I)_{r=a} = (\Phi_A)_{r=a}$ and the electric displacement $\big(\frac{\partial}{\partial r}\Phi_I\big)_{r=a} = \big(\frac{\partial}{\partial r}\Phi_A\big)_{r=a}$ at the surface of the Onsager sphere. The potentials inside and outside the Onsager sphere read

$$\Phi_I = \frac{\mu}{r^2}\cos\Theta - \frac{2(\epsilon-1)}{2\epsilon+1}\frac{\mu}{a^3} r\cos\Theta, \tag{3.2}$$

$$\Phi_A = \frac{3}{2\epsilon+1}\frac{\mu}{r^2}\cos\Theta. \tag{3.3}$$

The resulting electric field inside the cavity is a superposition of the dipole field in vacuum and the uniform reaction field of the form

$$\mathbf{R}(\omega) = \frac{1}{a^3}\frac{2[\epsilon(\omega)-1]}{2\epsilon(\omega)+1}\boldsymbol{\mu}(\omega), \tag{3.4}$$

or,

$$\mathbf{R}(\omega) = X(\omega)\boldsymbol{\mu}(\omega). \tag{3.5}$$

This reaction field acts back on the central molecular dipole moment and is constant everywhere inside the uniform spherical cavity.

The reaction field of Eq. (3.5) as electrodynamic response of the solvent to the solute can now be exploit to understand basic solute dynamics in solution. To illustrate this, we now formulate a spectral density $J(\omega)$, according to Eq. (2.13) in Sec. 2.1 as collective effect of the bath influencing the system's dynamics, for the Onsager's model of solvation. The spectral density can be used to obtain time-dependent relaxation and dephasing in the solute in the presence of the solvent [39, 31, 26, 82]. The solute-solvent coupling $V_I = -\boldsymbol{\mu} \cdot \mathbf{R}$ is the central entity which contains all relevant information of the solvent dynamics in response to the solute motion. This interaction energy typically lowers the total energy and forms a stable structure [39]. To illustrate the timely evolving solute in form of a Onsager cavity in presence of a solvent, we model a two-level system with a single active transition of energy ϵ, a coupling Δ for tunneling between the two levels and assume the solute has a permanent dipole moment in the ground and in the excited state, given by $\boldsymbol{\mu}_g$ and $\boldsymbol{\mu}_e$ respectively. We note that the direction of the dipole moment of the solute in the ground and excited state points in the same direction, such that we only use its absolute values in the two states $\mu = \begin{pmatrix} \mu_e & 0 \\ 0 & \mu_g \end{pmatrix}$. The two-state solute and the solute-solvent interaction Hamiltonian together reads

$$H_{S+I} = \frac{1}{2}\epsilon\sigma_z - \frac{1}{2}\Delta\sigma_x + \frac{1}{2}\sigma_z\Delta\mu R + \frac{1}{2}\mathbb{I}(\mu_e + \mu_g)R, \tag{3.6}$$

with $\Delta\mu = \mu_e - \mu_g$, the 2×2 Pauli matrices σ_z and σ_x and the 2×2 unitary matrix $\mathbb{I}$ [2]. We quantize the reaction field with its modes ω_α and its amplitudes e_α according to $R(t) = \sum_\alpha e_\alpha[a_\alpha e^{-i\omega_\alpha t} + a^\dagger e^{i\omega_\alpha t}]$. a_α and $a_\alpha^\dagger$ are the bosonic anhilation and creation operators such that the solvent is considered as bath of independent harmonic oscillators with the total solvent energy $H_B = \sum_\alpha \omega_\alpha a_\alpha^\dagger a_\alpha$. This *spin-boson model* describes relaxation and decoherence of an initially coherent excitation due to its coupling to the solvent with the resulting spectral density $J(\omega) = \pi \sum_\alpha e_\alpha^2 \delta(\omega - \omega_\alpha)$ [5, 26, 39]. We now relate the spectral density $J(\omega)$ to the zero-temperature fluctuations in the uncoupled environment as done in Refs. [4, 39]. We consider the expectation value of the reaction field as $\langle R(t) \rangle = 0$ and define the reaction field correlation function

$$C_R(t) = i\langle R(t)R(0)\rangle \equiv i \langle 0| e^{iH_B t} R e^{-iH_B t} R |0\rangle \, \Theta(t), \tag{3.7}$$

where $|0\rangle$ is the ground state of the solvent harmonic oscillators. We find that the Fourier

---

[2] The Pauli matrices are $\sigma_z = \begin{pmatrix} 1 & 0 \\ 0 & -1 \end{pmatrix}$ and $\sigma_x = \begin{pmatrix} 0 & 1 \\ 1 & 0 \end{pmatrix}$.

transform of $C_R(t)$ can be related to the spectral density via

$$\mathrm{Im}\, C_R(\omega) = \pi \sum_\alpha \delta(\omega - \omega_\alpha) |\langle 0| R |\alpha\rangle|^2 = \pi \sum_\alpha \delta(\omega - \omega_\alpha) {e_\alpha}^2 = J(\omega)/(\Delta\mu)^2. \tag{3.8}$$

Here we have used the orthogonality of the solvent states $\langle\alpha|\alpha'\rangle = \delta_{\alpha\alpha'}$ and expand R into its normal modes. We see that all terms $\langle 0| R |\alpha\rangle$ describe transitions of the single solvent oscillators from a ground state to a singly occupied state with energy $\hbar\omega_\alpha$, and $\langle 0| R |\alpha\rangle = e_\alpha$. The response $X(\omega)$ of Eqs. (3.4) or (3.4) relates the changing dipole moment to the solvent reaction field. From the quantum fluctuation-dissipation relation [20, 39, 26] we find that the imaginary part of $X(\omega)$ is related to the field fluctuations by the form

$$X''(\omega) = -\frac{i}{2}(1 - e^{-\beta\omega}) C_R(\omega), \tag{3.9}$$

which reduces to $C_R(\omega) = 2iX''(\omega)$ at zero temperature and confirms the general relation between the spectral density and the imaginary part of the response function, $J(\omega) \propto X''(\omega)$, by exploiting Eq. (3.8). Using the Debye formula for the dielectric function of Eq. (2.26) of Subsec. 2.2.2 and Eq. (3.8), the spectral density for the Onsager model reads

$$J(\omega) = \frac{2(\Delta\mu)^2}{a^3} \frac{6(\epsilon_\infty - \epsilon_s)}{(2\epsilon_s + 1)(2\epsilon_\infty + 1)} \frac{\omega\tau_E}{\omega^2\tau_E^2 + 1}, \tag{3.10}$$

where $\tau_E = (2\epsilon_\infty + 1)(2\epsilon_s + 1)^{-1}\tau_D$ [39].

The basis of the established model is the assumption that time-dependent changes in the electronic configuration of the solute are not too large such that the back action of the solvent polarization on the solute can be calculated in terms of linear response theory. Then, the fluctuation-dissipation theorem of Eq. (3.9) holds, the fluctuations are thermal, and a bath spectral density exists in the established form of Eq. (3.10) [26]. Despite microscopic details of the system and solute, the Onsager model captures the essential physics of the solvation process [39, 82]. Based on the derived spectral density (3.10), where experimentally obtainable parameters enter, spectroscopic features such as shifting and broadening of an absorption spectrum can be explained [39]. Thus, nonequilibrium but timely stationary solvation processes become measurable [53, 58, 31].

3.2 Generalization to a time-dependent Onsager model [3]

Up to present, a generalization of the Kirkwood-Onsager continuum theory of quantum solvation to explicitly include time-dependent solute or solvent properties has not been established. In this section, I formulate a theory of nonequilibrium quantum solvation in which parameters of the solute become explicitly time-dependent. We assume in a simplest approach a spherical molecular Onsager cavity with a time-dependent radius. The precise functional form of the time-dependence is imposed from outside and we consider two cases: a shrinking Onsager sphere (Subsec. 3.2.3), and, a breathing Onsager sphere with a transient expansion followed by a shrinking to the original size (Subsec. 3.2.4) [77]. In particular, we are interested in how the relaxation properties of an excited electronic state of the solute and its frequency-dependent response are influenced by the time-dependent solute cage. We consider a molecular point dipole dissolved in water. Since all parameters are kept explicit, other dielectric solvents can readily be addressed as well. In general, the frequency-dependent response functions are non-stationary and explicitly depend on time. For a shrinking Onsager sphere we find a frequency-dependent susceptibility which grows over time by up to 40%. In case of the breathing sphere we find a non-monotonous dependence of the solute relaxation rate on the breathing rate and a resonant suppression of damping when both rates are comparable. From the point of view of the theory of dissipative quantum systems, a time-dependent solute radius amounts to a time-dependent system-bath coupling and to a break-down of the stationarity of the environmental fluctuations. This calls for a generalization of the formalism to nonequilibrium baths. In particular, a standard form of the spectral density, see Eq. (3.10) for the stationary Onsager model, which is connected to a time-translationally invariant susceptibility and a damping kernel for the generalized Langevin equation (2.14) in Sec. 2.2 [26], cannot be formulated. This is also different to a previously calculation of an externally driven harmonic bath in which an external time-dependent field drives the harmonic bath oscillators [83, 84]. By this, a net external force on the central systems is composed by the bath, but it still can be described by a spectral density.

This leads to the following structure of this section. In Subsec. 3.2.1, I derive a model for a molecular dipole moment embedded in Onsager cavity with a time-dependent radius by

---

[3] The model presented in this section is based on the publication : H. Kirchberg, P. Nalbach and M. Thorwart, "Nonequilibrium quantum solvation with a time-dependent Onsager cavity," J. Chem. Phys. **148**, 164301 (2018).

means of a non-stationary Langevin equation. Subsec. 3.2.2 gives the physical parameters chosen for the model of solvation. In Subsec. 3.2.3, I solve the established equation and calculate the relaxation dynamics for the molecular dipole moment and its response to an external electric field in a shrinking Onsager cavity. Subsec. 3.2.4 shows the corresponding results for the case of a breathing Onsager cavity. Subsec. 3.2.5 concludes.

3.2.1 Model and nonequilibrium Langevin equation

One considers a solute molecule in the form of an electric dipole which is exposed to the reaction electric field generated by the back action of the polarized solvent. The electrons are bound to the positively charged nuclei and can be brought out of their equilibrium position by the fluctuating reaction field. In the simplest form of a homogeneous, isotropic model, the effective potential for the electron (with a charge e) near its equilibrium position is assumed harmonic with the characteristic frequency ω_0, and the fluctuations induce damping of its time-dependent displacement $\mathbf{q}(t)$ [61, 85]. The induced dipole moment of the solute is along the z-axis and given by $\boldsymbol{\mu}(t) = e\,q(t)\hat{\mathbf{e}}_z$. The dipole is placed inside a spherical Onsager cavity whose radius $a(t)$ is now assumed to be explicitly time-dependent in comparison to the static Onsager model in Sec. 3.1. One assumes that the time-dependence is created by some external mechanism, for instance, upon photoexcitation of the solute and a subsequent reconfiguration of the solute or the solvent (see introduction of this Chapter 3 for specific examples). The spherical cage is surrounded by a dielectric medium with a given frequency-dependent complex permittivity $\varepsilon(\omega) = \varepsilon'(\omega) + i\varepsilon''(\omega)$ according to Eq. (2.26) of Subsec. 2.2.2.

To calculate the Onsager reaction field by means of Maxwell's equations for a time-dependent radius, we assume that the radius $a(t) = a_0 + a_1(t)$ is composed of a time-independent part a_0 =const. and only changes weakly in a small range by the magnitude $a_1(t)$ over time. This allows us to neglect any charge current density and to use the much simpler laws of electrostatics [73, 38]. Therefore we use the electrostatic potential obtained for the region outside the Onsager sphere in the dielectric medium ($r > a(t)$) described by Eq. (3.3) and inside the sphere ($r < a(t)$) according to Eq. (3.2). All contributions of the magnetic field induced by the displacement current at the boundary of the slowly changing sphere are negligible.

With this, the reaction field is found to include an explicitly time-dependent radius $a(t)$ in comparison to that one derived in Eq. (3.4). The reaction field is homogeneous and points in z-direction, $\mathbf{R}(t) = R(t)\hat{\mathbf{e}}_z$, like the molecular dipole moment $\mu(t) = eq(t)$, so that it is given by

$$R(t) = \frac{1}{a(t)^3} \int_{-\infty}^{t} dt' \chi(t-t') \mu(t') \,. \tag{3.11}$$

With the Debye dielectric permittivity of Eq. (2.26) in time space we find the time-dependent response function or susceptibility

$$\chi(t) = \chi_D e^{-\omega_D t} \Theta(t), \tag{3.12}$$

where we have defined $\omega_D = (2\varepsilon_s + 1)/(3\tau_D)$, $\chi_D = \frac{2(\varepsilon_s - 1)}{3\tau_D}$ and choose $\epsilon_\infty = 1$ (cf. Subsec. 3.2.2 for further discussions). This yields the response function in the Laplace space [4], which we define for later purpose, according to

$$\chi(z) = -\frac{\chi_D}{z + i\omega_D} \,. \tag{3.13}$$

The total Hamiltonian for the electron forming the molecular dipole moment in harmonic approximation which couples to the reaction field via minimal coupling $V_I = -\mu R$ according to Eq. (2.35) reads

$$H = H_S + V_I = \frac{1}{2m} p^2 + \frac{m}{2} \omega_0^2 q^2 - eqR, \tag{3.14}$$

where p is the momentum of the electron e, q its displacement and m its mass.

The reaction field is a field operator whose expectation value $\langle R(t) \rangle$ gives rise to a time-dependent expectation value for the external force $e\langle R(t) \rangle$. Using the Hamiltonian of Eq. (3.14) and the Heisenberg equation of motion for the momentum $\langle p \rangle \equiv m\langle \dot{q} \rangle$ of the electron with mass m leads to a Langevin-type equation for the expectation value of the displacement with an explicit time-dependent memory kernel (resulting from reaction field of Eq. (3.11)) in form

$$m\langle \ddot{q}(t) \rangle + m\omega_0^2 \langle q(t) \rangle = e\langle R(t) \rangle = \frac{e^2}{a(t)^3} \int_0^t dt' \chi(t-t') \langle q(t') \rangle \,, \tag{3.15}$$

where $\langle q(t) \rangle = 0$ for $t < 0$ has been assumed. The electron displacement and the resulting dipole moment begins at $t = 0$ which also yields the lower limit $t = 0$ of the integral

---

[4] Laplace transform is defined by $f(z) = i\int_0^\infty dt\, e^{izt} f(t)$, where $f(z)$ is analytic for Im(z) > 0 and $f(t \to \infty) < \infty$.

in the memory kernel of Eq. (3.15). In the frequency domain, the response function in the memory kernel $\chi(\omega) = \chi'(\omega) + i\chi''(\omega)$ can be separated into the real and imaginary part, where the real part $\chi'(\omega)$ leads to a shift of the potential $V(q) = \frac{m}{2}\omega_0^2 q^2$ in Eq. (3.14) and the imaginary part $\chi''(\omega)$ induces damping of the displacement motion (see denominator polynomial in Eq. (3.20) where $-i\chi_0(\mathrm{Re}[z]) = \chi_0(\omega)$). We emphasize again that for a static Onsager radius $a(t) = a_0$ the damping kernel can be associated to the spectral density $J(\omega)$ of an equilibrium or stationary environment (see Eq. (3.10)). For the nonequilibrium solvent with a time-dependent Onsager radius, this is no longer possible, since the fluctuations of the nonequilibrium bath are no longer time-translational invariant (or, stationary). In the following, we therefore shall use the equation of motion in the form of Eq. (3.15).

3.2.2 Model parameters

Throughout this work, we study a test molecule with an eigenfrequency $\omega_0 = 1.183 \times 10^{15}$ Hz, which sets the natural system time scale of the dipole dynamics comparable to the ones of molecules and atoms in the ultraviolet regime. Furthermore, the choice of ω_0 is restricted to the regime above a minimal magnitude for stability reasons within the model (see Sec. 3.2.3 and Appendix A.1). The relevant mass is given by the electron mass $m = 9.11 \times 10^{-28}$ g. Then, the natural length scale of the displacements $q(t)$ is given by the oscillator length $q_d = \sqrt{\hbar/(m\omega_0)} = 3.1$ Å$= 3.1 \times 10^{-8}$cm. Note that we work in cgs units in which the electron charge is $e = 3 \times 1.602 \times 10^{-10}$esu.

For the solvent, we use the values of bulk water (at 20°C) according to $\varepsilon_s = 78.3$, $\tau_D = 8.2$ ps of the dipolar solvent and $\omega_D = 6.4$ THz $= 5.4 \times 10^{-3}\omega_0$. Moreover, $\chi_D = 6.3$ THz. For simplicity, we set $\varepsilon_\infty = 1$ in the high-frequency limit, while other values ($\varepsilon_\infty > 1$) for this limit lead to small constant shifts of the potential (see Eq. (A.6) in Appendix A.1 for details). The scale a_0 of the radius of the static Onsager sphere is assumed to be $a_0 = 6 \times 10^{-8}$cm. Hence, $\omega_0 \gg \omega_D; \chi_D$, and under these conditions, the scale of the right-hand side of Eq. (3.15) becomes $\sqrt{e^2/(ma_0^3)} = 1.1 \times 10^{15}$ Hz $\simeq \omega_0$. Moreover the quantity $e^2/(m\omega_0^2) = \alpha_m$ is related to the molecular polarizability (cf. Eq. (2.27) of Subsec. 2.2.3) for molecules without a permanent dipole moment [61] and reads within the model $\alpha_m = 0.84a_0^3$ which is comparable to the polarizability of Sr where $\alpha_m \simeq 30$ Å^3 [86, 87, 88][5].

---

[5] Value for α_m is appropriate for cgs units. To convert to SI, we utilize the relation $\alpha_m(\mathrm{SI})/\mathrm{Cm}^2\mathrm{V}^{-1} = 4\pi\epsilon_0 10^{-6}\alpha_\mathrm{m}(\mathrm{cgs})/\mathrm{cm}^3$.

3.2.3 Shrinking Onsager sphere

First, we consider the relaxation dynamics of the dipole in a shrinking Onsager sphere. We assume that the radius varies with time from the larger radius $a_0 + a_1$ to the smaller one a_0 according to

$$a(t) = a_0 + a_1(t) = a_0 + a_1 e^{-\alpha t}\Theta(t). \tag{3.16}$$

α denotes the shrinking rate. We assume that the initial electron displacement coincides with the shrinking of the sphere at $t = 0$.

From now on, I write all expectation values as $\langle q(t)\rangle \equiv q(t)$ and $\langle R(t)\rangle \equiv R(t)$ for better readability.

Time evolution of the dipole moment

To calculate the expectation value of the dipole moment $\mu(t)$, one needs to solve Eq. (3.15) which is a linear integro-differential equation. This is not possible in general in an analytic manner. To proceed, we employ the Laplace transform and need to use an approximation for the prefactor $1/a(t)^3$. In doing so, we expand the prefactor in a Taylor series up to first order in the time-dependent part. This is valid when the overall magnitude a_1 by which the radius changes over time is much smaller than the static radius a_0, which is usually the case in a concrete physical situation. In fact, the molecule is typically much larger than the change of its size induced by photoexcitation.

Hence, we have for $a_1 \ll a_0$ that

$$\frac{1}{a(t)^3} = \frac{1}{(a_0 + a_1 e^{-\alpha t})^3} \simeq \frac{1}{a_0^3}\left[1 - \frac{3a_1}{a_0} e^{-\alpha t}\right]. \tag{3.17}$$

For convenience, we define the rescaled linear susceptibilities for the case of fast shrinking according to

$$\begin{aligned} \chi_0(t) &= \frac{e^2}{m a_0^3}\chi(t), \\ \chi_1(t) &= \frac{3a_1}{a_0}\chi_0(t)\,. \end{aligned} \tag{3.18}$$

Here, $\chi_0(t)$ only depends on the static radius a_0 while $\chi_1(t)$ is of first order in a_1/a_0.

In first order in the ratio a_1/a_0, we obtain the Laplace transform [6] of Eq. (3.15) in the form

$$-z + [\omega_0^2 - z^2 + i\chi_0(z)]q(z) = i\chi_1(z + i\alpha)q(z + i\alpha)\,. \tag{3.19}$$

The solution immediately follows as

$$\begin{aligned} q(z) &= q_0(z) + q_1(z) \\ &= \frac{zq(t=0)}{\omega_0^2 - z^2 + i\chi_0(z)} + \frac{i\chi_1(z+i\alpha)q_0(z+i\alpha)}{\omega_0^2 - z^2 + i\chi_0(z)}\,. \end{aligned} \tag{3.20}$$

Here, $q(t = 0)$ denotes the initial expectation value of the displacement at $t = 0$ and we have assumed that the initial expectation value of the velocity $\dot{q}(t = 0) = 0$. For specific calculations below, we set $q(t = 0) = q_d$. Moreover, one has defined $q_0(z)$ which includes the contribution from the static smaller sphere with the final radius a_0, while all contributions from the time-dependent radius are contained in $q_1(z)$. Since we need to make sure that the second term $q_1(z)$ only contains contributions up to first order in a_1/a_0 (which is realized by the prefactor $\chi_1(z+i\alpha)$), we need to replace $q(z+i\alpha)$ by $q_0(z+i\alpha)$ for consistency here. Thus, we first calculate $q_0(z)$ for the static case by setting $a_1 = 0$. Then, we calculate the first-order term $q_1(z)$ which reflects the influence of the time-dependent radius $a_1(t)$. Finally, we transform the results back to the time domain to obtain the overall time-dependent expectation value of the displacement $q(t) = q_0(t) + q_1(t)$.

To obtain a stable solution of $q_0(t)$ as Laplace back transform of $q_0(z)$, we have to restrict the frequency domain such that $\omega_0 > \omega_{0,\mathrm{min}}$ (see Eq. (A.6) in Appendix A.1 for details). If we choose a smaller eigenfrequency, we will obtain an additional solution of $q_0(t)$ which diverges in time. The molecular dipole moment would then be completely distorted beyond the harmonic limit, and a real molecule, based on the Onsager model, would be deformed in terms of its extensional and electronic properties which is unphysical.

To transform $q_0(z)$ (first term of Eq. 3.20) back into the time domain, we first calculate the roots of the denominator polynomial $D(z)$ according to

$$q_0(z) = \frac{q(t=0)z}{\omega_0^2 - z^2 + i\chi_0(z)} = \frac{q(t=0)(-z^2 - iz\omega_D)}{z^3 + i\omega_D z^2 - \omega_0^2 z + i(-\omega_0^2\omega_D + \Phi)} = \frac{q(t=0)(-z^2 - iz\omega_D)}{D(z)}. \tag{3.21}$$

---

[6] Laplace transform is defined by $f(z) = i\int_0^\infty dt\, e^{izt} f(t)$, where $f(z)$ is analytic for Im(z) > 0 and $f(t \to \infty) < \infty$.

The resulting equation

$$D(z) = z^3 + i\omega_D z^2 - \omega_0^2 z + i(-\omega_0^2\omega_D + \Phi) = 0, \tag{3.22}$$

can now be solved in several steps, where $\Phi = \frac{e^2}{ma_0^3}\chi_D$. First, we substitute $z = i\lambda$ and obtain

$$\lambda^3 + \omega_D\lambda^2 + \omega_0^2\lambda + \omega_0^2\omega_D - \Phi = 0\,. \tag{3.23}$$

With the shift $\lambda = \tilde{z} - \omega_D/3$, it follows that

$$\tilde{z}^3 + p\tilde{z} + r = 0, \tag{3.24}$$

where $p = \omega_0^2 - \omega_D^2/3$ and $r = 2\omega_D^3/27 + 2\omega_0^2\omega_D/3 - \Phi$. The cubic equation can be solved by Cardano's method and one obtains

$$\tilde{z}_1 = u + v\,, \tag{3.25}$$

$$\tilde{z}_2 = u\epsilon_1 + v\epsilon_2\,, \tag{3.26}$$

$$\tilde{z}_3 = u\epsilon_2 + v\epsilon_1, \tag{3.27}$$

where $\epsilon_1 = -1/2 + i\sqrt{3}/2$, $\epsilon_2 = -1/2 - i\sqrt{3}/2$, $u = (-r/2 + \sqrt{\Delta})^{1/3}$, $v = (-r/2 - \sqrt{\Delta})^{1/3}$ and $\Delta = (r/2)^2 + (p/3)^3$. After back-substitution, the roots read

$$z_1 = i\left(u + v - \frac{\omega_D}{3}\right) \equiv -ic\,, \tag{3.28}$$

$$z_2 = -\frac{i}{2}\left(u + v + \frac{2\omega_D}{3}\right) - \frac{\sqrt{3}}{2}(u - v) \equiv -i\Gamma_0 - \Omega\,, \tag{3.29}$$

$$z_3 = -\frac{i}{2}\left(u + v + \frac{2\omega_D}{3}\right) + \frac{\sqrt{3}}{2}(u - v) \equiv -i\Gamma_0 + \Omega\,. \tag{3.30}$$

Here, we have introduced the parameters

$$c = -u - v + \frac{\omega_D}{3}\,, \tag{3.31}$$

$$\Gamma_0 = \frac{1}{2}\left(u + v + \frac{2\omega_D}{3}\right)\,, \tag{3.32}$$

$$\Omega = \frac{\sqrt{3}}{2}(u - v)\,. \tag{3.33}$$

The inverse Laplace transformation can be carried out by solving

$$q_0(t) = \frac{1}{2\pi i}\int_{-\infty}^{\infty} dz e^{-izt}\frac{q(t=0)(-z^2 - i\omega_D z)}{(z-z_1)(z-z_2)(z-z_3)} = -2\pi i \sum_j \mathrm{Res}(q_0, z_j)\,. \tag{3.34}$$

Next, we exploit the relations between the parameters which are typical for a Debye solvent, and, in the present case, for water in the Debye approximation. Plugging in the parameters discussed in Subsec. 3.2.2, we find that $\Phi \approx \omega_0^2\omega_D$ and that $p \approx \omega_0^2$. Moreover, we have that $r \approx 2\omega_0^2\omega_D/3 - \Phi \approx -\omega_0^2\omega_D/3 < 0$. This ensures that $\Delta \simeq \omega_0^6/3^3 > 0$, such that three linearly independent solutions exist, since $\omega_0 \gg \omega_D$. Using this physically motivated approximations from the model parameters in Subsec. 3.2.2, we have that $u \simeq \omega_0/\sqrt{3}$ and $v = -u$, such that

$$c \simeq \frac{\omega_D}{3}\,, \tag{3.35}$$

$$\Gamma_0 \simeq \frac{\omega_D}{3}\,, \tag{3.36}$$

$$\Omega \simeq \omega_0\,. \tag{3.37}$$

In time-domain $q_0(t)$ finally reads

$$q_0(t) \simeq e^{-\Gamma_0 t} q(t=0)\left[\frac{2}{9}\frac{\omega_D^2}{\omega_0^2} + \left(\frac{2}{9}\frac{\omega_D^2}{\omega_0^2} + 1\right)\cos\omega_0 t - \frac{\omega_D}{3\omega_0}\sin\omega_0 t\right] \tag{3.38}$$

$$\simeq e^{-\Gamma_0 t} q(t=0)\cos\omega_0 t\,. \tag{3.39}$$

For the given parameters, it follows that the damping strength is $\Gamma_0 \simeq \omega_D/3$, see Eq. (3.36). Only then, the oscillation frequency is given by ω_0, and other components (such as that coming from the sine) are negligible. Moreover, we note that for a fixed parameter combination and without the neglect of the small terms in Eq. (3.34), we find that the damping, defined in Eq. (3.32), $\Gamma_0 \propto 1/a_0^3$, i.e., an increased radius results in a smaller damping [89].

With this result at hand, we investigate next the first-order term $q_1(t) \sim a_1/a_0$ obtained from the inverse Laplace transform of $q_1(z)$ in Eq. (3.20).

$q_1(z)$ can be expressed as

$$\begin{aligned} q_1(z) &= \frac{i\chi_1(z+i\alpha)q_0(z+i\alpha)}{\omega_0^2 - z^2 + i\chi_0(z)} \\ &= iQ_1 \frac{1}{z-z_0}\,\frac{z+i\omega_D}{(z-z_1)(z-z_2)(z-z_3)}\,\frac{z^2+i\omega_D z-\alpha^2-\omega_D\alpha+2i\alpha z}{(z-\bar{z}_1)(z-\bar{z}_2)(z-\bar{z}_3)}\,, \end{aligned} \tag{3.40}$$

where $\bar{z}_i = z_i - i\alpha$ are the shifted roots z_i of Eqs. (3.28)-(3.30),

$$z_0 = -i(\alpha + \omega_D)\,, \tag{3.41}$$

and

$$Q_1 = \frac{3a_1}{a_0}\frac{e^2}{ma_0^3}\chi_D q(t=0)\,. \tag{3.42}$$

After performing the inverse Laplace transform back to the time domain by using the theorem of residues and the physically motivated approximations of Eqs. (3.35)-(3.37), we obtain three terms such that

$$q_1(t) = Q_1 \sum_{j=1}^{3} q_1^{(j)}(t)\,, \tag{3.43}$$

with

$$\begin{aligned} q_1^{(1)}(t) &= \frac{e^{-\omega_D t/3}}{3}\,\frac{\omega_D}{\omega_0^2}\,\frac{1}{\alpha(\alpha^2+\omega_0^2)}\left\{\frac{2}{3}\omega_D + \alpha - \frac{\alpha(5\omega_D-9\alpha)}{2\omega_D+3\alpha} - e^{-\alpha t}\left(\frac{2}{3}\omega_D - \alpha\right)\right\}\,, \\ q_1^{(2)}(t) &= \frac{e^{-\omega_D t/3}}{9\omega_0^2\alpha} \\ &\quad\times \mathrm{Re}\left\{e^{i\omega_0 t}\frac{3\omega_0 - i2\omega_D}{3\omega_0 - i(2\omega_D+3\alpha)}\,\frac{2\omega_D^2+9\omega_0^2-3\omega_D\alpha-9\alpha^2-i(3\omega_D\omega_0+18\alpha\omega_0)}{(i\alpha-\omega_0)(i\alpha-2\omega_0)}\right\}\,, \end{aligned} \tag{3.44}$$

$$q_1^{(3)}(t) = \frac{e^{-[\omega_D/3+\alpha]t}}{9\omega_0^2\alpha}\mathrm{Re}\left\{e^{i\omega_0 t}\frac{3\omega_0 - i(2\omega_D-3\alpha)}{3\omega_0 - i2\omega_D}\,\frac{2\omega_D^2+9\omega_0^2-i3\omega_D\omega_0}{(i\alpha+\omega_0)(i\alpha+2\omega_0)}\right\}\,. \tag{3.45}$$

The results for $q_0(t)$ (black curve) and for $q_1(t)$ (blue curve) with $a_1/a_0 = 0.1$ are shown graphically in Fig. 3.2 for a rather quick shrinking with $\alpha = 5\Gamma_0 \simeq 9\times 10^{-3}\omega_0$. The additional term $q_1(t)$, which reflects the shrinking, is in phase with $q_0(t)$ and has the same frequency as $q_0(t)$. The amplitudes for $q_1(t)$ first grow, reach a maximum and finally decay to zero.

For the chosen shrinking rate $\alpha = 5\Gamma_0$ the maximum magnitude of $q_1(t)$ is reached around $t \approx 150\,\omega_0^{-1}$. After that, the central dipole experiences the shrinking sphere and, thus, an enhanced damping, such that the amplitude of $q_1(t)$ decreases. The maximum

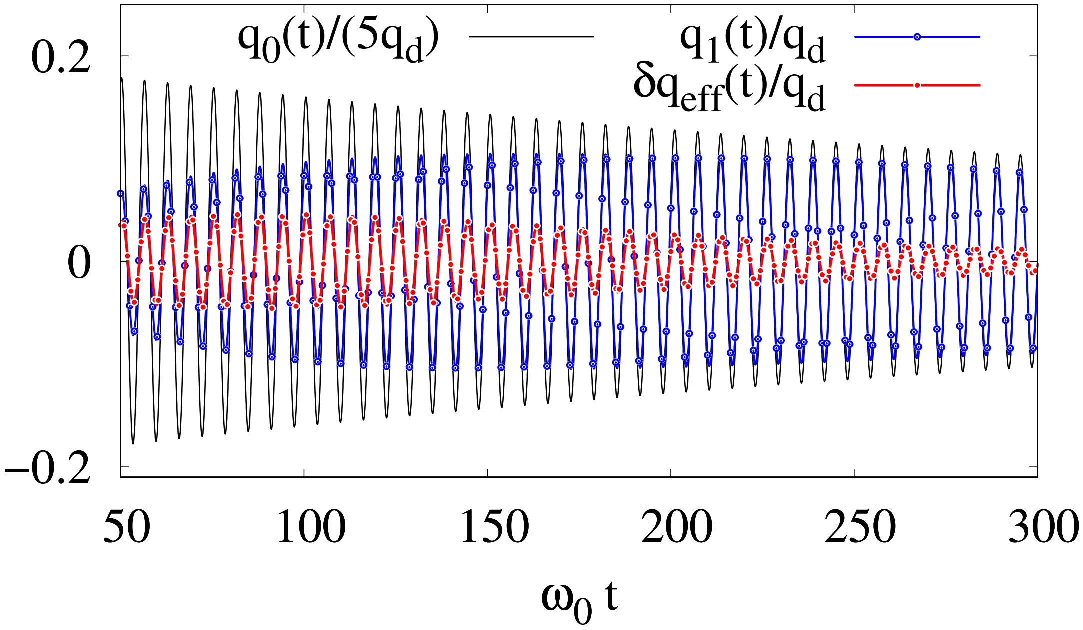

Figure 3.2: Time-dependent displacement $q_0(t)$ (black, reduced by a factor of 0.2) and first-order contribution $q_1(t)$ for $a_1/a_0 = 0.1$ and for the shrinking rate $\alpha = 5\Gamma_0$ (blue) for the parameters given in Sec. 3.2.2. The red curve shows the estimated effective correction $\delta q_{\text{eff}}(t) = q_{\text{eff}}(t) - q_0(t)$ obtained by substituting a_0 in Φ in Eq. (3.22) by the full time-dependent radius $a(t)$ which leads to $q_{\text{eff}}(t)$ for $a_1/a_0 = 0.1$ (see text).

amplitude occurs on a time scale $\alpha^{-1} \simeq 120\,\omega_0^{-1}$. For an increased shrinking rate, the maximal magnitude of the additional term $q_1(t)$ is reached earlier as the sphere shrinks faster. A larger magnitude of a_1 results in a bigger initial radius $a(t = 0) = a_0 + a_1$ of the Onsager sphere where the fluctuating solvent molecules are located further away from the dipole. This gives rise to a more rapid initial increase in $q_1(t)$, see Fig. 3.3. During the shrinking, the fluctuating solvent molecules come closer and their impact increases which happens on the characteristic timescale α^{-1}, before going to zero at infinite time when the final radius a_0 is reached.

As the magnitude a_1 by which the radius changes is much smaller than the static radius a_0, one may approximate the time-dependent $q(t)$ by an effective $q_{\text{eff}}(t)$ which is obtained from the exact $q_0(t)$ in Eq. (3.34) with the constant decay rate Γ_0 of Eq. (3.32) being replaced by a time-dependent decay rate $\Gamma(t) \propto 1/[a(t)]^3$. The resulting $\delta q_{\text{eff}}(t) = q_{\text{eff}}(t) - q_0(t)$ is shown in Fig. 3.2 by the red line for $a_1/a_0 = 0.1$. One observes that

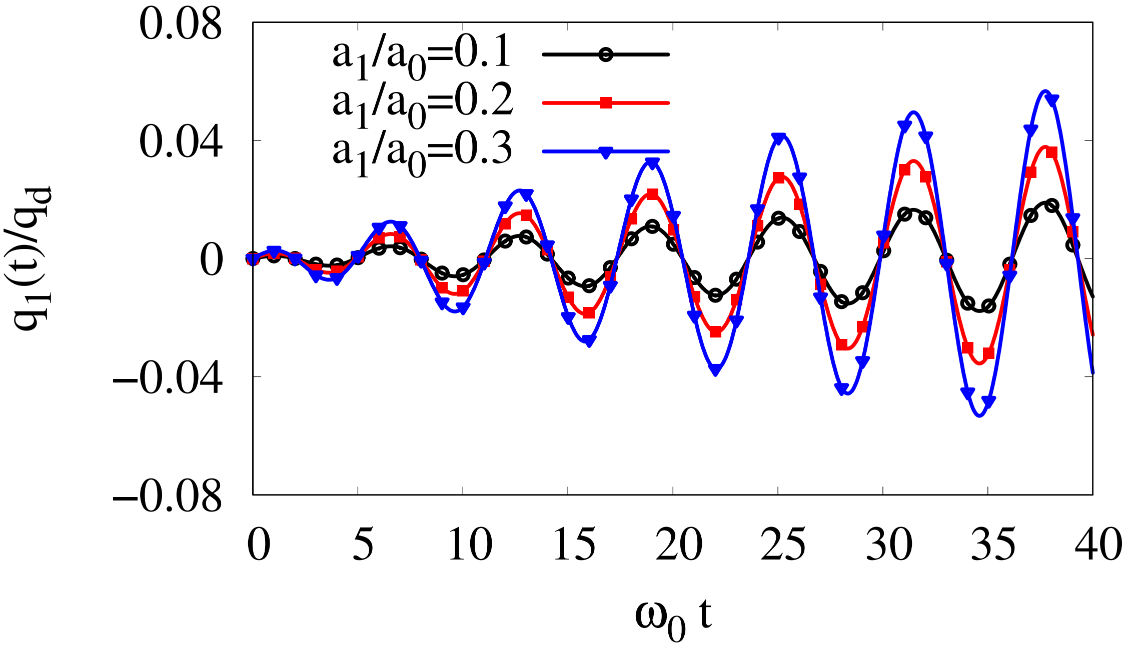

Figure 3.3: Time-dependent first-order contribution $q_1(t)$ for short times for different values of $a_1/a_0 = 0.1$ (black), 0.2 (red), and 0.3 (blue) for $\alpha = 5\Gamma_0$.

this simply estimated correction to $q_0(t)$ considerably underestimates the fully dynamical time evolution. Hence, the time-dependent $a(t)$ induces more involved emerging collective effects which are not captured by an adiabatic approach.

With the expectation value $q(t) = q_0(t) + q_1(t)$ at hand, we can determine the expectation value of the reaction field, given in Eq. (3.11), in response to the dipole moment $\mu(t)$ together with Eq. (3.12). The result is shown in Fig. 3.4. The reaction field of the surrounding medium shows a phase shift of $\pi/2$ relative to the dipole moment $\mu(t) = eq(t)$ and therefore acts as a damping force. The phase shift reflects the rearrangement time of the caging solvent molecules to the momentary configuration of the central dipole moment.

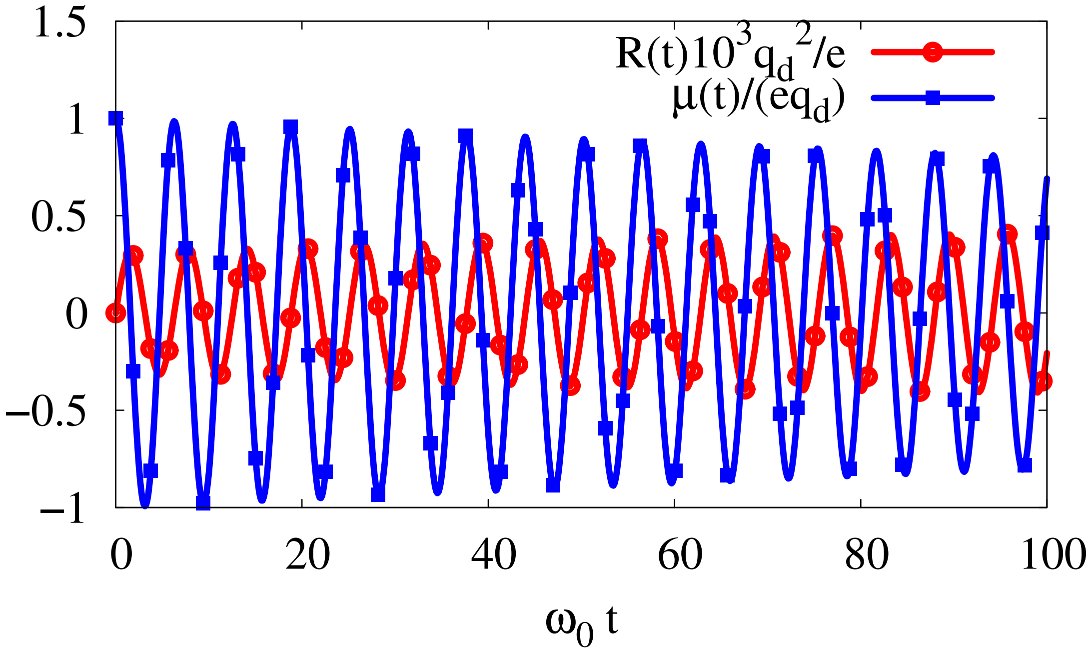

Figure 3.4: Time dependent reaction field $R(t)$ for the time-dependent dipole moment $\mu(t) = eq(t)$ for the parameters given in Sec. 3.2.2, $\alpha = 5\Gamma_0$ and $a_1/a_0 = 0.3$.

Influence of the shrinking rate on damping

To reveal the impact of the shrinking rate α on the damping of the central solute dipole, we consider the driven dynamics with a finite $q_1(t)$. Physically, a larger value of α brings the solvent more rapidly closer to the center of the Onsager sphere and damping is enhanced. The two limiting cases can be obtained from the Onsager radius Eq. (3.17) and the dependence $\Gamma \propto \frac{1}{a^3}$. For $\alpha \to \infty$, the damping rate Γ is given by $\Gamma_0 \propto \frac{1}{a_0^3}$, as is clear from Eq. (3.17). For the opposite limit $\alpha \to 0$, one may set $e^{-\alpha t} \simeq 1$ and obtain the rate Γ_α by replacing the prefactor $\frac{1}{a_0^3} \to \frac{1}{a_0^3}\left[1 - \frac{3a_1}{a_0}\right]$ in the expression for Γ_0, i.e., $\Gamma \to \Gamma_\alpha = (1 - 3a_1/a_0)\Gamma_0$.

To obtain the crossover between the two limiting cases, we exploit the fact that the additional contribution to the expectation value $q_1(t)$ has the same frequency and no phase shift relative to $q_0(t)$. To determine the damping rate Γ, we fit the function $q_{\text{ft}}(t) = q(t = 0)e^{-\Gamma t}\cos[\omega_0 t]$ to $q(t) = q_0(t) + q_1(t)$ in the regime of long times, i.e., in the time window $[100, 200]\omega_0^{-1}$, where possibly fast decaying contributions are suppressed. The result for the dependence of Γ on the shrinking rate α is shown in Fig. 3.5 for $a_1/a_0 = 0.01$. The full result correctly interpolates between the two limits.

For comparison, we also show the damping rate Γ_{eff} determined from fitting the decaying exponential in the same time window as above to the adiabatic time-dependent $q_{\text{eff}}(t)$ in which the static Onsager radius has been replaced by the momentary value $a(t)$. The result is shown in Fig. 3.5 by the red symbols. One observes that the assumption of an effective dynamics leads to an overestimated damping rate as compared to the true dynamics of $q(t)$. This is consistent with the results shown in Fig. 3.2. Hence, we conclude that the relaxation properties of the central dipole are significantly influenced by a time-dependent radius of the Onsager sphere.

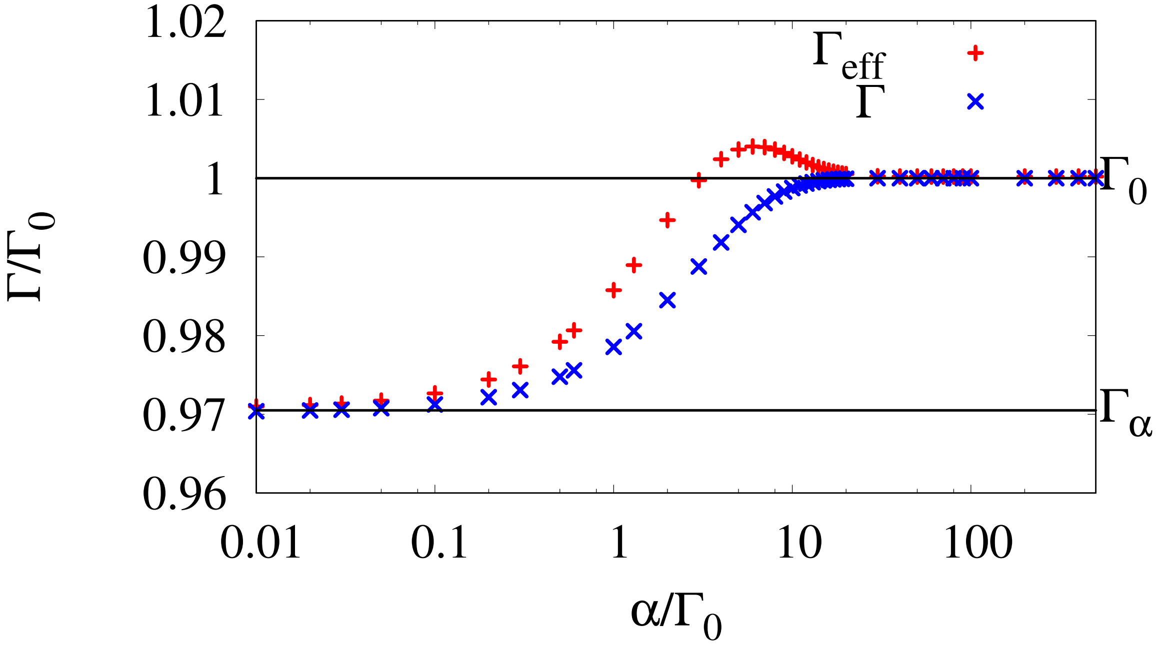

Figure 3.5: Damping rate Γ (blue symbols) as a function of the shrinking rate α for $a_1/a_0 = 0.01$ and for the parameters given in Sec. 3.2.2. The limiting cases are $\Gamma \to \Gamma_0$ for $\alpha \to \infty$ and $\Gamma \to \Gamma_\alpha = \Gamma_0(1 - 3a_1/a_0)$ for $\alpha \to 0$. The red symbols show the effective rate Γ_{eff} obtained from a fit to the approximated dynamics q_{eff}.

Dipole response

We study next the frequency-dependent linear response of the expectation value $\mu(t) = eq(t)$ of the dipole moment in a temporally shrinking sphere to an external harmonic electric force $eE(t)$. The response function contains information about the refraction and the absorption behavior of the test molecule (see Sec. 2.3 and Eq. (2.41) for the response of a continuous dielectric medium). For this, we couple an additional time-dependent external electric field $E(t)$ to $\mu(t)$ via $V_I(t) = -\mu(t)E(t)$ under the assumption that the wavelength of the external field is much larger than the sphere radius a_0 of the Onsager sphere, so that one can disregard any spatial dependence. Additionally, we assume for simplicity that the direction of E is parallel μ.

To determine the response, we again perform the approximation for the prefactor $1/a(t)^3$ as above. Next, we extend the equation of motion (3.15) by the driving term and perform the Laplace transform $f(z) = i\int_0^\infty dte^{izt}f(t)$ to obtain $q_R(z) = q(z) + \delta q(z)$ (see Eq. (A.9) in Appendix A.2). The first term represents the homogeneous part and is discussed in detail in the previous Sec. 3.2.3, while we identify the second term $\delta q(z)$ as the term of the response term to the applied external field, i.e.,

$$\delta q(z) = X_0(z)[E(z) + iW_1(z+i\alpha)E(z+i\alpha)], \tag{3.46}$$

where

$$\begin{aligned} X_0(z) &= \frac{e}{m[\omega_0^2 - z^2 + i\chi_0(z)]}, \\ W_1(z) &= \frac{\chi_1(z)}{\omega_0^2 - z^2 + i\chi_0(z)}. \end{aligned} \tag{3.47}$$

In the real-time domain and for $a_1 \ll a_0$, $\delta q(t)$ can be written in the form

$$\delta q(t) = i\int_0^t dsX(t,s)E(t-s), \tag{3.48}$$

where $s \leq t$ and where

$$\begin{aligned} X(t,s) &= X_0(s) - e^{-\alpha t}\int_0^s due^{\alpha u}X_0(u)W_1(s-u) \\ &= X_0(s) - e^{-\alpha t}X_1(s). \end{aligned} \tag{3.49}$$

Adiabatic limit

In order to obtain a frequency-dependent response function, which depends explicitly on the time t, we again perform a Laplace transform of Eq. (3.48), while one is only interested in the real part of z, which is the frequency part. According to the chosen definition of the Laplace transform, we identify the physical response function as $X(t, \omega) \equiv -iX(t, \mathrm{Re}[z])$. The adiabatic limit holds when the shrinking rate $\alpha \ll \Gamma_0$, where Γ_0 in Eq. (3.39) is the decay rate of $X_0(s)$. Then, the time-dependent prefactor $e^{-\alpha t}$ can be treated adiabatically and the response function in the frequency domain reads

$$X(t, \omega) = X_0(\omega) + ie^{-\alpha t} X_0(\omega - i\alpha) W_1(\omega) \,. \tag{3.50}$$

The response function in the adiabatic limit contains two terms. The first one reflects the response of the dipole moment to the external field for a static sphere with constant radius a_0. The second term includes all shrinking effects and is linear in a_1/a_0. Figures 3.6 and 3.7 show the real and imaginary part of the response function at different times t after initial preparation of the dipole moment $\mu(t = 0) = eq_d$ at $t = 0$.

At time $t = 0$, the impact of the shrinking on the response function is most pronounced due to the second term of Eq. (3.49). The real part of the response function is associated with the refraction of the incoming light and the imaginary part is connected to the absorption of the central dipole moment in the shrinking Onsager cavity according to (molecular) absorption of general dielectric media discussed in Sec. 2.3. The imaginary part has a maximum at ω_0 and shows an enhancement of up to 40% (Fig. 3.6 b) for its maximum, which decays exponentially with time (e.g., Fig. 3.7 b at intermediate time $t = 40\Gamma_0^{-1}$). The exponential decay of the maximum is shown in Fig. 3.8.

Interestingly, a bigger shrinking rate α shows an initially more pronounced response which rapidly decays with time, while the response function for a smaller α decreases more slowly. The physical meaning is that for a slower shrinking, the final radius a_0 is reached later, the action of the fluctuating environment comes later closer to the dipole, such that effectively, damping is reduced and the response is enhanced for a longer time period. In turn, the broadening of the imaginary part is narrower for longer times.

As a side remark, one may fit a Lorentzian to the imaginary part $X''(\omega)$ of Eq. (3.50) and read of its full width at half maximum which is equal to Γ for different shrinking rates α shown in Fig. 3.5 for $a_1/a_0 = 0.01$.

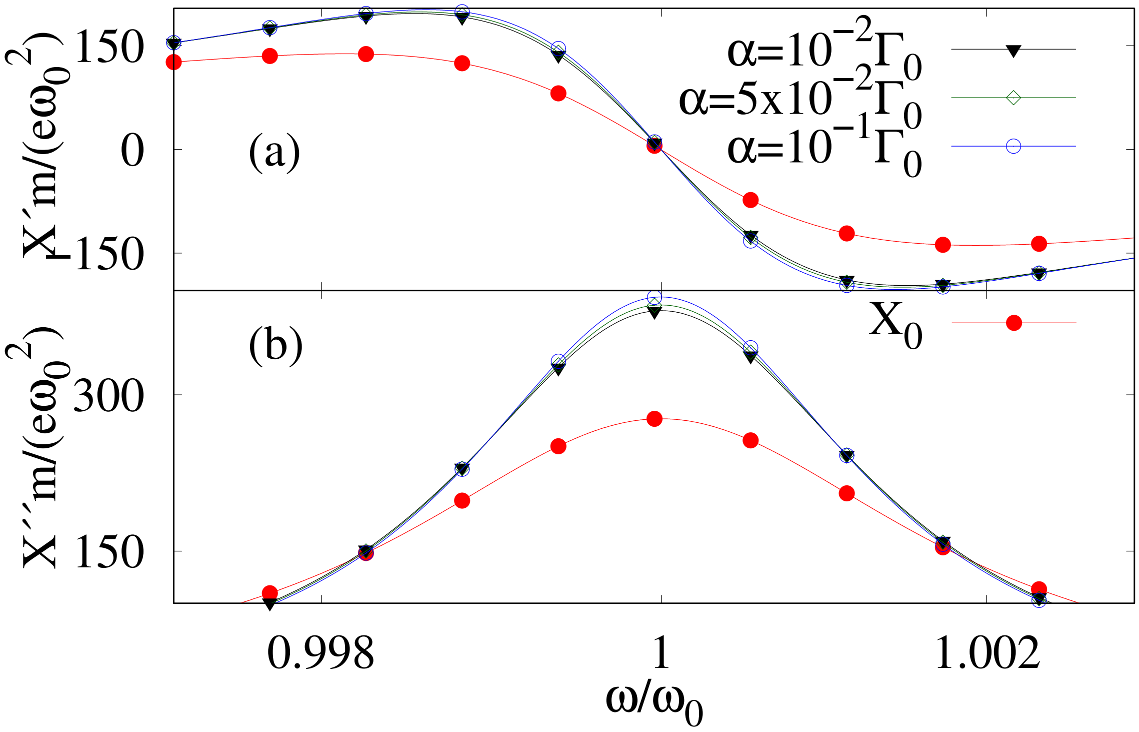

Figure 3.6: Real (a) and imaginary (b) part of the response function $X(t=0,\omega)$ at initial time $t=0$ in the adiabatic limit for different shrinking rates α for $a_1 = 0.1a_0$ for the solvent parameters of water (see text).

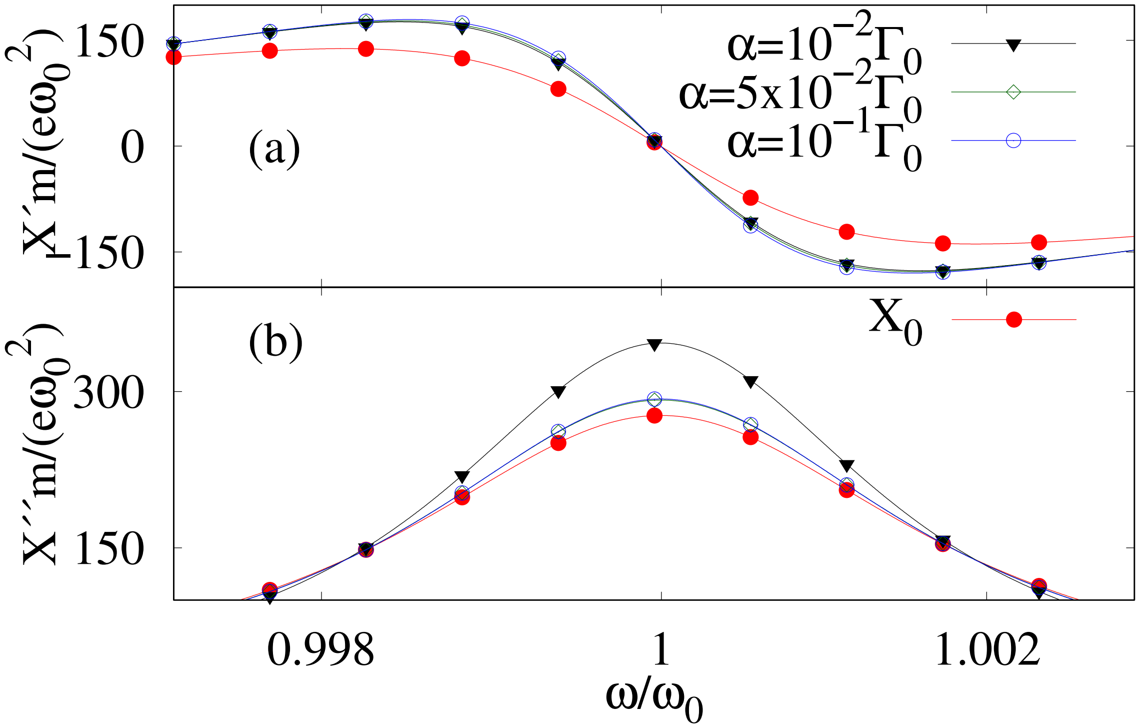

Figure 3.7: Real (a) and imaginary (b) part of the response function $X(t=40\Gamma_0^{-1},\omega)$ at intermediate time $t=40\Gamma_0^{-1}$ in the adiabatic limit for different shrinking rates α for $a_1 = 0.1a_0$.

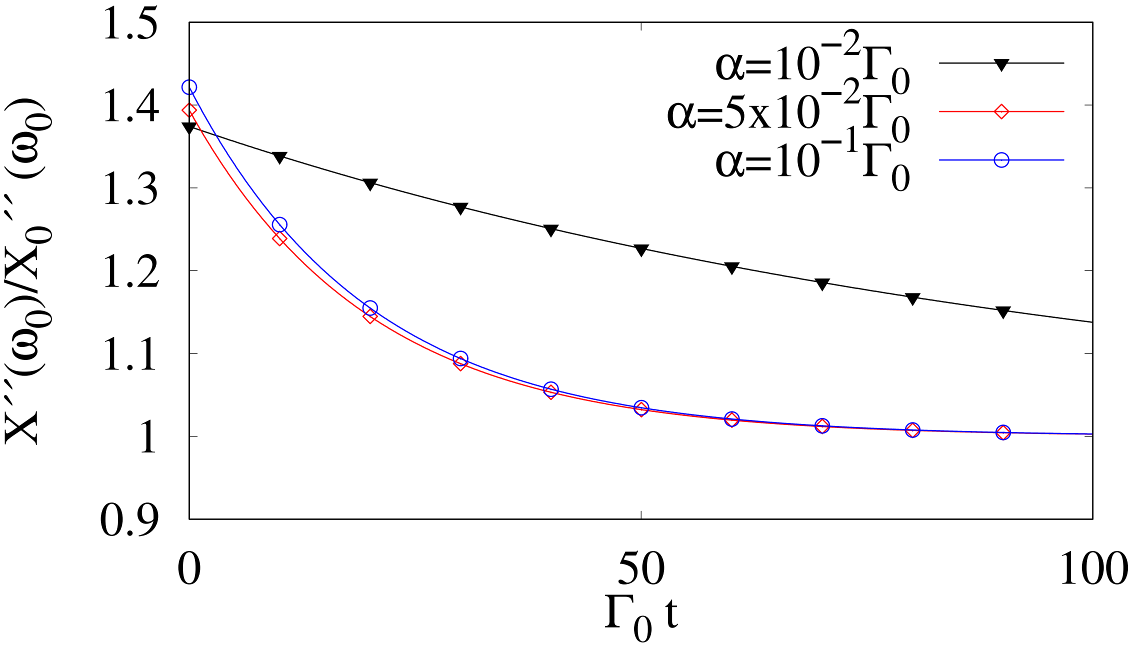

Figure 3.8: The maximum of the imaginary part $X''(t,\omega_0)/X_0''(t,\omega_0)$ at different times for different shrinking rates α for $a_1 = 0.1a_0$.

Beyond the adiabatic limit

In order to get information about the dipole response beyond the adiabatic limit for larger shrinking rates, we couple the dipole to an explicit monochromatic electric field $E(t) = E_0 \cos[\omega_{ex} t]$. We are then able to calculate the response $-i\delta q(\mathrm{Re}[z]) \equiv \delta q(\omega)$ according to Eq. (3.46) to this specific choice of the electric field. We define the effective response function $\delta q(\omega)/E(\omega)$ and show the results in Fig. 3.9. If the frequency of the external field is in resonance with the dipole frequency, $\omega_{ex} = \omega_0$, we finds an interesting behavior. For $0 \leq \alpha \leq 0.5\Gamma_0$, the maximum at $\omega = \omega_0$ turns into a dip and two peaks around the dipole eigenfrequency appear in the imaginary part of the response. With increasing shrinking rate, the two peaks move further apart from each other and disappear again at $\alpha \geq 0.5\Gamma_0$ while the central linewidth becomes broader. The analysis of calculating the damping rate Γ of the dipole moment leads back to the idea of fitting a single Lorentzian to the imaginary part around the eigenfrequency ω_0 which becomes broader for faster shrinking. We note that the effective response function $\delta q(\omega)/E(\omega)$ still contains functional signatures of the applied electric field since the charge displacement $\delta q(\omega)$ and the stimulating field $E(\omega)$ depend on each other in a nonlinear way, see Eq. (3.46). The effective response reflects only a global responsive behavior away from the frequency ω_{ex} of the incoming light field. The observed dip results from the sharp feature of the monochromatic electric field around ω_{ex}. We observe that the incoming field enters as $E(\omega + i\alpha)$ in the nonlinear response of Eq. (3.46) and depends on the shrinking rate α. We thus conclude that the distance between the two maximum frequencies forming the dip, $w = \omega_{max,2} - \omega_{max,1}$, can be used to determine the shrinking rate α. Fig. 3.10 represents the distance between the maximum frequencies for different shrinking rates. Their distance grows with enhanced shrinking rate before it drops and eventually disappears. For small shrinking rates, $a \leq 0.1\Gamma_0$, we find that the distance of the maximum frequencies shows a dependence $w \propto \sqrt{\alpha}$.

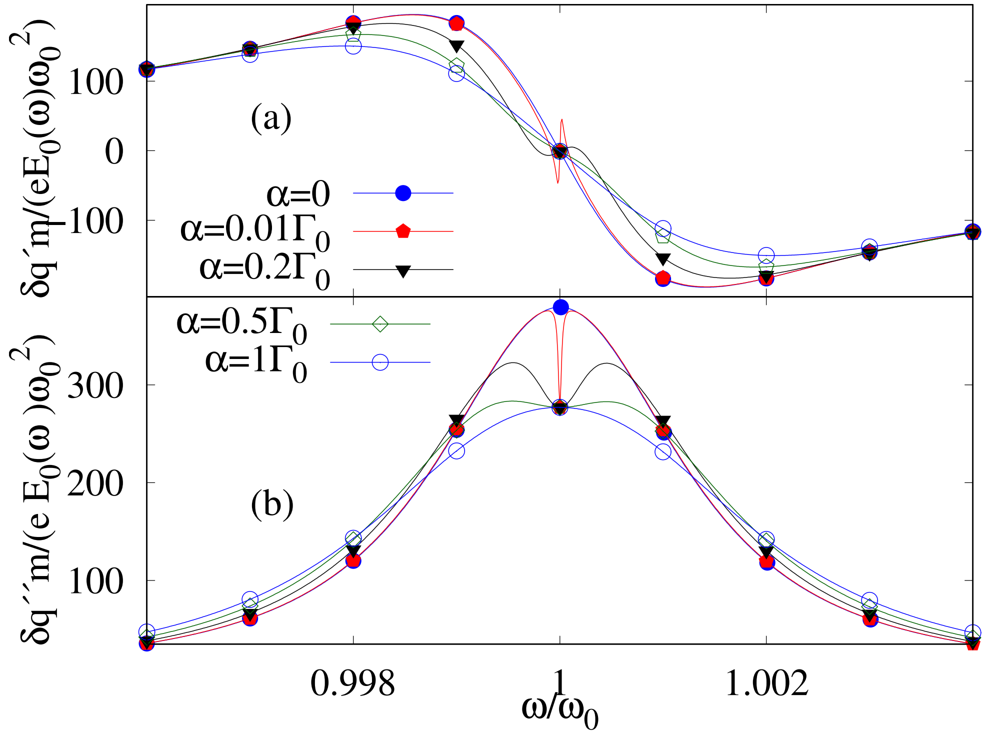

Figure 3.9: The (a) real and (b) imaginary part of the effective response $\delta q(\omega)/E(\omega)$ for a monochromatic electric field with $\omega_{ex} = \omega_0$ for $a_1 = 0.1a_0$ for different shrinking rates α.

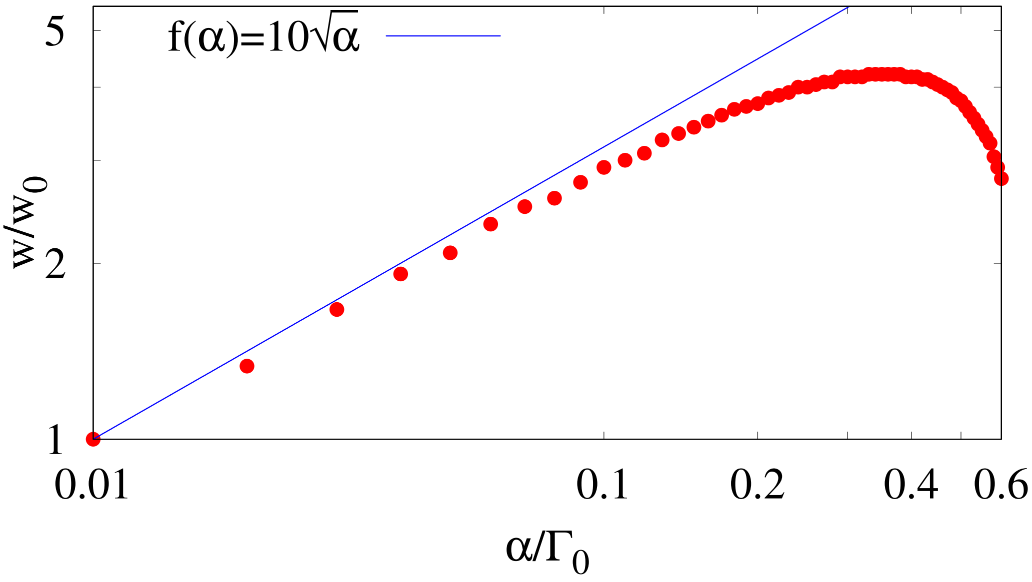

Figure 3.10: Distance between the maximum frequencies $w = \omega_{max,2} - \omega_{max,1}$ of the effective response $\delta q(\omega)/E(\omega)$ for a monochromatic electric field with $\omega_{ex} = \omega_0$ for $a_1 = 0.1a_0$ for different shrinking rates α. The difference w_0 is determined for the rate $\alpha = 0.01\Gamma_0$. The function $f(\alpha) = 10\sqrt{a}$ is a fit to the data for small shrinking rates.

3.2.4 Breathing Onsager Sphere

Another physically relevant configuration is a breathing Onsager sphere with the dynamic radius

$$a(t) = a_0 + a_2(t) = a_0 + a_2\,\alpha\,t\,e^{1-\alpha t}\,\Theta(t), \tag{3.51}$$

which is chosen such that we obtain the maximum value $a_{\max}(t_{\max} = 1/\alpha) = a_0 + a_2$ at $t_{\max} = 1/\alpha$. During this dynamics the radius first growths from $a(t = 0) = a_0$ to the maximum value $a(t_{\max}) = a_0+a_2$ and then returns to $a(t \to \infty) = a_0$. This time-dependent behavior covers excitation and de-excitation of photoexcited molecules accompanied by spatial breathing [77].

Time evolution of the dipole moment

We calculate the impact of the breathing Onsager sphere on the expectation value $\mu(t) = eq(t)$ of the central dipole moment. In following the same calculus as in Sec. 3.2.3, we again expand the prefactor $1/a(t)^3$ in a Taylor series up to first order in the time-dependent part. This is valid when the magnitude a_2 by which the radius changes is much smaller than the static radius a_0. One finds

$$\begin{aligned}\frac{1}{a(t)^3} &\simeq \frac{1}{a_0^3}\left[1 - \frac{3a_2}{a_0}\alpha t e^{1-\alpha t}\right] \\ &= \frac{1}{a_0^3}\left[1 - \frac{3a_2}{a_0}\alpha \exp[1]\left(-\frac{\partial}{\partial\alpha}\right)e^{-\alpha t}\right],\end{aligned} \tag{3.52}$$

so that we can again split the linear the response function into $\chi_0(t) + \chi_2(t)$, since we are only interested in first order contributions of a_2/a_0, the prefactor of $\chi_2(t) = 3a_2/a_0 \exp(1)\chi_0(t)$. We perform a Laplace transform of Eq. (3.15). It is helpful to define the Laplace transform of the susceptibility for the breathing

$$\chi_2(z) = -\frac{3a_2}{a_0}\exp(1)\frac{e^2}{ma_0^3}\frac{\chi_D}{(\omega_D - z)^2}\,. \tag{3.53}$$

To obtain an analytic solution in the form $q(t) = q_0(t) + q_2(t)$, we need to determine the inverse Laplace transform of the dynamic part

$$\begin{aligned} q_2(z) &= -\alpha\frac{\partial}{\partial\alpha}\frac{i\chi_2(z+i\alpha)q_0(z+i\alpha)}{\omega_0^2-z^2+i\chi_0(z)} \\ &= -iQ_2\frac{\partial}{\partial\alpha}\left[\frac{1}{z-z_0}\frac{z+i\omega_D}{(z-z_1)(z-z_2)(z-z_3)}\frac{z^2+i\omega_D z-\alpha^2-\omega_D\alpha+2i\alpha z}{(z-\bar{z}_1)(z-\bar{z}_2)(z-\bar{z}_3)}\right], \end{aligned} \tag{3.54}$$

where $\bar{z}_i = z_i - i\alpha = \bar{z}_i(\alpha)$ are the shifted roots z_i of Eqs. (3.28)-(3.30) and explicitly depend on α. Moreover, z_0 is given by Eq. (3.41) and also depends on α. Furthermore,

$$Q_2 = \frac{3a_1\alpha\exp(1)}{a_0}\frac{e^2}{ma_0^3}\chi_D q(t=0)\,. \tag{3.55}$$

Performing the inverse Laplace transform by exploiting the theorem of residues, we obtain the solution $q(t) = q_0(t) + q_2(t)$ in the time domain, where $q_0(t)$ is known from Eq. (3.34). The solution $q_2(t)$ reads with the assumption of the physical model parameters (Subsec. 3.2.2)

$$q_2(t) = Q_2\sum_{j=1}^{4} q_2^{(j)}(t), \tag{3.56}$$

with

$$\begin{aligned}
q_2^{(1)}(t) &= e^{-\omega_D t/3}\,\frac{2}{3}\frac{\omega_D}{\omega_0^2}\,\frac{1}{\alpha(\alpha^2+\omega_0^2)}\,\frac{2\omega_D^2-3\omega_D\alpha-9\alpha^2}{3\alpha+2\omega_D} \qquad (3.57)\\
&\times\left\{\frac{-\omega_D-6\alpha}{9(2\omega_D^2-3\omega_D\alpha-9\alpha^2)}-\frac{1}{3\alpha+2\omega_D}+\frac{1}{3\alpha}-\frac{2\alpha}{3(\omega_0^2+\alpha^2)}\right\}\,,\\
q_2^{(2)}(t) &= e^{-(\omega_D/3+\alpha)t}\,\frac{2\omega_D-3\alpha}{2\omega_0^2}\,\frac{1}{9\omega_D\alpha(\alpha^2+\omega_0^2)} \qquad (3.58)\\
&\times\left\{-3\omega_D+\omega_D^2\left(2t+\frac{2}{2\omega_D-3\alpha}+\frac{2}{\alpha}-\frac{4\alpha}{\omega_0^2+\alpha^2}\right)\right\}\,,\\
q_2^{(3)}(t) &= e^{-\omega_D t/3}\frac{1}{9\omega_0^2\alpha}\mathrm{Re}\\
&\left\{e^{i\omega_0 t}\frac{(2\omega_D+3i\omega_0)(-9\alpha^2-3\alpha\omega_D+2\omega_D^2+9\omega_0^2-18i\omega_0\alpha-3i\omega_D\omega_0)}{2\omega_D+3\alpha+3i\omega_0}\right.\\
&\times\left[\frac{-\omega_D-6i\omega_0-6\alpha}{3(2\omega_0^2-\alpha^2-3i\alpha\omega_0)(-9\alpha^2-3\alpha\omega_D+2\omega_D^2+9\omega_0^2-18i\omega_0\alpha-3i\omega_D\omega_0)}\right.\\
&-\frac{3}{(2\omega_0^2-\alpha^2-3i\alpha\omega_0)(2\omega_D+3\alpha+3i\omega_0)}+\frac{1}{(-\omega_0+i\alpha)^2(2i\omega_0+\alpha)}\\
&\left.\left.-\frac{2}{\alpha(-2\omega_0+i\alpha)^2}\right]\right\},\\
q_2^{(4)}(t) &= e^{-(\omega_D/3+\alpha)t}\frac{1}{\omega_0^2\alpha}\mathrm{Re}\left\{e^{i\omega_0 t}\frac{3\alpha-2\omega_D-3i\omega_0}{2\omega_0^2+3i\omega_0\alpha-\alpha^2}\left[\frac{-2\omega_D-12i\omega_0}{6\omega_D+9i\omega_0}-\frac{2\omega_D^2-3i\omega_D\omega_0+9\omega_0^2}{3(2\omega_D+3i\omega_0)^2}\right.\right.\\
&+\frac{(2\omega_D^2-3i\omega_D\omega_0+9\omega_0^2)t}{9(2\omega_D+3i\omega_0)}-\frac{2\omega_D^2-3i\omega_D\omega_0+9\omega_0^2}{3(2\omega_D+3i\omega_0)(-2\omega_D-3i\omega_0+3\alpha)}\\
&+(2\omega_D^2-3i\omega_D\omega_0+9\omega_0^2)\left(-\frac{1}{3(2\omega_D-3i\omega_0)^2}-\frac{-2i\omega_0+\alpha}{9(2\omega_0^2+3i\alpha\omega_0-\alpha^2)(2\omega_D+3i\omega_0)}\right.\\
&\left.\left.\left.-\frac{1}{9\alpha(2\omega_D+3i\omega_0)}+\frac{i\omega_0+\alpha}{9(2\omega_D+3i\omega_0)(2\omega_0^2+3i\alpha\omega_0-\alpha^2)}\right)\right]\right\}. \qquad (3.59)
\end{aligned}$$

The time-evolution of the dipole moment according to $q(t) = q_0(t) + q_2(t)$ is shown in Fig. 3.11. The driven part $q_2(t)$ is shown for different breathing rates and compared to the undriven part $q_0(t)$. For the breathing sphere, a relative phase shift between $q_0(t)$ and $q_2(t)$ can be observed. For smaller breathing rates $\alpha/\Gamma_0 < 1$, the phase shift persists much longer than for the larger breathing rates.

Next, we compare the two cases of a time-dependent shrinking $a_1(t)$ with the time-dependent breathing $a_2(t)$ Onsager radius regarding their impact on the time evolution of $q(t)$ at longer (but still non-asymptotic) times. The comparison is shown in Fig. 3.12 for the same value of the time constant $\alpha = 0.1\Gamma_0$ and for $a_{1/2} = 0.1a_0$. At long times,

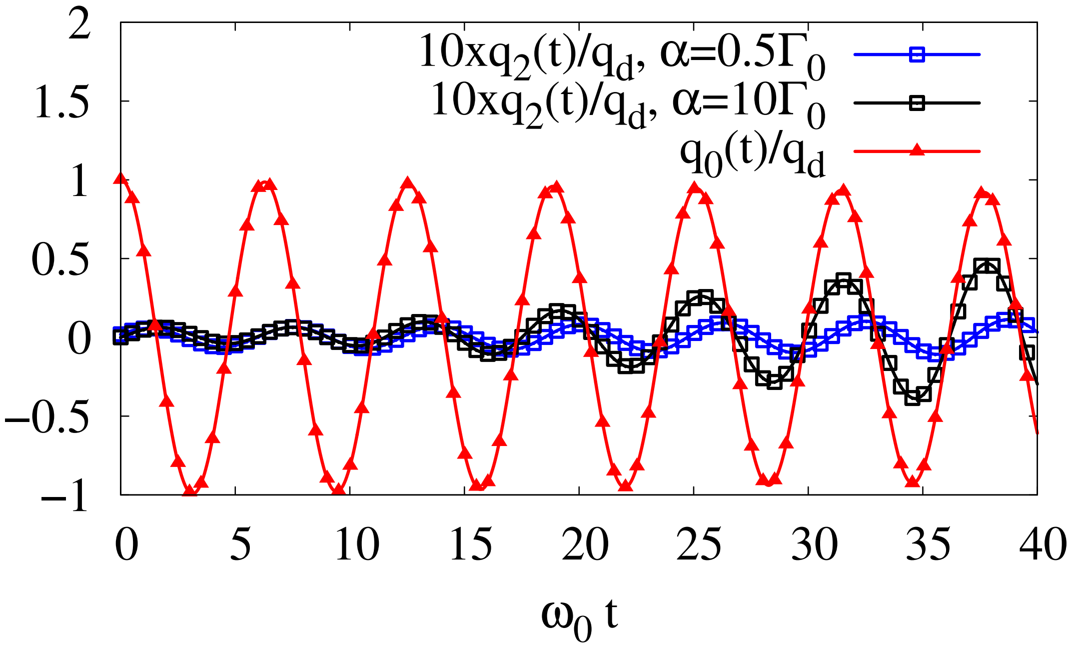

Figure 3.11: Dynamics of the dipole moment according to $q(t) = q_0(t) + q_2(t)$. The driven part $q_2(t)$ is shown for different breathing rates $\alpha = 0.5\Gamma_0$ (blue, scaled by a factor of 10) and $\alpha = 10\Gamma_0$ (black, scaled by a factor of 10) for $a_2/a_0 = 0.3$ and for the parameters as given in Sec. 3.2.2. The undriven part $q_0(t)$ is shown in red.

both cases show in-phase oscillations with $q_0(t)$. In general, the shrinking results in a more pronounced impact on the dipole oscillations than the breathing.

Influence of the breathing rate on damping

The parameter α determines the scale of the time-dependent breathing behavior of the Onsager radius $a(t) = a_0 + a_2(t)$. In turn, the time scale of the damping of the dipole is given by Γ_0 and the interplay of both can affect the overall damping rate Γ of the breathing system. In order to determine the overall damping rate Γ, we again fit the function $q_{\text{ft}}(t) = q(t = 0)e^{-\Gamma t} \cos[\omega_0 t]$ to $q(t)$, but now regarding the additional term which respects the breathing behavior of the Onsager radius $a(t) = a_0 + a_2(t)$. The initial phase shift is neglected by restricting the fitting to the time window $\omega_0 t > 300$. The result for the damping rate is shown in Fig. 3.13.

For small rates $\alpha \ll \Gamma_0$, the maximal extension of the sphere is reached only at long

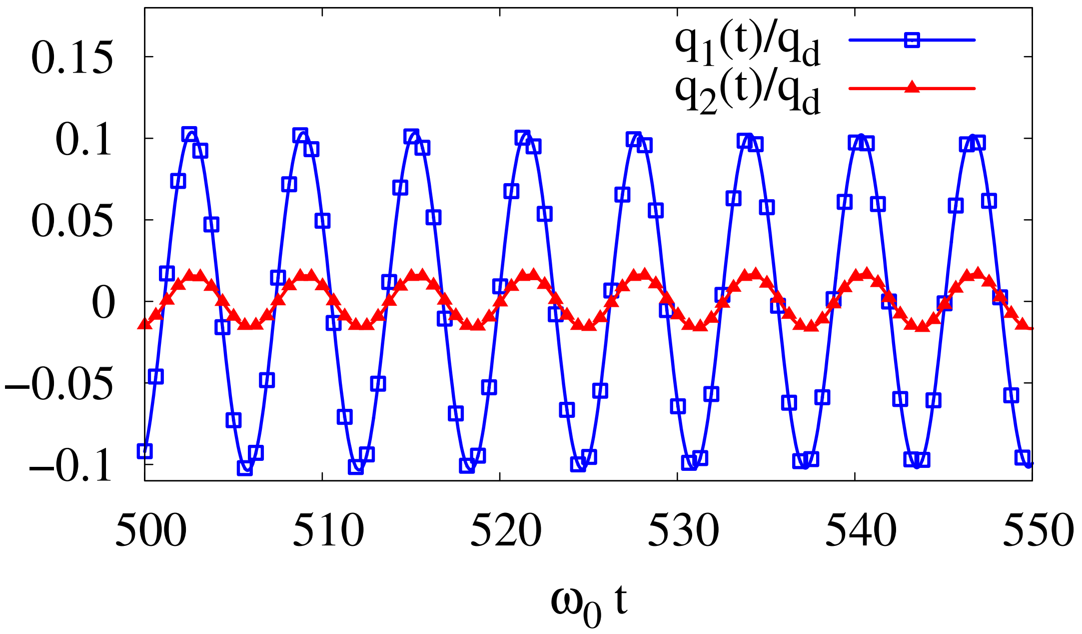

Figure 3.12: Dynamics of the driven parts $q_1(t)$ (shrinking sphere, blue) and $q_2(t)$ (breathing sphere, red) at intermediate times for $a_1 = a_2 = 0.1a_0$, $\alpha = 0.1\Gamma_0$, and for the parameters given in Sec. 3.2.2.

times $\sim 1/\alpha \to \infty$, so that the radius largely persists at a_0. Moreover, α enters as a prefactor in $a_2(t)$, so that the additional term of the dynamics $q_2(t)$ is negligible, and, thus, $\Gamma \to \Gamma_0$. For large breathing rates $\alpha \gg \Gamma_0$, the breathing occurs very rapidly, so that the dipole does not have enough time to respond and largely 'sees' again an Onsager sphere with radius a_0, so that $\Gamma \to \Gamma_0$. In between, when $\alpha \approx \Gamma_0$, the environmental solvent molecules are mostly pushed away from the central dipole while it relaxes, so that its damping is reduced. This effect is maximal when $\alpha = \Gamma_0$, pointing to an interesting resonant reduction of the damping. As can be seen for our choice of realistic model parameters, the reduction of the damping can amount to almost 30% in the resonance region, an effect that should be detectable by spectroscopic means.

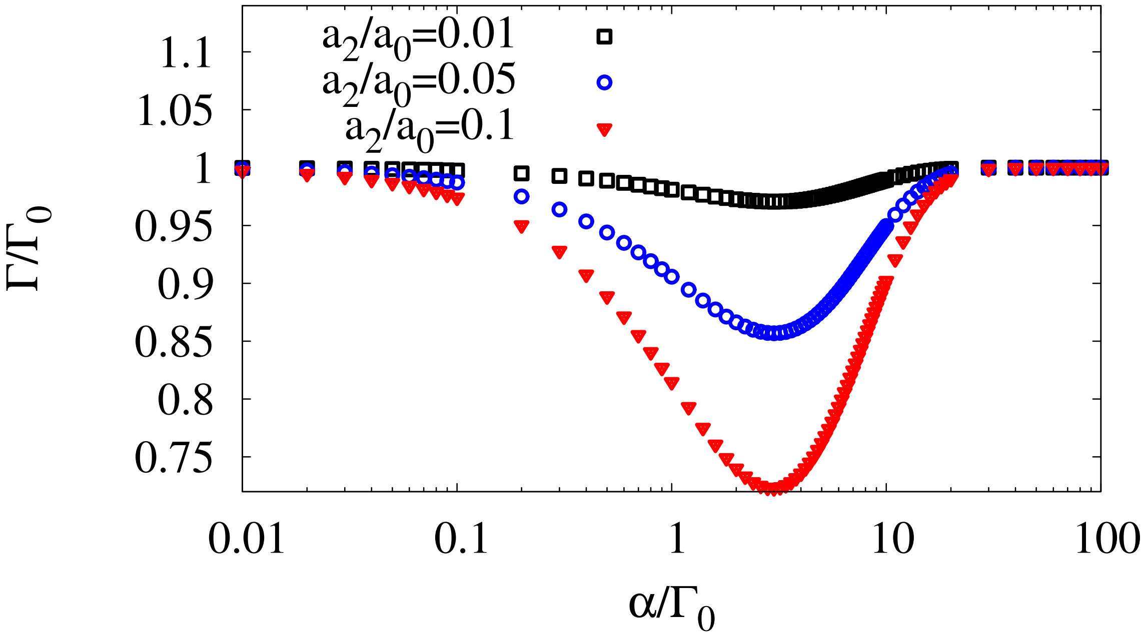

Figure 3.13: Dependence of the asymptotic damping rate Γ on the breathing rate α for different breathing amplitudes for the parameters given in Sec. 3.2.2.

Dipole response

We study next the linear response function of the dipole moment $\mu(t)$ in the breathing sphere to an externally driven electric field $E(t)$, analogously to Sec. 3.2.3. As before, the wavelength of the external field is assumed to be much larger than the static sphere radius a_0, so that we can disregard the spatial dependence of $E(t)$. Additionally, the external electric field $E(t)$ is assumed to be parallel to the dipole moment $\mu(t)$.

The equation of motion in Laplace space again takes the form $q_R(z) = q(z) + \delta q(z)$, where $q(z)$ (and its time equivalent) is studied in detail in Sec. 3.2.4 and the term $\delta q(z)$ arises from the external field $eE(z)$ (see Eq. (A.9) in Appendix A.2). $\delta q(z)$ is given by Eq. (3.46), where $W_1(z)$ now takes the form

$$W_1(z) = -\alpha \frac{\partial}{\partial \alpha} \frac{\chi_2(z)}{\omega_0^2 - z^2 + i\chi_0(z)}. \tag{3.60}$$

In the real-time domain,

$$\delta q(t) = i \int_0^t ds X(t,s) E(t-s)\,, \tag{3.61}$$

where

$$X(t,s) = X_0(s) + i\alpha \frac{\partial}{\partial \alpha} e^{-\alpha t} \int_0^s du e^{\alpha u} X_0(u) W_1(s-u). \tag{3.62}$$

Adiabatic limit

When performing the Laplace transform of $X(t,s)$, we again assume $\alpha \ll \Gamma_0$, the decay rate of $X_0(s)$. Thus, the time-dependent prefactor can be treated adiabatically. The Laplace transform of the response function for the breathing sphere then becomes

$$\begin{aligned} X(t,\omega) = X_0(\omega) + i\alpha t e^{-\alpha t} X_0(w - i\alpha) W_1(\omega) \\ - i\alpha e^{-\alpha t} \frac{\partial}{\partial \alpha} X_0(\omega - i\alpha) W_1(\omega)\,, \end{aligned} \tag{3.63}$$

where the real part of the Laplace variable $\mathrm{Re}[z] \equiv \omega$ reflects the frequency. According to our definition of the Laplace transform, the physical response is identified as $X(t,\omega) \equiv -iX(t,\omega = \mathrm{Re}[z])$.

At initial time $t = 0$, the response of the dipole moment in a breathing sphere does not differ from the dipole moment in the static sphere. We show the results for a later time $t =$

$20\Gamma_0^{-1}$ in Fig. 3.14. We observe again a more pronounced response function which finally drops to the form of a static sphere (Fig. 3.15, e.g., the imaginary part). Especially the imaginary part which reflects the absorption of the dipole moment is temporally enhanced by up to 40% as compared to the static case. A smaller breathing rate α shows a weaker impact on the response. Additionally the broadening of the line shape of the absorptive part is reduced at different times for different rates α. A intermittently smaller broadening is connected to a momentary reduced damping of the central dipole moment. The maximum radius $a(t = 1/\alpha) = a_0 + a_2$ of the breathing sphere is reached at the time $t = 1/\alpha$ where the fluctuating environment is spatially maximally far away from the dipole moment, while its damping is reduced the most. Thus, the time-dependent response function carries clear signatures of the breathing of the Onsager sphere.

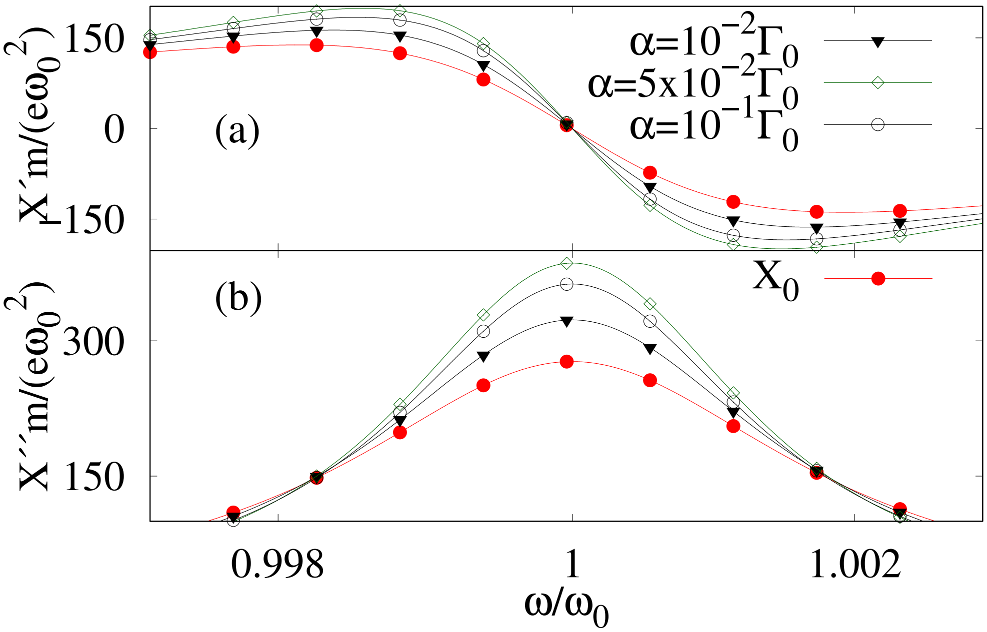

Figure 3.14: Real (a) and imaginary (b) part of the response function $X(t = 20\Gamma_0^{-1}, \omega)$ for different breathing rates α for $a_2 = 0.1a_0$ in the adiabatic limit. Note that $\Gamma_0 = 22.2 \times 10^{-4}\omega_0$ for the parameters given in Sec. 3.2.2.

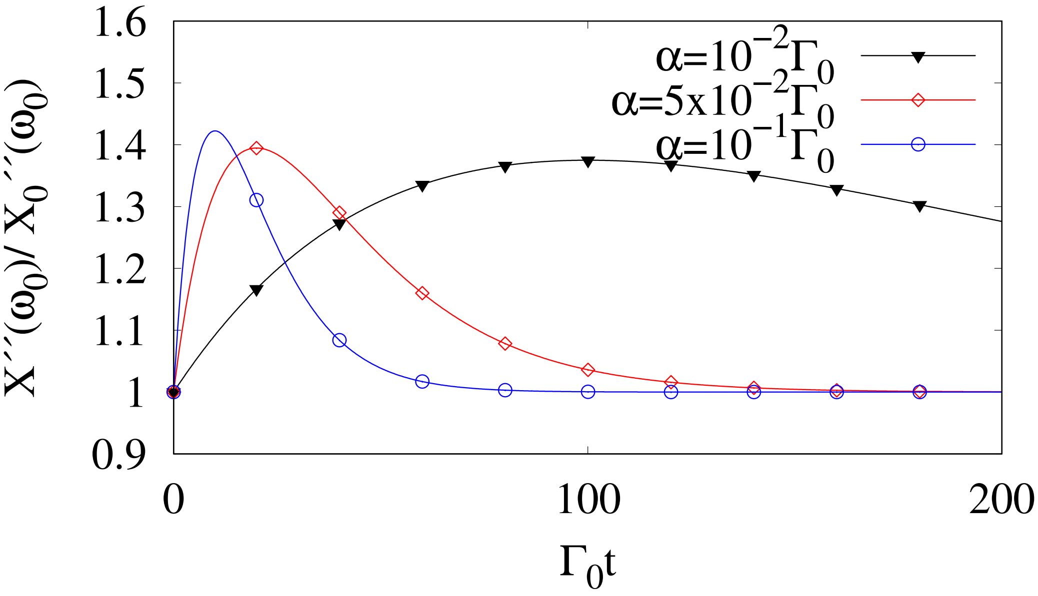

Figure 3.15: Time-dependent maximum of $X''(t, \omega_0)$ of the response function for $a_2 = 0.1a_0$ for different breathing rates.

Beyond the adiabatic limit

The effective response $\delta q(\omega)/E(\omega)$ to an electric field $E(t) = E_0 \cos[\omega_{ex} t]$ leads also to a split in two peaks shifted around the dipole eigenfrequency ω_0, while the central peak remains the most pronounced. This is shown in Fig. 3.16. The splitting first increases with an enhanced breathing rate until it disappears at $\alpha \geq 0.4\Gamma_0$. At $\alpha \approx \Gamma_0$ we observe the narrowest line width which eventually becomes broader with increasing breathing rate, see Fig. 3.16. This can be again recovered by recording the full width at half maximum of a single Lorentzian fit to the imaginary part, see discussion in Sec. 3.2.3. These results are shown in Fig. 3.13 as fitted damping rates to the real-time dipole dynamics $q(t)$. We emphasize again that the effective response $\delta q(\omega)/E(\omega)$ reflects only a global behavior away from the frequency ω_{ex} of the incoming light field while the behavior around $\omega_{ex} = \omega_0$ results from the sharp feature of the monochromatic electric field since the charge displacement $\delta q(\omega)$ is non-linearly related to the stimulating electric field $E(\omega)$, see Eq. (3.46). Due to the non-linearity of the response function of Eq. (3.46), the signatures of $E(\omega + i\alpha)$ results in pronounced dips in the effective response function varying with the breathing rate α. Fig. 3.17 shows the distance between the outer maximum frequencies forming the dips for different breathing rates. Their distance grows with enhanced breathing rate before it disappears. We find that the distance of the maxima shows an overall dependence $w \propto \sqrt{\alpha}$.

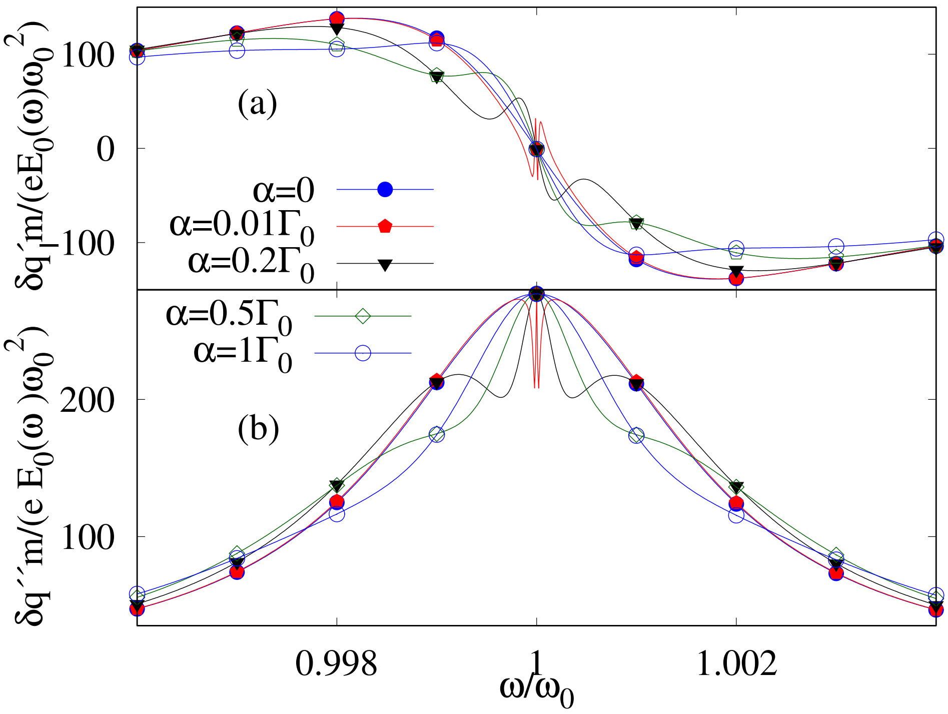

Figure 3.16: The (a) real and (b) imaginary part of the effective response $\delta q(\omega)/E(\omega)$ for a monochromatic electric field at eigenfrequency $\omega_{ex} = \omega_0$ for $a_1 = 0.1a_0$ and different breathing rates α.

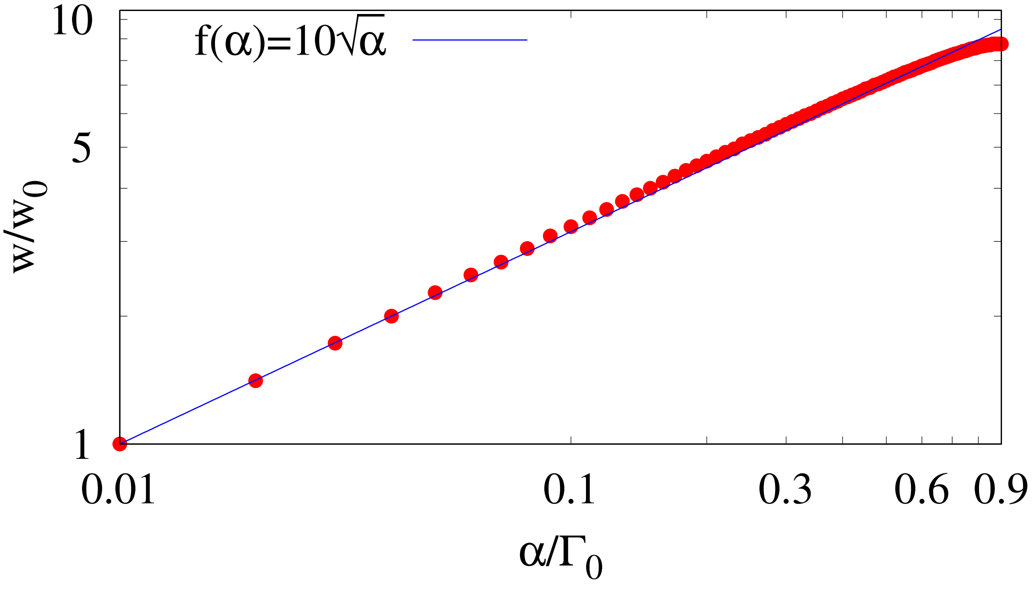

Figure 3.17: Distance between the maximum frequencies $w = \omega_{max,2} - \omega_{max,1}$ of the effective response $\delta q(\omega)/E(\omega)$ for a monochromatic electric field with $\omega_{ex} = \omega_0$ for $a_1 = 0.1a_0$ for different breathing rates α. The difference w_0 is determined for the rate $\alpha = 0.01\Gamma_0$. The function $f(\alpha) = 10\sqrt{a}$ is a fit to the data.

3.2.5 Conclusions for the time-dependent Onsager spheres

The time-dependent Onsager model portrays a solvated molecule which changes its spatial extensions in a time-dependent way due to an external stimulus. As an important consequence, the interaction of the molecular dipole moment with the dissipative solvent becomes time-dependent, such that the non-stationary effects of nonequilibrium quantum solvation can be investigated within a model-based approach. The cases of a shrinking and a breathing Onsager sphere are of particular physical interest.

For the case of a shrinking sphere, we find that the qualitative form of the response is close to the that of the static sphere, but is strongly time-dependent. The magnitude of the absorptive part is temporally enhanced up to 40%. The damping rate of the molecular dipole moment can be easily understood in the two limits of fast and slow shrinking and our results nicely interpolate between these two limits. The calculated results clearly show that the nonequilibrium quantum solvation cannot be described by a fully adiabatic approach which treats the momentary radius of the shrinking sphere as a parameter. In general, a shrinking sphere shows a stronger damping than the corresponding static sphere.

For the case of a breathing sphere, the real and the imaginary parts of the susceptibility show again a strong time dependence. A breathing Onsager sphere is accompanied by a globally reduced damping at intermediate shrinking rates. There, the damping rate shows a significant minimum for values of shrinking rates comparable to the static relaxation. This cross-over behavior nicely interpolates between the two limits of fast and slow breathing which both coincide with the relaxation behavior of a static sphere.

In both regimes an effective response function which relates the central molecular dipole moment dynamics to an external electric driving field in a non-linear way can be formulated. The non-monotonous behavior of the effective response around the resonance frequency is a variable means to determine the shrinking and breathing rates of the Onsager cavity and, thus, the dynamics of the solute.

The resonantly reduced damping which occurs for a breathing Onsager sphere illustrates the nontrivial role of a nonequilibrium environment for the relaxation properties of a damped system such as the central solute. It can only occur under nonequilibrium conditions and shows that a time-dependent dissipative environment away from thermal equilibrium can yield less detrimental implications than resulting from a thermal reservoir. The time-dependent Onsager model thus contributes to understanding the impact of dynamically and spatially varying molecular properties of dissolved molecules on the relaxation of its electronic degrees of freedom and, thus, its energy exchange with the solvent.

3.3 Nonconventional time-dependent Stokes shift[7]

Time-dependent fluorescence spectroscopy is used to probe molecular motion at the interfaces of dissolved molecules. By determining the maximum shift of the fluorescence emission spectrum at time t after excitation, solvent relaxation in the proximity of the solute, e.g., chromophores of biological macromolecules, can be recorded [90, 91, 92]. This time-dependent Stokes shift is measured after electronic excitation analogous to the Franck-Condon principle [93, 94], where the polar solvent arrangement still corresponds to the unexcited solute which is an energetically unfavorable solvent conformation when the solute is excited. Over time, the solvent adapts to the altered charge distribution of the solute, reaches energetically more favorable configurations, so that the energy of fluorescence emission decreases. The well-established Bagchi-Oxtoby-Fleming theory describes the time development of the Stokes shift in polar media by means of a continuum Onsager model [92]. It may be understood as a time-dependent description of the Ooshika-Lippert-Mataga equation of the average shift in frequency of the absorption and fluorescence transition in solution due to polar interactions [92, 95, 96, 97]. By determining linear response, it is possible to link the fluctuations of the solute-solvent interaction to the dipole correlation function, which depend on solvent time constants and dielectric properties only [92]. For the simplest case of a Debye-type dielectric medium (cf. Eq. (2.26)), the model predicts an exponential relaxation of the solvation energy proportional to the solvent's longitudinal relaxation time $\tau_L = [(2\epsilon_\infty + 1)/(2\epsilon_s + 1)]\tau_D$ which is also one outcome of the spectral density in Eq. (3.10). The relaxation time becomes observable by the time-dependent Stokes shift [92]. The continuous approach for time-resolved fluorescence spectroscopy is a powerful description until today because the fluorescence response is insensitive to the motion of individual water molecules but only to their collective motion [90, 91]. Spectroscopic measurements confirm relaxation time scales in accordance with τ_L which are much faster than reorientation of single-solvent molecules reflecting the fact that the solvent response involves the coupled response of many molecules. This prediction of τ_L forms a cornerstone for the comparison of experimental time-dependent Stokes shift results to theoretical models [98].

However, experimental data sometimes deviate from the prediction of a homogeneous continuum model. This may be understood from the microscopic picture. The solvent in

---

[7] The model presented in this section is based on the publication : H. Kirchberg and M. Thorwart, "Time-Resolved Probing of the Nonequilibrium Structural Solvation Dynamics by the Time-Dependent Stokes Shift," J. Phys. Chem. B **124**, 5717 (2020).

close proximity to the solute contains an insufficient number of molecules to attain the full cooperativity described by the τ_L response, but the solvent far away may look like a continuum fluid where τ_L pertains. Therefore, the overall relaxation may occur on several different time scales and may include single particle relaxation times up to τ_L and even leads to ultrafast relaxation contributions in a non-exponential manner [98, 99].

To this end, molecular dynamics (MD) simulations help to mimic at least the most prominent solvent reorientation and relaxation time scales to understand experimental time-dependent fluorescence studies. Neira and Nitzan, for example, have used MD simulations to confirm a slow dynamical solvent component associated with salt ions in electrolyte solutions which becomes visible by a slower time component in the Stokes shift in comparison to the conventional bulk water relaxation [100].

Recent experimental time-dependent fluorescence studies of aqueous proteins portray clear evidence of different dynamical components within the solvent [101, 90]. Heid and Braun, for example, successfully decompose the fluorescence Stokes shift into a water and protein component by performing MD simulations at nine different sites of the protein in water [90]. The water component dominates the static Stokes shift at short times, but decays rapidly, whereas the self-motion of the protein becomes visible after a few picoseconds. The resulting Stokes shift therefore leads to a bi- or multimodal time-dependent decay behavior [90, 91]. Despite the computational accessibility to describe different dynamical contributions of the solvation process, MD simulations may also be limited to a tractable number of solvent molecules to avoid extremely high numerical effort.

The aim of this section is to formulate an effective nonequilibrium theory for the time-dependent Stokes shift where explicit time-dependent motion beyond thermal fluctuations enters. To this end, we extend the Bagchi-Oxtoby-Fleming continuum theory by including a shrinking radius on a finite time scale according to the model discussed in the previous Section 3.2.

In this section, I develop a model for the bimodal time-dependent Stokes shift by the time-dependent Onsager model of solvation in Subsec. 3.3.1. In Subsec. 3.3.2, the results are discussed.

3.3.1 Model

We consider the time-dependent Stokes shift characterized by the function $S(t)$ for a photoexcited molecular complex with explicit molecular motions at the aqueous interface to a dipolar solvent. The Stokes shift function is defined by [31]

$$S(t) = \frac{\Delta E_{solv}(t) - \Delta E_{solv}(\infty)}{\Delta E_{solv}(0) - \Delta E_{solv}(\infty)}, \tag{3.64}$$

where $\Delta E_{solv}(t)$ is the resulting solvation energy difference between the excited and the ground state molecule at a given time t. $\Delta E_{solv}(t)$ results of the electrostatic interaction between the solute, i.e., its charge distribution, and the surrounding solvent. If there is only little internal vibrational excitation of the solution in the transition, the time-dependent Stokes shift mainly results from the time-dependent solvation energy [102].

We consider the model of the shrinking Onsager cavity of Sec. 3.2 where the central molecular dipole moment suddenly changes from an initial ground state $\boldsymbol{\mu}_g$ to $\boldsymbol{\mu}_e$ upon photoexcitation which initiates the geometrical 'shrinking'. The shrinking cavity radius may mimic generically motional changes at the solute-solvent interface such as the observed self-motion of dissolved proteins [91, 90].

The interaction energy of the dipole with the homogeneous and isotropic solvent is given by $V_I = -\boldsymbol{\mu}(t) \cdot \mathbf{R}(t) \equiv E_{solv}(t)$. The reaction field $\mathbf{R}(t)$ (cf. Eq. (3.11)) portrays the time-dependent back action on the dipole moment, where the geometric changes at the solute-solvent interface enters via a time-dependent Onsager radius $a(t)$. We follow the same arguments of a small dynamically shrinking Onsager radius (Eq. (3.17)) to split the reaction field into two terms according to Eq. (3.18)

$$\mathbf{R}(t) = \frac{1}{a_0^3} \int_{-\infty}^{t} dt' \left[\chi(t-t') - \frac{3a_1}{a_0} \exp[-\alpha t] \Theta(t) \chi(t-t') \right] \boldsymbol{\mu}(t'), \tag{3.65}$$

where the shrinking with rate α begins upon photoexcitation at time $t = 0$. We assume the optical excitation of the solute to occur instantaneously such that the dipole moment changes from $\boldsymbol{\mu}_g$ to $\boldsymbol{\mu}_e$ at $t = 0$ which coincides with the beginning of the radial shrinking. Moreover, we assume that the dipole moment does not change its direction but its magnitude. Therefore the dipole moment reads

$$\boldsymbol{\mu}(t) = \mu_g \hat{\mathbf{e}}_z + \Theta(t)(\mu_e - \mu_g)\hat{\mathbf{e}}_z, \tag{3.66}$$

where $\Theta(t)$ is the unit Heaviside function. Then, the reaction field in Eq. (3.65) yields

$$\mathbf{R}(t) = \frac{1}{a_0^3}\chi_s\mu_g\hat{\mathbf{e}}_z + \frac{1}{a_0^3}\int_{-\infty}^{t} dt' \left[\chi(t-t') - \frac{3a_1}{a_0}\exp[-\alpha t]\chi(t-t')\right]\Theta(t')\Delta\mu\hat{\mathbf{e}}_z, \qquad (3.67)$$

where, exploiting Eq. (3.12), $\chi_s = \int_{-\infty}^{t} dt'\chi(t-t') = \frac{2(\epsilon_s-1)}{2\epsilon_s+1}$ and $\Delta\mu = \mu_e - \mu_g$. The first term in Eq. (3.67) describes the static reaction field before excitation when the solvent is in equilibrium with the ground state dipole moment $\boldsymbol{\mu}_g$. The second term is the change of $\mathbf{R}(t)$ after the sudden change of the dipole moment to $\boldsymbol{\mu}_e$ where the solvent has to readjust to. In addition, due to the excitation, the molecular radius begins to shrink from its initial value $a_0 + a_1$ to a_0, which gives rise to an additional explicit time-dependent contribution given by the third term.

At time t the solute suddenly fluoresces and reaches again its ground state such that also its dipole moment goes back to $\boldsymbol{\mu}_g$ where the solvent will immediately react in the continuum's approach with the fast (or optical) contribution ϵ_∞ (cf. Eq. (2.26)). We set this value to $\epsilon_\infty = 1$ according to the physical parameters in Subsec. 3.2.2 such that there is no further contribution to the reaction field coming from the sudden dipole change arising from $\chi_\infty = 2a(t)^{-3}(\epsilon_\infty - 1)(2\epsilon_\infty + 1)^{-1}$.

The solvation energy difference between the excited state and the ground state of the molecule at time t thus reads

$$\begin{aligned}\Delta E_{solv}(t) &= -\boldsymbol{\mu}_e\mathbf{R}(t) + \boldsymbol{\mu}_g\mathbf{R}(t) \qquad (3.68)\\ &= -\frac{1}{a_0^3}\mu_g\chi_s\Delta\mu - \frac{\Delta\mu^2}{a_0^3}\int_{-\infty}^{t} dt'\left[\chi(t-t') - \frac{3a_1}{a_0}\exp[-\alpha t]\chi(t-t')\right]\Theta(t')\\ &= -\frac{1}{a_0^3}\mu_g\chi_s\Delta\mu + \Delta E(t),\end{aligned}$$

where only the second term is time-dependent such that the first term cancels out in determining $S(t)$ of Eq. (3.64). We then perform a complex Fourier transform [8] of $\Delta E(t)$, by using the convolution theorem and the Fourier transform of the Heaviside step function

---

[8] One defines the complex Fourier transform by $f(z) = \int_{-\infty}^{\infty} dt\, e^{-izt} f(t) = \mathcal{F}[f(t)]$, where $f(z)$ is analytic for Im(z) < 0 and $f(t \to \infty) < \infty$.

$\mathcal{F}[\Theta(t)] = \frac{1}{iz}$, and find

$$\Delta E(z) = -\frac{\Delta\mu^2}{a_0^3}\left[\frac{\chi(z)}{iz} - \frac{3a_1}{a_0}\frac{\chi(z-i\alpha)}{i(z-i\alpha)}\right], \tag{3.69}$$

where $z = \omega - i\eta$ with ω real and η representing a small positive number [102]. The inverse transform of Eq. (3.69) for $t \geq 0$ leads to

$$\begin{aligned}
\Delta E(t) &= -\frac{\Delta\mu^2}{2\pi a_0^3}\int_C dz e^{izt}\left[\frac{\chi(z)}{iz} - \frac{3a_1}{a_0}\frac{\chi(z-i\alpha)}{i(z-i\alpha)}\right] && (3.70)\\
&= -\frac{4\Delta\mu^2}{\pi a_0^3}\int_0^\infty d\omega \frac{\cos[\omega t]}{\omega}\,\mathrm{Im}\left[\frac{\epsilon(\omega)-1}{2\epsilon(\omega)+1}\right] - \frac{\Delta\mu^2\chi_s}{a_0^3}\left[1 - 3\frac{a_1}{a_0}e^{-\alpha t}\right] && (3.71)\\
&= \frac{\Delta\mu^2}{a_0^3}\left\{\left[\frac{2(\epsilon_s-1)}{2\epsilon_s+1}e^{-\omega_D t}\right] - \chi_s\left[1 - 3\frac{a_1}{a_0}e^{-\alpha t}\right]\right\}. && (3.72)
\end{aligned}$$

The contour C of integration in Eq. (3.70) is a path parallel to but slightly below the real axis in the complex plane. Further details for calculating the first term in Eq. (3.70) are given in Appendix B while we apply the residue theorem for the second term at the singularity $z = i\alpha$. We use the Debye relaxation for $\epsilon(\omega)$ (cf. Eq. (2.26)) to evaluate the integral in Eq. (3.71). The resulting $\omega_D = (2\epsilon_s + 1)/(3\tau_D)$ in Eq. (3.72) is already defined for the response function of Eq. (3.12) and is the inverse dipolar longitudinal relaxation time $\omega_D = \tau_L^{-1}$ [92].

The time-dependent fluorescence Stokes shift of Eq. (3.64) then yields

$$S(t) = \frac{1}{1+Q}e^{-\omega_D t} + \frac{1}{1+Q^{-1}}e^{-\alpha t}, \tag{3.73}$$

where $Q = 3\frac{a_1}{a_0}$.

3.3.2 Results and discussions

The calculated Stokes shift of Eq. (3.73) clearly indicates a bi-exponential decay where the first term reflects the collective bulk water relaxation while the second term describes the motional changes at the solute-solvent interface associated with a possible self-motion of the solute and the corresponding shrinking rate α. Fig. 3.18 shows the resulting Stokes shift for different shrinking rates, which are equal to (black-star line), larger than the inverse longitudinal relaxation time (black-diamond line) or smaller (red-diamond line).

The bimodal experimental fit to time-dependent fluorescent Stokes shift of the dye

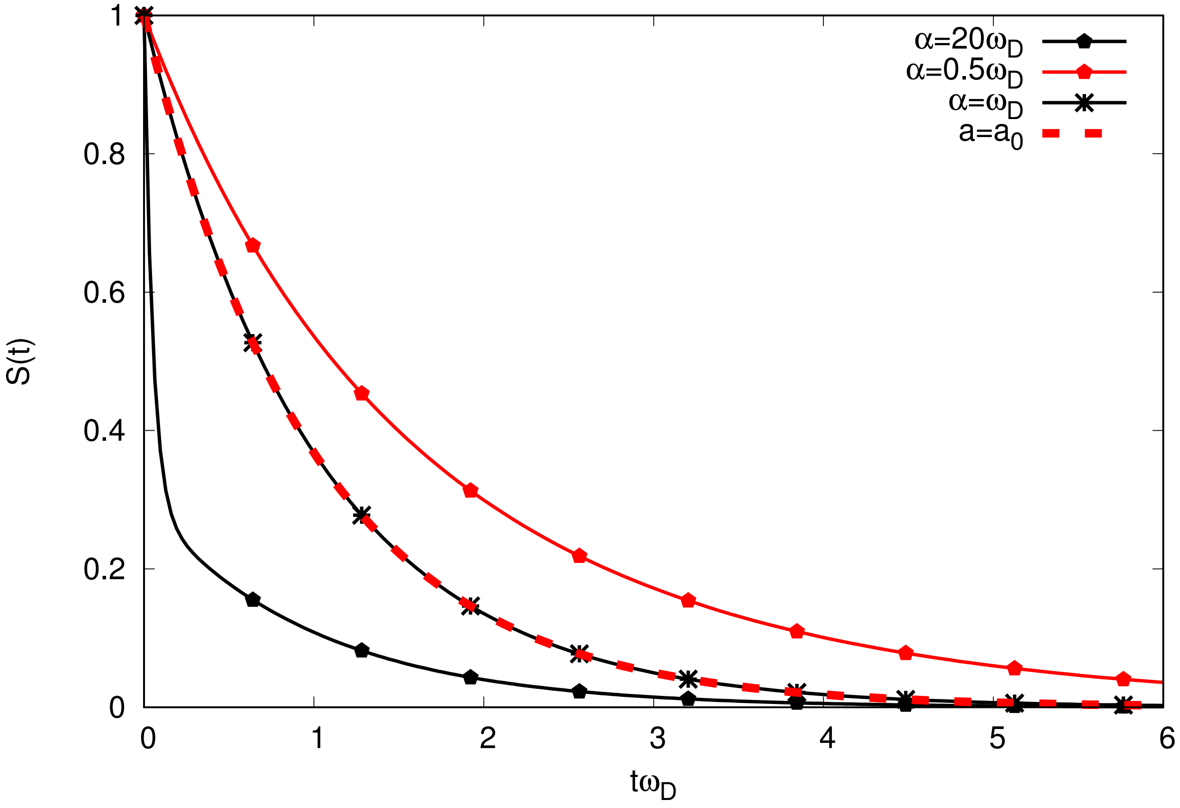

Figure 3.18: The time-dependent Stokes shift due to a suddenly changing dipole moment upon fluorescence in an shrinking Onsager cavity of different shrinking rates for $a_1 = 0.01a_0$. The dashed red line portrays the time-dependent Stokes shift in an Onsager cavity of constant radius.

Hoechst 33258 in solution with DNA shows clear evidence of different motional contributions. The experimental recorded Stokes-shift confirms that water solvating the dye bound to DNA is slowed down but contributes to the fast relaxation times (0.2 and 1.2 ps), while the DNA self-motion (∼20 ps) changes the long-time components (1.4 and 19 ps) of the solvation response. [103, 104].

Hence, the standard Onsager continuum model for the time-dependent Stokes shift can be extended to a generic model for an explicit time-dependent motion at the interfacial region of the solute to solvent. Many experimental fluorescence Stokes shifts show two or more components which decays on different time scales. Molecular dynamics simulations examine the origin of the Stokes shift data and find that the bulk water component dominates at short times but rapidly decays. The long-time behavior is more dominated by the solute dynamics, i.e., mostly the self-motion of a dissolved protein [91].

3.4 Formation of a hydrophobic hydration shell [9]

We study next the time-dependent formation of the hydration shell around a hydrophobic solute on the basis of a Onsager model with a varying hydration shell around it. The growth process is imposed from outside and is described phenomenologically within two approaches. First, we consider a time-dependent thickness of the hydration layer which grows from zero to a finite value over a finite time range. Second, we assume a time-dependent variation of the dielectric properties in the form of a time-dependent complex permittivity within a finite layer around the central Onsager sphere. In the first approach, we assumes that the hydration shell has different dielectric properties and, in particular, a slower solvent reorganization (or, Debye) time. We find a time-dependent frequency shift down to the blue of the resonant response of the dipole, together with a dynamically decreasing line width. The blue shift directly indicates the work which the systems performs to form the hydration layer and is a directly measurable quantity. The reduced line width reveals the less effective damping of the hydration shell which has slower fluctuations and also removes the fast bulk fluctuations further away from the central dipole.

This section is structured as follows. In Subsec. 3.4.1, I point out time-dependent extensions of hydration shells determined from spectroscopic measurements and build a Onsager model with a dynamic hydration shell. Then, I first derive a time-dependent layered Onsager model with a growing hydration shell around in Subsec. 3.4.2 and calculate the response function of the molecular dipole to an external applied field. In Subsec. 3.4.3, I formulate a layered Onsager model with a hydration shell of fixed extension but with time-dependent dielectric permittivity before determining the resulting response behavior of the central molecular dipole moment. Subsec. 3.4.4 summarizes.

3.4.1 Layered dynamic Onsager model

To describe the impact of a time-dependent formation of the hydration shell on the relaxation properties of a test dipole dissolved in a polar solvent, we generalize the static Onsager model of Sec. 3.1 [38, 105, 106] to include time-dependent nonequilibrium effects

---

[9] The model presented in this section is based on the publication : H. Kirchberg, P. Nalbach, C. Bressler and M. Thorwart, "Spectroscopic Signatures of the Dynamical Hydrophobic Hydration Shell Formation," J. Chem. Phys. B **123**, 2106 (2019).

due to a dynamic hydration shell. To mimic the growth of the hydration shell, we assume a dynamic layer thickness growing from zero to a final value r. The precise time protocol of this growth is left unspecified and only enters phenomenologically into the model. Outside the shell, the water shows its usual bulk behavior.

This model is motivated by the experiment [49] with a negatively charged hydrophilic iodide which is ionized by an X-ray pulse. Around the resulting neutral and hydrophobic iodine, an expanded water layer forms containing around 27 water molecules [78]. The extracted size of the entire complex, i.e., the central iodine plus the hydration shell of one layer of water molecules after the shell formation is approximately $b = 6.5$Å. This value is found from the iodine-oxygen radial distribution function, where a second maximum appears signaling a high density of water atoms beyond the shell and the continuous interface to the bulk water [78]. The initial size of the dissolved iodide is estimated as $a = 3.6$Å from the first maximum of the iodide-oxygen radial distribution. The resulting layer thickness after neutralization can thus be obtained as $r = 2.9$Å$= 0.8a$. We neglect in the derived model the hydration shell around the initial iodide formed by approximately eight water molecules in the first solvation shell [39, 78]. We now ready to study the two different scenarios for the hydration shell formation. Within the first one (Subsec. 3.4.2), we consider a time-dependent growth of a hydration layer with a time-dependent thickness, which has a complex permittivity different from the bulk. In the second situation (Subsec. 3.4.3), we assume a static Onsager sphere, but a time-dependent complex permittivity within a well-defined spatial range associated with the fixed shell extension. Outside the hydration layer, bulk water is assumed as solvent. In comparing the results of both scenarios, we obtain interesting insights into the dynamic formation of a hydration shell leading to the hydrophobic behavior.

3.4.2 Growing water layer

In the layered Onsager model, the solvent is described as continuous, homogeneous and uniform and is associated with the time translationally invariant dielectric function $\epsilon_x(t-t')$ [39]. The index x refers to different components of the environment, i.e., the hydration shell ($x = H$) and the bulk ($x = B$). Throughout this model, we consider again the Debye form of the dielectric function (cf. Eq. (2.26) for its equivalent in frequency space in Subsec.

2.2.2)

$$\epsilon_x(t-t') = \epsilon_{x,\infty}\delta(t-t') + \frac{\epsilon_{x,s}-\epsilon_{x,\infty}}{\tau_{x,D}} \exp\left[-\frac{t-t'}{\tau_{x,D}}\right]\Theta(t-t'), \tag{3.74}$$

where each component x has its own specific Debye relaxation time $\tau_{x,D}$, its static dielectric constant $\epsilon_{x,s}$ and its high-frequency dielectric constant $\epsilon_{x,\infty}$. For bulk water at room temperature, $\epsilon_{B,s} = 78.3$, $\epsilon_{B,\infty} = 4.21$, and $\tau_{B,D} = 8.2$ps [39, 57]. The dielectric properties of the hydration shell continuum are less clear, but in general, a higher structural order of the water molecules in the first few layers around the solute implies weaker fluctuations and, thus, $\epsilon_{B,s} \gg \epsilon_{H,s}$ [39, 79, 107, 108]. This reflects the fact, that the water molecules are stronger bound in a hydrogen network and are less polarizable. Due to this enhanced interaction in the layer, the relaxation time is slower by a factor of 5 to 10 [79], such that $\tau_{H,D} \gg \tau_{B,D}$ [108]. A reduced dielectric constant of water is also recorded in water strongly confined in small tubes of several nanometers [109]. Here, water exhibits a less flexible structure near surfaces and is difficult to reorient by applying an electric field.

In our time-dependent layered Onsager model, we assume that the shell formation process is phenomenologically well described by a radial increase of the total radius $b(t)$ of the central Onsager sphere plus layer of the form

$$b(t) = a + r[1 - e^{-\alpha(t-t_0)}]\Theta(t-t_0), \tag{3.75}$$

where the shell formation begins at time t_0 from the static radius a with the rate α of formation. The final shell thickness is r and the final total Onsager radius is $b = a + r$. This form of the growth reflects a gradual shell formation, where the environmental dipole moments adjust themselves first more rapidly layer by layer in a stronger bound network and then successively slower if further away from the central hydrophobic molecule.

Reaction field

To determine the time-dependent response to the dynamic hydration shell formation, we calculate the resulting electric field induced by the polar environment. The central time-dependent dipole moment polarizes both components of the polar environment, the hydration shell and the bulk water, such that both create a fluctuating reaction field. We assume again that the dipole moment $\boldsymbol{\mu}(t) = \mu(t)\hat{\mathbf{e}}_z$ does not change its direction but its magnitude.

Due to the spherical symmetry, the electric potentials in the cavity, the shell and the bulk water sectors are expressed in terms of Legendre polynomials [73] as in Sec. 3.2. From the potentials, all resulting electric fields in all sectors result by imposing the boundary conditions at a and b, i.e., (i) the continuity of the electric potentials and (ii) the continuity of the normal components of the electric displacement. The boundary conditions follow as

$$R(t)a^3 + \mu(t) = A(t)a^3 + B(t), \tag{3.76}$$

$$R(t)a^3 - 2\mu(t) = \int_{t^*}^{t} dt' \epsilon_H(t-t')\Big[A(t')a^3 - 2B(t')\Big], \tag{3.77}$$

$$A(t)b(t)^3 + B(t) = C(t), \tag{3.78}$$

$$\int_{t^*}^{t} dt' \epsilon_H(t-t')\Big[A(t')b(t)^3 - 2B(t')\Big] = -2\int_{t^*}^{t} dt' \epsilon_B(t-t')C(t')\,, \tag{3.79}$$

where $R(t)$ is the magnitude of the reaction field and $\mu(t)$ the magnitude of the dipole moment. $A(t)$ is the reaction field and $B(t)$ the field of the induced dipole moment in the shell, while $C(t)$ is the induced dipole field in the bulk water. We have to ensure that the layer formation is slow enough to disregard any dynamic magnetic field induced by the displacement current. We further disregard the spatial variation of the dielectric function, but assume it as homogeneous inside the bulk and the shell. The time t^* marks the beginning of measuring the response of the dipole moment, when the molecular charge is brought out of its equilibrium, and may differ from the time t_0 of the beginning of the shell formation in Eq. (3.75). The two processes may be recorded experimentally by two different sharp coherent pulses, like in an experimental pump-probe set-up.

When performing a Fourier transform [10] of Eqs. (3.76) and (3.77), we want to treat the time-dependent total radius $b(t)$ adiabatically in order to be able to proceed. This is possible as long as the shell formation in Eq. (3.75) is slower than all time-decaying processes of the electric fields induced by the environment, or, equivalently, the rate α is the smallest of all inverse time scales of the problem. In doing so, $b(t,t_0)^3 \to b(t^*,t_0)^3$ contributes as a constant parameter and can be taken out of the Fourier integral which starts effectively at time t^*, while the shell formation has already started at t_0. This approach requires $t^* \geq t_0$ such that the beginning of the shell formation is at the same time or before the beginning of the measurement. Below, we will ensure self-consistently that α fulfills this requirement. From Eqs. (3.76)-(3.79), we obtain for the reaction field in

---

[10] The Fourier transform is defined here by $\mathcal{F}[f(t)] = \int_{t^*}^{\infty} dt \exp(i\omega t) f(t)$.

Fourier space

$$R(\omega) = \frac{\mu(\omega)}{a^3} \frac{-2[\epsilon_H(\omega)+2][\epsilon_H(\omega)-\epsilon_B(\omega)]a^3 + 2[\epsilon_H(\omega)-1][2\epsilon_B(\omega)+\epsilon_H(\omega)]b(t_0,t^*)^3}{2[\epsilon_H(\omega)-1][\epsilon_H(\omega)-\epsilon_B(\omega)]a^3 - [2\epsilon_B(\omega)+\epsilon_H(\omega)][2\epsilon_H(\omega)+1]b(t_0,t^*)^3} \tag{3.80}$$

$$= \xi(\omega, t_0, t^*)\mu(\omega),$$

where $b(t^*, t_0)^3$ enters parametrically and the dipole moment may be understood as $\mu(\omega) = eq(\omega)$. This relation defines the frequency-dependent susceptibility $\xi(\omega, t_0, t^*)$ which depends parametrically on t_0 and t^*.

Equation of motion for the molecular dipole moment

We investigate next again the time-dependent expectation value $\langle \mu(t) \rangle = e \langle q(t) \rangle$ of the molecular dipole moment. The net charge of the molecule is zero, but it can be polarized such that within the harmonic approximation, with the potential $V(q) = \frac{1}{2} m\omega_0^2 q^2$ in H_S of Eq. (3.14), the charge of mass m oscillates with a characteristic frequency ω_0 around its equilibrium position, forming the time-dependent molecular dipole moment. The dipole moment couples linearly via the coupling $V_I = -\mu[R + E]$ to the reaction field and an additional external electric driving field. We assume again perfect alignment of the dipole moment to the direction of the reaction and electric field, such that we can operate with their absolute values. To obtain a Langevin-type equation for the expectation value of the charge displacement, we can again derive again the Heisenberg equation of motion for $\langle p(t) \rangle \equiv m \langle \dot{q}(t) \rangle$ by exploiting the Hamiltonian of Eq. (3.14) while we take into account the reaction field, the environmental back action of the bulk water and the gradually growing hydration shell given in Eq. (3.80). The reaction field couples to the dipole moment via the force $e \langle R(t) \rangle$. The resulting Langevin-type integro-differential equation of motion follows as

$$m \langle \ddot{q}(t) \rangle + m\omega_0^2 \langle q(t) \rangle - e^2 \int_{t^*}^{t} dt' \xi(t^*, t_0, t') \langle q(t') \rangle = eE(t), \tag{3.81}$$

with the electron mass m, the electron charge e and a typical molecular frequency $\omega_0 = 2.5 \times 10^{15}$Hz in the near ultraviolet spectrum. The associated molecular polarizability (cf. Eq. (2.27) in Subsec. 2.2.3) $\alpha_m = e^2/(m\omega_0^2) = 11.26\text{Å}^3$ for a polarizable molecule without a permanent dipole moment matches perfectly with the value for diatomic iodine I_2 [61, 110]

[11]. Although one wants to mimic the hydration shell formation around monoatomic iodine with a less polarizability the use of the polarizability for diatomic iodine may be a good approximation. The reason for this is that the associated X-ray absorption experiment $\mathrm{I}^- \rightarrow \mathrm{I}$ clearly hints to a transient complex species $\mathrm{I}^0(\mathrm{OH}_2)$ which may have a higher polarizability [49]. Moreover, all information about the molecular extension a, the final hydration shell thickness r, its formation rate α and the time t_0 of the onset of the formation enter via the the response term $\xi(\omega, t_0, t^*)$ of Eq. (3.80). A Fourier transform of Eq. (3.81) leads to

$$\langle q(\omega)\rangle = \frac{\langle \dot{q}(t^*)\rangle\, e^{i\omega t^*} - i\omega\,\langle q(t^*)\rangle\, e^{i\omega t^*} + (e/m)E(\omega)}{\omega_0^2 - \omega^2 - (e^2/m)\xi(\omega, t_0, t^*)}, \tag{3.82}$$

with the initial charge displacement $\langle q(t^*)\rangle$ and its initial velocity $\langle \dot{q}(t^*)\rangle$, while $\langle q(t \to \infty)\rangle = \langle \dot{q}(t \to \infty)\rangle = 0$ as the functions are integrable. We note that $\mathrm{Re}[\xi(\omega, t^*, t_0)]$ induces a renormalization of the potential frequency in the denominator polynomial of Eq. (3.82), while $\mathrm{Im}[\xi(\omega, t^*, t_0)]$ leads to damping.

To obtain the electric reaction field $A(t)$ and the dipole field $B(t)$ in the hydration shell, we transform $\langle q(\omega)\rangle$ in Eq. (3.82) back into the time domain. By this, we obtain the dipole moment $\langle \mu(t)\rangle = e\,\langle q(t)\rangle$ and the resulting reaction field given in Eq. (3.80) in the Onsager sphere and can calculate then the associated fields $A(t)$ and $B(t)$ as given in Eqs. (3.76)-(3.79). This allows us to verify self-consistently that we can treat $b(t, t_0)$ in Eqs. (3.78) and (3.79) adiabatically. We are free to choose the initial time t^*, when the dipole begins to oscillate, while the hydration shell formation has begun at an earlier time t_0, i.e., $t^* \geq t_0$. We set $t_0 = 0$ such that t^* directly refers to the time span during which the hydration shell grows. Additionally, we switch off the driving field $E(\omega) = 0$ to see the damping induced by the environment, set $\langle \dot{q}(t^*)\rangle = 0$ and choose the typical oscillator length for the initial expectation value for the charge displacement as $\mathrm{Re}[\langle q(t^*)\rangle\, e^{i\omega t^*}] = \sqrt{\frac{\hbar}{m\omega_0}}$. The results are shown in Fig. 3.19.

It is clear that $b(t)^3$ increases slowly enough in comparison to $A(t)$ and $B(t)$ for a proper choice of the formation rate α such that the time dependence of the total radius can be treated adiabatically in Eqs. (3.78) and (3.79), i.e., $b(t)^3 \equiv b(t^*)^3 =$const. We also have to ensure that the resulting damping has to comply with $\Gamma \gg \alpha$ for different sphere radii a, for all given final hydration shell thicknesses r and for all chosen times t^* for the initial displacement. For the specific choice of the neutralization of iodine ($\mathrm{I}^- \rightarrow \mathrm{I}^0$) with

---

[11] Note that we work in cgs units in which the electron charge is $e = 3 \times 1.602 \times 10^{-10}$esu.

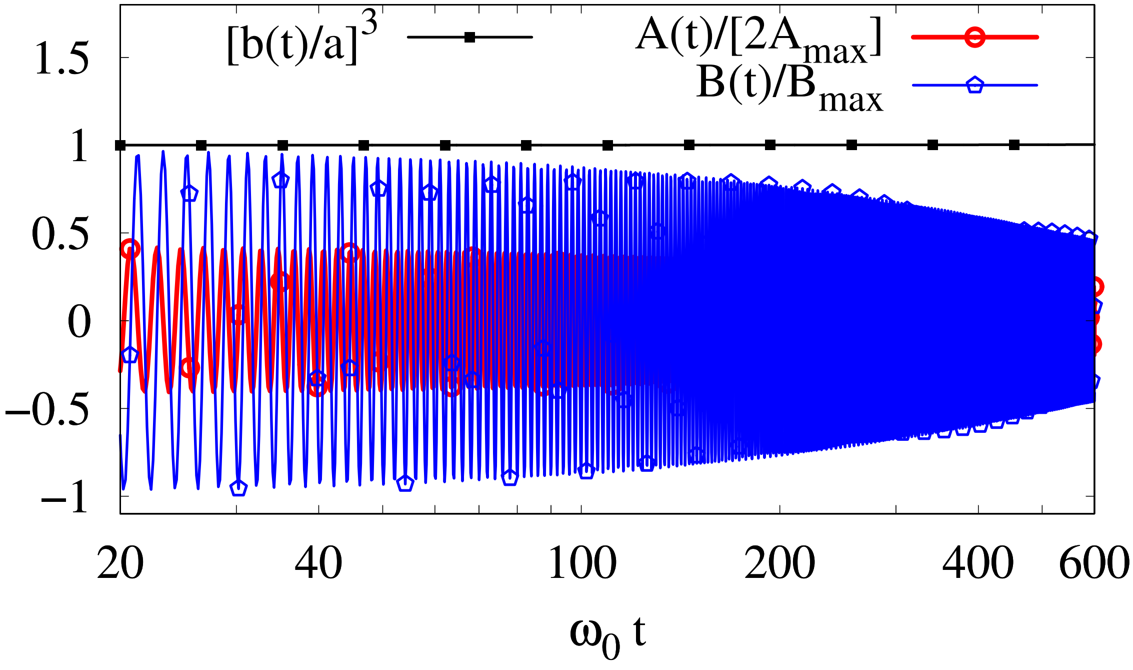

Figure 3.19: Dipole field $A(t)$ and reaction field $B(t)$ in the hydration shell which has begun to grow at $t_0 = 0$ before we start the observation at $t^* = 10\omega_0^{-1}$. The inner (constant) sphere radius is $a = 3.6$ Å, while the final shell thickness is set to $r = 0.8a$. $\Gamma = 2.6 \times 10^{-4}\omega_0$ is the resulting decay rate of the electric fields. The formation rate is chosen as $\alpha = 0.1\Gamma$ and the Debye dielectric parameters are set to $\epsilon_{H,\infty} = \epsilon_{B,\infty}$, $\epsilon_{H,s} = 0.1\epsilon_{B,s}$ and $\tau_{D,H} = 10\tau_{D,B}$.

$a = 3.6$Å and $r = 0.8a$, we find $\Gamma = 2.6 \times 10^{-4}\omega_0$, where the oscillation begins at $t^* = 10\omega_0^{-1}$ after the hydration shell formation. We choose $\alpha = 0.1\Gamma$, which refers to a typical time scale of the hydration shell formation of $\alpha^{-1} \sim$ ps [49, 107]. The shell formation requires a breaking of the hydrogen bonds between the solvent molecules with the just neutralized and hydrophobic iodine and a reformation of strong hydrogen bonds among each other. The measured average molecular reorientation times for bulk water is 2.5 ps [107, 111].

The dynamics of the displacement of the central dipole is damped with the damping rate Γ. The results for Γ for different given parameters are shown for increasing time t^* in Fig. 3.20. An overall decrease of the damping is observed with increasing time delay t^* between the onset of the shell formation and the initial charge displacement. The fact that Γ is time-dependent reflects the nonequilibrium situation of the time-dependent environment with the growing hydration layer. The maximal damping rate is observed at $t^* = 0$, where no shell exists. While the shell forms out, the bulk water as the source of fluctuations is further pushed away from the central dipole by the intermediate hydration layer. The dielectric properties within the newly created hydration shell are assumed to be weakened as the water molecules hold stronger together due to the formation of hydrogen bonds. This reduces damping of the charge displacement and hence of the induced electric fields $A(t)$ and $B(t)$. As can be seen, for larger inner sphere radii a, the damping decreases because the environment is spatially further away from the central dipole, see Fig. 3.20. Qualitatively similar results have been obtained previously for the relaxation time of an excited vibrational state of a molecular complex with a finite, but static hydration shell around [89]. If the hydration shell grows to a bigger final thickness r, damping is more reduced as the strongly fluctuating bulk water is gradually replaced by the less polarizable water confined in the hydration shell. This effect is less recorded for a smaller final shell extension r in Fig. 3.20.

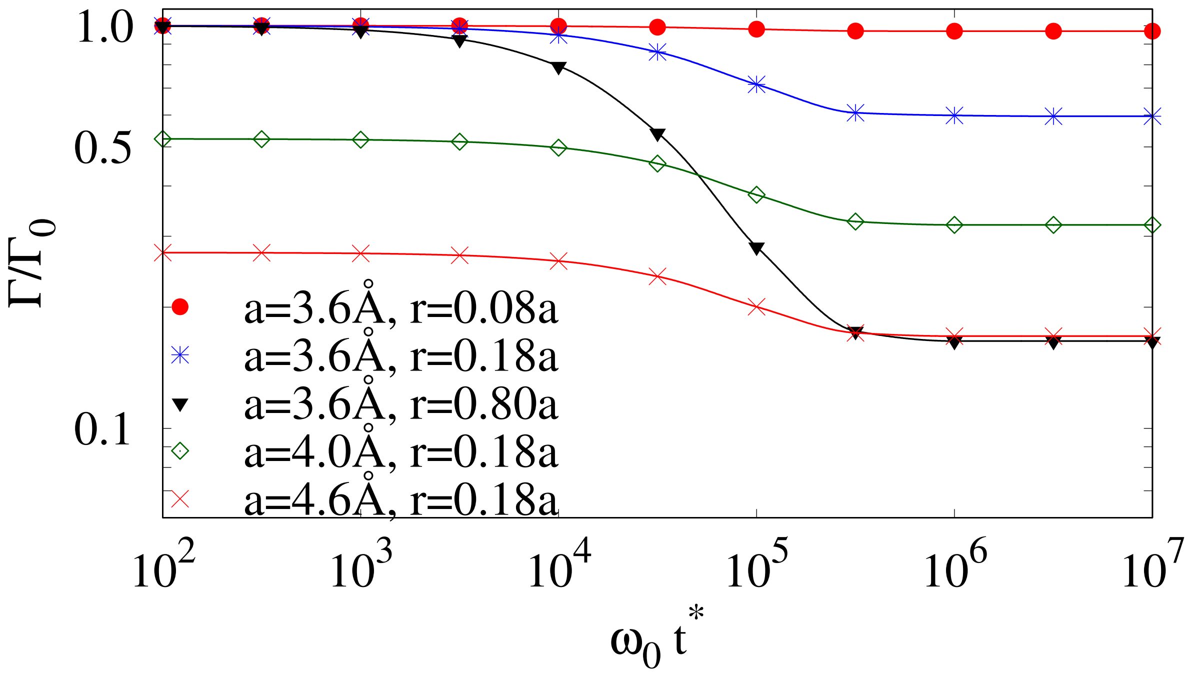

Figure 3.20: Damping rate in dependence of the time t^* between the start of the shell formation and initial displacement for different sphere radius a and final shell extensions r. The damping is recorded relative to the damping $\Gamma_0 = 2.6 \times 10^{-4}\omega_0$ for $a = 3.6$Å and $r = 0.8a$ at $t_0 = 0$. Moreover, $\epsilon_{H,\infty} = \epsilon_{B,\infty}$, $\epsilon_{H,s} = 0.1\epsilon_{B,s}$ and $\tau_{H,D} = 10\tau_{B,D}$.

Response function

When we are only interested in the response of the dipole moment to the external electric field, we set the initial conditions $\langle q(t^*)\rangle = 0$ and $\langle \dot{q}(t^*)\rangle = 0$ in Eq. (3.82). The external electric field drives the charge, which follows with a characteristic but fixed phase delay and amplitude difference after a transient time. On the one hand, the pulse has to be long enough that the dipole displacement follows its stationary oscillation, but on the other hand, it should be short enough that the time-dependent total radius $b(t) \equiv b(t^*)$ can be treated adiabatically. This can expressed as $\Gamma_{\rm min}^{-1} < T < \alpha^{-1}$, where T is the pulse duration. $\Gamma_{\rm min}$ is the minimal damping which occurs when the shell formation process is completed (Fig. 3.20). The resulting response to the external driving field can be evaluated as

$$\langle q(\omega)\rangle = \frac{e}{m}\frac{1}{\omega_0^2 - \omega^2 - (e^2/m)\xi(t^*,\omega)}E(\omega) = \chi(\omega,t^*)E(\omega)\,, \tag{3.83}$$

where the susceptibility $\chi(\omega,t^*)$ contains information about the time evolution via t^* of the increasing radius $b(t^*)$.

The real part of the susceptibility is shown in Fig. 3.21(a) and is connected to the refractive behavior of the molecule, while the imaginary part of the response, shown in Fig. 3.21(b) is related to its absorptive behavior (see Eq. (2.41) in Sec. 2.3).

With increasing time t^* since the onset of the shell formation, the resonances in the absorptive part shifts in frequency to the blue. This results in a smaller relative shift $\delta\omega_m(t^*) = \omega_m(t^*) - \omega_0$ of the peak maximum at $\omega_m(t^*)$ with respect to the eigenfrequency ω_0 until the shell is fully formed out. The resonance frequency is smaller than the eigenfrequency $\omega_m(t^*) < \omega_0$ due to the renormalization due to the polar environment. Thus, the incoming light will be absorbed from the molecule at higher frequencies when the hydration shell around it is more pronounced. This up-shift to the blue of the absorption frequency corresponds to an energy which may be understood as a part of the energy needed to build up the hydrogen-bond network within the hydrophobic hydration shell.

To quantify this work performed, one can use the Gibbs free energy of solvation for our model with $\Delta G = \Delta H - T\Delta S = \Delta E + p\Delta V - T\Delta S$, while ΔH is the enthalpic change, ΔE is the change of the internal energy, $p\Delta V$ the volume work and $T\Delta S$ the heat exchange during the solvation. The change of internal energy $\Delta E = \Delta W - p\Delta V + T\Delta S$ contains a contribution of non-expansion work ΔW, while one keeps the pressure and temperature constant. The defined Gibbs free energy then reads $\Delta G = \Delta W$, which reflects

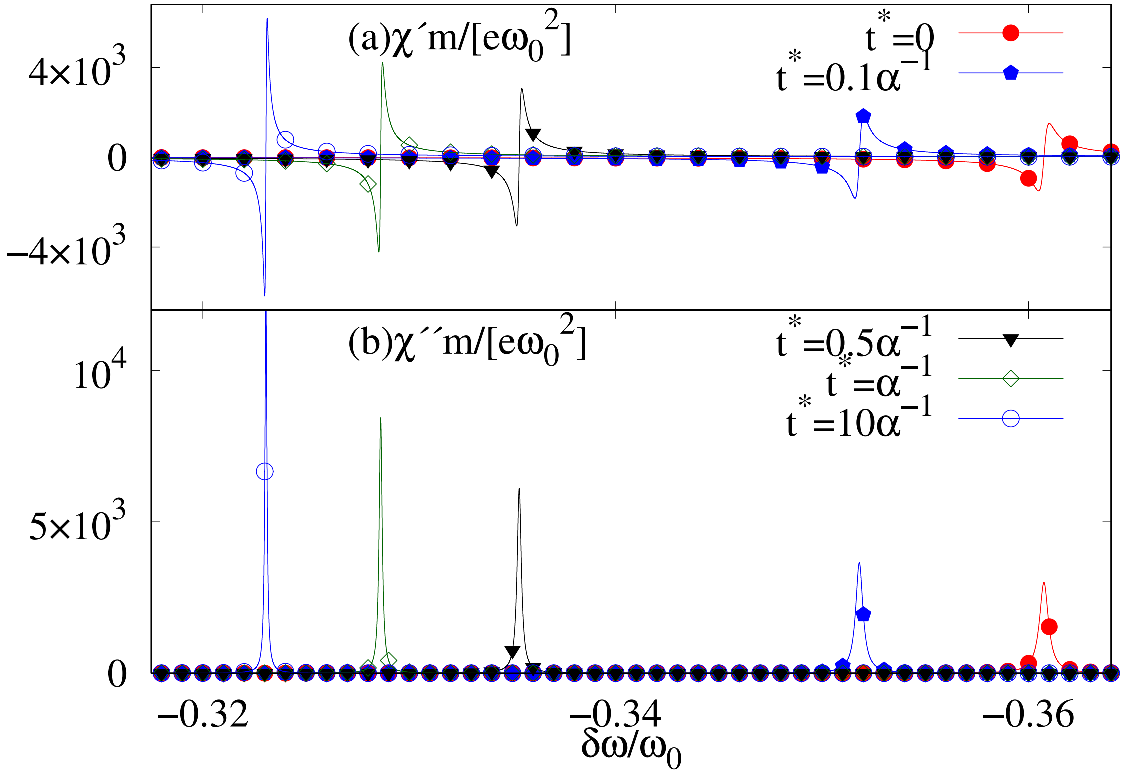

Figure 3.21: Real (a) and imaginary (b) part of the susceptibility $\chi(\omega, t^*)$ to an external field at different times, with $\delta\omega = \omega_m - \omega_0$, $\alpha = 10^{-5}\omega_0$,$\tau_{H,D} = 10\tau_{B,D}$, $\epsilon_{H,s} = 0.1\epsilon_{B,s}$, $\epsilon_{H,\infty} = 0.8\epsilon_{B,\infty}$. The sphere extension is $a = 3.6$Å and $r = 0.8a$.

the maximal amount of work that can be extracted from the solute ($\Delta G < 0$), or has to be added to the solute ($\Delta G > 0$) during solvation in order to letting it dissolve. In the given case, ΔG will be positive since we have to perform work to electrostatically orient the water to form a hydration shell. In fact, to be quantitative, we can extract this work from the blue shift of the peaks in the susceptibility, see, e.g., Fig. 3.21(b). For the parameters used there, we can read off the frequency difference of $\Delta\delta\omega = 0.04\omega_0$, such that $\Delta G = \Delta W = 0.04\hbar\omega_0$. The performed work stems from the explicitly time-dependent shell thickness performed from outside. The total required Gibbs free energy $\Delta G > 0$ for the whole hydrophobic solvation process is positive, reflecting the low solubility of iodine and, thus, the hydrophobic character. The frequency shift is directly measurable in the absorption spectrum of the solute.

In MD simulations of hydrophobic solvation of noble gases the positive free Gibbs energy $\Delta G = \Delta H - T\Delta S > 0$ results out of an extremely large loss of entropy and hence a negative ΔS at room temperature. This also has been confirmed experimentally by

[112, 113]. A prominent interpretation is that the water molecules in the hydration shell are more strongly coupled among each other and to the solute which reduces their mobility, and hence, the entropy of the system. Therefore, the entropic penalty for the hydrophobic solvation becomes directly measurable.

Additionally, one observes a strongly reduced line width when t^* is growing. This is shown in Fig. 3.21 (b) and, more explicitly, in Fig. 3.22, and perfectly reflects the reduced damping of the central dipole. The basic physical origin are the less flexible water molecules of the shell and the strengthened hydrogen bonds of the water molecules, see also Fig. 3.20. The range of the hydrogen bonds in the shell is smaller as compared to bulk water, which indicates a high structural ordering. In the Debye model, this effect is included by a smaller static and high-frequency dielectric constant in the shell [108]. The line width, measured by the full width at half maximum of the peak in the absorptive part of the response, is more reduced with time t^* if the static dielectric constant is more reduced in the shell, as shown in Fig. 3.22. The final width is reached faster, with a more rapid shell formation.

To be more quantitative, we show in Fig. 3.23 the total blue shift $\delta\omega$ of the resonance frequency over time t^*. It increases for a larger final shell thickness r, as more energy is needed to form the hydrophobic shell. This result coincides with the higher energy required to dissolve hydrophobic molecules with a bigger volume, because a molecule with thicker hydration shell takes up an enlarged volume in the solution [114]. The shift to the blue occurs faster for a quicker shell formation. Moreover, a strong up-shift is observed with a reduced high-frequency dielectric constant $\epsilon_{H,\infty}$ of the bound water. This is seen by changing the parameter c and shown in Fig. 3.23. In contrast, no impact on the frequency shift is found for a reduced static dielectric constant $\epsilon_{H,s}$. Analytically, this can be understood via the impact of the high-frequency dielectric constant on the real part of the susceptibility ξ in the denominator polynomial of Eq. (3.82) which leads to a frequency renormalization, while the static dielectric constant has an imperceptible impact on ω_0.

The maximum of the absorption peak increases with time t^* until the hydration shell is finally formed out, which is shown in Fig. 3.23 (inset). This enhanced response is due to the fact that the strongly damping bulk water is more and more replaced by the less damping water more tightly bound in the shell. The final value of the peak maximum is faster reached with a more rapid shell formation. This effect is more pronounced for a thicker shell. The reduced damping and the increase of the absorption maximum validate the decreased linewidth in Fig. 3.22. We also find an enhanced growth of the peak maximum and a smaller line width (shown in Fig. 3.22) for a smaller static dielectric constant $\epsilon_{H,s}$,

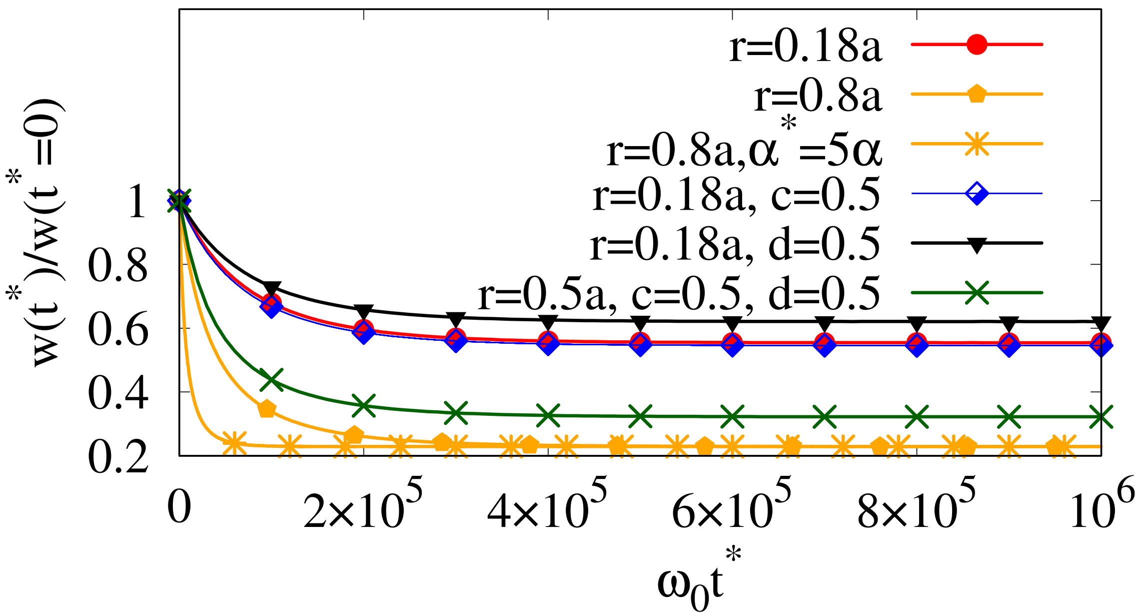

Figure 3.22: Full width at half maximum $w(t^*)/w(t^*=0)$ of the peak in the imaginary part of the susceptibility $\chi(\omega, t^*)$ in dependence of the time t^* elapsed since hydration shell formation has started, for different final shell extensions r. The high-frequency dielectric constant is set to $\epsilon_{H,\infty} = c\epsilon_{B,\infty}$ with $c = 0.8$, if not stated otherwise. The static dielectric constant $\epsilon_{H,s} = d\epsilon_{B,s}$ with $d = 0.1$, if not stated otherwise. The inner Onsager sphere radius reads $a = 3.6$Å and $\alpha = 10^{-5}\omega_0$, $\alpha^* = 5\alpha$ and the Debye times are $\tau_{D,H} = 10\tau_{D,B}$.

while this effect is not visible for a smaller high-frequency dielectric constant, see inset of Fig. 3.23. We thus can conclude that the high-frequency constant $\epsilon_{H,\infty}$ contributes more to a renormalization of the eigenfrequency ω_0, while the static constant $\epsilon_{H,s}$ strongly influences the damping and hence the absorption maximum of the central dipole moment.

3.4.3 Time-dependent dielectric permittivity

In the second approach, the shell formation is described by a time-dependent decrease of the static $\epsilon_{H,s}$ and the high-frequency $\epsilon_{H,\infty}$ dielectric parameters of the dielectric continuum in a layer region with finite fixed thickness r around the Onsager cavity within a Debye model. Once the ion has been neutralized by a light pulse, a hydrogen network will be gradually formed associated with its specific dielectric constant. During this process, the dielectric parameters will progressively decrease from their initial values of bulk water to

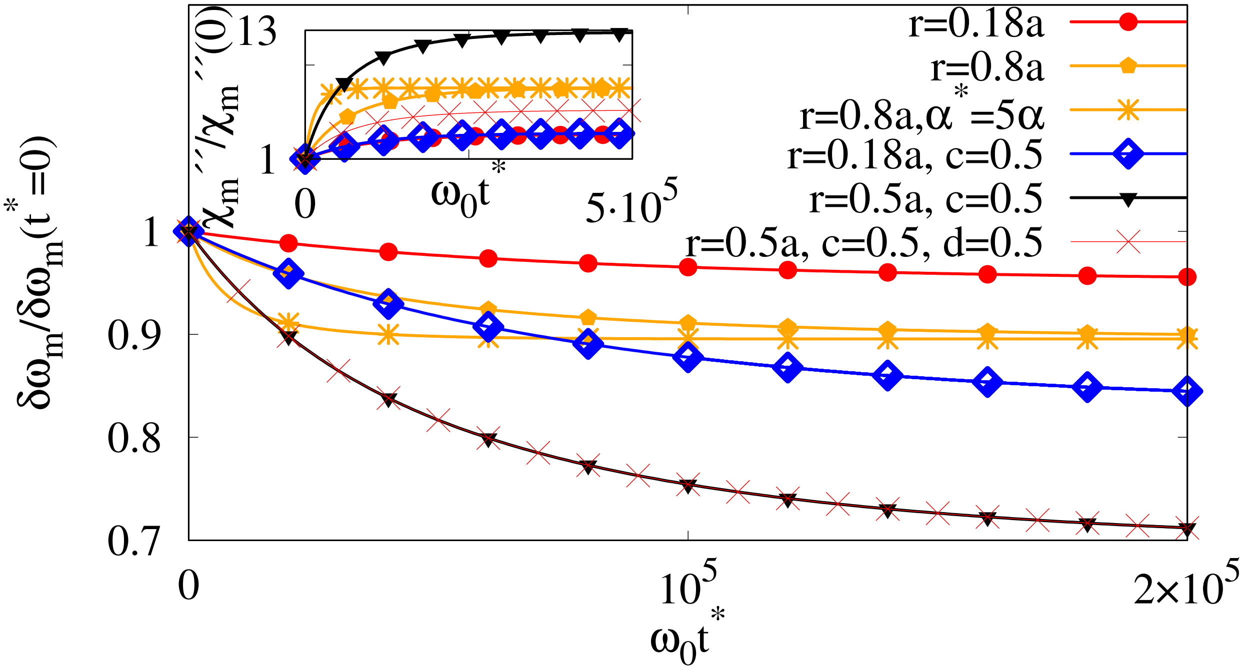

Figure 3.23: Relative frequency shift $\delta\omega_m(t^*) = \omega_m(t^*) - \omega_0$ of the peak in the imaginary part $\chi''_m(t^*)$ in dependence of t^* for different final shell extensions r. The high-frequency dielectric constant is $\epsilon_{H,\infty} = c\epsilon_{B,\infty}$ with $c = 0.8$, if not specified otherwise. The static dielectric constant is $\epsilon_{H,s} = d\epsilon_{B,s}$ with $d = 0.1$, if not specified otherwise. Inset: Evolution of the peak maximum in the imaginary part in dependence of t^*. The inner Onsager sphere radius is $a = 3.6$Å, $\alpha = 10^{-5}\omega_0$, $\alpha^* = 5\alpha$ and $\tau_{D,H} = 10\tau_{D,B}$.

the their final values. Within this picture, the small environmental dipole moments arrange themselves successively in a network of hydrogen bonds within the fixed shell thickness r. The overall temporal Debye form will be kept unchanged with the fixed relaxation time $\tau_{H,D} = \tau_{B,D}$, see Eq. (3.74), while the prefactors decrease according to

$$g(t, t_0) = 1 - h[1 - e^{-\alpha(t-t_0)}]\Theta(t - t_0)\,, \tag{3.84}$$

where $1-h$ describes the final magnitude of the dielectric parameters within the shell, while t_0 is again the time when the shell formation starts. α defines the rate of the decrease of the dielectric parameter. The exponential decrease in Eq. (3.84) is chosen because the hydration shell forms out more rapidly at the beginning, before it successively reaches its final dielectric properties. The model parameter is chosen as $0 < h < 1$ because the more strongly coupled water network of the shell can be described by a reduced dielectric constant and the dipoles in the shell are less polarizable than bulk water.

Again with the same idea as before, we treat $g(t)$ adiabatically in Eqs. (3.76)-(3.79). After Fourier transforming the resulting reaction field, we find

$$\begin{aligned} R(\omega) &= \frac{\mu(\omega)}{a^3}\frac{2[g(t^*,t_0)-1][2+g(t^*,t_0)\epsilon_B(\omega)]a^3-2[2+g(t^*,t_0)][g(t^*,t_0)\epsilon_B(\omega)-1]b^3}{[g(t^*,t_0)\epsilon_B(\omega)-1][g(t^*,t_0)-1]2a^3-[2+g(t^*,t_0)][2g(t^*,t_0)\epsilon_B(\omega)+1]b^3} \\ &\equiv \xi(\omega,t_0,t^*)\mu(\omega) = e\xi(\omega,t_0,t^*)q(\omega), \end{aligned} \tag{3.85}$$

where $\xi(\omega,t_0,t^*)$ contains all information about the adiabatically decreasing dielectric parameter within the solvation shell. One has to ensure that $\alpha \ll \Gamma$, where Γ is the damping of the induced reaction field $A(t)$ inside the hydration shell. Hence, $g(t) \equiv g(t^*)$ can be treated parametrically. As before, the time $t_0 = 0$ marks the onset of the hydration shell formation, while t^* is the beginning of the evaluation of the response, the lower boundary of the Fourier transform, reflecting the arrival of the external pulse, where $t^* \geq t_0$. We are now able to study the response to an external electric field with the reaction field given in Eq. (3.85), which we insert into Eq. (3.83). As before in the approach with a growing layer (Subsec. 3.4.2), one also finds here a relative frequency up-shift in the absorptive part of the response function. This is shown in Fig. 3.24, where we compare the results of both approaches.

For the dynamically increasing radius, scenario in Subsec. 3.4.2 (labeled with A in Fig. 3.24), the frequency shift decreases faster with time than for the decreasing dielectric parameter of the present scenario (labeled with B in Fig. 3.24). Formally, this may be understood by the fact that $b(t)^3$ enters cubic in Eq. (3.80) while $g(t)$ appears as linear in Eq. (3.85). The surface of the hydration shell grows quadratically in growing scenario of Subsec. 3.4.2 and, thus, also the number of involved environmental dipoles, whereas the total number of the involved dipoles in the present scenario is constant and they adjust themselves all together at the same time. With a more reduced dielectric constant in the shell, its polarizability decreases in comparison to the bulk and the total up-shift is more pronounced, as seen in Fig. 3.24.

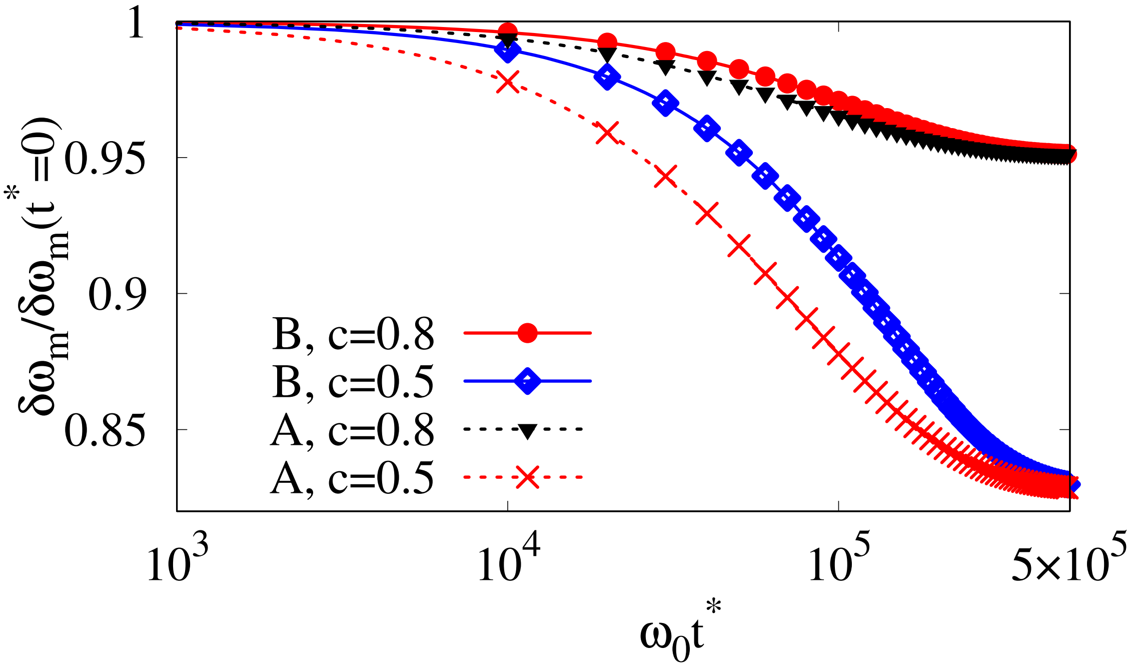

Figure 3.24: Relative frequency shift $\delta\omega_m(t^*) = \omega_m(t^*) - \omega_0$ of the peak in the imaginary part of the susceptibility $\chi''_m(t^*)$ in dependence of the time t^* since hydration shell formation has started, as described by the growing approach (labeled with A) of Subsec. 3.4.2 with an increasing radius $b(t)$, and by the time-dependent dielectric approach (labeled with B) of Subsec. 3.4.3 with a gradual reduction of the dielectric constant in the layer region. The high-frequency and static dielectric constants are $\epsilon_{H,\infty/s} = c\epsilon_{B,\infty/s}$. The inner Onsager sphere radius is $a = 3.6$Å, the shell thickness $r = 0.8a$ and $\alpha = 10^{-5}\omega_0$. The Debye times are here $\tau_{D,H} = \tau_{D,B}$ for both scenarios.

3.4.4 Summary

We have studied the time-resolved response of a molecule, becoming a hydrophobic agent, which is embedded in water as a highly polar environment, around which a layer of hydrated water grows dynamically. This model refers to the abstraction of an electron of iodide which results in its neutral but strongly hydrophobic iodine partner [49]. After the formation of the apolar hydrophobic solute, hydrogen bonds in the water have to be broken up and the water molecules have to rearrange. This hydrophobic solvation process is accompanied by a formation of a hydration shell which leads to a reduction of the overall entropy such that the solubility is energetically highly unfavorable. In the very proximity of the hydrophobic agent, the polarizability of the water is assumed to be reduced since water molecules form strengthened hydrogen bonds and the fluctuations are slowed down as compared to bulk water. This is modeled by a continuous hydration layer with reduced dielectric constants.

With this continuum model, we are able to calculate the time-dependent response of the central probe dipole in this nonequilibrium environment to an external electric field. Within our calculation, we have assumed that the electric probe pulse is long enough to drive the dipole to a stationary oscillation, but short enough to treat the change of the radius of the cluster adiabatically. In good agreement with the experiment, we find a time scale of the shell formation of $\alpha^{-1} \sim$ ps [49, 111]. We have studied two scenarios of the hydration shell formation, where, within the first one (Subsec. 3.4.2), the thickness of the spherical shell grows progressively, while, in the second one (Subsec. 3.4.3), the Debye dielectric permittivity decreases gradually for a fixed shell extension. Both approaches yield a relative dynamical frequency up-shift of the resonance in the absorptive part of the response function during the shell formation, which signals a positive free energy during the hydrophobic solvation. The time-dependent frequency blue shift is accompanied by a reduced line width in the absorptive peak which additionally indicates less damping due to a more rigid structural order and stronger hydrogen bonds of the water molecules in the shell as compared to bulk water. For both scenarios, the dynamic frequency shifts of the absorption resonance reveals the dynamics of the hydration shell formation. Further experimental investigation by pico- and femtosecond absorption spectroscopy will lead to more detailed insights to elucidate the hydrophobic solvation process on the atomic scale, and, in particular, into the dielectric properties inside the hydration shell.

Chapter 4

Charge transfer in molecular junction in non-equilibrated solvents[1]

Metal-molecule-metal junctions that operate in dielectric solvent are common in many applications, for example in junctions controlled by electrochemical gating. Transport in such junctions often occur by successive electron hopping between molecular sites as well as between the molecule and the metal leads [115]. In the simplest model when the molecule supports only one electron localization site, this site is repeatedly occupied and de-occupied as electrons hop between meal and molecule. Each such hopping event is accompanied by solvent relaxation (so called reorganization) to accommodate the molecule charging state and determines the time for transient localization. The overall conduction in this case is determined by metal-molecule coupling, the solvent-imparted stabilization (reorganization energy or polaron formation energy) and solvent fluctuations needed to overcome the localization barrier.

Theoretical treatments of such sequential hopping events usually rely on the Marcus electron transfer theory [115] introduced in Subsec. 2.4.3. This is a transition-state type theory that assumes that solvent relaxation between hopping events proceeds to full thermal equilibrium so that the next electron transfer event takes place out of an equilibrium distribution solvent configurations (see nonadiabatic charge transfer rate in Eq. (2.60) in Subsec. 2.4.3). Such behavior can be realized when solvent reorganization in response to charge localization on the connecting molecule is fast relative to the molecule-leads' tunneling rates. The other extreme limit, where the solvent is not sensitive to the molecular

---

[1] The model presented in this chapter is based on the publication : H. Kirchberg, M. Thorwart and A. Nitzan, "Charge Transfer Through Redox Molecular Junction In Non-Equilibrated Solvents," J. Phys. Chem. Lett., accepted for publication (2020).

charge redistribution, corresponds to co-tunneling transport that is described by the Landauer theory. However, even when localization and solvent relaxation make consecutive hopping the dominant mechanism, the assumption of full thermal relaxation embedded in the Marcus theory is not necessarily valid, and extension of Marcus theory to situations where the electron transfer rate is 'solvent controlled', in the sense that it depends on the solvent relaxation dynamics, are abundant [116, 117, 118, 119].

Most relevant to the present chapter are studies that focus on solvent dynamic effects in bridge-mediated electron transfer [120, 121], where solvent dynamics is not manifested just in the electron-transfer rate but in the determination of the very nature of the processes between the limiting forms of cotunneling (or superexchange) and sequential hopping. The publications cited above are representative of a substantial body of literature that analyzes deviations of the electron transfer rate from its transition state theory (TST) form due to finite solvent relaxation time. TST becomes valid when this relaxation is assumed fast, implying that bridge mediated transfer is sequential, with the individual hopping rates assuming their Marcus form (see Eq. (2.60) in Subsec. 2.4.3). As discussed extensively in the context of the classical theory of barrier crossing, slow relaxation does not necessarily imply weak coupling to the solvent [50, 122, 123]. Indeed, solvent relaxation in response to solute state-change is manifested in classical barrier crossing rates as a crossover between the low- and high-friction limits [123, 124, 125], with the rate increasing or decreasing with increasing friction at the low- (underdamped) and high- (overdamped) friction limits, while the TST approximation provides an upper bound on the rate in the intermediate crossover region. Most treatments of such effects in electron transfer have focused on the case of low friction although the other limit has also been considered [126].

In this chapter, we consider the effect of finite solvent-induced relaxation on the hopping conduction in molecular junctions, thus going beyond the standard treatments of transport in solvated molecular junctions that rely on Marcus theory. We maintain other assumptions of this theory: electron tunneling is conditional on the possibility to conserve the total (electronic and nuclear) energy, and broadening of molecular electronic levels due to their interaction with the metal leads is disregarded so that electron-transfer (ET) rates into or out of the metal electron level ϵ are proportional to $\Gamma f(\epsilon)$ and $\Gamma[1-f(\epsilon)]$, respectively, where Γ is a golden rule rate associated with the molecule-metal coupling, and $f(\epsilon)$ the Fermi function [127, 31]. The corresponding Marcus rates k_{AB} (from the electrode to the molecule) and the reverse $k_{B\to A}$ are

$$k_{AB} = \int d\epsilon \Gamma(\epsilon) f(\epsilon) F(E_{AB} + \epsilon) \tag{4.1}$$

$$k_{BA} = \int d\epsilon \Gamma(\epsilon)[1 - f(\epsilon)] F(\Delta E - \epsilon), \tag{4.2}$$

where $E_{AB} = E_A - E_B$ is the energy difference between the molecular state A and B and the rate derived for donor-acceptor ET in Eq. (2.60) of Subsec. 2.4.3

$$F(x) = \frac{1}{\sqrt{4\pi E_R k_B T}} \exp\left\{ -\frac{(x - E_R)^2}{4E_R k_B T} \right\}, \tag{4.3}$$

with T and k_B denoting the temperature and the Boltzmann constant, respectively (throughout this chapter we assume that the temperature of the metal electrodes and the solvent are equal) and E_R is the solvent reorganization energy - the free energy released by relaxation of the solvent to its stable (equilibrium) configuration following a sudden transition between the oxidized and reduced molecular states (see discussion in Subsec. 2.4.3). Eq. (4.3) is the high-temperature limit of the average, over a thermal (Boltzmann) distribution of solvent configurations, of Franck-Condon factors (see Eq. (2.60) in Subsec. 2.4.3) that reflect the dependence of the solvent configuration on the molecular electronic state. When the finite timescale of the solvent relaxation is taken into account, this thermal distribution is replaced by a time-dependent probability distribution that reflects this relaxation.

In the following model, I describe this dynamics by diffusion (Smoluchowski) equations that take different forms in the high- and low-friction limits. In analogy to the Kramers theory of activated barrier crossing [50], the high-friction (overdamped) limit is characterized by diffusion along the position coordinate, while the low-friction is described by diffusion in energy space. In either case, we find that the average junction current resulting from this calculation depends on the friction parameter γ that determines the solvent relaxation rate. Of further significance is the dependence of the current noise on this relaxation rate. For small damping we show that the process is Markovian and the hopping statistics is Poissonian. When solvent relaxation occurs on a finite timescale, successive electron hopping events are correlated. We suggest that a combined measurement of average current and current noise may serve to identify such situations in solvated electronic junctions.

This leads to the following structure of this chapter: In Sec. 4.1 we derive the theoretical model for the ET transfer in solvent that relaxes on a finite timescale. To this end, we solve the diffusion equation in the overdamped regime for a solvent reaction coordinate and in the regime of low damping for the total solvent energy as diffusive variable, respectively. We construct a suitable Monte Carlo simulation procedure to calculate the average charge current and the charge current correlation function, which is described in Sec. 4.2. In Sec. 4.3, we analyze the calculated average current and current correlation for the different modes of operation in the overdamped and low-damping regime. Finally, we discuss the possibility to realize these limiting behaviors through the dependence of solvent relaxation dynamics on its geometrical confinements. Sec. 4.4 summarizes this chapter.

4.1 Theoretical Model

We consider a molecular system weakly coupled to two metal electrodes R (right) and L (left) which are modeled as free electron reservoirs characterized by their respective chemical potentials μ_K and the potentials $\phi_K (K = L, R)$ due the external applied voltage. The associated Fermi functions for the electron energy ϵ read

$$f_K(\epsilon) = \frac{1}{\exp\left(\frac{\epsilon - \mu_K + e\Phi_K}{k_B T}\right) + 1}, \tag{4.4}$$

where $K = L, R$, and e, k_B and T are the electron charge, the Boltzmann constant and the temperature, respectively.

The molecular system comprises a single channel, a two-state system with an oxidized state A, with $N-1$ electrons, with energy E_A, and a reduced state B, with N electrons, with energy E_B. The molecular system is embedded in a polar solvent that imposes a fluctuating environment and responds electrodynamically to the charging state of the molecule [2]. In the Marcus theory [43, 44], this response is expressed by a distribution of solvent configurations along a single reaction coordinate, x, determined by free energy surfaces that depend on the molecular electronic state according to (see Eqs. (2.45) and

---

[2] As discussed in Subsec. 2.4.1, the electron transfer theory may be represented by a standard spin-boson model, with the solvent represented as bosonic environment coupled linearly to the molecular electronic occupation [64, 65]. A standard polaron transformation of this Hamiltonian yields a system with two electronic levels system, a harmonic bath comprising independent normal modes and coupling that connects transitions between the two electronic levels with shifts in the equilibrium position of these modes.

(2.47) in Subsec. 2.4.1 for a single solvent mode and Ref. [31])

$$E_A(x) = E_A + \frac{1}{2}\hbar\omega_0 x^2 + \epsilon \tag{4.5}$$

$$E_B(x) = E_B + \frac{1}{2}\hbar\omega_0 (x-d)^2. \tag{4.6}$$

In this shifted harmonic surfaces model, E_A and E_B are the electronic energies at the equilibrium solvent configurations, chosen as $x_A = 0$ and $x_B = d$ for the state A and B respectively. The harmonic forms and the identical curvatures of these surfaces correspond to the assumption that the solvent responds linearly to the charging state of the molecule and has the consequence that the reorganization energy

$$E_R = \frac{1}{2}\hbar\omega_0 d^2 \tag{4.7}$$

is the same irrespective of the process direction from A to B or vice versa.

The single-electron energy ϵ is added to the molecular energy in state A (cf. Eq. (4.5)), expressing the fact that when the molecule is oxidized, the electron removed from it is occupying a single electron state of energy ϵ in the metal. The integrals over ϵ in Eqs. (4.1) and (4.2) reflect the broad band of single electron states in the metal. The Marcus theory makes two further simplifying assumptions: the small molecule-metal coupling and the high-temperature limit. Together they have several implications. First, the assumption that $\hbar\Gamma \ll k_B T$, allows to disregard level broadening due to the finite lifetime of excess electron or holes on the molecule. Secondly, in the high-temperature limit, nuclear tunneling can be disregarded in evaluating the electron hopping rate, namely such events are assumed to be dominated by crossings of nuclear potential surfaces. Finally, the small electronic coupling Γ makes it possible to use perturbation theory to the lowest order in the electronic coupling for evaluating the electron hopping probability, essentially disregarding level splitting in this calculation (e.g., using the non-adiabatic limit of the Landau-Zenner expression for this probability). Under these assumptions, electron transfer events are dominated by nuclear configurations where $E_A(x) = E_B(x)$, namely at the transition point along the reaction coordinate given by

$$x_{TR} = \frac{E_B - E_A - \epsilon + \frac{1}{2}\hbar\omega_0 d^2}{\hbar\omega_0 d}. \tag{4.8}$$

Marcus theory [43, 44] is based on transition state theory of reaction rates. It provides a framework for representing the solvent sate in a one-dimensional free-energy surface defined with respect to a single reaction coordinate that the electronic energies in states A and B depend only on a single solvent quantifier, in the present case, the local solvent polarization. Extending this theory to the dynamical regime requires an additional assumption, tacitly made in most studies like those cited above, that the same free energy surfaces $E_A(x)$ and $E_B(x)$ can be used as potential energy surfaces for the reaction coordinate x, provided that account is taken for the fact that this coordinate can exchange energy with all other solvent degrees of freedom [3]. Making the additional assumption that this dynamics is Markovian, the motion of the reaction coordinate, when the molecule is in state A or B, can be described by a Langevin equation by augmenting Newtonian dynamics on the potential surfaces (4.5) or (4.6) by a friction γ and a random noise terms that satisfy the standard fluctuation-dissipation relations according to Sec. 2.1. Equivalently, the probability distribution $P_j(x, v; t)$ for the molecular states $j = A, B$ obeys under these conditions the Fokker-Planck equation

$$\frac{\partial P_j(x,v;t)}{\partial t} = \omega_0 \frac{d\bar{V}_j}{dx}\frac{\partial P_j}{\partial v} - \omega_0 v \frac{\partial P_j}{\partial x} + \gamma \left[\frac{\partial}{\partial v}(vP_j) + \frac{k_B T}{\hbar\omega_0}\frac{\partial^2 P_j}{\partial v^2}\right]. \tag{4.9}$$

In Eq. 4.9, the normalized potential surfaces are $\bar{V}_j = V_j/(\hbar\omega_0)$ with $V_A(x) = \frac{1}{2}\hbar\omega_0 x^2$ and $V_B(x) = \frac{1}{2}\hbar\omega_0(x-d)^2$. We note that the position and velocity variables in Eqs. (4.5),(4.6) and (4.9) are dimensionless, and related to their dimensioned counterparts $\bar{x}, \bar{v}$ by $x = \sqrt{m\omega_0/\hbar}\bar{x}$ and $v = \sqrt{m/(\hbar\omega_0)}\bar{v}$. The solvent properties that enter at this level of description are manifested via the parameters ω_0 and γ that can be obtained from fitting of an observed dielectric response of the solvent to standard dielectric response models which will be described in more detail for γ in Subsec. 4.3.4. The solvent-molecule coupling enters through the parameter d that determines the solvent reorganization energy E_R as given in Eq. (4.7) and discussed in the system-bath model in Subsec. 2.4.1. We note that the overdamped limit of Eq. (4.9) has been used in the Zusman generalization of the Marcus theory [116, 117]

In the following Subsections 4.1.1 and 4.1.2, in analogy to Kramers treatments of activated barrier crossing [50], we consider the implications of this dynamics in two limits. In the overdamped limit, $\gamma \gg \omega_0$, Eq. (4.9) leads to a Smoluchowski equation that describes

---

[3] A detailed theoretical treatment may be the reaction coordinate mapping. Here one incorporates a distinct bath degree of freedom, the reaction coordinate, into an enlarged system Hamiltonian, which is then treated explicitly. The remaining reservoir degrees of freedom are again traced out in the usual pertubative manner [128].

diffusion along the x coordinate,

$$\begin{aligned} \frac{\partial}{\partial t} P_j(x,t|x'_{TR},t_{TR}) &= -\frac{\partial}{\partial x}[\dot{x} P_j(x,t|x'_{TR},t_{TR})] \\ &= \frac{\omega_0}{\hbar\beta\gamma}\frac{\partial}{\partial x}\left[\frac{\partial}{\partial x} + \beta\hbar\omega_0 \frac{d\bar{V}_j(x)}{dx}\right] P_j(x,t|x'_{TR},t_{TR})\,, \end{aligned} \tag{4.10}$$

where $\beta = (k_BT)^{-1}$. In the opposite underdamped limit, $\gamma \ll \omega_0$, the relaxation implied by Eq. (4.9) may be reduced, after phase averaging [31], to diffusion in energy space, described by

$$\begin{aligned} \frac{\partial P(E)}{\partial t} &= \frac{\partial}{\partial E}\left[\gamma E\left[1 + k_BT\frac{\partial}{\partial E}\right]P(E)\right] \\ &= \frac{\partial}{\partial E}\gamma\left[E - k_BT\right]P(E) + \frac{\partial^2}{\partial E^2}\gamma E k_BT P(E). \end{aligned} \tag{4.11}$$

The distribution functions $P(x,t)$ from Eq. (4.10) or $P(E,t)$ from Eq. (4.11) replace the Boltzmann distribution in the evaluation of the instantaneous probability for electron transfer, leading to time-dependent rates that will replace the rates of Eqs. (4.1) and (4.2). We note that the stationary solution of both Eqs. (4.10) and (4.11) is the Boltzmann distribution, implying that transition-state theory will be recovered when relaxation is fast, $\gamma \to 0$ in Eq. (4.10) or $\gamma \to \infty$ in Eq. (4.11).

We are now ready to solve Eqs. (4.10) and (4.11) to obtain charge transfer rates in the respective limits to investigate their implications for standard observables like the average charge current noise.

4.1.1 Overdamped regime

The probability densities resulting from the Smoluchowski equation (4.10) for the overdamped reaction coordinate x ($\gamma \gg \omega_0$) can be calculated exactly. In this limit, the probability densities are velocity independent. Eq. (4.10) should be solved now for every time segment between electron transfer events with the initial condition

$$P_j(x,t_{TR}|x'_{TR},t_{TR}) = \delta(x - x'_{TR})\ , \tag{4.12}$$

where $t_{TR} < t$ is the time of the preceding electron transfer event, given that the event occurred with the reaction coordinate at position x'_{TR}. The solutions are (see also illustration

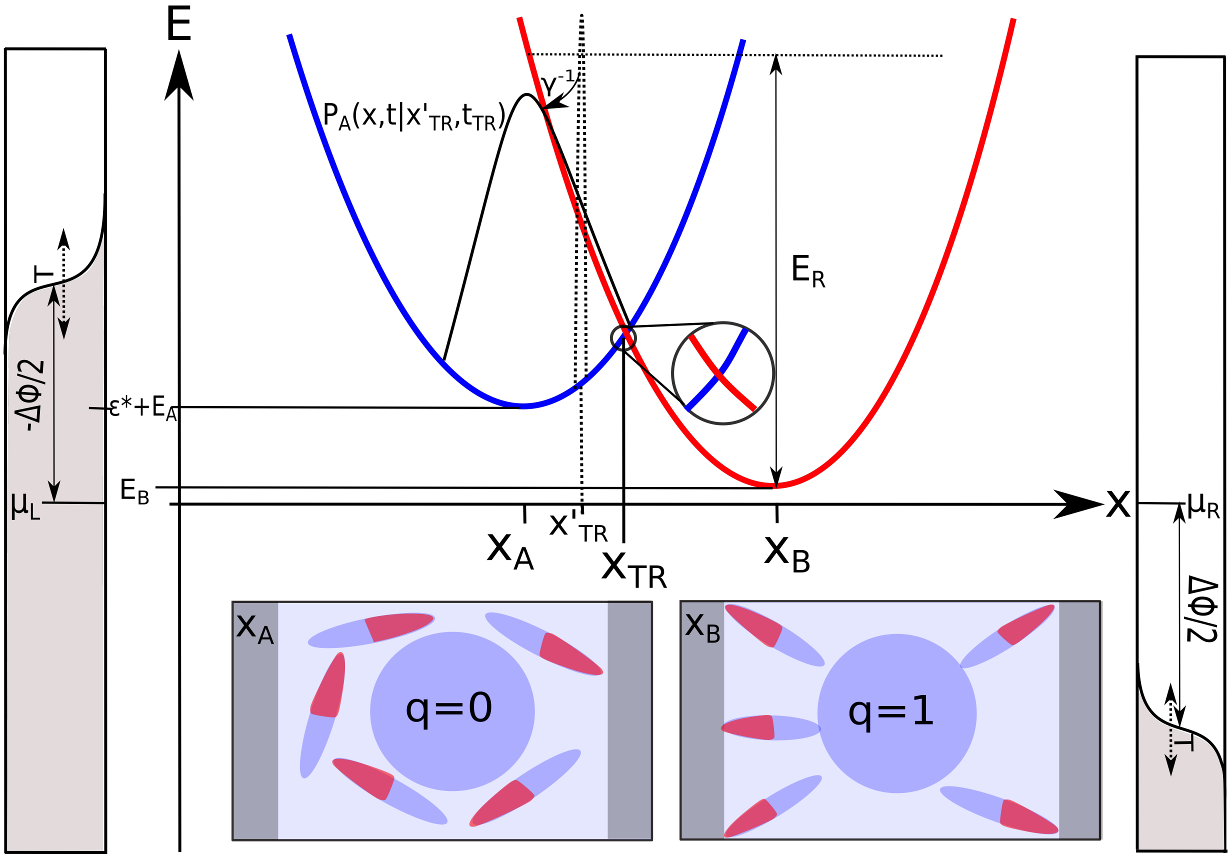

Figure 4.1: Energy representation of the electron transfer process. The blue diabat represents the oxidized state A including the energy alignment with a charge of an arbitrarily chosen energy ϵ^*, the red diabat the reduced state B. The energy distribution of the charges and vacancies in the left ($K = L$) and right ($K = R$) electrode follows out of the Fermi distribution $f_K(\epsilon)$ (or $1 - f_K(\epsilon)$), respectively, of Eq. (4.4) with temperature T. The state energy strongly depends on the solvent configuration described by the reaction coordinate x (see Eqs. (4.5) and (4.6)). The relaxation of the reaction coordinate x after a previous transition at x'_{TR} is described by its probability density (black colored) under the action of the damping γ. The boxes show the equilibrium solvent configuration $x_A = 0$ for the oxidized state and $x_B = d$ for the reduced state indicating the fluctuating dipole of the solvent molecules.

in Fig. 3.2)

$$P_A(x,t|x'_{TR},t_{TR}) = \sqrt{\frac{D}{2\pi[1-a^2(t-t_{TR})]}} \exp\left\{-\frac{D}{2}\frac{[x-a(t-t_{TR})x'_{TR}]^2}{1-a^2(t-t_{TR})}\right\} , \qquad (4.13)$$

$$P_B(x,t|x'_{TR},t_{TR}) = \sqrt{\frac{D}{2\pi[1-a^2(t-t_{TR})]}} \exp\left\{-\frac{D}{2}\frac{[x-d-a(t-t_{TR})(x'_{TR}-d)]^2}{1-a^2(t-t_{TR})}\right\} , \qquad (4.14)$$

where $D = \beta\hbar\omega_0$ and $a(t) = \exp\left[-\frac{\omega_0^2}{\gamma}t\right]$. For $\gamma \to 0$, $a(t) \to \infty$ for all time $t > 0$, indication "instantaneous" relaxation to an equilibrium Boltzmann distribution in the corresponding wells.

$P_A(x,t|x'_{TR},t_{TR})dx$ is the probability to find a solvent configuration with a reaction coordinate in $[x, x+dx]$ for the the oxidized state A at time t, given that the previous transition from the reduced state B has occurred at the solvent configuration x'_{TR} at time t_{TR}. Correspondingly, $P_B(x,t|x'_{TR},t_{TR})dx$ describes the equivalent for the reduced state B. It is important to notice that the next electronic transition can take place at any x. This x then becomes the next transition configuration x_{TR} for which the energy $\epsilon(x_{TR})$ and consequently the probabilities to find a corresponding metal level occupied $f_K(x)$ or unoccupied $1 - f_K(x)$ are determined from Eq. (4.8).

Correspondingly, the ET rates (probabilities per unit time), k_{AB} into the molecule, and k_{BA} out of the molecule, are given in this high-friction limit by

$$k^K_{AB}(t - t_{TR}; x'_{TR}) = \Gamma \int_{-\infty}^{\infty} dx P_A(x,t|x'_{TR},t_{TR}) f_K(x) \tag{4.15}$$

$$k^K_{BA}(t - t_{TR}; x'_{TR}) = \Gamma \int_{-\infty}^{\infty} dx P_B(x,t|x'_{TR},t_{TR}) \big(1 - f_K(x)\big), \tag{4.16}$$

where $K = L$ or R. Γ is assumed to be independent of the solvent configuration x while Γ^{-1} characterizes the time span between the electron hopping events.

We emphasize again that the integration over all solvent configuration in Eqs. (4.15) and (4.16) can be extended to $\pm\infty$ because a transition may occur at every solvent configuration along the reaction coordinate, subjected to the Pauli principle that is accounted in Eqs. (4.15) and (4.16). In agreement with the above observation that the limit $\gamma \to 0$ correspond to "infinitely fast" relaxation to equilibrium, the rates given in Eqs. (4.15) and (4.16) become the thermal Marcus rates of Eqs. (4.1) and (4.2).

Using the rates of Eqs. (4.15) and (4.16), we can calculate the average current and its correlation with a numerical Monte Carlo procedure (Sec. 4.2). The solvent dynamics is propagated using Eq. (4.13) or (4.14) depending on the present state of the molecule, and at any time step transition is attempted using the probabilities (4.15) or (4.16) depending again on the current molecular state.

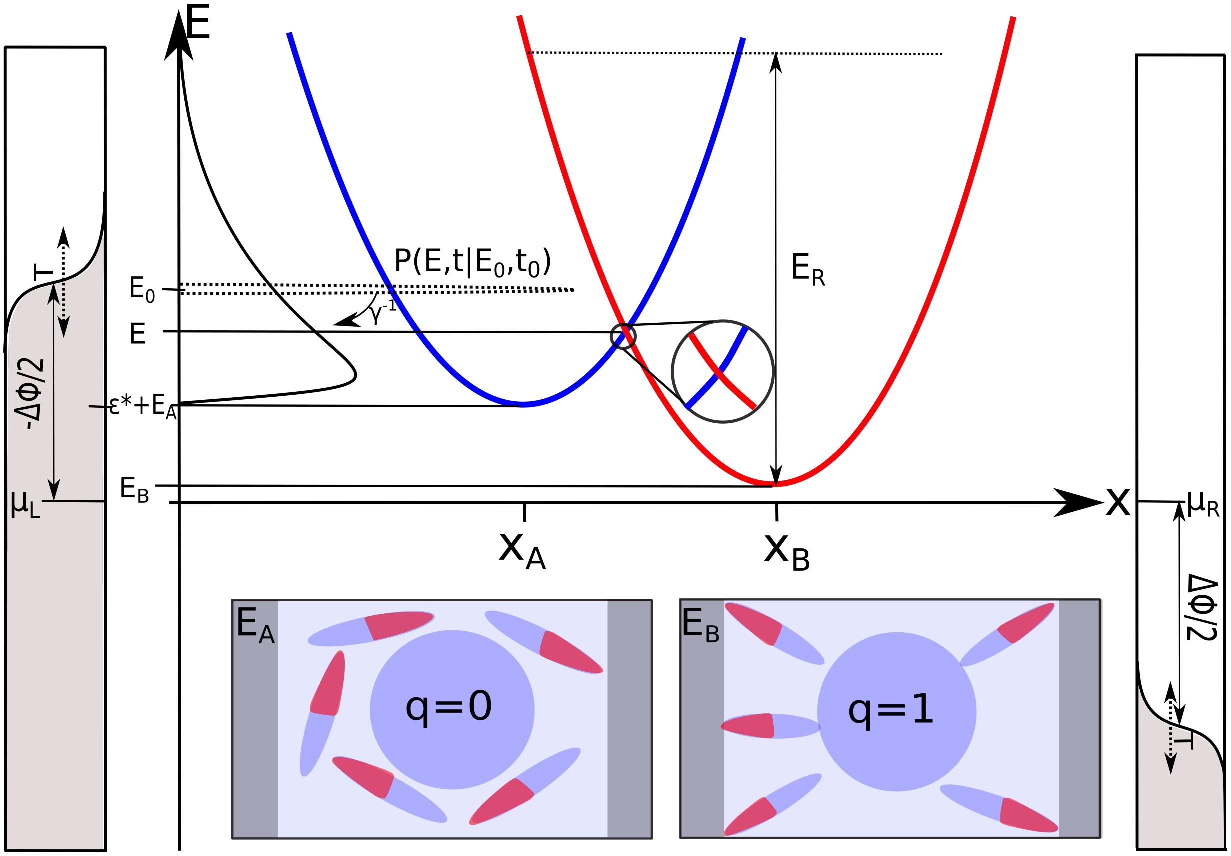

Figure 4.2: Energy representation of the electron transmission process. The blue diabat represents the oxidized state A including the energy alignment with a charge of arbitrarily chosen energy ϵ^*, the red diabat the reduced state B. The energy distribution of the charges and vacancies in the left ($K = L$) and right ($K = R$) electrode follows out of the Fermi distribution $f_K(\epsilon)$ $(1 - f_K(\epsilon))$ (Eq. (4.4)) with temperature T. The state energy strongly depends on the solvent configuration described by the solvent energy E, see Eqs. (4.5) and (4.6). The relaxation of the energy E after a previous transition with E_0 is described by its probability density (black colored) influenced by the damping γ. The boxes show the equilibrium energy E_A for the oxidized state and E_B for the reduced state by means of adjustable dipoles where the solvent energy has its minimum respectively.

4.1.2 Low-damping regime

In the regime of low damping, $\gamma \ll \omega_0$, the reaction coordinate oscillates many times under its harmonic restoring force before appreciable relaxation occurs. In this case, as in the Kramers [50] regime of low damping, the parameter that determines the probability of electron transfer and relaxes due to the interaction with the thermal environment is the energy. In the Kramers case, the rate in this limit is determined by the inverse mean first-passage time to reach a critical energy. Here, the rate can be obtained from the golden rule (see Eq. 2.55 in Subsec. 2.4.3 by including the electronic states of the metal) say for the $A \to B$ transition, in the form

$$k_{AB} = \frac{2\pi}{\hbar}\int_{-\infty}^{\infty} d\epsilon \rho_M(\epsilon) f(\epsilon) \sum_{v;v'} |\langle v|\hat{V}_{A,B}|v'\rangle|^2 \delta(E_A - E_B + \epsilon + E_b(v) - E_b(v')) \,, \quad (4.17)$$

where $E_A(v)$, $E_B(v')$ are eigenvalues of the solvent Hamiltonian (harmonic oscillator state on the potential surfaces $E_A(x)$ and $E_B(x)$), $\hat{V}_{AB}$ is the interstate coupling and $\rho_m(\epsilon)$ is the density of single electron states in the metal. We further consider the density of states $\rho_M(\epsilon) = \rho_M =$ const. as independent of the electron energy.

In the Appendix C, we show that Eq. (4.17) can be transformed into the expression

$$k_{AB} = \Gamma \int_{-\infty}^{\infty} d\epsilon f(\epsilon) \int_{-\infty}^{\infty} dt e^{i(E_A - E_B + \epsilon)t/\hbar} e^{-ig^2 \sin(\omega_0 t) + g^2[2n(t)+1][\cos(\omega_0 t) - 1]}, \quad (4.18)$$

where $\Gamma = \frac{\rho_M |V_{A,B}|^2}{\hbar^2}$ is the conditional rate and g determines the coupling between the solvent (oscillator) states and the molecular state A or B. Eqs. (4.17) and (4.18) are not limited to the semi-classical limit used in the Marcus theory and, in fact constitute, for this low-damping limit, an extension of the Marcus formalism. Keeping, for simplicity, the Marcus level of treatment, we exploit an additional approximation which is equivalent to the high-temperature limit used in the transition state theory limit (see derivation for Eq. (2.60) in Subsec. 2.4.3): Assuming $n(t) \gg 1$ in the relevant range of solvent energy, and because the reaction coordinate x interacts in this energy range with many solvent degrees of freedom, the integrand is very short-lived [129] and can be approximated by expanding the sine term up to first and the cosine term up to second order in the argument $\omega_0 t$. This short-time expansion leads to

$$\begin{aligned} k_{AB} =& \Gamma \int_{-\infty}^{\infty} d\epsilon f(\epsilon) \int_{-\infty}^{\infty} dt e^{i(E_A - E_B + \epsilon)t/\hbar - itg^2\omega_0 - t^2 g^2 \omega_0^2 [2n(t)+1]/2} \\ =& \Gamma \sqrt{\frac{\pi}{a}} \int_{-\infty}^{\infty} d\epsilon f(\epsilon) e^{-\frac{(E_A - E_B + \epsilon - E_R)^2}{4\hbar^2 a}}, \end{aligned} \quad (4.19)$$

where we consider $n(t)$ to evolve only slightly in time for slow energy relaxation ($\gamma \ll \omega_0$). Moreover, we perform the time integral in Eq. (4.19) by regarding $n(t)$ as a constant parameter. We introduce $a = (2n(t)+1)g^2\omega_0^2/2 \simeq E(t)E_R/\hbar^2$ as well as the reorganization energy $E_R = \hbar g^2 \omega_0$ and the solvent energy $E(t) = \hbar\omega_0 n(t)$ in Eq. (4.19).

The rates for the electron insertion and removal process accompanied by slow energy relaxation finally follow as

$$k_{AB}(t;E|E_0) = \Gamma\sqrt{\frac{\pi}{E(t)E_R}}\int_{-\infty}^{\infty} d\epsilon f(\epsilon) e^{-\frac{(E_A-E_B+\epsilon-E_R)^2}{4E(t)E_R}} \tag{4.20}$$

$$k_{BA}(t;E|E_0) = \Gamma\sqrt{\frac{\pi}{E(t)E_R}}\int_{-\infty}^{\infty} d\epsilon [1-f(\epsilon)] e^{-\frac{(E_B-E_A-\epsilon-E_R)^2}{4E(t)E_R}}. \tag{4.21}$$

Remarkably, the final result under this short-time approximation is similar to Marcus' result of Eq. (2.60) in Subsec. 2.4.3, except that the thermal energy k_BT is replaced by $E(t)$ - the (time-dependent) solvent energy expressed by the energy content in the reaction coordinate, calculated at time t, which is the time elapsed since the proceeding electron has hopped onto or out off the molecule, and subject to the initial condition $E(t=0) = E_0$, which is the energy at which the proceeding hopping took place.

Next, we consider the energy relaxation (or diffusion) dynamics, sketched in Fig. 4.2. As before, we look at the time evolution between two electron hopping events. For definiteness, we assume that the next electron hopping will be an $A \to B$ transition and the proceeding $B \to A$ event happened at time t_0 under system energy E_0. Following this event, the probability to find the system at time t with energy E is the solution of Eq. (4.11) with the initial condition $P(E,t_0|E_0,t_0) = \delta(E-E_0)$.

The solution of Eq. (**??**) may be found by performing a Fourier transform according to $P(c) = \int dE e^{icE} P(E)$, which yields

$$\frac{\partial P(c)}{\partial t} + \left[\gamma c - ic^2\gamma k_BT\right]\frac{\partial}{\partial c}P(c) = ick_BT\gamma P(c). \tag{4.22}$$

It can be solved by using the methods of characteristics $P(c,t) \to P(c(\tau),t(\tau))$, which implies

$$\frac{\partial P}{\partial \tau} = \frac{\partial P}{\partial c}\frac{\partial c}{\partial \tau} + \frac{\partial P}{\partial t}\frac{\partial t}{\partial \tau}. \tag{4.23}$$

Comparison of the coefficients leads to the ordinary differential equations

$$\frac{\partial t}{\partial \tau} = 1 \tag{4.24}$$

$$\frac{\partial c}{\partial \tau} = \gamma c - ic^2 \gamma k_B T \tag{4.25}$$

$$\frac{\partial P}{\partial \tau} = ick_B T \gamma P(c(\tau), t(\tau)). \tag{4.26}$$

Eq. (4.24) and Eq. (4.25) lead to

$$t = \tau \,, \tag{4.27}$$

$$\frac{\partial}{\partial t}\left[\frac{1}{c}\right] + \frac{\gamma}{c} - i\gamma k_B T = 0 \,, \tag{4.28}$$

and with $1/c \to z$, we find

$$\frac{\partial z}{\partial t} + \gamma z - i\gamma k_B T = 0, \quad \Rightarrow z(t) = ae^{-\gamma t} + \left(1 - e^{-\gamma t}\right) ik_B T, \tag{4.29}$$

while a is determined by the initial condition. Hence, this gives with $c(t = 0) = c_0 \Rightarrow a = 1/c_0$

$$c(t) = \frac{1}{ae^{-\gamma t} + (1 - e^{-\gamma t}) ik_B T} = \frac{c_0}{e^{-\gamma t} + (1 - e^{-\gamma t}) ik_B T c_0} \,. \tag{4.30}$$

Eq. (4.26) then leads to

$$P(t) = Ae^{\int_0^t dt' ik_B T c(t')} \tag{4.31}$$

$$= Ae^{\ln\left(1 - ik_B T c_0 + ik_B T c_0 e^{\gamma t}\right)} \tag{4.32}$$

$$= A\left(1 - ik_B T c_0 + ik_B T c_0 e^{\gamma t}\right), \tag{4.33}$$

where A may be defined by the initial conditions. With $c_0 = ce^{-\gamma t}/[1 - cik_B T(1 - e^{-\gamma t})]$, we get

$$P(c, t) = \frac{A}{1 - cik_B T(1 - e^{-\gamma t})}. \tag{4.34}$$

The initial condition $c(t=0)=c_0$ and the fixed initial energy E_0 translates to

$$P(c_0, t=0) = \int_{-\infty}^{\infty} dE e^{ic_0 E}\delta(E-E_0) = e^{ic_0E_0} \equiv A\,. \tag{4.35}$$

One now transforms $P(c,t)$ back to $P(E,t)$ and finds

$$\begin{aligned} P(E,t) &= \frac{1}{2\pi}\int_{-\infty}^{\infty} dc \exp\left(-iEc\right)\exp\left[\frac{iE_0ce^{-\gamma t}}{1-cik_BT(1-e^{-\gamma t})}\right]\frac{1}{1-cik_BT(1-e^{-\gamma t})} && (4.36)\\ &= \frac{1}{2\pi}\int_{-\infty}^{\infty} dc P(c,t). && (4.37)\end{aligned}$$

We identify $c_p = -i/[k_BT(1-e^{-\gamma t})] = -ih$ as a simple pole and can solve the integral by taking the real axis as contour of integration and an infinite semicircle in the lower half-plane towards the imaginary axis to end up with the residue of the lower half-plane. We have

$$\begin{aligned} P(E,t) &= \frac{1}{2\pi}\oint dc P(c,t) = \lim_{R\to\infty}\int_{-R}^{R} dc P(c,t) + \lim_{R\to\infty}\int_{0}^{\pi} d\theta P(Re^{i\theta},t)iRe^{i\theta} && (4.38)\\ &= \frac{-2\pi i}{2\pi}\mathrm{Res}_{c=-ih}P(c,t), && (4.39)\end{aligned}$$

where one uses $c = Re^{i\theta}$ in the second integral which one can neglect afterwards because $\lim_{|c|\to\infty} P(c,t) \to 0$, if $E \geq 0$. We further rewrite the function $P(c,t)$ as an infinite sum, which leads to

$$\begin{aligned} P(E,t) &= \frac{1}{2\pi}\int_{-\infty}^{\infty} dc \sum_{n=0}^{\infty}\frac{(iE_0ce^{-\gamma t} - iEc - Ec^2/h)^n (ih)^{n+1}}{n!(ih+c)^{n+1}}\Theta(E) && (4.40)\\ &= \frac{1}{2\pi}\int_{-\infty}^{\infty} dc \sum_{n=0}^{\infty}\frac{F(c)^n (ih)^{n+1}}{n!(ih+c)^{n+1}}\Theta(E). && (4.41)\end{aligned}$$

One can use the theorem of residue for each summand, while one has a simple pole at $c=-ih$ of each different power of n. This yields

$$P(E,t) = \frac{-2\pi i}{2\pi}\mathrm{Res}_{c=-ih}P(c,t)\Theta(E) = -i\sum_{n=0}^{\infty}\frac{(ih)^{n+1}(\partial^n/\partial c^n)F(c)^n|_{c=-ih}}{n!^2}\Theta(E). \tag{4.42}$$

Before calculating each summand, we evaluate the derivatives $(\partial^n/\partial c^n)F(c)$ at $c=-ih$, where we define $(\partial^n/\partial c^n)F(c) = F^{(n)}(c)$.

$$F(-ih) = E_0 h e^{-\gamma t}, \tag{4.43}$$

$$F^{(1)}(-ih) = i[E_0 e^{-\gamma t} + E], \tag{4.44}$$

$$F^{(2)}(-ih) = -2E/h, \tag{4.45}$$

$$F^{(3)}(-ih) = F^{(n)}(-ih) = 0; \text{ for } n \geq 3. \tag{4.46}$$

We now evaluate the summands of Eq. (4.41) to obtain

$$n = 0 \;\; ih \tag{4.47}$$

$$n = 1 \;\; -ih^2[E_0 e^{-\gamma t} + E] \tag{4.48}$$

$$n = 2 \;\; ih^3[2![E_0 e^{-\gamma t} + E]^2 + 4EE_0 e^{-\gamma t}]/2!^2 \tag{4.49}$$

$$n = 3 \;\; -ih^4[3![E_0 e^{-\gamma t} + E]^3 + 36EE_0 e^{-\gamma t}[E_0 e^{-\gamma t} + E]]/3!^2 \tag{4.50}$$

$$n = 4 \;\; ih^5[4![E_0 e^{-\gamma t} + E]^4 + 144EE_0 e^{-\gamma t}[E_0 e^{-\gamma t} + E]^2 + 72E^2 E_0^2 e^{-2\gamma t}]/4!^2 \tag{4.51}$$

$$n = 5 \;\; -ih^6[5![E_0 e^{-\gamma t} + E]^5 + 2400EE_0 e^{-\gamma t}[E_0 e^{-\gamma t} + E]^3 + 3600E^2 E_0^2 e^{-2\gamma t}[E_0 e^{-\gamma t} + E]]/5!^2 \tag{4.52}$$

...

After some reorganization effort one finds

$$P(E,t) = h \sum_{n=0}^{\infty} \frac{(-h)^n [E_0 e^{-\gamma t} + E]^n}{n!} \cdot \sum_{m=0}^{\infty} \frac{h^{2m} E^m E_0^m e^{-m\gamma t}}{m!^2} \Theta(E) \tag{4.53}$$

$$= \frac{1}{k_B T(1 - e^{-\gamma t})} \exp\left[\frac{-(E_0 e^{-\gamma t} + E)}{k_B T(1 - e^{-\gamma t})}\right] \sum_{m=0}^{\infty} \frac{\left[\frac{EE_0 e^{-\gamma t}}{k_B^2 T^2 (1 - e^{-\gamma t})^2}\right]^m}{m!^2} \Theta(E). \tag{4.54}$$

The infinite series in the last expression (4.54) represents the modified Bessel function of first kind and zeroth order [4].

---

[4] The modified Bessel function of the first kind and of zeroth order reads

$$I_0(x) = \sum_{k=0}^{\infty} \frac{(\frac{1}{4}x^2)^k}{k!^2} \tag{4.55}$$

$$\lim_{x\to\infty} I_0(x) = \sqrt{\frac{1}{2\pi x}} e^x. \tag{4.56}$$

We check the normalization by using again $h = 1/[k_B T(1 - e^{-\gamma t})]$,

$$\int_0^\infty dEP(E,t) = he^{-hE_0 e^{-\gamma t}} \sum_{m=0}^{\infty} \frac{h^{2m} E_0^m e^{-m\gamma t}}{m!^2} \underbrace{\int_0^\infty dE e^{-hE} E^m}_{\frac{m!}{h^{m+1}}} = e^{-hE_0 e^{-\gamma t}} \sum_{m=0}^{\infty} \frac{(hE_0 e^{-\gamma t})^m}{m!} \tag{4.57}$$

$$= 1.$$

In the limit $t \to \infty$, we find

$$\lim_{t\to\infty} P(E) = \frac{1}{k_B T} \exp\left(\frac{-E}{k_B T}\right) \Theta(E)\,, \tag{4.58}$$

which is the Boltzmann distribution. Moreover, the limit $t \to 0$ corresponds to the limit $h \to \infty$, which yields

$$\lim_{t\to 0} P(E) = \lim_{h\to\infty} P(E) = \sqrt{\frac{1}{2\pi 2h\sqrt{EE_0}}} \cdot e^{2h\sqrt{E_0 E}} \cdot h \cdot e^{-h[E_0+E]}\Theta(E) = \begin{cases} 0 & \text{for} \quad E \neq E_0 \\ \infty & \text{for} \quad E = E_0 \end{cases} \tag{4.59}$$

$$= \delta(E - E_0)\Theta(E)\,. \tag{4.60}$$

Using the energy dependent rates of Eqs. (4.20) and (4.21) and the evolving probability distribution for this energy, Eq. (4.54), we have constructed a numerical Monte Carlo procedure for generating a sequence of electronic transitions in the following Sec. 4.2 from which the average current as well as the current noise can be evaluated.

4.2 Numerical Methods

4.2.1 Charge current

We calculate the charge current through the molecule by means of a random walk simulation (Monte Carlo) for a sequence of electron insertion (removal) events into (out of) the molecule. The rates for these processes, corresponding to transfer from (to) the left ($K = L$) and right ($K = R$) electrode are given by Eqs. (4.15) and (4.16) in the overdamped limit and by Eqs. (4.20) and (4.21) for the low-damping regime, respectively.

The stochastic current is defined as the difference between the sequence of insertion

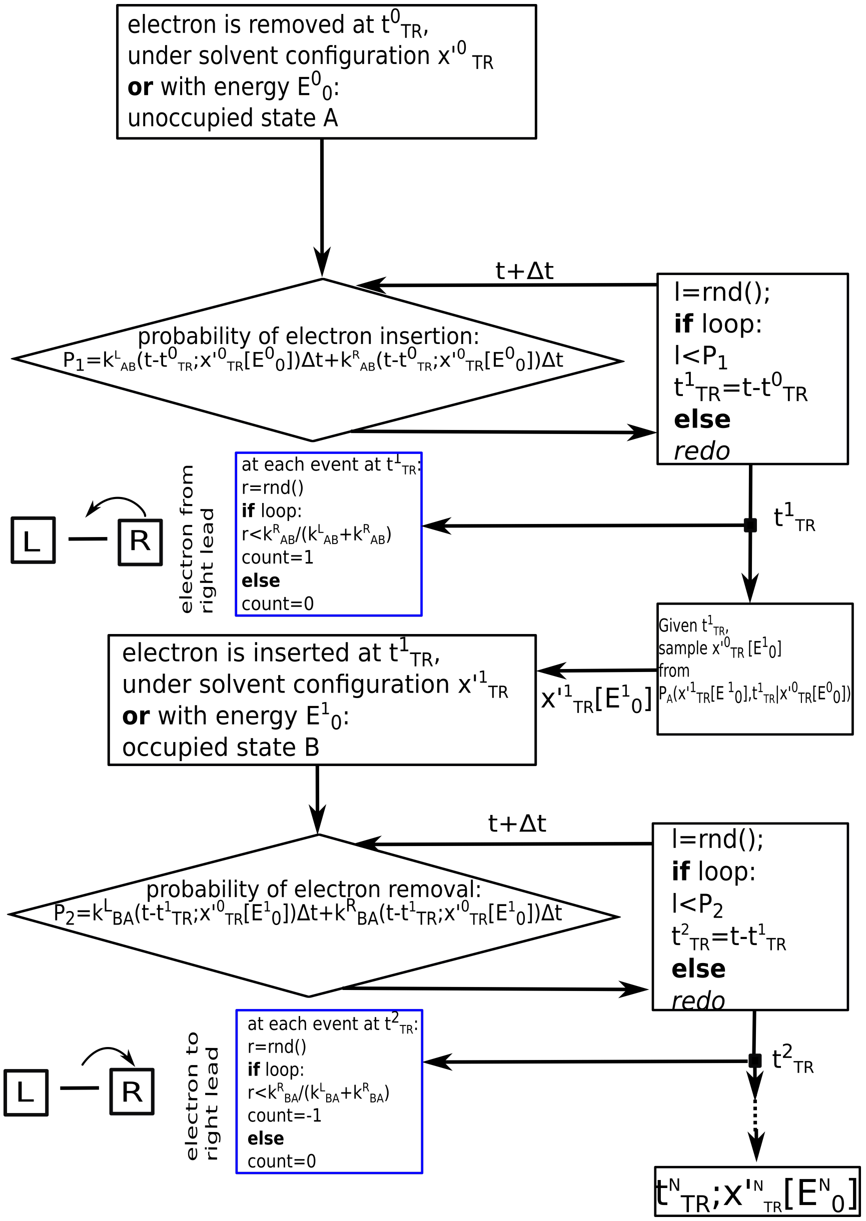

Figure 4.3: Flow chart of the Monte Carlo algorithm to calculate the charge current.

events and the sequence of removal events from and to a given electrode, where each event is represented by the delta-function spike (see Eq. (4.61) below). Once an insertion or removal event is recorded at time t^N_{TR}, one determines the electrode involved in this exchange (see Fig. 4.3). Fig. 4.4 represents an example of individual electron moves with respect to the right lead.

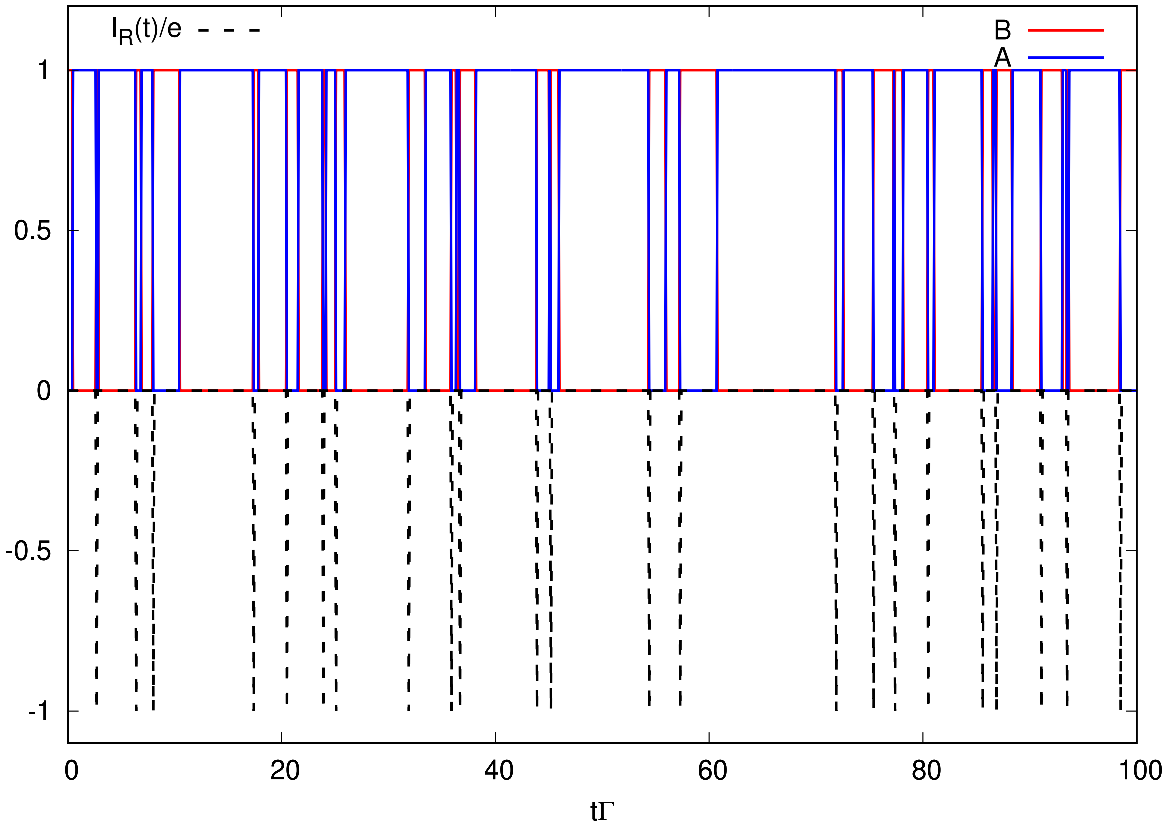

Figure 4.4: Specific sequence of hopping events between the states A and B at ambient temperature $T = 300K$ for the damping rate $\gamma = 0.001\omega_0$ (overdamped regime) and the bias potential of $\Delta\Phi = 300$mV. The electron injection AB from the right lead is recorded with the normalized current $I_R(t)/e$, where e is the electron charge. We set $\mu_R = \mu_L = \Delta E = E_B - E_A$.

The stochastic current associated with the lead K $(K = L, R)$ is then written as

$$I_K(t) = e\Big[\sum_i \delta(t - t_{Ki}) - \sum_j \delta(t - t_{Kj})\Big], \tag{4.61}$$

where e is the electron charge and where the first sum goes over all time t_{Ki} at which the electron was inserted in lead K, and the second accounts similarly for removal events at t_{Kj}. The expectation value of the current $\langle I \rangle$ at the respective lead reads

$$\langle I \rangle = \frac{e}{\tau}\int_0^\tau dt\Big[\sum_i \delta(t - t_i) - \sum_j \delta(t - t_j)\Big] = \frac{e}{\tau}[N - M], \tag{4.62}$$

where we detect N electron insertion and M removal processes to a given lead within the time period τ. We assume a steady-state current for the observation time window between $(0,\tau)$ for ideally long observation times $\tau \to \infty$.

4.2.2 Current noise

Next, we examine the correlation characteristics of resulting current time-series. The autocorrelation function of the current is defined by

$$C_I(t') = \frac{1}{\tau}\int_0^\tau (I(t) - \langle I\rangle)(I(t+t') - \langle I\rangle)dt, \tag{4.63}$$

where τ is the time interval of observation. Now, we apply Eqs. (4.61) to (4.63) to find the autocorrelation of the δ-current pulses as

$$\begin{aligned} C_I(t') = {} & \frac{e^2}{\tau}\sum_{i;i'}\sum_{j;j'}\int_0^\tau dt\Big[\delta(t-t_i)\delta(t-t_{i'}+t') - \delta(t-t_i)\delta(t-t_{j'}+t') \\ & - \delta(t-t_j)\delta(t-t_{i'}+t') + \delta(t-t_j)\delta(t-t_{j'}+t')\Big] - \langle I\rangle^2 \\ = {} & \frac{e^2}{\tau}\sum_{i;i'}\sum_{j;j'}\Big[\delta(t_i-t_{i'}+t') - \delta(t_i-t_{j'}+t') \\ & - \delta(t_j-t_{i'}+t') + \delta(t_j-t_{j'}+t')\Big] - \langle I\rangle^2. \end{aligned} \tag{4.64}$$

We examine the term $I(t)I(t+t')$ as all other terms lead to $-\langle I\rangle^2$. The current variance is defined by $\sigma_I^2 \equiv C(t'=0)$. In evaluating this term, we use the fact that only δ-functions for $i=i'$ and $j=j'$ remain in $I(t)I(t)$ of Eq. (4.64), while all other δ-functions cancel. If we detect N insertion and M removal processes to a given lead, we find

$$\sigma_I^2 = C(t'=0) = \frac{e^2}{\tau}[N+M]\delta(0) - \langle I\rangle^2 = \lim_{\tau'\to 0}\frac{e^2}{\tau\tau'}[N+M] - \langle I\rangle^2 = \langle I^2\rangle - \langle I\rangle^2, \tag{4.65}$$

where we replace the δ-function by the inverse of the infinitely small time span τ'^{-1}.

To obtain an autocorrelation signal in a numerically efficient way, one broadens the δ-functions of Eq. (4.64) to normalized Lorentzian functions. They do not influence the current as long as their characteristic width is smaller than the expected waiting time between the individual electron occupation and deoccupation events onto and from the molecule. This is of the order of Γ^{-1}.

Experimental current auto-correlograms are often fitted to an exponential function [130], such that one considers exponential current correlation of the form

$$C_I(t') = \sigma_{I,P}^2 \tau' \left[\delta(t') + \frac{\alpha}{\tau_c} e^{-\frac{t'}{\tau_c}} \right] = \sigma_{I,P}^2 \tau' \left[\frac{1}{\tau'} + \frac{\alpha}{\tau_c} e^{-\frac{t'}{\tau_c}} \right], \tag{4.66}$$

where $\sigma_{I,P}^2$ is the variance of the current for uncorrelated Poissonian electron injection and removal events and τ_c is the correlation time. τ' is the small time span describing the δ-function. Thus, the variance calculated from Eq. (4.66) reads $C_I(t'=0) = \sigma_I^2 = \sigma_{I,P}^2(1+\alpha)$, where $\tau' \simeq \tau_c$ such that α characterizes the correlation between the electron events. For a Possonian process $\alpha = 0$ and the Fano factor $F = 1 + \alpha = \sigma_I^2 / \langle I \rangle = 1$. If $F > 1$, the current has positive correlations, while if $F < 1$, the current has negative correlations.

4.3 Results and discussion

4.3.1 Overdamped regime

Current

The average charge current $\langle I \rangle$ obtained from the Monte Carlo procedure of Subsec. 4.2 is shown in Fig. 4.5 as a function of the bias voltage and the solvent induced damping γ. We set $\mu_R = \mu_L = \Delta E = E_B - E_A$ in Eqs. (4.4) to (4.6) and apply a symmetric bias voltage $\Phi_R = -\Phi_L = \Delta\Phi/2$ between the leads. Depending on the voltage bias, three modes of behavior are seen. (a) When the applied bias voltage is moderately larger than the thermal energy, i.e. $e\Delta\Phi/2 > k_B T$, (while $k_B T \sim 25$meV at ambient temperature of 300K) the current increases, then saturates, with increasing γ (see Fig. 4.5 for 200-400 mV). The reason for this behavior is that for large γ relaxation is slow. Therefore, the system remains close to a transition configuration, i.e., energy barrier to the transition does not develop quickly enough. (b) For considerably larger bias (1000 mV in Fig. 4.5) there is no sensitivity to solvent configuration (states are vacant on one lead and occupied on the other for any configuration), hence no effect on the average current at which this configuration evolves is seen. (c) For small bias (100 mV in Fig. 4.5) increasing γ initially enhances the electronic current for the same reason as in (a): At large γ, staying in the small energy window at which transfer can occur, implies a larger probability of an electron transfer. However, some relaxation is needed to stabilize the "product" of this transfer. Further increase of γ makes such relaxation to slow and leads to current reduction because

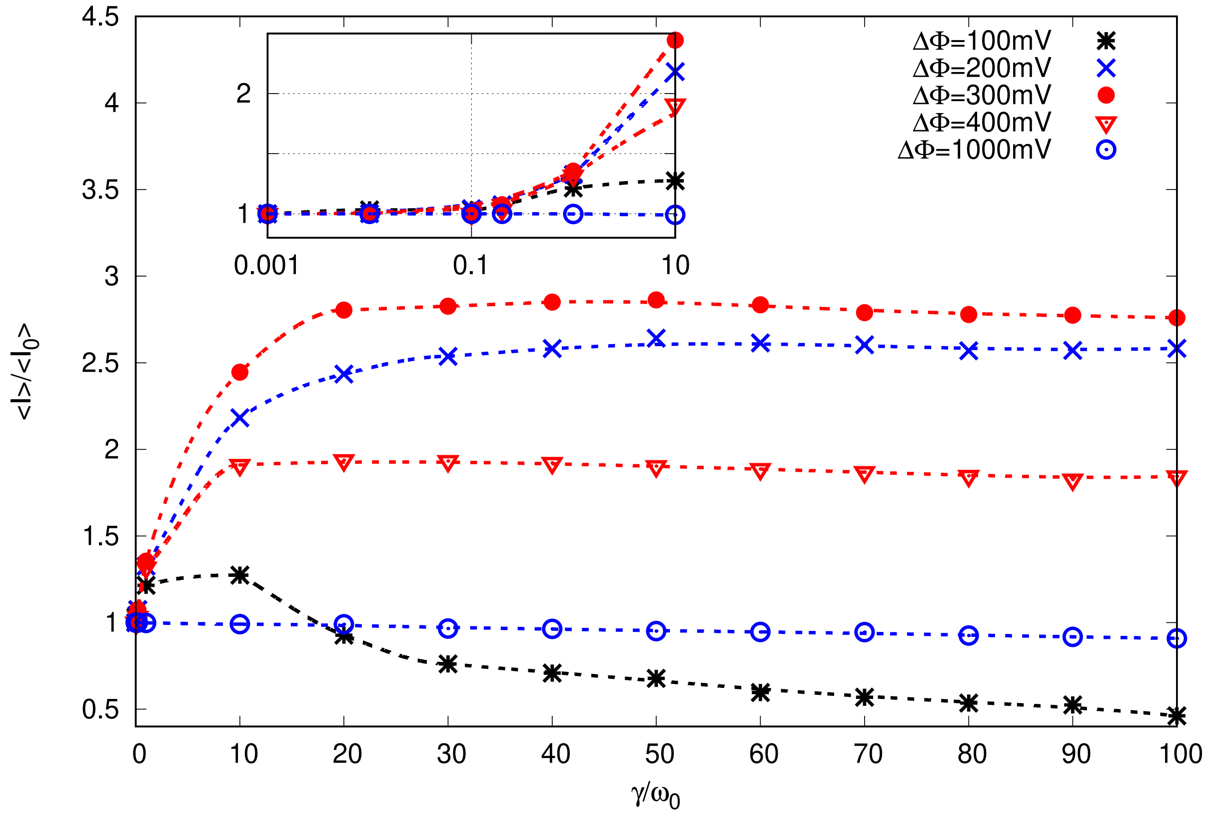

Figure 4.5: Expectation value of the current $\langle I\rangle/\langle I_0\rangle$ at ambient temperature $T = 300\text{K}$ for the reorganization energy $E_R = 200\text{meV}$ at different applied bias potentials $\Delta\Phi$ by varying the damping rate γ. $\langle I_0\rangle$ is the current for fast solvent relaxation, $\gamma \to 0$. The dotted lines are functional fits to the data points for better readability.

for such large γ the dot level sticks in an energy region with finite probability to return to the electrode where it originated.

Reiterating, a larger friction γ implies, in the limit under consideration, a slower solvent-induced stabilization of the electron on the molecular bridge. The initial increase of the current with growing γ for small damping for all modes of operation (see inset Fig. 4.5) may be understood as solvent-mediated stabilization of the molecular transition state configuration. For larger γ, this stabilization results in a frozen configuration that is more ($e\Delta\Phi/2 > k_BT$) or less ($e\Delta\Phi/2 \sim k_BT$) favorable to subsequent electron transfer events.

We note that, although the diffusion equation in the overdamped regime is strictly valid only for $\gamma \gg \omega_0$, it reproduces the Boltzmann distribution as a solution for $\gamma = 0$. However, the calculated average current in the intermediate regime $\gamma \sim \omega_0$ may be seen as an interpolation between the tractable limits of zero and strong damping.

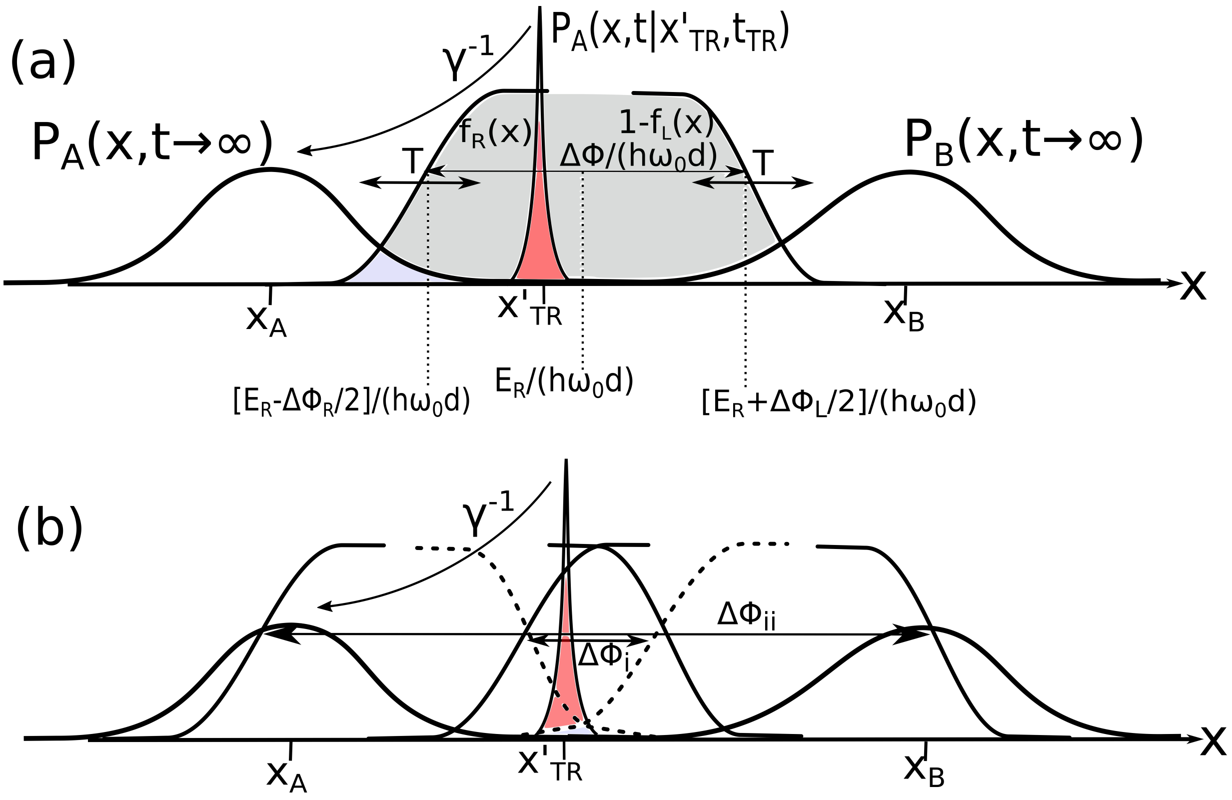

Figure 4.6: Illustration of the rate integral in Eq. (4.15) which comprises a probability density P_A (P_B) and the Fermi function $f_K(x)$ $(1 - f_K(x))$ of the respective lead ($K = R$ or $K = L$) where the probability density and Fermi function have a time-dependent shift relative to each other. Figure (a) shows the time-dependent probability distribution of state A reflecting the solvent relaxation along the x-coordinate to an equilibrium Boltzmann distribution. An enhanced damping γ stabilizes the distribution near a transition point and leads to an overall larger integral value in comparison to the equilibrium distribution. This results in an increased charge injection rate. Figure (b) shows the same scenario, but for a different applied bias potential $\Delta\Phi_i \equiv \Delta\Phi_i(\hbar\omega_0 d)^{-1}$ and $\Delta\Phi_{ii} \equiv \Delta\Phi_{ii}(\hbar\omega_0 d)^{-1}$. For $e\Delta\Phi_i \sim k_BT$, there arises a finite probability for a distribution stabilized near a transition point of a charge injection from opposed directed leads which decreases the charge current. For a large applied $e\Delta\Phi_{ii} > 2E_R$, the Fermi functions are shifted in a way that the probability density around equilibrium or near a transition point leads to comparable integral values. The current is therefore less sensitive to the solvent damping γ along x. Since the bias voltage is applied symmetrically, one may discuss the same scenario for the rate of electron removal in Eq. (4.16).

Mathematically all modes of operation can be directly understood by investigating the ET rates (Eqs. (4.15) and (4.16)) where two contributions, (i) the probability distribution and (ii) the Fermi function (Eq. (4.4) with transformation $\epsilon \rightarrow x$), form the integral (see illustration in Fig. 4.6). With enhanced γ, the solvent probability distributions P_A, Eq. (4.13), and P_B, Eq. (4.14), relax slower to their equilibrium Boltzmann-like properties around $x_A = 0$ or $x_B = d$, respectively. Their initial position depends on the solvent configuration under which an ET process has occurred. The increased γ 'freezes' the configuration and hence stabilizes the distribution near a possible transition point (see Fig. 4.6). The integral values of Eqs. (4.15) as well as (4.16), and, hence, the rate for an electron injection and removal, to the right and left lead, respectively, increases with bigger solvent damping and, thus, the current. For $e\Delta\Phi/2 \sim k_BT$, the more localized solvent distributions with increased γ may also form a finite integral with the lead of the opposite direction such that an injection and removal process may occur from and to the same lead. This suppresses the charge current.

By calculating the average current over the reorganization energy, we observe that the average current drops suddenly if the reorganization energy is $E_R = \Delta\Phi/2$ for an extremely small damping. This represents the Marcus ET transfer regime (see $\gamma = 0.001\omega_0$ in Fig. 4.7). For $E_R = \Delta\Phi/2$ and $\gamma \ll 1$, the ET rates of Eq. (4.15) as well as Eq. (4.16) clearly portray that the Fermi function cuts half the Boltzmann distribution in Fig. 4.6 such that the rate and the current are halved. In general, an enhanced reorganization energy results in a pronounced horizontal shift between the potential minimum of state A and B, i.e. a larger distance between x_A and x_B in Fig. 4.1, such that the transition becomes energetically less favored. However, a greater solvent damping stabilizes the molecular state near a transition state such that the current drops at higher reorganization energies with enhanced damping (see Fig. 4.7). In addition, the sudden drop is more stiff with enhanced damping γ, since the solvent fluctuates less freely. Thus, the rigid behavior in the current-reorganization behavior with larger γ may be associated to a less fluctuating solvent. A similar effect is observed for the increase of current-voltage characteristic before a steady state current is reached (inset in Fig. 4.7). For enhanced solvent damping, the steady state current is reached for smaller applied bias voltage due to solvent stabilization near a transition point.

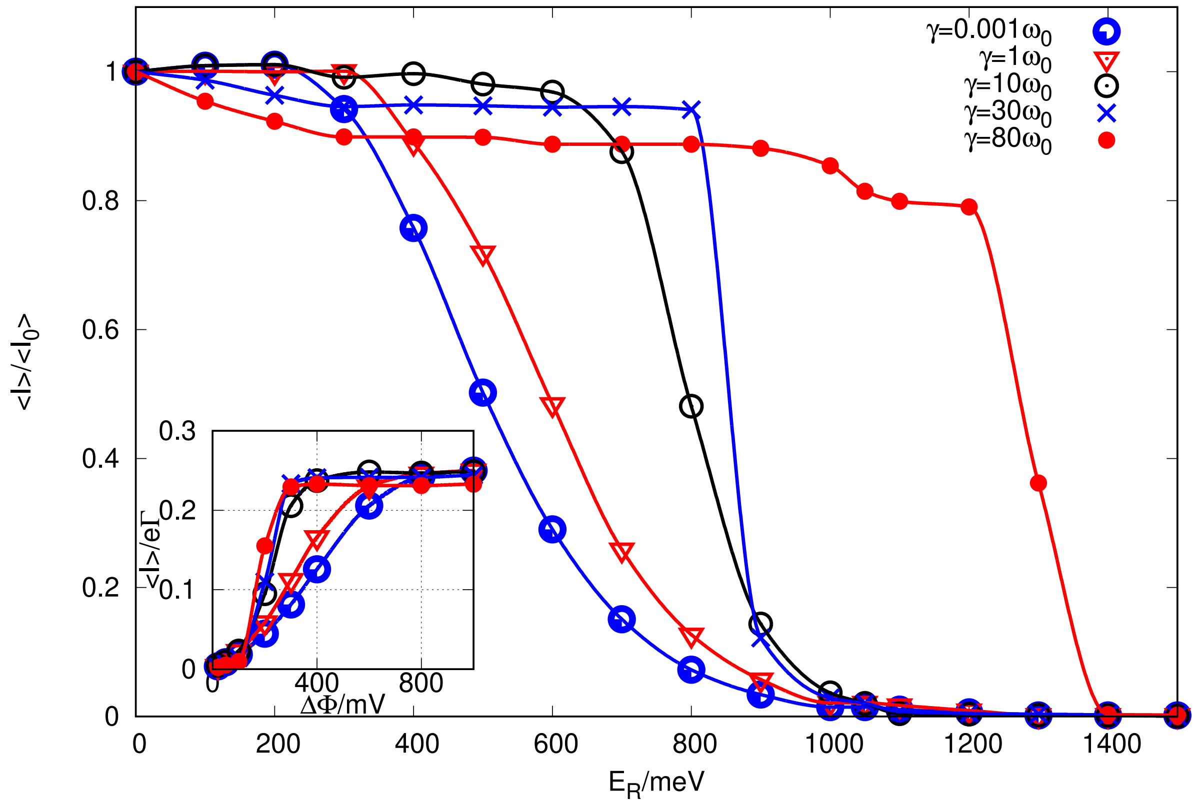

Figure 4.7: Expectation value of the current $\langle I\rangle/\langle I_0\rangle$ at ambient temperature $T = 300\text{K}$ for different damping strengths γ at a bias potential $\Delta\Phi = 1000\text{mV}$ by varying the reorganization energy. $\langle I_0\rangle$ is the current for the reorganization energy $E_R = 0$. The solid lines are functional fits to data points. Inset: $\langle I\rangle/e\Gamma$ at ambient temperature $T = 300\text{K}$ for different damping strengths γ at a reorganization energy of $E_R = 500\text{meV}$ and varying the applied bias potential $\Delta\Phi$. The observation time for the average current (see Eq. (4.62)) is $\tau = 50000\Gamma^{-1}$, Γ is the characteristic transition rate and e the elementary charge.

Current correlation and Fano factor

The current correlation $C_I(t)$ (see Eq. (4.64)), as shown in Fig. 4.8, drops faster with time by applying a higher bias voltage. This is evident since a higher applied voltage is able to align the molecular level with more occupied or vacant energy states in the leads such that the charge current is less correlated. In contrast, a longer correlation expresses the solvent mediated ET, where the 'frozen' solvent configuration holds the molecular state near a transition state which becomes more visible when applying a smaller bias potential. Since a bigger γ describes a slower solvent relaxation, the current is more correlated with growing γ. The solvent fluctuates less and the ET events are stronger influenced by previous charge configurations on the molecule and their related solvent configurations. Interestingly, for $e\Delta\Phi/2 \sim k_BT$, small damping $\gamma = \omega_0$ shows higher correlation than larger damping with $\gamma = 70\omega_0$ (Fig. 4.8 for $\Delta\Phi = 50$meV). This behavior reflects again the effect of a possible ET in inverse directions, since the transition state may align the molecular energy level with electronic states of the opposite lead.

The current variance σ_I (see Eq. (4.65)) first grows with γ for $e\Delta\Phi \sim k_BT$ (inset in Fig. 4.8 for $\Delta\Phi = 50$meV and $\Delta\Phi = 100$meV) and confirms an initially enhanced current deviation from the mean, which decreases with growing γ. A molecular picture: The solvent fluctuates less which aligns at first the molecular state with more occupied or vacant metal states leading to a higher current variance. Later with growing γ the molecular state can be aligned with the metal levels of opposite directed leads which results in a reduced current variance. For $e\Delta\Phi > k_BT$, the current deviation about the mean increases with γ before a steady state is reached when the solvent configuration stabilizes the molecular state near a transition state (inset in Fig. 4.8 for $\Delta\Phi = 200$meV).

The calculated Fano factor [130, 131] $F = \frac{\langle I^2\rangle - \langle I\rangle^2}{\langle I\rangle} > 1$ (see discussion of Subsec. 4.2) shows clear evidence of a non-Poissonian (correlated) ET process for non-vanishing friction, while Poissonian statistics characterizes the limit $\gamma \to 0$ (fast solvent relaxation). Once the applied bias voltage is large enough, the solvent relaxation shows no impact on the ET because the position of the dot "level" does not change its orientation relative to empty and occupied single electron states of the metal, hence $F = 1$ for all γ. For an applied bias potential in the regime of relevant thermal fluctuations, i.e., $e\Delta\Phi \sim k_BT$, the Fano factor first increases before it declines to a steady value when the molecular "state" is localized in a region when its sees probabilities of similar magnitudes for vacancies or occupation on the leads of both sides (see $\Delta\Phi = 50$mV and $\Delta\Phi = 100$mV in Fig. 4.9). Yet, the reduced Fano factor signals a less correlated ET since the charge transfer may occur spontaneously in opposite directions. The inset in Fig. 4.9 shows the correlation time τ_c, defined by fitting $C_I(t)$ (see Eq. (4.64)) to an exponential $C(t) \propto \exp\left[-\frac{t}{\tau_c}\right]$. An increased correlation time τ_c with enhanced damping directly signals a stronger current correlation and confirms the prior observations.

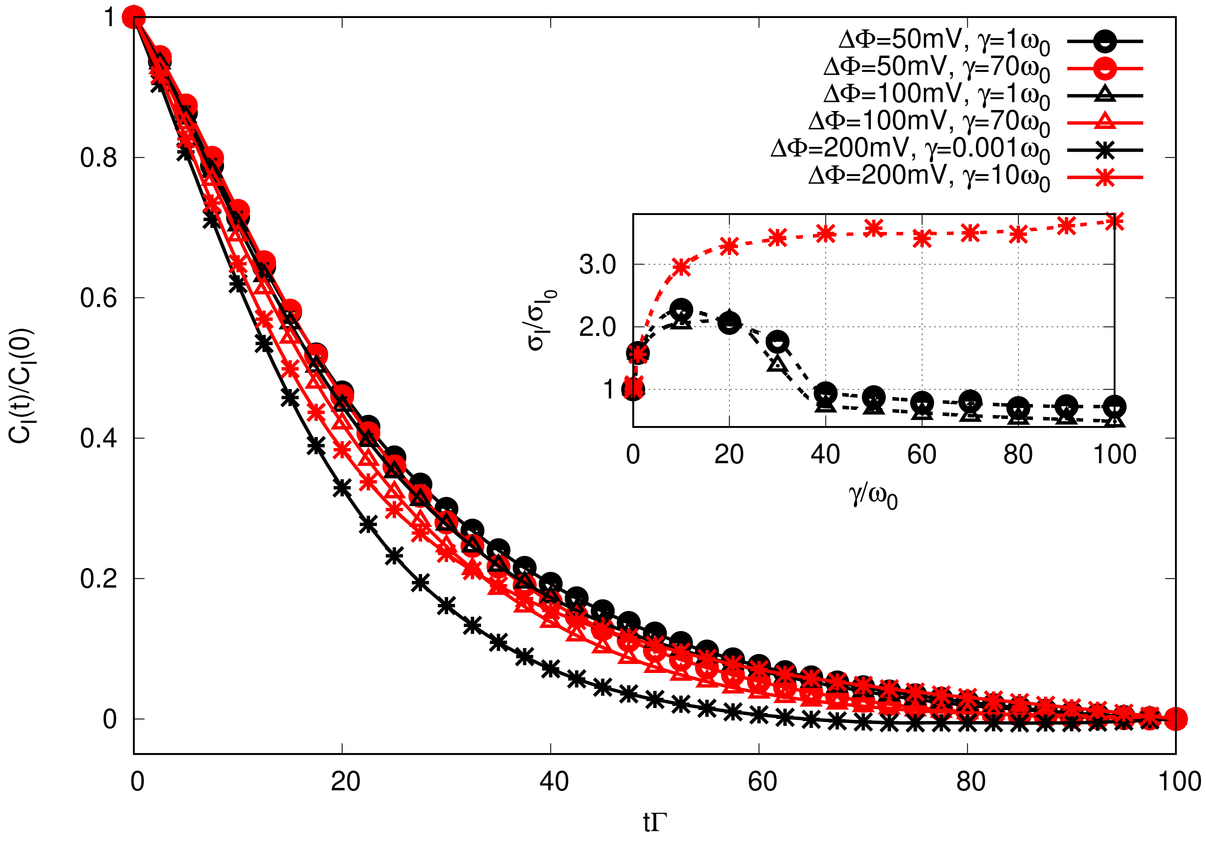

Figure 4.8: Normalized current correlation function $C_I(t)/C_I(0)$ at ambient temperature $T = 300$K for the reorganization energy $E_R = 200$meV at different applied bias potentials $\Delta\Phi$ and different values of the damping strength γ. Inset: Normalized current variance σ_I/σ_{I_0} for varying the damping γ. The black circles portray the variance for the potential $\Delta\Phi = 50$mV, the black triangles for $\Delta\Phi = 100$mV and the red stars for $\Delta\Phi = 200$mV. The dotted lines are functional fits to the data points for better readability. I_0 is the current for $\gamma \to 0$ (fast solvent relaxation).

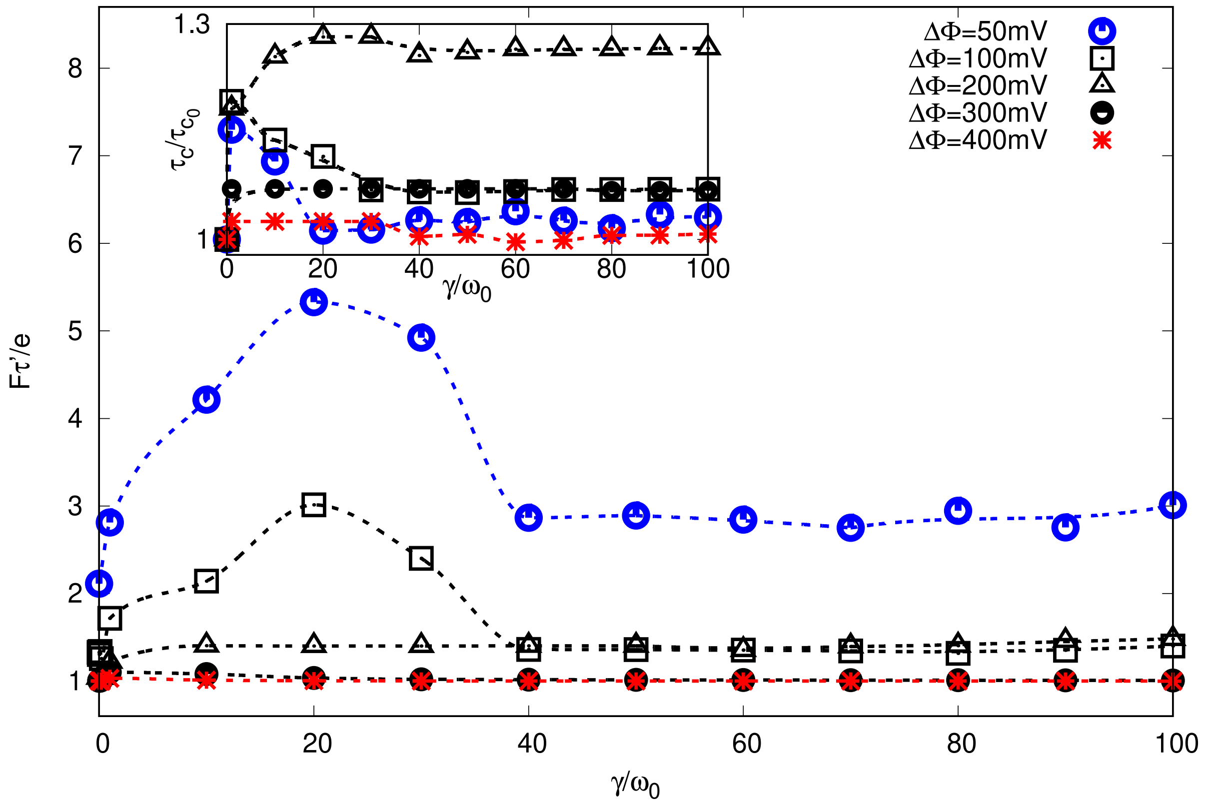

Figure 4.9: Normalized Fano factor $F\tau'/e$ at ambient temperature $T = 300$K for different applied bias potentials $\Delta\Phi$ for the reorganization energy $E_R = 200$meV by varying the damping rate γ. τ' is the observation time (see Eq. (4.65)), e the electron charge. Inset: Normalized correlation time τ_c/τ_{c_0} for varying the damping strength γ from a fit of $C(t)$ to Eq. (4.66). τ_{c_0} is the correlation time for fast solvent relaxation, $\gamma \to 0$. The dotted lines are functional fits to the data points for better readability.

4.3.2 Low-damping regime

Current

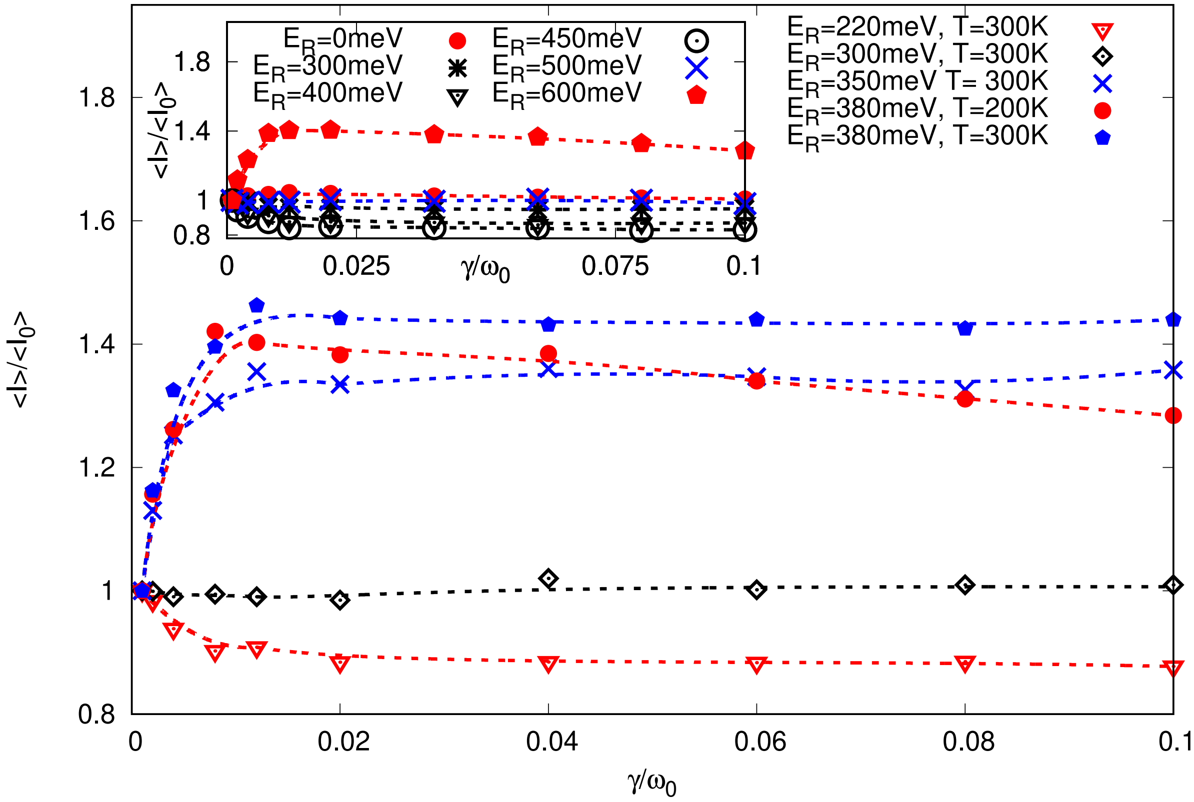

Figure 4.10: Expectation value of the current $\langle I \rangle / \langle I_0 \rangle$ for different reoganization energies E_R for varying the damping γ. The bias potential is set to $\Delta\Phi = 600\text{mV}$. $\langle I_0 \rangle$ is the current for infinitely small solvent energy relaxation, $\gamma \to 0$. Inset: $\langle I \rangle / \langle I_0 \rangle$ for different reoganization energies E_R for the bias potential $\Delta\Phi = 1000\text{mV}$ at temperature $T = 300\text{K}$. The dotted lines are functional fits to the data points for better readability.

We consider the average current in Fig. 4.10 and recall that in the low-damping regime energy relaxation is faster for larger γ. We set again $\mu_R = \mu_L = \Delta E = E_B - E_A$ (Eqs. (4.4) to (4.6)) and a symmetric bias voltage $\Phi_R = -\Phi_L = \Delta\Phi/2$ (Eq. (4.4)) at the leads. For $e\Delta\Phi/2 < E_R$, the average current increases with growing solvent-induced damping γ (see Fig. 4.10 for $E_R = 380\text{meV}$ and $E_R = 350\text{meV}$). This increase appears to stem from the fact that the energy distribution becomes broader in time, such that more metal states can be accessed. This enhances the rates and hence the current through the molecule for growing γ. It is evident that this effect becomes more pronounced at higher temperature (see Fig. 4.10 for $E_R = 380$meV at $T = 200$K and $T = 300$K) since the thermal fluctuations are enhanced, thus leading to thermally activated ET processes. If the reorganization energy becomes much larger than the applied bias voltage, the broadening of the molecular states becomes irrelevant since the alignment with the Fermi states of the leads vanishes. When the bias voltage $\Delta\Phi$ satisfies $e\Delta\Phi/2 = E_R$ (see Fig. 4.10 for $E_R = 300$meV or inset of Fig. 4.10 for $E_R = 500$meV), the average current shows no sensitivity to an increasing damping γ. The reason appears to be the fact that in this case the molecular energy state aligns with the occupied/vacant electronic energy levels in the leads. For $e\Delta\Phi/2 > E_R$, the average current decreases with increasing solvent induced damping γ (see Fig. 4.10 for $E_R = 220$meV). In this case, the molecular states which are broadened due to γ drop out of the conduction window of the leads. This reduces the ET rates (Eqs. (4.20) and (4.21)) and, thus, the current through the molecule.

We may again analyze the rate for the electron insertion (Eq. (4.20)) where the integral includes the probability distribution P_A for an electron to enter the molecule with the given molecular and environmental energy configuration weighted by the Fermi distribution of the given lead. For $e\Delta\Phi/2 < E_R$, the Fermi distribution $f(\epsilon)$ has a negative offset while the width of P_A increases with γ such that the overlap increases and with it the rate (see Fig. 4.11). The same is observed for the removal process but now with the distribution $1 - f(\epsilon)$ of vacant states of the electrode. In the mode of operation $e\Delta\Phi/2 = E_R$, the average current shows no sensitivity to increasing damping γ (see Fig. 4.10 for $E_R = 300$meV). The molecular energy states aligns with the occupied or vacant electronic energy levels in the leads. For the rates for the electron insertion and removal process, the Fermi distribution has no offset with respect to the probability distribution P_A (P_B) such that the friction-depending width of P_A (P_B) does not affect the integral value and, hence, the rate. For $e\Delta\Phi/2 > E_R$, the average current decreases with increasing solvent induced damping γ (see Fig. 4.10 for $E_R = 220$meV). In this case, the broadened molecular states with enhanced γ exceed the conduction window of the leads. This reduces the ET rates (Eqs. (4.20) & (4.21)) and, thus, the current through the molecule.

By calculating the average current for different reorganization energies, we observe that the average current drops suddenly if the reorganization energy is $E_R = \Delta\Phi/2$ (Fig. 4.12). The sudden drop is more smooth with enhanced damping γ. A larger γ allows the solvent to fluctuate more freely due to the ambient temperature. Thus, the flattened dependence in current-reorganization characteristics with enhanced γ may be associated to a more strongly fluctuating solvent. The same effect is observed for the current-voltage

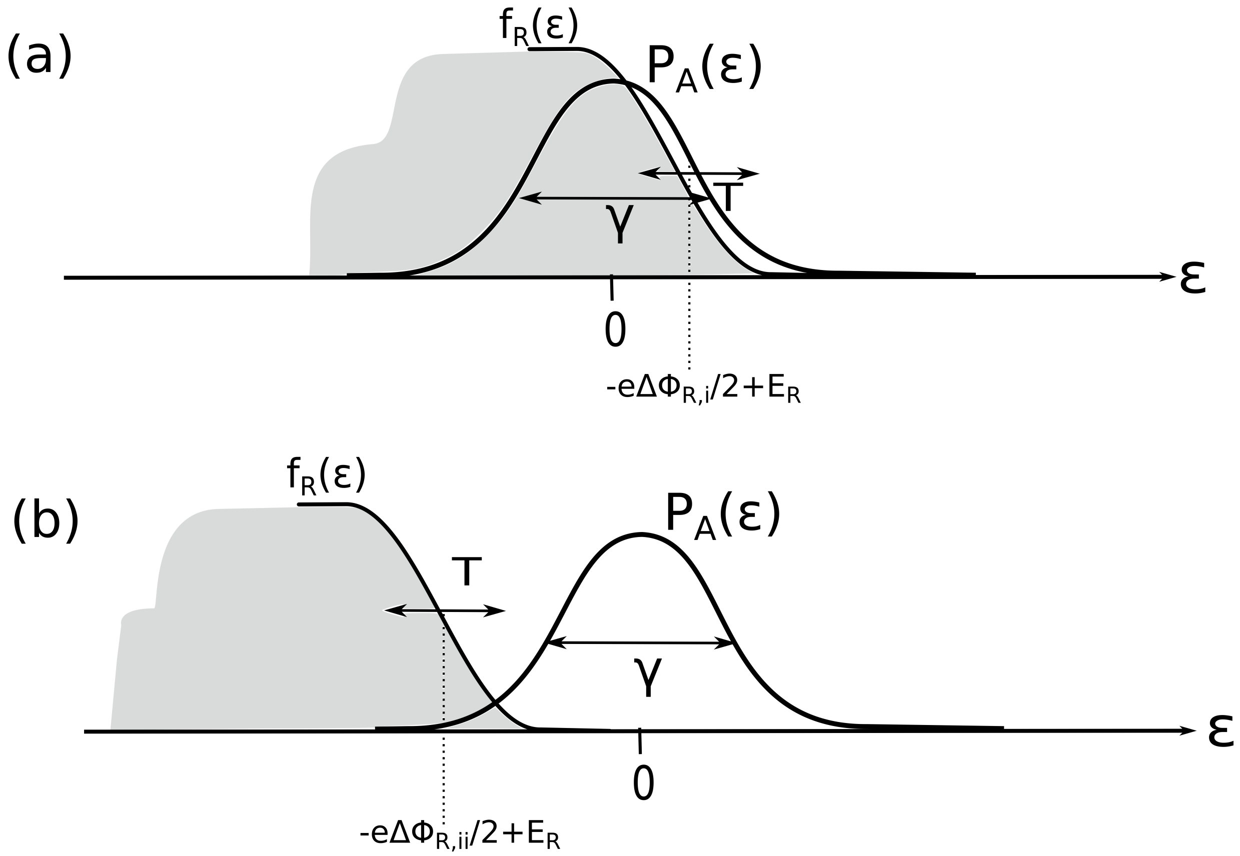

Figure 4.11: Illustration of the rate integral in Eq. (4.20) which comprises a probability density and the Fermi function of the right lead which can be shifted with respect to each other by the applied bias voltage. Figure (a) shows the fluctuating probability distribution of state A reflecting the solvent fluctuation proportional to γ along the energy coordinate. The applied bias potential is smaller than the reorganization energy, i.e., $e\Delta\Phi_{R,i}/2 < E_R$. An increased magnitude of γ leads to a broadened distribution such that the integral value in Eq. (4.20) is reduced due to the smaller overlap with the Fermi function. The current is thus reduced. Figure (b) shows the same scenario but for a bias larger than the reorganization energy $\Delta\Phi_{R,ii} > E_R$. Here the overlap with the Fermi function increases in the integral value and, thus, the current.

characteristics once half the bias voltage reaches the reorganization energy (see inset in Fig. 4.12).

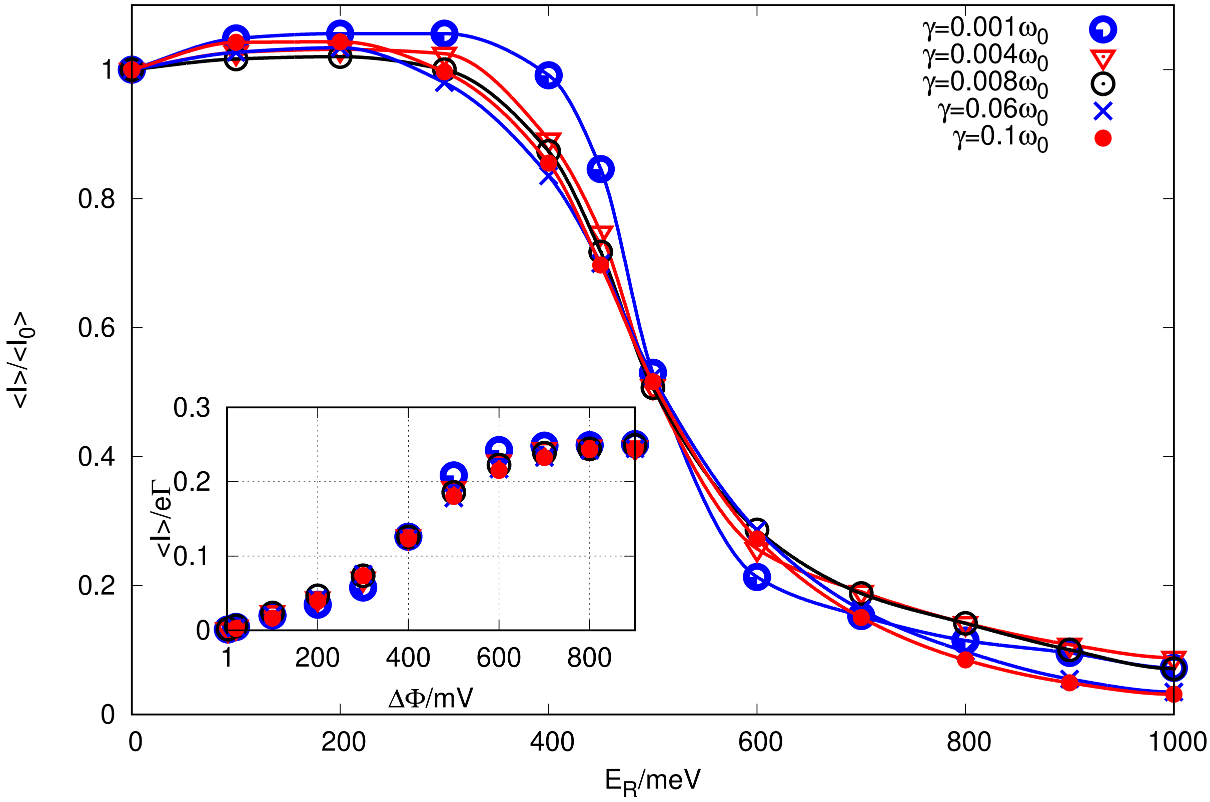

Figure 4.12: Expectation value of the current $\langle I\rangle/\langle I_0\rangle$ at ambient temperature $T = 300$K for different damping strengths γ for a potential $\Delta\Phi = 1000$mV for varying reorganization energies. $\langle I_0\rangle$ is the current for the reorganization energy $E_R = 0$. The solid lines are functional fits to data points. Inset: $\langle I\rangle/e\Gamma$ at ambient temperature $T = 300$K for different damping strengths γ at reorganization energy $E_R = 200$meV for varying the applied bias $\Delta\Phi$. The observation time for the average current (see Eq. (4.62)) is $\tau = 50000\Gamma^{-1}$, Γ is the characteristic transition rate and e the elementary charge.

Current correlation and Fano factor

The calculated current correlation function $C_I(t)$ (see Eq. (4.64)) is shown in Fig. 4.13. It drops again faster with time by applying a higher bias voltage since the successive ET is increased and less correlated. However, the current shows more correlation for larger γ which describes a faster solvent energy relaxation. In this situation, the ET events are stronger influenced by the solvent energy of previous molecular charge states and, thus, more correlated.

The current variance σ_I, statistically determined from Eq. (4.65), (inset in Fig. 4.13) grows with γ for $e\Delta\Phi/2 < E_R$ and confirms enhanced current variations about the mean (inset in Fig. 4.13 for $e\Delta\Phi = 300\text{mV}$). The solvent energy relaxes faster which aligns the molecular state with more occupied or vacant metal states leading to a higher current which varies more. For $e\Delta\Phi = 0$, the average current is zero which varies even less for enhanced solvent energy relaxation. For $e\Delta\Phi/2 = E_R$ the current deviation about the mean is independent of the solvent energy relaxation and, therefore, independent of γ (inset in Fig. 4.13 for $\Delta\Phi = 400\text{mV}$). For $\Delta\Phi/2 > E_R$, the current variance is reduced with larger γ since fast solvent energy relaxation leads to less molecular energy-metal energy alignments such that the current is reduced. It varies only little around its average (inset in Fig. 4.13 for $\Delta\Phi = 500\text{mV}$).

The calculated Fano factor $F = \frac{\langle I^2\rangle - \langle I\rangle^2}{\langle I\rangle} > 1$ is shown in Fig. 4.14 and reveals a strongly non-Poissonian ET process for a small bias voltage in comparison to a large reorganization energy. Here, the effect of the broadening of the molecular level induced by larger γ leads to electron hopping correlated in time. This correlation disappears if the applied voltage exceeds the reorganization energy considerably. Again by fitting an exponential $C \propto \exp\left[-\frac{t}{\tau_c}\right]$ (see Eq. (4.66)) to the normalized calculated correlation function the impact of damping on the current can be directly quantified (see inset in Fig. 4.14). An increased correlation time τ_c with enhanced damping directly signals a higher current correlation and confirms the prior observations.

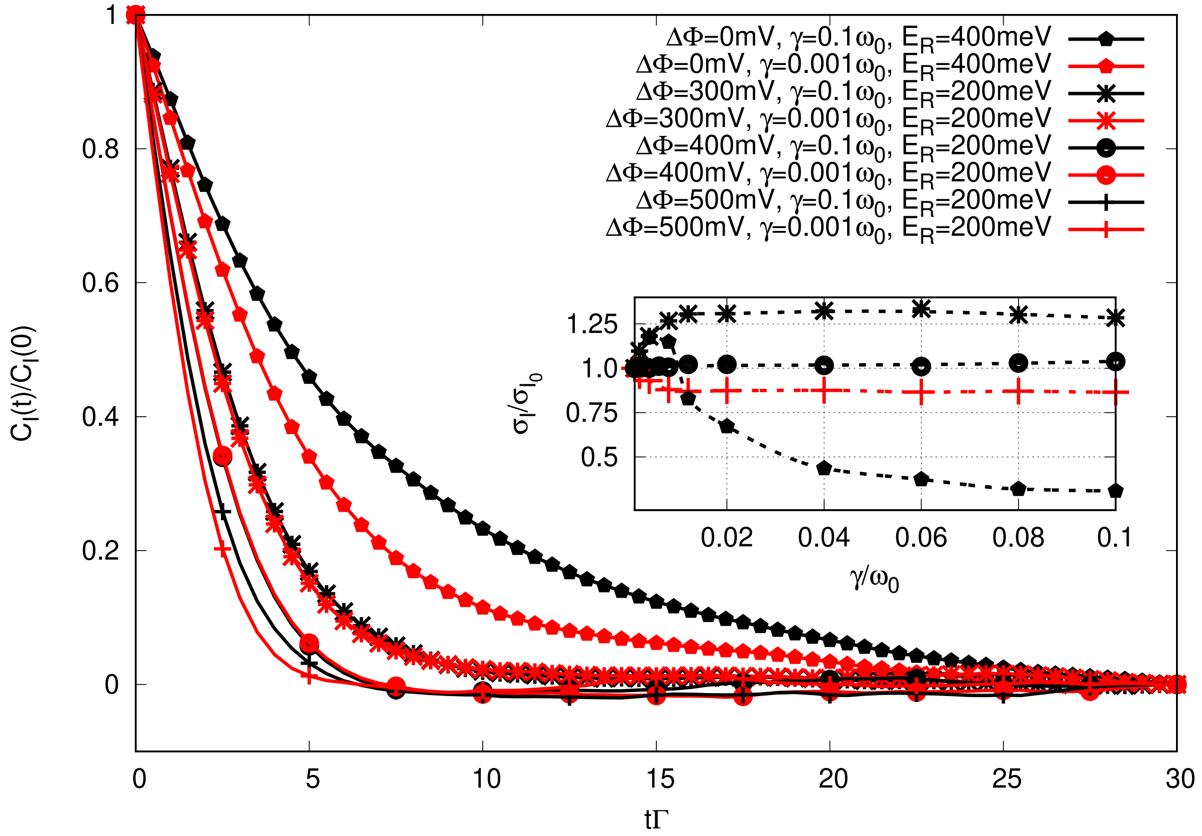

Figure 4.13: Normalized current correlation $C_I(t)/C_I(0)$ at ambient temperature $T = 300\text{K}$ for different reorganization energies E_R at different applied bias potentials $\Delta\Phi$ and different damping strengths γ. Inset: Normalized current variance σ_I/σ_{I_0} for varying damping γ. The variance for the potential $\Delta\Phi = 0$ is displayed with diamonds, for $\Delta\Phi = 300\text{mV}$ displayed with stars, for $\Delta\Phi = 400\text{mV}$ displayed with circles and for $\Delta\Phi = 500\text{mV}$ displayed with pluses. I_0 is the current for small solvent energy relaxation, $\gamma \to 0$.

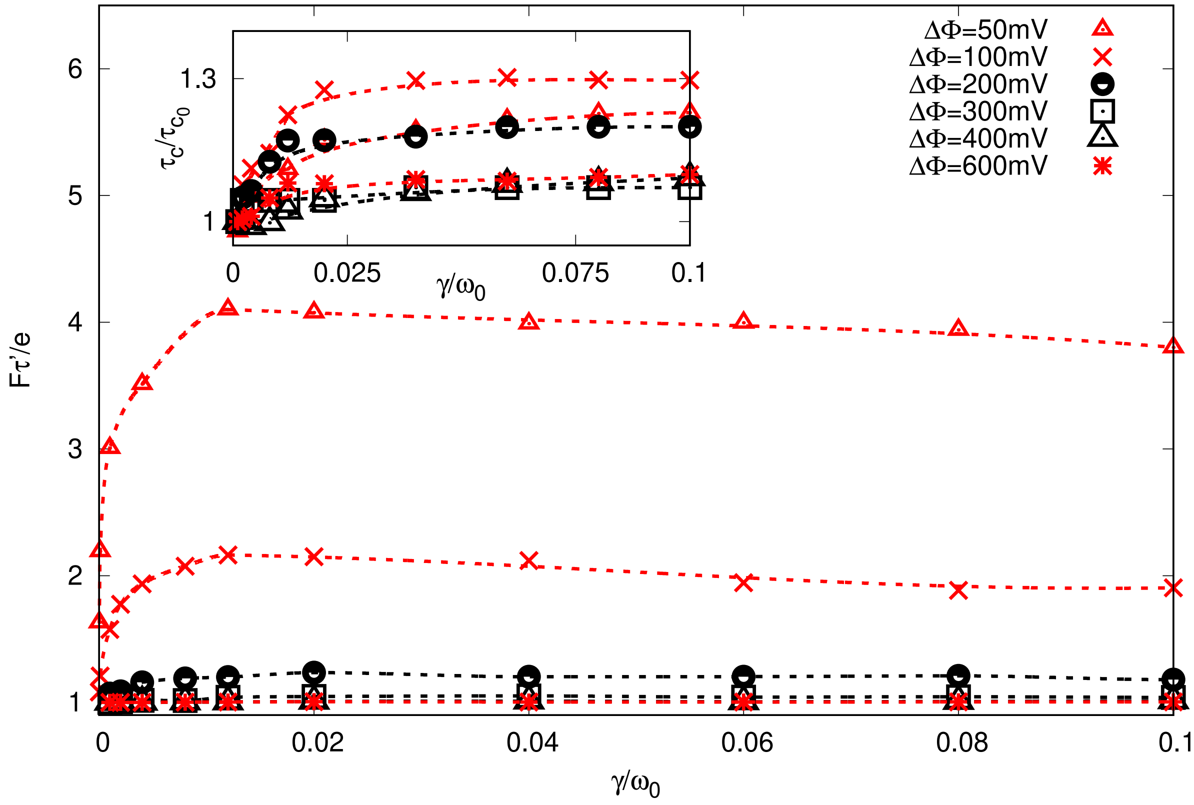

Figure 4.14: Normalized Fano factor $F\tau'/e$ at ambient temperature $T = 300\text{K}$ for the reorganization energy $E_R = 200\text{meV}$ for different bias potentials $\Delta\Phi$ and different damping γ. τ' is the observation time, e the electron charge. Inset: Normalized correlation time τ_c/τ_{c_0} for varying damping γ from fitting $C(t)$ to Eq. (4.66). τ_{c_0} is the correlation time for for small solvent energy relaxation $\gamma \to 0$. The dotted lines are functional fits to the data points for better readability.

4.3.3 Kramers-like turnover

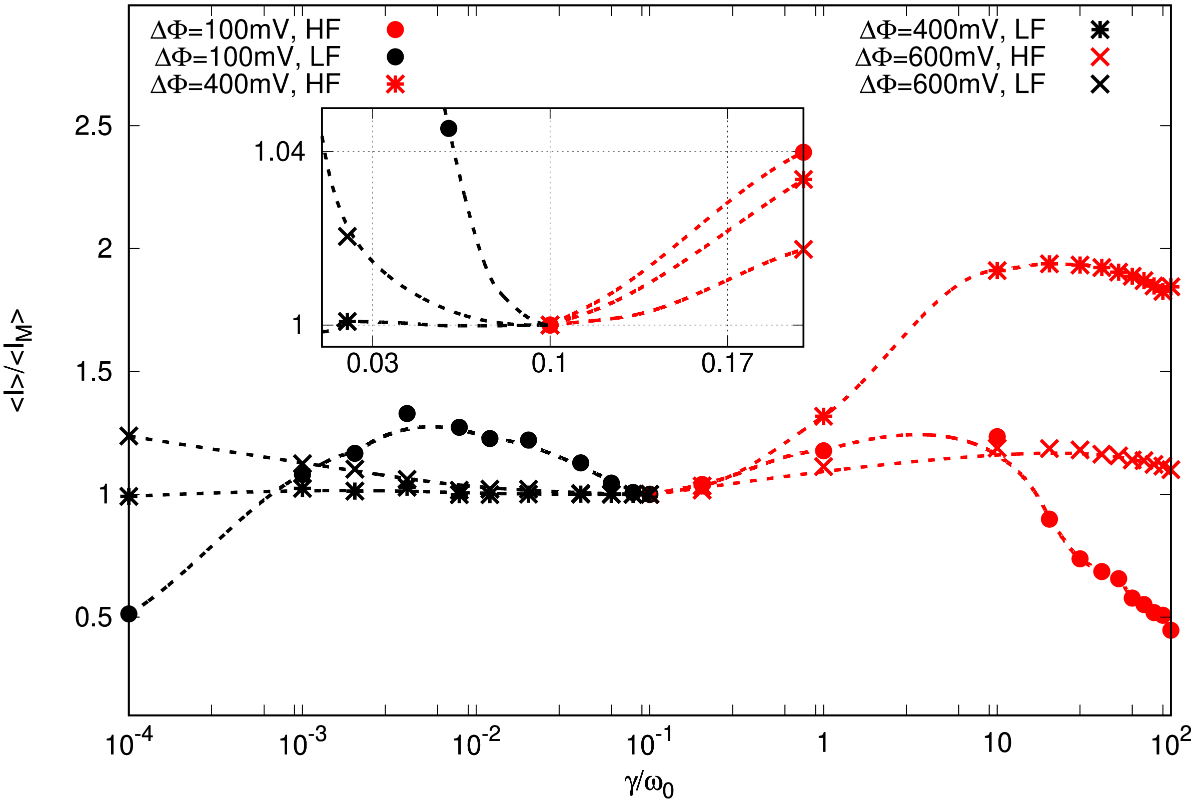

Figure 4.15: The ratio $\langle I \rangle / \langle I_M \rangle$ between the actual average current $\langle I \rangle$ and the current obtained in the TST (Marcus) limit ($\gamma \to 0$ in the high-friction calculation (red dots) or $\gamma \to \infty$ in the low-friction one (black dots)), plotted as a function of γ in a range encompassing both low- and high-friction (LF and HF, respectively) regimes and displayed for different values of the bias potential $\Delta\Phi$. The reorganization energy is set to $E_R =$ 200meV and the temperature is taken to $T = 300$K. The dotted lines are functional fits to the data points for better readability. Inset: Focus on the transition from low to high friction of the average current.

It is interesting to consider the dependence of the average current on the damping strength. This is shown in Fig. 4.15. For $e\Delta\Phi/2 < E_R$, we see in Fig. 4.15 for $\Delta\Phi = 100$mV in the low-friction regime that $\langle I \rangle \propto \gamma$ and that the current is controlled by energy diffusion and the resulting broadening of the molecular level inside the conduction window. In the high-damping regime, we find that $\langle I \rangle \propto \gamma^{-1}$ for small bias voltage, $e\Delta\Phi/2 \sim k_B T$, and the current is strongly influenced by the configurational change along the reaction coordinate. For large damping, the solvent configurations freeze the molecular state at a transition state which may fall into occupied or vacant electronic levels in the leads of opposite directions. This reduces the current. For $e\Delta\Phi/2 > E_R$ for the low-friction regime, see Fig. 4.15 for $\Delta\Phi = 600$mV, the molecular level broadening exceeds the width of the conduction window for small but growing γ such that $\langle I\rangle \propto \gamma^{-1}$ while for $e\Delta\Phi/2 > k_BT$ the solvent stabilizes a possible transition state in the high-damping regime where $\langle I\rangle \propto \gamma$.

The 'turnover' between the regimes of low- and the high-damping, reminiscent of the Kramers turnover of activated barrier crossing rates [50]. Despite a conceptual similarity, there is an important difference: We consider the average current which is composed in the sequential transport regime of four different time-dependent ET rates describing electron insertion and removal to/from the molecular dot via the left/right contact. All four rates depend on the solvent damping and the applied bias voltage. Therefore, there is no one-to-one mapping of the charge current to the Kramers rate as shown in Chapter 14 of Ref. [31] in the strict sense. However, the analogy is obvious.

4.3.4 Proposal for experimental control of solvent damping

The question may arise how to suitably tune the damping strength γ in a real junction experiment. Since the solvent adjusts to the charge distribution on the molecule, its relaxation properties are determined by electromagnetic properties (see discussion of for continuous dielectrics in Sec. 2.2). In particular, for a polar solvent, they depend via the spectral density linearly on the dielectric function as derived in Eq. (2.72) of Subsec. 2.4.4 [58]. Provided that the damping experienced by the Marcus reaction coordinate stems from the solvent, we may aim to control damping by tuning the dielectric properties of the solvent. This is indeed possible in a dielectric solvent confined on the nanoscale and can be realized by tuning the geometry of the confinement. A proof-of-principle is the recent observation of the dependence of the dielectric function of water confined in nanochannels [109].

To illustrate this connection in more detail, we use the spectral density of a fluctuating dipolar solvent specified by Eq. (2.72) in Subsec. 2.4.4 with the Debye type dielectric function of Eq. (2.26) in Subsec. 2.2.1

$$J(\omega) = \frac{2E_R}{\pi\hbar}\frac{\omega_D}{\omega}\frac{1}{\omega^2+\omega_D^2}, \tag{4.67}$$

where $\omega_D = \epsilon_s/(\epsilon_\infty\tau_D)$ with the low- (ϵ_s) and high- (ϵ_∞) frequency dielectric constants and the Debye relaxation time τ_D for solvent relaxation described by the Onsager continuum model of the solvent with Debye relaxation in Subsec. 3.2.1. In the Ohmic regime where $\omega_D \gg \omega_0$ (see Eq. 2.16 in Sec. 2.2), the damping kernel (Eq. 2.15 in Sec. 2.2) for the Langevin equation for the diffusive coordinates x or E can be evaluated as $\tilde{\gamma}(t) = \Theta(t)\omega_0 \int_0^\infty d\omega J(\omega)\omega\cos(\omega t) = \Theta(t)\omega_0 \frac{E_R}{\hbar} e^{-\omega_D t} = \omega_0 \frac{\epsilon_\infty}{\epsilon_0} \frac{E_R \tau_D}{\hbar} \delta(t) = \gamma\delta(t)$. For the latter equation, we use the definition of the damping kernel of Ref. [26], but multiply $J(\omega)$ by ω^2 (we note the different definition of the spectral densities of Refs. [58] and [26] as discussed in Sec. 2.4) and the limit $\omega_D \to \infty$ to obtain the δ-distribution.

It is interesting to see that Fumagalli *et al.* [109] have found experimentally an anomalous decline of the static dielectric constant following the phenomenological relation $\epsilon_s(h) = h/[2h_i/\epsilon_i + (h - 2h_i)/\epsilon_{bulk}]$ for water confined in nanochannels of height h with $\epsilon_i = 2.1$, $\epsilon_\infty = 1.8$ and $h_i = 7.4$ Å. They explain the strong reduction of $\epsilon_s(h)$ for the nanostructured water channel as compared to the bulk configuration with a restricted mobility of the water dipoles at the boundary surfaces which the nanochannel forms with the host material in which they are immersed.

The relationship between the damping constant and the reorganization energy implies in turn that the friction experienced by a solute in a dielectric solvent depends on the dielectric function. For example, using the common relation $E_R = A\left[\frac{1}{\epsilon_\infty} - \frac{1}{\epsilon_s}\right]$ [58], A being a solvent/solute dependent coefficient with the dimension of an energy, we find a connection between γ and ϵ and consequently between γ and any geometrical parameter that may affect ϵ. In detail, we find a geometry-dependent damping strength

$$\gamma(h) = \left[\frac{1}{\epsilon_\infty} - \frac{1}{\epsilon_s(h)}\right] \omega_0 \frac{\epsilon_\infty}{\epsilon_s(h)} \frac{A\tau_D}{\hbar}\,, \tag{4.68}$$

where the strong change of the static dielectric constant in confined geometries enters.

Obviously, we can effectively tune the damping strength γ by tuning the height h of the nanochannel, i.e., the degree of confinement of the solvent, in which the metal-molecule-metal junction operates. The resulting dependance of γ on h is shown in Fig. 4.16. This effect intensifies further if one takes into account the enhanced relaxation time τ_D for water molecules restricted in their mobility [108]. For different modes of operation, i.e., for different relations of E_R, $\Delta\Phi$ and $k_B T$, we thus may control the current $\langle I \rangle$ by tuning γ. Even though the change of γ may not lead to a turnover from low to high damping or vice versa, the characteristic $\langle I \rangle \propto \gamma$ or $\langle I \rangle \propto \gamma^{-1}$ indicates the high- or low-damping regime.

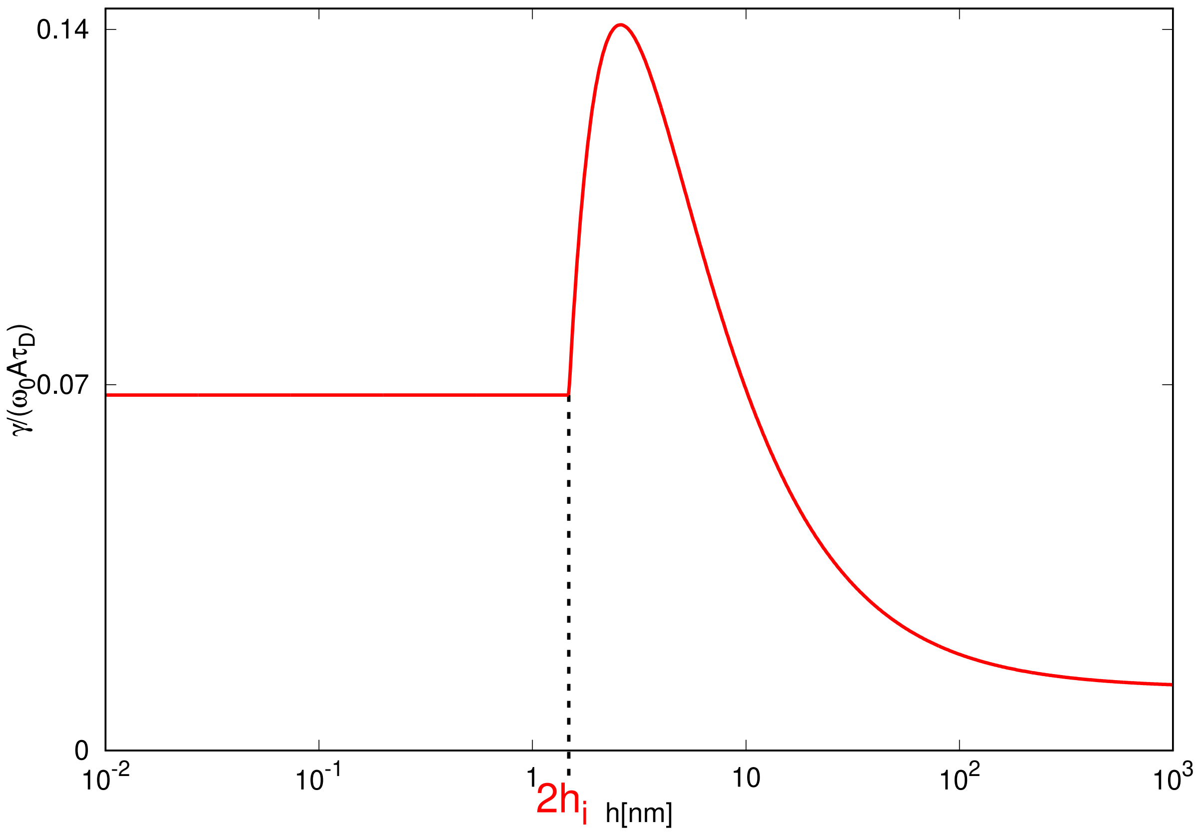

Figure 4.16: Effective frequency-dependent damping $\gamma/(\omega_0 A\tau_D)$, for $\hbar \equiv 1$, in confined nanochannels of height h filled with water based on data taken from Fumagalli *et al.* [109].

4.4 Summary

To summarize, we have calculated the average charge current for a sequential electron transfer in a metal-molecule-metal junction, where consecutive events of charge transfer my be strongly influenced by relaxation of surrounding solvent, thereby affecting the observed current and its fluctuations. The resulting dynamics was described by a kinetic model that comprises rates of electron exchange between molecules and leads with relaxation of the thermal environment in response to the changing molecular charge. This relaxation is described by a diffusion process that focuses on the reaction coordinate in the high-friction regime and on its associated energy in the low-friction limit. We have considered the average current as well as the current noise. In the regime of low friction, an increasing solvent damping strength leads to an increasingly fluctuating energy level which is associated to an effective broadening of the molecular energy level that lies inside ($e\Delta\Phi/2 < E_R$) or outside ($e\Delta\Phi/2 > E_R$) the conduction window of the metal-molecular-metal junction (using the language of a combined Marcus-Landauer model [132, 133]). Consequently, the average current is enhanced ($e\Delta\Phi/2 < E_R$) or reduced ($e\Delta\Phi/2 > E_R$) when friction becomes larger in this regime. In the regime of large damping, increasing friction implies a more slowly relaxing configuration along the reaction coordinate. Therefore, in the course of successive electron transfer events the molecular configuration remains more localized near a transition point. This leads to an average current that increases with friction when $e\Delta\Phi/2 > k_BT$ but decreases when an enhanced localization leads to an increased probability of back ET, which becomes possible when $e\Delta\Phi/2 \sim k_BT$. A unified look at both regimes indicates a Kramers-like turnover of electron transfer which translates into a corresponding turnover behavior of the overall current as a function of the damping strength. This clearly reflects the nonequilibrium fluctuations at work under an applied bias voltage.

It should be noted that ”turnover” is a generic mode of behavior of rate (or transport) processes. The overall transport dynamics determined by the underlying rate(s) changes its character between different regimes by varying some control parameter. In the Kramer problem this parameter is the friction on the reaction coordinate while in our case it is the (not unrelated) dielectric relaxation associated with the solvation coordinate (as defined by Marcus). Other mechanisms have been considered, see, e.g. Refs. [134, 135] where the control parameter changes the dephasing of local energy levels leading to turnover in exciton transport behavior. To the best of our knowledge, our present work is the first where the consequence of such turnover is considered not only for the average rate (or transport coefficient) but also for the noise in the ensuing current.

The calculated Fano factor indicates a non-Poissonian current statistics for an enhanced damping in both regimes for a small applied bias voltage and a large reorganization energy. Once the applied voltage is large enough, the solvent-induced friction has no impact on the ET, because the solvent-mediated orientation (in the high-damping regime) or the broadening (in the low-damping regime) of the molecular level does not change relative to empty and occupied single-electron states in the metal. The calculated current autocorrelation functions and the related correlation times confirms the observations. Therefore, current noise as an additional observable may help to distinguish between different modes of operation. Additionally, this mechanism may help to interpret current-voltage observations (see Ref. [136]).

Furthermore, we illustrate a viable means to tune the damping strength γ of the solvent which depends on the dielectric properties of the solvent via the static dielectric constant. For this, we illustrate a possible way of how to effectively use experimentally measured data which report an extreme decline of the static dielectric constant of water in confined nanochannels of variable height. By this, we deduce a direct dependence of γ on the height of the nanochannel which can be readily used to observe and control the characteristic current-damping behavior in molecular junctions.

Chapter 5

Summary and outlook

In the present thesis, a generalized theory of a dynamical solvent has been introduced in order to analyze 'non-conventional' time-dependent phenomena in guest-host correlated quantum systems. All associated experimental setups refer to dissolved single molecules or molecular systems when one faces solute and solvent dynamics on same and, thus, competing time scales. These situations where specific highly nonequilibrium solute-solvent effects, such as a hydration shell formation, take place [49] require a theoretical description beyond standard Green-Kubo like correlations known from equilibrium quantum solvation [20]. Therefore, the explicit solutions of equations of motion for distinct solute or solvent degrees of freedom may now enable predictions for energy absorption and charge transfer in a dynamical and strongly non-equilibrated solvent.

The dynamics of complex many-body quantum systems as those characterizing solute-solvent systems is often calculated in terms of the effective dynamics of a relevant small set of observables characterizing the solute or solvent. Depending on the context, these observables are related to the macroscopic world, e.g., the molecular dipole moment as considered in the first part of the thesis, or to a reaction coordinate describing the solvent degrees of freedom for charge transfer processes as investigated in the second part of this thesis. The utilized Langevin equations lead to a mean-field-type description of the solvent which enters in a memory kernel of the equation of motion where, within the continuum approach, macroscopic dielectric solvent properties are integrated.

In the first part of the thesis, I have established a novel nonequilibrium theory for time-irreversible changes in the geometrical structure of the solute or solvent. To this end, I have formulated a theory of nonequilibrium quantum solvation based on the Onsager model in which parameters of the solute or solvent are explicitly depending on time. Up to present, a generalization of the Onsager continuum equilibrium theory of quantum solvation to explicitly include time-dependent solvent properties has not been established. I have solved the resulting generalized Langevin equation for the molecular dipole moment where the memory kernel has now an explicit time dependence reflecting the non-stationary solute-solvent dynamics.

Inspired by experimental results revealing the structural dynamics of photoexcited complexes such as $[\mathrm{Co(terpy)_2}]^{2+}$ in aqueous solution where the photoexcitation leads to an elongation of the Co-N bonds[77], we have analyzed the relaxation properties of molecular point dipole by the results of the corresponding non-stationary Langevin equation. We have considered two different scenarios: a shrinking Onsager sphere and a breathing Onsager sphere. Due to the time-dependent solvent, the frequency-dependent response function of the dipole becomes explicitly time-dependent. For a shrinking Onsager sphere, the dipole relaxation is in general enhanced. In contrast, a breathing sphere reduces damping as compared to the static sphere. We have identified a difference in the dipole relaxation in comparison to a stationary quasiadiabatic Onsager model where the time-dependent solvent has been incorporated parametrically. Interestingly, we find a non-monotonous dependence of the relaxation rate on the breathing rate and a resonant suppression of damping when both rates are comparable. Moreover, the line width of the absorptive part of the response function is strongly reduced for times when the breathing sphere reaches its maximal extension.

Since the model is very generic, we have used the approach of a shrinking sphere to develop a model for the observed bimodal dynamic behavior of the solvent correlation function. This behavior can be experimentally revealed by a time-dependent Stokes shift [103, 104, 101]. By using linear response theory, we have explicitly decomposed the fluorescence Stokes shift into a component which originates from the solvent and into a component reflecting the 'self-motion' of the solute. Thus, we have extended the well-established Bagchi-Oxtoby-Fleming theory of solvent relaxation towards non-stationary molecular motions.

Finally, we have modeled the dynamic build-up of the hydration shell around a hydrophobic solute on the basis of solving the non-stationary Langevin equation for the generalized Onsager model by including a time-dependent hydration shell. Most notably, we have found a time-dependent frequency shift down to the blue of the resonant absorption of the dipole, together with a dynamically decreasing line width compared to bulk water. The blue shift reflects the work performed against the network of hydrogen bonds in the bulk solvent and is a directly measurable quantity. The results are in agreement with an experiment on the hydrophobic solvation of iodine in water. The experimental XAS study has demonstrated the dynamic expansion of the solvent layer within a time of 5ps after the transfer $I^- \rightarrow I^0$, accompanied by an increase of the radius of the hydrated cluster by up to 80% [49, 78].

In the second part of the thesis, I have investigated the effect of a dynamic solvent-induced relaxation on the 'hopping' conduction of electrons in molecular junctions. This approach goes beyond the standard treatment of transport in solvated molecular junctions that rely on Marcus theory. In analogy to Kramers' treatment of activated barrier crossing [50], we have formulated a diffusion (Smoluchowski) equation for the reaction coordinate, a distribution of specific solvent configurations. Its dynamics can be described by a Langevin equation where a friction γ and a random noise terms enter. They satisfy the standard fluctuation-dissipation relations. We then have considered the implications of the solvent dynamics in two limits. In the overdamped limit, a Smoluchowski equation describes diffusion along the reaction coordinate. In the opposite underdamped limit, the relaxation may be reduced, after phase averaging, to diffusion in energy space. After solving the Smoluchowski equations, we have formulated the electron transfer rates which now depend explicitly on the time elapsed since the last transfer process. The average charge current through the junction results from the statistical calculation based on a Monte Carlo simulation by exploiting the time-dependent electron transfer rates. It depends on the friction strength that determines the solvent relaxation rate. For the regime of low damping, we have found that an enhanced damping leads to an effective broadening of the molecular energy level that falls into or exceeds the conduction window of the metal-molecular-metal junction arrangement, depending whether the bias voltage window is smaller or larger than the reorganization energy. Therefore, the average current is correspondingly enhanced or reduced. In turn, in the regime of large damping and slowly relaxing configuration along the reaction coordinate, the molecular state is more localized at a transition point with increasing damping such that the average current increases or decreases when thermal fluctuations make an inverse ET possible. This depends whether the bias voltage window is larger than or comparable to the thermal energy. Both regimes together show a Kramers-like turnover of the current in dependence of the damping, but now under true nonequilibrium conditions of an applied bias potential. Moreover, I have investigated the dependence of the current noise on this relaxation rate. For low damping the process is Markovian and the hopping statistics is Poissonian. When solvent relaxation occurs on a finite timescale, successive electron hopping events are correlated. Finally, we illustrate a viable means to tune the damping strength of the solvent which depends on the dielectric properties of the solvent via the static dielectric constant. Therefore, we show a possible way of how to effectively use experimentally measured data which report an extreme decline of the static dielectric constant of water in confined nanochannels of variable height. By this, we deduce a direct dependence of the solvent induced damping on the height of the nanochannel which can be readily used to observe and control the characteristic current-damping behavior in molecular junctions.

In both parts of the present thesis, I have investigated the impact of the solvent dynamics on a finite time scale on physical measurable observables, such as the transport current and the time-dependent molecular dipole moment. We see that, in both cases, the observable strongly depends on the underlying nonequilibrium solvent dynamics which needs to be controlled. To do so, we have reduced the enormously complex network of time-dependent interaction characterizing solute-solvent systems to relevant properties. In the first part, I have formulated a non-stationary solvent response to the system's dipole moment dynamics where the explicit solvent degrees of freedom have been eliminated. In the second part, I have derived a time-dependent probability distribution for a reduced set of the solvent degrees of freedom, the reaction coordinate. Both approaches yield a tremendous reduction and come along with coarse-grained solvent variables which may be related to macroscopic solvent properties such as the dielectric constant and relaxation times. Such parameters can be experimentally determined with the ultimate goal that energy and charge transfer may be efficiently controlled.

Several experimental, numerical and theoretical approaches still exist to study and understand the dynamics of water as solvent surrounding (bio-)molecules and control their charge- and energy-transfer properties. One example of many is the study of energy exchange of a vibrationally excited solute to the interfacial water shell [137, 138, 139]. Energy transfer from the solute to the hydration shell occurs on subpico- to picosecond time scales and strongly depends on the local hydration geometries and particular type of excitation [140]. This opens further promising tasks to understand the solvent-solute interplay and to deduce consequences on the properties and on the function of the dissolved molecules, including their elementary (bio-)chemical reactions also *in vivo* [140]. Time-resolved structure sensitive experimental methods from X-ray diffraction, scattering or absorption may elucidate further insights in the functionality of solute-solvent interactions. One possibility could arise when the water dynamics in the vicinity of the solute changes time-local dielectric properties and, thus, influence whether charges can easily enter the solute to initiate a chemical reaction [140]. In this direction, new theoretical developments will be required to quantify nonequilibrium and time-dependent effects in more complex models. A theory of higher-order (X-ray) spectroscopy [141] combined with time-dependent non-stationary Langevin equations for the relevant observables [40], where system and bath are strongly correlated, may be a promising route. Once the origin of (time-dependent) solvent-solute interactions is understood, suitable manipulation of the solvent environment can yield a control of the reactivity and product selectivity of chemical processes [142].

Appendix A

Time-dependent Onsager sphere

This Appendix establishes background information for the developed generalized Onsager model in Sec. 3.2. In Sec. A.1, we rewrite the equation of motion in the usual form in which a Stokes damping force appears which is proportional to the velocity of the particle. In Sec. A.2, we provide the details for the time-dependent response function to an external applied electric field.

A.1 Equation of motion in time domain

The expectation value $\langle \mu(t) \rangle = e\langle q(t) \rangle$ of the dipole moment embedded in the center of the Onsager sphere follows from the solution of the generalized Langevin equation in which the expectation value of the reaction field $\langle R(t) \rangle = \frac{e^2}{a(t)^3} \int_0^t dt' \chi(t-t') \langle q(t') \rangle$ acts as an external force $e\langle R(t) \rangle$ on the dipole moment. For better readability, we set $\langle q(t) \rangle \equiv q(t)$ and $\langle R(t) \rangle \equiv R(t)$. The equation of motion then reads

$$m\ddot{q}(t) + m\omega_0^2 q(t) - \frac{e^2}{a(t)^3} \int_0^t dt' \chi(t-t') q(t') = 0, \tag{A.1}$$

where the third term is the back action of the dielectric medium, the solvent, on the dipole. To obtain the usual form of the equation of motion with a damping force proportional to the velocity, we express the response function $\chi(t)$ with the dielectric function in Debye form (see Eq. (2.26) in Subsec. 2.2.2) and with $\epsilon_\infty \neq 1$ as

$$\begin{aligned}\chi(t) = &\exp\left[-\frac{2\epsilon_s+1}{(2\epsilon_\infty+1)\tau_D}t\right]\frac{2(\epsilon_s-1)}{(2\epsilon_\infty+1)\tau_D}\Theta(t) \\ &-\exp\left[-\frac{2\epsilon_s+1}{(2\epsilon_\infty+1)\tau_D}t\right]\frac{2(2\epsilon_s+1)(\epsilon_\infty-1)}{(2\epsilon_\infty+1)^2\tau_D}\Theta(t) \\ &+\exp\left[-\frac{2\epsilon_s+1}{(2\epsilon_\infty+1)\tau_D}t\right]\frac{2(\epsilon_\infty-1)}{(2\epsilon_\infty+1)}\delta(t).\end{aligned} \tag{A.2}$$

The resulting damping kernel reads with $\epsilon_\infty = 1$ according to

$$\gamma(t) = \int_t^\infty ds \chi(s) = \frac{\chi_D}{\omega_D}e^{-\omega_D t}\,, \tag{A.3}$$

where $\omega_D = (2\epsilon_s+1)/(3\tau_D)$ and $\chi_D = \frac{2(\epsilon_s-1)}{3\tau_D}$ according to Eq. (3.12) in Subsec. 3.2.1. With this, one can now write the third term of Eq. (A.1) in terms of the damping kernel in the form

$$m\ddot{q}(t) + m\omega_0^2 q(t) + \frac{e^2}{a(t)^3}\int_0^t dt' \dot{\gamma}(t-t')q(t') = 0\,. \tag{A.4}$$

After an integration by parts and obeying the relation $\dot{\gamma}(t-t') = \partial\gamma(t-t')/\partial(t-t') = -\partial\gamma(t-t')/\partial t'$, we find

$$m\ddot{q}(t) + m\omega_0^2 q(t) - \frac{e^2}{a(t)^3}\left[\gamma(0)q(t) - \gamma(t)q(0) - \int_0^t dt'\gamma(t-t')\dot{q}(t')\right] = 0\,. \tag{A.5}$$

or, equivalently,

$$m\ddot{q}(t) + m\left[\omega_0^2 - \frac{e^2}{ma(t)^3}\gamma(0)\right]q(t) + \frac{e^2}{a(t)^3}\int_0^t dt'\gamma(t-t')\dot{q}(t') = -\frac{e^2}{a(t)^3}\gamma(t)q(0). \tag{A.6}$$

The second term describes a renormalized potential where the renormalization occurs due to the coupling to the dielectric medium, where the effective frequency follows from $\omega_{\text{eff}}^2 = \omega_0^2 - [\Delta\omega(t)]^2$, with $[\Delta\omega(t)]^2 = e^2\gamma(0)/(ma(t)^3)$. The biggest renormalization occurs for the smallest magnitude of the sphere radius a_0 such that we set

$$\Delta\omega \equiv \Delta\omega(t\to\infty) = \sqrt{\frac{\Phi}{\omega_D}}\,, \tag{A.7}$$

with

$$\Phi = \frac{e^2}{ma_0^3}\chi_D\,. \tag{A.8}$$

If $\omega_0^2 < (\Delta\omega)^2$, the effective potential has a negative curvature and describes an unstable situation of the dipole moment in the Onsager sphere. So, since we are only interested in the damping of the dynamics of the dipole induced by the dielectric medium and not in an unstable renormalization of the potential, one needs to ensure that $\Delta\omega < \omega_0$ which is fulfilled for our choice of parameters in the main text of Sec. 3.2.

The third term of Eq. (A.6) describes the damping force acting on the dipole in the Onsager sphere due to the response of the environment to the dipolar dynamics. This damping kernel is related to the spectral density $J(\omega) = M\omega \int_0^\infty dt\gamma(t)\cos(\omega t)$ in case of a static Onsager radius $a(t) = a_0$ of an equilibrium environment described as an infinite set of harmonic oscillators as inversion of the Fourier integral of Eq. (2.15) of Sec. 2.2. The inhomogeneous term on the right-hand side of Eq. (A.6) is an initial slip resulting from the present assumption of factorizing initial conditions for the system-bath dynamics [26].

A.2 Response function

When one adds an external force $eE(t)$ on the right hand side of Eq. (3.15) in Sec. 3.2 and then perform a Laplace transform, we find

$$\begin{aligned} q_R(z) &= q(z) + \delta q(z) \\ &= \frac{zq(t=0)}{\omega_0^2 - z^2 + i\chi_0(z)} + \frac{i\chi_1(z+i\alpha)q_0(z+i\alpha)}{\omega_0^2 - z^2 + i\chi_0(z)} \\ &+ \frac{e}{m}\frac{1}{\omega_0^2 - z^2 + i\chi_0(z)}\left[E(z) + \frac{i\chi_1(z+i\alpha)E(z+i\alpha)}{\omega_0^2 - (z+i\alpha)^2 + i\chi_0(z+i\alpha)}\right], \end{aligned} \tag{A.9}$$

where we again replace $q(z+i\alpha)$ by $q_0(z+i\alpha)$ in the second term of Eq. (A.9) since we need to make sure that the latter one only contains contributions up to first order in a_1/a_0 (which is realized by the prefactor $\chi_1(z+i\alpha)$). The second term $\delta q(z)$ reflects the response of the dipole moment to the external force and reads

$$\delta q(z) = X_0(z)[E(z) + iW_1(z+i\alpha)E(z+i\alpha)], \tag{A.10}$$

with

$$X_0(z) = \frac{e}{m[\omega_0^2 - z^2 + i\chi_0(z)]}, \tag{A.11}$$

$$W_1(z) = \frac{\chi_1(z)}{\omega_0^2 - z^2 + i\chi_0(z)}. \tag{A.12}$$

With the Laplace transform

$$f(z) = i\int_0^\infty dz e^{izt} f(t) = L[f(t)], \tag{A.13}$$

where $z \in \mathbb{C}$ and $\mathrm{Im}[z] > 0$, the convolution rule follows as

$$L[\int_0^t ds f(t-s)q(s)] = -if(z)q(z). \tag{A.14}$$

In the real-time domain, $\delta q(t)$ takes the form (for small but finite radius a_1)

$$\delta q(t) = i\int_0^t ds X_0(t-s)\left[E(s) - e^{-\alpha s}\int_0^s du W_1(s-u)E(u)\right]. \tag{A.15}$$

This may be written as

$$\delta q(t) = i\int_0^t X(t,s)E(t-s), \tag{A.16}$$

where

$$X(t,s) = X_0(s) - e^{-\alpha t}\int_0^s du e^{\alpha u} X_0(u) W_1(s-u) = X_0(s) - e^{-\alpha t} X_1(s). \tag{A.17}$$

The Fourier transform of $X(t,s)$ leads to the response function. An explicit form of it can only be obtained in the adiabatic limit: We assume $\alpha \ll \Gamma_0$, while Γ_0 is the decay rate of $X_0(s)$, so that the time-dependent prefactor $e^{-\alpha t}$ can be treated adiabatically. We define the Fourier transform as

$$f(\omega) = \int_{-\infty}^\infty dt e^{i\omega t} f(t) = F[f(t)]. \tag{A.18}$$

As all functions $f(t) = 0$ for $t < 0$ in our problem, we performs a Laplace transform, so that we may write $f(\omega) \equiv -if(\mathrm{Re}[z])$ in view of our definition of the Laplace transform in

Eq. (A.13).

Appendix B

Analysis for the Stokes shift equation

For the first term in Eq. (3.70) of Sec. 3.3, we follow the back transform given in the publication of *Hsu et al.* [102].

$$\Delta E(t) = \frac{-\Delta\mu^2}{2\pi a_0^3}\int_C dz \frac{\chi(z)}{iz} e^{izt} \tag{B.1}$$

$$= -\frac{-\Delta\mu^2}{2\pi a_0^3}\int_C dz \frac{\chi(z)-\chi(0)}{iz} e^{izt} - \frac{-\Delta\mu^2}{2\pi a_0^3}\int_C dz \frac{\chi(0)}{iz} e^{izt}, \tag{B.2}$$

while C is the contour parallel but slightly below the real axis. The second term by exploiting the residue theorem is equal to $-\frac{\Delta\mu^2}{a_0^3}\chi(0)\Theta(t)$. $\chi(z)$ is analytic on the real axis and $\chi(0)$ is a real number. Since $\frac{\chi(z)-\chi(0)}{z} = [\frac{d\chi(z)}{dz}]_{z=0} + O(z)$ (second integrand of Eq. (B.2)) for $z \to 0$ and since $d\chi(z)/dz$ has no singularity at $z = 0$, the term does not possess a pole at $z = 0$.

The contour C may now therefore coincide with the real axis such that with $\chi(\omega) = \mathrm{Re}[\chi(\omega)] + i\,\mathrm{Im}[\chi(\omega)]$ and the fact that $\chi(-\omega) = \chi^*(\omega)$ because $\chi(t)$ is real, we find

$$\int_C dz \frac{\chi(z)-\chi(0)}{iz} e^{izt} = 2\int_0^\infty d\omega \frac{\mathrm{Im}[\chi(\omega)]}{\omega}\cos(\omega t) + 2\int_0^\infty d\omega \frac{\mathrm{Re}[\chi(\omega)]-\chi_s}{\omega}\sin(\omega t). \tag{B.3}$$

Thus, Eq. (B.2) reads

$$\Delta E(t) = \frac{-\Delta\mu^2}{\pi a_0^3}\left[\int_0^\infty d\omega \frac{\mathrm{Im}[\chi(\omega)]}{\omega}\cos[\omega t] + \int_0^\infty d\omega \frac{\mathrm{Re}[\chi(\omega)]-\chi_s}{\omega}\sin[\omega t] + \pi\chi_s\Theta(t)\right]. \tag{B.4}$$

Since $\Delta E(t) = 0$ for $t < 0$ and the first and second integrand are equal for positive t. Eq. (B.4) yields

$$\Delta E(t) = \frac{-2\Delta\mu^2}{\pi a_0^3} \int_0^\infty d\omega \frac{\mathrm{Im}[\chi(\omega)]}{\omega} \cos[\omega t] - \frac{\Delta\mu^2}{a_0^3} \chi_s \Theta(t). \tag{B.5}$$

Appendix C

Evaluation of the nonadiabatic electron transfer rate

Here we derive the transfer rate of Eq. (4.18) in Subsec. 4.1.2. We start with the golden rule ET rate given by Eq. (4.17) in Subsec. 4.1.2 for the $A \to B$ transition

$$k_{AB} = \frac{2\pi}{\hbar} \int_{-\infty}^{\infty} d\epsilon \rho_M(\epsilon) f(\epsilon) \sum_{v;v'} |\, \langle v | \hat{V}_{A,B} | v' \rangle \,|^2 \delta(E_A - E_B + \epsilon + E_b(v) - E_b(v'))\,, \qquad \text{(C.1)}$$

where $E_A(v)$ and $E_B(v')$ are the eigenvalues of the nuclear (solvent) Hamiltonian (i.e., the harmonic oscillator state on the potential surfaces $E_A(x)$ and $E_B(x)$), $\hat{V}_{AB}$ is the interstate coupling and $\rho_M(\epsilon)$ is the density of single electron states in the metal. We further assume the wide-band limit, i.e., the density of states $\rho_M(\epsilon) = \rho_M =$ const. being independent of the electron energy in the following.

We use the definition of the interstate coupling $\hat{V}_{A,B} = V_{A,B} e^{g(\hat{a}^\dagger - \hat{a})}$ (while $\hat{V}_{A,B}^\dagger = \hat{V}_{B,A}$) according to the spin-boson model after a polaron transformation. Here, $\hat{a}^\dagger$ and $\hat{a}$ are the creation and annihilation operators of the harmonic oscillator state while g describes its coupling strength to the molecular energy states (see Ref. [31] , Chapter 12). Next, we use the identity $\delta(x) = (2\pi\hbar)^{-1}\int_{-\infty}^{\infty} dt e^{ixt/\hbar}$ and write Eq. (C.1) in Subsec. 4.1.2 in the form

$$\begin{aligned} k_{AB} &= \frac{\rho_M}{\hbar^2}\int_{-\infty}^{\infty} d\epsilon f(\epsilon)\sum_{v;v'}\langle v|\hat{V}_{AB}|v'\rangle\langle v'|\hat{V}_{BA}|v\rangle\int_{-\infty}^{\infty} dt e^{i(E_A-E_B+\epsilon+E_b(v)-E_b(v'))t/\hbar} \\ &= \frac{\rho_M}{\hbar^2}\int_{-\infty}^{\infty} d\epsilon f(\epsilon)\int_{-\infty}^{\infty} dt e^{i(E_A-E_B+\epsilon)t/\hbar}\sum_{v}\langle v|e^{i\hat{H}_B t/\hbar}\hat{V}_{AB}e^{-i\hat{H}_B t/\hbar}\sum_{v'}|v'\rangle\langle v'|\hat{V}_{BA}|v\rangle \\ &= \frac{\rho_M|V_{A,B}|^2}{\hbar^2}\int_{-\infty}^{\infty} d\epsilon f(\epsilon)\int_{-\infty}^{\infty} dt e^{i(E_A-E_B+\epsilon)t/\hbar}\sum_{v}\langle v|e^{g(\hat{a}^\dagger e^{i\omega_0 t}-\hat{a}e^{-i\omega_0 t})}e^{g(\hat{a}^\dagger-\hat{a})}|v\rangle\ , \end{aligned} \tag{C.2}$$

where $\hat{H}_B$ is the Hamilton for the harmonic oscillator, ω_0 is the harmonic mode and $\sum_{v'}|v'\rangle\langle v'|$ is the completeness relation in the oscillator subspace whose orthonormal states obey $\langle v|v'\rangle = \delta_{v,v'}$. We utilize the identity

$$K \equiv \sum_{v}\langle v|e^{\alpha_1\hat{a}+\beta_1\hat{a}^\dagger}e^{\alpha_2\hat{a}+\beta_2\hat{a}^\dagger}|v\rangle = e^{(\alpha_1+\alpha_2)(\beta_1+\beta_2)(n+1/2)+(\alpha_1\beta_2-\beta_1\alpha_2)/2}\ , \tag{C.3}$$

where $n = \sum_v\langle v|\hat{a}^\dagger\hat{a}|v\rangle$ [31]. Since the the oscillator interacts with many solvent degrees of freedom, it exchanges irreversibly energy with the solvent, such that the energy can be defined by $E(t) = n(t)\hbar\omega_0$. Using the definition $n(t) = E(t)/(\hbar\omega_0)$, Eq. (C.2) in Subsec. 4.1.2 becomes

$$k_{AB} = \Gamma\int_{-\infty}^{\infty} d\epsilon f(\epsilon)\int_{-\infty}^{\infty} dt e^{i(E_A-E_B+\epsilon)t/\hbar-ig^2\sin(\omega_0 t)+g^2[2n(t)+1][\cos(\omega_0 t)-1]}\ , \tag{C.4}$$

which equals Eq. (4.18) in Subsec. 4.1.2 after introducing the conditional rate $\Gamma = \frac{\rho_M|V_{A,B}|^2}{\hbar^2}$.

References

[1] R. Zwanzig, "Ensemble Method in the Theory of Irreversibility," J. Chem. Phys. **33**, 1338–1341 (1960).

[2] H. Mori, "Transport, Collective Motion, and Brownian Motion," Prog. Theor. Phys. **33**, 423–455 (1965).

[3] R. Zwanzig, "Nonlinear Generalized Langevin Equations," J. Stat. Phys. **9**, 215–220 (1973).

[4] A. O. Caldeira and A. J. Leggett, "Influence of Dissipation on Quantum Tunneling in Macroscopic Systems," Phys. Rev. Lett. **46**, 211–214 (1981).

[5] A. J. Leggett, S. Chakravarty, A. T. Dorsey, Matthew P. A. Fisher, Anupam Garg, and W. Zwerger, "Dynamics of The Dissipative Two-State System," Rev. Mod. Phys. **59**, 1–85 (1987).

[6] M. Thorwart, P. Reimann, and P. Hänggi, "Iterative Algorithm versus Analytic Solutions of the Parametrically Driven Dissipative Quantum Harmonic Oscillator," Phys. Rev. E **62**, 5808–5817 (2000).

[7] E. Joos, H.D. Zeh, C. Kiefer, D.J.W. Giulini, J. Kupsch, and I.-O. Stamatescu, *Decoherence and the Appearance of a Classical World in Quantum Theory* (Springer Berlin Heidelberg, 2003).

[8] R. Braun, *The Miscellanious Work of Robert Brown* (Robert Hardwicke, London, 1866).

[9] A. Einstein, "Über die von der molekularkinetischen Theorie der Wärme geforderte Bewegung von in ruhenden Flüssigkeiten suspendierten Teilchen," Ann. Phys. (Berlin) **322**, 549–560 (1905).

[10] M. v. Smoluchowski, "Zur kinetischen Theorie der Brownschen Molekularbewegung und der Suspensionen," Ann. Phys. (Berlin) **326**, 756–780 (1906).

[11] P. Langevin, "Sur la Théorie du Mouvement Brownien," Comptes Rendues **146**, 530 (1908).

[12] J. v. Neumann, "Wahrscheinlichkeitstheoretischer Aufbau der Quantenmechanik," Nachrichten von der Gesellschaft der Wissenschaften zu Göttingen, Mathematisch-Physikalische Klasse **1927**, 245–272 (1927).

[13] L. Landau, "Das Dämpfungsproblem in der Wellenmechanik," Z. f. Phys. **45**, 430–441 (1927).

[14] F. Bloch, "Nuclear Induction," Phys. Rev. **70**, 460–474 (1946).

[15] G. E. Uhlenbeck and L. S. Ornstein, "On the Theory of the Brownian Motion," Phys. Rev. **36**, 823–841 (1930).

[16] V. Weisskopf and E. Wigner, "Berechnung der natürlichen Linienbreite auf Grund der Diracschen Lichttheorie," Z. f. Phys. **63**, 54–73 (1930).

[17] H. Grabert, *Projection Operator Technics in Nonequilibrium Statistical Mechanics* (Springer Berlin Heidelberg, 1982).

[18] P. C. Hohenberg and B. I. Halperin, "Theory of Dynamic Critical Phenomena," Rev. Mod. Phys. **49**, 435–479 (1977).

[19] M. S. Green, "Markoff Random Processes and the Statistical Mechanics of Time-Dependent Phenomena. II. Irreversible Processes in Fluids," J. Chem. Phys. **22**, 398–413 (1954).

[20] R. Kubo, "Statistical-Mechanical Theory of Irreversible Processes. I. General Theory and Simple Applications to Magnetic and Conduction Problems," J. Phys. Soc. Jpn. **12**, 570–586 (1957).

[21] A. G. Redfield, "The Theory of Relaxation Processes," in *Advances in Magnetic Resonance*, Advances in Magnetic and Optical Resonance, Vol. 1, edited by John S. Waugh (Academic Press, 1965) pp. 1–32.

[22] J. Thingna, J.-S. Wang, and P. Hänggi, "Generalized Gibbs State with Modified Redfield Solution: Exact Agreement up to Second Order," J. Chem. Phys. **136**, 194110 (2012).

[23] Y. Tanimura and R. Kubo, "Time Evolution of a Quantum System in Contact with a Nearly Gaussian-Markoffian Noise Bath," J. Phys. Soc. Jpn **58**, 101–114 (1989).

[24] N. Makri, "Numerical Path Integral Techniques for Long Time Dynamics of Quantum Dissipative Systems," J. Mat. Phys. **36**, 2430–2457 (1995).

[25] C. V. Raman, "A new radiation," Indian J. Phys. **74**, 382–386 (1928).

[26] U. Weiss, *Quantum Dissipative Systems* (World Scientific Publishing, Singapore, 2010).

[27] S. Mukamel, "Multidimensional Femtosecond Correlation Spectroscopies of Electronic and Vibrational Excitations," Annu. Rev. Phys. Chem. **51**, 691–729 (2000).

[28] J. T. Hynes, "Chemical Reaction Dynamics in Solution," Annu. Rev. Phys. Chem. **36**, 573–597 (1985).

[29] A. L. Harris, J. K. Brown, and C. B. Harris, "The Nature of Simple Photodissociation Reactions in Liquids on Ultrafast Time Scales," Annu. Rev. Phys. Chem. **39**, 341–366 (1988).

[30] N. A. Abul-Haj and D. F. Kelley, "Geminate Recombination and Relaxation of Molecular Iodine," J. Chem. Phys. **84**, 1335–1344 (1986).

[31] A. Nitzan, *Chemical Dynamics in Condensed Phases* (Oxford University Press, Oxford, 2006).

[32] M. v. Smoluchowski, "Versuch einer mathematischen Theorie der Koagulationskinetik kolloider Lösungen." Z. Phys. Chem. **92**, 129–168 (1918).

[33] J. Franck and E. Rabinowitsch, "Some Remarks about Free Radicals and the Photochemistry of Solutions," Trans. Faraday Soc. **30**, 120–130 (1934).

[34] M. Lehni and H. Fischer, "Effects of Diffusion on the Self-Termination Kinetics of Isopropylol Radicals in Solution," Int. J. Chem. Kinet. **15**, 733–757 (1983).

[35] M. Lehni, H. Schuh, and H. Fischer, “Rate Constants for the Termination of Benzyl Radicals in Solution,” International Journal of Chemical Kinetics **11**, 705–713 (1979).

[36] J. N. Murrell, A. J. Stace, and R. Dammel, “Computer Simulation of the Cage Effect in the Photodissociation of Iodine,” J. Chem. Soc., Faraday Trans. 2 **74**, 1532–1539 (1978).

[37] Orozco M. Gelpí J. L. Hospital A., Goni J. R., “Molecular Dynamics Simulations: Advances and Applications,” Adv Appl Bioinform Chem. **8**, 3747 (2015).

[38] L. Onsager, “Electric Moments of Molecules in Liquids,” J. Am. Chem. Soc. **58**, 1486–1493 (1936).

[39] J. Gilmore and R. H. McKenzie, “Spin Boson Models for Quantum Decoherence of Electronic Excitations of Biomolecules and Quantum Dots in a Solvent,” J. Phys.: Condens. Matt. **17**, 1735–1746 (2005).

[40] B. Mennucci, “Continuum Solvation Models: What Else Can We Learn from Them ?” J. Phys. Chem. Lett. **1**, 1666–1674 (2010).

[41] P. Debye, Ver. Deut. Phys. Gesell. **15**, 77 (1913).

[42] P. Drude, “Zur Elektronentheorie der Metalle,” Ann. Phys. (Berlin) **306**, 566–613 (1900).

[43] R. A. Marcus, “On the Theory of Oxidation-Reduction Reactions Involving Electron Transfer. I,” J. Chem. Phys. **24**, 966–978 (1956).

[44] R. A. Marcus, “Electrostatic Free Energy and Other Properties of States Having Nonequilibrium Polarization. I,” J. Chem. Phys. **24**, 979–989 (1956).

[45] C. Cappelli, S. Corni, B. Mennucci, R. Cammi, and J. Tomasi, “Vibrational Circular Dichroism within the Polarizable Continuum Model: A Theoretical Evidence of Conformation Effects and Hydrogen Bonding for (S)-()-3-Butyn-2-ol in CCl4 Solution,” J. Phys. Chem. A **106**, 12331–12339 (2002).

[46] R. Cammi and J. Tomasi, “Nonequilibrium Solvation Theory for the Polarizable Continuum Model: A New Formulation at the SCF Level with Application to the Case of the Frequency-Dependent Linear Electric Response Function,” Int. J. Quantum Chem **56**, 465–474 (1995).

[47] D. Ben-Amotz, "Hydration-Sell Vibrational Spectroscopy," J. Am. Chem. Soc. **141**, 10569–10580 (2019).

[48] J. Grdadolnik, F. Merzel, and F. Avbelj, "Origin of Hydrophobicity and Enhanced Water Hydrogen Bond Strength Near Purely Hydrophobic Solutes," Proc. Natl. Acad. Sci. U.S.A. **114**, 322–327 (2017).

[49] V.-T. Pham, T. J. Penfold, R. M. van der Veen, F. Lima, A. El Nahhas, S. L. Johnson, P. Beaud, R. Abela, C. Bressler, I. Tavernelli, C. J. Milne, and M. Chergui, "Probing the Transition from Hydrophilic to Hydrophobic Solvation with Atomic Scale Resolution," J. Am. Chem. Soc. **133**, 12740–12748 (2011).

[50] H. A. Kramers, "Brownian Motion in a Field of Force and The Diffusion Model of Chemical Reactions," Physica (Utrecht) **7**, 284–304 (1940).

[51] H. Eyring, "The Activated Complex in Chemical Reactions," J. Chem. Phys. **3**, 107–115 (1935).

[52] S. Chandrasekhar, "Stochastic Problems in Physics and Astronomy," Rev. Mod. Phys. **15**, 1–89 (1943).

[53] J. Tomasi, B. Mennucchi, and R. Cammi, "Projection Operator Technics in Nonequilibrium Statistical Mechanics," Chem. Rev. **105**, 299 (2005).

[54] R. P. Feynman and F. L. Vernon, "The Theory of a General Quantum System Interacting with a Linear Dissipative System," Ann. Phys. (New York) **24**, 118–173 (1963).

[55] R. K. Wangsness and F. Bloch, "The Dynamical Theory of Nuclear Induction," Phys. Rev. **89**, 728–739 (1953).

[56] A. C. Fogarty and D. Laage, "Water Dynamics in Protein Hydration Shells: The Molecular Origins of the Dynamical Perturbation," J. Phys. Chem. B **118**, 7715–7729 (2014).

[57] R. Buchner, J. Barthel, and J. Stauber, "The Dielectric Relaxation of Water Between 0°C and 35°C," Chem. Phys. Lett. **306**, 57 – 63 (1999).

[58] V. May and O. Kühn, *Charge and Energy Transfer Dynamics in Molecular Systems* (Wiley-VCH, Weinheim, 2011).

[59] M. L. Horng, J. A. Gardecki, A. Papazyan, and M. Maroncelli, "Subpicosecond Measurements of Polar Solvation Dynamics: Coumarin 153 Revisited," J. Phys. Chem. **99**, 17311–17337 (1995).

[60] H. A. Lorentz, *The Theory of Electrons* (B. G. Teuber, Leipzig, 1916).

[61] J. D. Jackson, *Classical electrodynamics* (Wiley, New York, 1999).

[62] R. Clausius, *Die Mechanische Behandlung der Electricität* (Vieweg+Teubner, Wiesbaden, 1879).

[63] O. F. Mossotti, Memorie di Mathematica e di Fisica della Società Italiana della Scienza Residente in Modena **24** (1850).

[64] V. G. Levich and R. R. Dogonadze, Dokl. Akad. Nauk **124** (1954).

[65] V. G. Levich and R. R. Dogonadze, Coll. Czech. Chem. Comm. **26** (1961).

[66] M. Born and R. Oppenheimer, "Zur Quantentheorie der Molekeln," Ann. Phys. (Berlin) **389**, 457–484 (1927).

[67] S. A. Arrhenius, "Über die Dissociationswärme und den Einfluss der Temperatur auf den Dissociationsgrad der Elektrolyte," Z. Physik. Chem. **4**, 96 (1889).

[68] S. A. Arrhenius, "Über die Reaktionsgeschwindigkeit bei der Inversion von Rohrzucker durch Säuren," Z. Physik. Chem. **4**, 226 (1889).

[69] H. J. Kim and J. T. Hynes, "Role of Solvent Electronic Polarization in Electron-Transfer Processes," J. Phys. Chem. **94**, 2736–2740 (1990).

[70] H. J. Kim and J. T. Hynes, "Equilibrium and Nonequilibrium Solvation and Solute Electronic Structure. I. Formulation," J. Chem. Phys. **93**, 5194–5210 (1990).

[71] H. J. Kim and J. T. Hynes, "Equilibrium and Nonequilibrium Solvation and Solute Electronic Structure. II. Strong Coupling Limit," J. Chem. Phys. **93**, 5211–5223 (1990).

[72] H. J. Kim and J. T. Hynes, "Equilibrium and Nonequilibrium Solvation and Solute Electronic Structure. III. Quantum Theory," J. Chem. Phys. **96**, 5088–5110 (1992).

[73] C. J. F. Böttcher, *Theory of Electric Polarization* (Elsevier, Amsterdam, 1973).

[74] C. Bressler, W. Gawelda, A. Galler, M. M. Nielsen, N. Sundström, G. Doumy, A. M. March, S. H. Southworth, L. Young, and L. Vankò, "Solvation Dynamics Monitored by Combined X-ray Spectroscopies and Scattering: Photoinduced Spin Transition in Aqueous [Fe(bpy)3]2+," Faraday Discuss. **171**, 169–178 (2014).

[75] L. Daku, M. Latévi, and A. Hauser, "Ab Initio Molecular Dynamics Study of an Aqueous Solution of [Fe(bpy)3](Cl)2 in the Low-Spin and in the High-Spin States," J. Phys. Chem. Lett. **1**, 1830–1835 (2010).

[76] T. J. Penfold, B. F. E. Curchod, I. Tavernelli, R. Abela, U. Rothlisberger, and M. Chergui, "Simulations of X-ray Absorption Spectra: the Effect of the Solvent," Phys. Chem. Chem. Phys. **14**, 9444–9450 (2012).

[77] E. Biasin, T. B. van Driel, K. S. Kjær, A. O. Dohn, M. Christensen, T. Harlang, P. Chabera, Y. Liu, J. Uhlig, M. Pápai, Z. Németh, R. Hartsock, W. Liang, R. Zhang, J.and Alonso-Mori, M. Chollet, J. M. Glownia, S. Nelson, D. Sokaras, T. A. Assefa, A. Britz, A. Galler, W. Gawelda, C. Bressler, K. J. Gaffney, H. T. Lemke, K. B. Møller, M. M. Nielsen, V. Sundström, G. Vankó, K. Wärnmark, S. E. Canton, and K. Haldrup, "Femtosecond X-Ray Scattering Study of Ultrafast Photoinduced Structural Dynamics in Solvated $[\mathrm{Co(terpy)_2}]^{2+}$," Phys. Rev. Lett. **117**, 013002 (2016).

[78] S. Koneshan, J. C. Rasaiah, R. M. Lynden-Bell, and S. H. Lee, "Solvent Structure, Dynamics, and Ion Mobility in Aqueous Solutions at 25°C," J. Phys. Chem. B **102**, 4193–4204 (1998).

[79] D. Laage, T. Elsaesser, and J. T. Hynes, "Water Dynamics in the Hydration Shells of Biomolecules," Chem. Rev. **117**, 10694–10725 (2017).

[80] M. Born, "Über die Beweglichkeit der elektrolytischen Ionen," Zeitschrift für Physik **1**, 221–249 (1920).

[81] J. G. Kirkwood, "Statistical Mechanics of Fluid Mixtures," J. Chem. Phys. **3**, 300–313 (1935).

[82] J. R. Lakowicz, *Principles of Fluorescence Spectroscopy* (Springer Science+Business Media, LLC, Boston, MA, 2006).

[83] H. Grabert, P. Nalbach, J. Reichert, and M. Thorwart, “Nonequilibrium Response of Nanosystems Coupled to Driven Quantum Baths,” J. Phys. Chem. Lett. **7**, 2015–2019 (2016).

[84] J. Reichert, P. Nalbach, and M. Thorwart, “Dynamics of a Quantum Two-State System in a Linearly driven Quantum Bath,” Phys. Rev. A **94**, 032127 (2016).

[85] M. Wegner, *Extreme Nonlinear Optics* (Springer, Berlin, 2004).

[86] E. Bichoutskaia and N. C. Pyper, “Polarizability of the Iodide Ion in Crystal,” J. Phys. Chem. C **111**, 9548–9561 (2007).

[87] A. L. McClellan, *Tables of Experimental Dipole Moments* (W. H. Freeman, San Francisco, 1963).

[88] P. Schwerdtfeger and J. K. J. K. Nagle, “2018 Table of Static Dipole Polarizabilities of the Neutral Elements in the Periodic Table,” Molecular Physics **117**, 1200–1225 (2019).

[89] P. Nalbach, A. J. A. Achner, M. Frey, M. Grosser, C. Bressler, and M. Thorwart, “Hydration Shell Effects in the Relaxation Dynamics of Photoexcited Fe-II Complexes in Water,” J. Chem. Phys. **141**, 044304 (2014).

[90] E. Heid and D. Braun, “Fundamental Limitations of the Time-Dependent Stokes Shift for Investigating Protein Hydration Dynamics,” Phys. Chem. Chem. Phys. **21**, 4435–4443 (2019).

[91] L. Nilsson and B. Halle, “Molecular Origin of Time-Dependent Fluorescence Shifts in Proteins,” Proc. Natl. Acad. Sci. U.S.A. **102**, 13867–13872 (2005).

[92] B. Bagchi, D. W. Oxtoby, and G. R. Fleming, “Theory of the Time Development of the Stokes Shift in Polar Media,” Chem. Phys. **86**, 257 – 267 (1984).

[93] J. Franck and E. G. Dymond, “Elementary Processes of Photochemical Reactions,” Trans. Faraday Soc. **21**, 536–542 (1926).

[94] E. U. Condon, “Nuclear Motions Associated with Electron Transitions in Diatomic Molecules,” Phys. Rev. **32**, 858–872 (1928).

[95] Y. Ooshika, “Absorption Spectra of Dyes in Solution,” J. Phys. Soc. Jpn. **9**, 594–602 (1954).

[96] N. Mataga, Y. Kaifu, and M. Koizumi, “Solvent Effects upon Fluorescence Spectra and the Dipolemoments of Excited Molecules,” Bull. Chem. Soc. Jpn. **29**, 465–470 (1956).

[97] E. Lippert, “Spektroskopische Bestimmung des Dipolmomentes aromatischer Verbindungen im ersten angeregten Singulettzustand,” Zeitschrift für Elektrochemie, Berichte der Bunsengesellschaft für physikalische Chemie **61**, 962–975 (1957).

[98] M. Maroncelli and G.R. Fleming, “Computer Simulation of the Dynamics of Aqueous Solvation,” J. Chem. Phys. **89**, 5044–5069 (1988).

[99] B. Bagchi and A. Chandra, “Ultrafast Solvation Dynamics: Molecular Explanation of Computer Simulation Results in a Simple Dipolar Solvent,” J. Chem. Phys. **97**, 5126–5131 (1992).

[100] E. Neria and A. Nitzan, “Semiclassical Evaluation of Nonadiabatic Rates in Condensed Phases,” J. Chem. Phys. **99**, 1109–1123 (1993).

[101] S. Cerveny and J. Swenson, “Water Dynamics in the Hydration Shells of Biological and Non-Biological Polymers,” J. Chem. Phys. **150**, 234904 (2019).

[102] C.-P. Hsu, X. Song, and R. A. Marcus, “Time-Dependent Stokes Shift and Its Calculation from Solvent Dielectric Dispersion Data,” J. Phys. Chem. B **101**, 2546–2551 (1997).

[103] K. E. Furse and S. A. Corcelli, “The Dynamics of Water at DNA Interfaces: Computational Studies of Hoechst 33258 Bound to DNA,” J. Am. Chem. Soc. **130**, 13103–13109 (2008).

[104] K. E. Furse and S. A. Corcelli, “Effects of an Unnatural Base Pair Replacement on the Structure and Dynamics of DNA and Neighboring Water and Ions,” J. Phys. Chem. B **114**, 9934–9945 (2010).

[105] H. Kirchberg, P. Nalbach, and M. Thorwart, “Nonequilibrium Quantum Solvation with a Time-Dependent Onsager Cavity,” J. Chem. Phys. **148**, 164301 (2018).

[106] T.-W. Nee and R. Zwanzig, “Theory of Dielectric Relaxation in Polar Liquids,” J. Chem. Phys. **52**, 6353–6363 (1970).

[107] D. Laage, T. Elsaesser, and J. T. Hynes, “Perspective: Structure and Ultrafast dynamics of Biomolecular Hydration Shells,” Struc. Dyn. **4**, 044018 (2017).

[108] K.-J. Tielrooij, J. Hunger, R. Buchner, M. Bonn, and H. J. Bakker, “Influence of Concentration and Temperature on the Dynamics of Water in the Hydrophobic Hydration Shell of Tetramethylurea,” J. Am. Chem. Soc. **132**, 15671–15678 (2010).

[109] L. Fumagalli, A. Esfandiar, R. Fabregas, S. Hu, P. Ares, A. Janardanan, Q. Yang, B. Radha, T. Taniguchi, K. Watanabe, G. Gomila, K. S. Novoselov, and A. K. Geim, “Anomalously Low Dielectric Constant of Confined Water,” Science **360**, 1339–1342 (2018).

[110] K. J. Miller, “Calculation of the Molecular Polarizability Tensor,” J. Am. Chem. Soc. **112**, 8543–8551 (1990).

[111] H. J. Bakker, Y. L. A. Rezus, and R. L. A. Timmer, “Molecular Reorientation of Liquid Water Studied with Femtosecond Midinfrared Spectroscopy,” J. Phys. Chem. A **112**, 11523–11534 (2008).

[112] F. Sedlmeier, D. Horinek, and R. R. Netz, “Entropy and Enthalpy Convergence of Hydrophobic Solvation Beyond the Hard-Sphere Limit,” J. Chem. Phys. **134**, 055105 (2011).

[113] S. Garde, G. Hummer, A. E. García, M. E. Paulaitis, and L. R. Pratt, “Origin of Entropy Convergence in Hydrophobic Hydration and Protein Folding,” Phys. Rev. Lett. **77**, 4966–4968 (1996).

[114] D. Chandler, “Interfaces and the Driving Force of Hydrophobic Assembly,” Nature **437**, 640647 (2005).

[115] J. Zhang, A.r M. Kuznetsov, I. G. Medvedev, Q. Chi, T. Albrecht, P. S. Jensen, and J. Ulstrup, “Single-Molecule Electron Transfer in Electrochemical Environments,” Chem. Rev. **108**, 2737–2791 (2008).

[116] L. D. Zusman, “Outer-Sphere Electron Transfer in Polar Solvents,” Chem. Phys. **49**, 295 – 304 (1980).

[117] L. D. Zusman, “Dynamical Solvent Effect in Electron Transfer Reactions Occurring in a Mixture of Two Polar Solvents,” J. Chem. Phys. **102**, 2580–2584 (1995).

[118] R. A. Marcus and H. Sumi, “Solvent Dynamics and Vibrational Effects in Electron Transfer Reactions,” J. Electroanal. Chem. **204**, 59–67 (1986).

[119] E. M. Kosower and D. Huppert, “Excited State Electron and Proton Transfers,” Annu. Rev. Phys. Chem. **37**, 127–156 (1986).

[120] H. Sumi and T. Kakitani, “Unified Theory on Rates for Electron Transfer Mediated by a Midway Molecule, Bridging between Superexchange and Sequential Processes,” J. Phys. Chem. B **105**, 9603–9622 (2001).

[121] K. Saito and H. Sumi, “Unified Expression For the Rate Constant of The Bridged Electron Transfer Derived by Renormalization,” J. Chem. Phys. **131**, 134101 (2009).

[122] A. Nitzan, “Activated rate processes in condensed phases: the kramers theory revisited,” in *Adv. Chem. Phys.* (John Wiley and Sons, Ltd, 2007) pp. 489–555.

[123] P. Hänggi, P. Talkner, and M. Borkovec, “Reaction-Rate Theory: Fifty Years After Kramers,” Rev. Mod. Phys. **62**, 251–341 (1990).

[124] V. I. Melnikov and S. V. Meshkov, “Theory of Activated Rate Processes: Exact Solution of the Kramers Problem,” J. Chem. Phys. **85**, 1018–1027 (1986).

[125] E. Pollak, H. Grabert, and P. Hänggi, “Theory of Activated Rate Processes for Arbitrary Frequency Dependent Friction: Solution of the Turnover Problem,” J. Chem. Phys. **91**, 4073–4087 (1989).

[126] A. Okada, “Qualitative Features of Electron Transfer Reaction for High Viscosity of Solvent and Low Activation Barrier,” J. Phys. Chem. A **104**, 7744–7750 (2000).

[127] R. A. Marcus, “Chemical and Electrochemical Electron-Transfer Theory,” Annu. Rev. Phys. Chem. **15**, 155–196 (1964).

[128] A. Nazir and G. Schaller, “The reaction coordinate mapping in quantum thermodynamics,” in *Thermodynamics in the Quantum Regime. Fundamental Theories of Physics* (Springer, Cham, 2018) pp. 551–577.

[129] J. Jortner, "Temperature Dependent Activation Energy for Electron Transfer between Biological Molecules," J. Chem. Phys. **64**, 4860–4867 (1976).

[130] A. Renart, R. Moreno-Bote, X.-J. Wang, and N. Parga, "Mean-Driven and Fluctuation-Driven Persistent Activity in Recurrent Networks," Neural Comput. **19**, 1–46 (2007).

[131] U. Fano, "Ionization Yield of Radiations. ii. The Fluctuations of the Number of Ions," Phys. Rev. **72**, 26–29 (1947).

[132] A. Migliore, P. Schiff, and A. Nitzan, "On the Relationship Between Molecular State and Single Electron Pictures in Simple Electrochemical Junctions," Phys. Chem. Chem. Phys. **14**, 13746–13753 (2012).

[133] L. Yuan, L. Wang, A. R. Garrigues, L. Jiang, H. V. Annadata, M. Anguera Antonana, E. Barco, and C. A. Nijhuis, "Transition from Direct to Inverted Charge Transport Marcus Regions in Molecular Junctions via Molecular Orbital Gating," React. Chem. Eng. **13**, 322–329 (2018).

[134] J. Wu, R. J. Silbey, and J. Cao, "Generic Mechanism of Optimal Energy Transfer Efficiency: A Scaling Theory of the Mean First-Passage Time in Exciton Systems," Phys. Rev. Lett. **110**, 200402 (2013).

[135] E. Zerah-Harush and Y. Dubi, "Universal Origin for Environment-Assisted Quantum Transport in Exciton Transfer Networks," J. Phys. Chem. Lett. **9**, 1689–1695 (2018).

[136] E-D. Fung, D. Gelbwaser, J. Taylor, J. Low, J. Xia, L. M. Davydenko, I.and Campos, S. Marder, U. Peskin, and L. Venkataraman, "Breaking Down Resonance: Nonlinear Transport and the Breakdown of Coherent Tunneling Models in Single Molecule Junctions," Nano Lett. **19**, 2555–2561 (2019).

[137] C. T. Middleton, B. Cohen, and B. Kohler, "Solvent and Solvent Isotope Effects on the Vibrational Cooling Dynamics of a DNA Base Derivative," J. Phys. Chem. A **111**, 10460–10467 (2007).

[138] S. Hassan, M. Schade, Christopher P. Shaw, R. Lévy, and P. Hamm, "Response of Villin Headpiece-Capped Gold Nanoparticles to Ultrafast Laser Heating," J. Phys. Chem. B **118**, 7954–7962 (2014).

[139] R. Costard, C. Greve, I. A. Heisler, and T. Elsaesser, "Ultrafast Energy Redistribution in Local Hydration Shells of Phospholipids: A Two-Dimensional Infrared Study," J. Phys. Chem. Lett. **3**, 3646–3651 (2012).

[140] D. Laage, T. Elsaesser, and J. T. Hynes, "Water Dynamics in the Hydration Shells of Biomolecules," Chem. Rev. **117**, 10694–10725 (2017).

[141] S. Mukamel, D. Healion, Y. Zhang, and J. D. Biggs, "Multidimensional Attosecond Resonant X-Ray Spectroscopy of Molecules: Lessons from the Optical Regime," Annu. Rev. Phys. Chem. **64**, 101–127 (2013).

[142] J. J. Varghese and S. H. Mushrif, "Origins of Complex Solvent Effects on Chemical Reactivity and Computational Tools to Investigate Them: a Review," React. Chem. Eng. **4**, 165–206 (2019).

Acknowledgment

First, I would like to thank Prof. Dr. Michael Thorwart for the proposal of the great topic of my PhD-project. It was very nice to get into a complete new field of ultrafast and nonequilibrium quantum solvation with promising experimental realizations at the new-established research unit in Hamburg - the European XFEL. During my whole PhD-period Michael Thorwart encouraged me in establishing new theories and new approaches. Throughout the plenty of discussions, he helped me as expert of nonequilibrium quantum dynamics and statistics to more and more learn about different approaches and exact calculations. He also promoted an international research stay at the University of Pennsylvania and the Tel Aviv University to enlarge my knowledge of molecular energy and charge transfer in non-equilibrated solution. Finally, he continuously supported my research and my personal development with great aid.

Furthermore, I really thank Prof. Dr. Abraham Nitzan for giving me the great opportunity to host me in Philadelphia and Tel Aviv. During this time, I could enlarged my knowledge in the field of molecular dynamics in condensed phases. Abraham Nitzan gave me excellent insights into newest approaches and problems of the research community. It was a great pleasure to continue to collaborate in such an international context and to successfully accomplish a joint-project. He unceasingly encouraged me during my research and welcomed me in the US and Israel with greatest hospitality.

In addition, I would like to thank Prof. Dr. Peter Nalbach for his support and discussions when I established a newly approach for molecular absorption in nonquilibrium solvation. As expert in quantum many-body dynamics he gave me deep insights into the field, especially in mathematical descriptions ranging from exact numerical to generalized analytic approaches. I have learned so much from him.

Furthermore, I really liked to be part of an amazing and inspirational working group with excellent colleagues. We had a great time together. I thank you all.

I enjoyed the financial support from the SFB 925 "Light Induced Dynamics and Control

of Correlated Quantum Systems" as well as from the cluster of excellence AIM "Advanced Imaging of Matter". It was a great pleasure to be part of the respective graduate schools which offered nice extra-curricular programs and workshops.

Finally, I thank my family and friends for their love, support and endless understanding.

Eidesstattliche Versicherung/ Declaration on oath

Hiermit versichere ich an Eides statt, die vorliegende Dissertationsschrift selbst verfasst und keine anderen als die angegebenen Hilfsmittel und Quellen benutzt zu haben.

Die eingereichte schriftliche Fassung entspricht der auf dem elektronischen Speichermedium.

Die Dissertation wurde in der vorgelegten oder einer ähnlichen Form nicht schon einmal in einem früheren Promotionsverfahren angenommen oder als ungenügend beurteilt.

Hamburg, den 19.02.2020

Henning Kirchberg